NORTHWESTERN UNIVERSITY

Function of Discrete MARTX Toxin Domains in *Vibrio vulnificus* Intragastric Pathogenesis

A DISSERTATION

SUBMITTED TO THE GRADUATE SCHOOL
IN PARTIAL FULFILLMENT OF THE REQUIREMENTS

for the degree

DOCTOR OF PHILOSOPHY

Field of Life Sciences

By

Hannah Elizabeth Gavin

EVANSTON, ILLINOIS

June 2018

ABSTRACT

In 2015, the United States Department of Agriculture (USDA) reported that 1 in 6 Americans fall ill with a foodborne infection annually, resulting in more than 3000 fatalities and an estimated $15 billion in economic burden due to combined medical costs, productivity loss, and death. On a per-case basis, infections caused by the marine bacterium *Vibrio vulnificus* are the most burdensome foodborne illness at $3.3 million/case. *V. vulnificus*-associated fatality rates are reported to exceed 50 percent. Yet, the bacterium's major virulence factor and its relationship to foodborne infection remain poorly understood. As infection incidence climbs in conjunction with rising sea surface temperature, studies elucidating pathogenic mechanisms of *V. vulnificus* are increasingly critical.

This study investigates the pathogenic mechanisms of *V. vulnificus* as mediated by its primary virulence factor, the Multifunctional Autoprocessing Repeats-in-Toxins (MARTX) toxin. The MARTX toxin, product of the *rtxA1* gene, has been identified as the dominant secreted virulence factor in the intragastric mouse model of *V. vulnificus* infection. MARTX toxins are classified as repeats-in-toxins (RTX) family members by virtue of characteristic amino acid repeats at the protein C-terminus. MARTX toxins are further defined as a unique sub-family of RTX proteins possessing: 1) tandem amino acid repeats at the N-terminus; 2) a cysteine protease domain (CPD) for autoprocessing; and 3) a section of effector domains situated between N-terminal repeats and CPD. Functional roles for each toxin region have been previously postulated but only recently experimentally investigated. This study employs a combination of bacterial genetic manipulation, *in vitro* assays, and *in vivo* intragastric mouse infection. We

demonstrate that the same native MARTX toxin effector domain repertoire that is dispensable for toxin secretion, toxin delivery to host cells, and cell lysis *in vitro* is essential for induction of rapid intestinal epithelial barrier dysfunction, bacterial dissemination from the mouse intestine, and anti-phagocytosis activity against macrophages. Moreover, the MARTX toxin effector domain repertoire is essential for bacterial virulence potential.

We also investigate roles for individual effector domains within the larger repertoire. Each of the five investigated MARTX effector domains exhibit functional redundancy in the ability to disrupt phagocytic activity and intestinal barrier integrity. However, individual domains confer different virulence potential. This is demonstrated by altered survival outcomes of mice infected with strains harboring deletions in discrete effector domains. Together our results support a model in which the MARTX toxin repeat regions and CPD together function as a delivery platform for diverse effector cargo that define toxin potency and directly impact *V. vulnificus* virulence potential in mammalian hosts.

ACKNOWLEDGEMENTS

To Dr. Karla Satchell: I am so grateful for your mentorship. From day one, you outlined a path to success and helped me to walk that path. Thank you for all the constructive criticisms, timely insights, and communicative interactions. Thank you for promoting my scientific independence by helping me to develop as a researcher, writer, and academic. Your guidance has never led me astray, and your support has shaped my career in ways both tangible and intangible.

I have also benefited from time with many wonderful members of the Satchell lab. I am particularly appreciative of the ever-patient microbiology tutoring of Byoung Sik Kim. Marco Biancucci and Patrick Woida were together the most wonderful and consistent lab presence in my graduate career. I am especially thankful for their camaraderie. Thanks to the particular efforts of multiple lab members, the group vibe has never been better. I hope for such a positive social dynamic in my new lab.

I am grateful for the guidance of my committee members, Drs. Hank Seifert, Alan Hauser, and Patrick Seed, as well as the bacteriology faculty in the Northwestern University Department of Microbiology-Immunology. I can think of specific feedback from each of you that has shaped my experiments and my thinking. Thank you all for molding me into an appropriately skeptical scientist. I aim to represent the best of Northwestern as I move on to new endeavors.

The Driskill Graduate Program has supported me from interview, through candidacy, all the way to graduation. The program and its leadership – specifically Dr. Steve Anderson, Dr. Pamela Carpentier, and Judy Brown – are true assets to any DGP student. The DGP leadership has continuously supported my well-being and promoted my success. Likewise, interactions with fellow DGP students have been overwhelmingly positive throughout my time at Northwestern.

I will always appreciate the Cell and Molecular Basis of Disease (CMBD) training grant. It provided me with financial support and the ability to give a chalk talk. The Science Club program, co-administered by Northwestern Science in Society and the Boys and Girls Clubs of Chicago, also holds a special place in my graduate experience. Weekly interactions with my co-mentor, Tom Fauvell, and our middle school students have kept me grounded and laughing even on the most difficult of laboratory days.

To my friends and loved ones: science is cool, but it's you who make life wonderful! To my family – you are the foundation on which I build my life. I feel constantly privileged/honored/ecstatic to be a Gavin.

STATEMENT OF PUBLICATION

Portions of the Abstract and Chapters 1-5 have been published previously in the following reports:

Gavin HE and Satchell, KJF (2015) MARTX toxins as effector delivery platforms (review). *FEMS Pathogens and Disease*, 73(9):ftv092.

Kim BS, Gavin HE, Satchell KJF (2015) Distinct roles of the repeats-containing regions and effector domains of the *Vibrio vulnificus* multifunctional-autoprocessing repeats-in-toxin (MARTX) toxin. *mBio* 6: e00324-15.

Gavin HE, Beaubier NT and Satchell KJF (2017) The effector domain region of the *Vibrio vulnificus* MARTX toxin confers biphasic epithelial barrier disruption and is essential for systemic spread from the intestine. *PLoS Pathogens*, 13(1): e1006119.

Gavin HE and Satchell KJF. (2017) Surface hypothermia predicts murine mortality in the intragastric *Vibrio vulnificus* infection model. *BMC Microbiology,* 17(1): 136.

TABLE OF CONTENTS

ABSTRACT

ACKNOWLEDGEMENTS

STATEMENT OF PUBLICATION

TABLE OF CONTENTS

LIST OF TABLES

LIST OF FIGURES

CHAPTER 1 – INTRODUCTION

1.1. *Vibrio* biology

1.1. *V. vulnificus* epidemiology

1.2. *V. vulnificus* pathogenesis

1.2.1. Infection progression

1.2.2. Pre-disposing conditions

1.2.3. Experimental models of pathogenesis

1.3. Virulence determinants in *V. vulnificus*

1.3.1. Resistance to host

1.3.2. Motility and adhesion

1.3.3. Iron acquisition

1.3.4. Secreted factors

1.4. MARTX toxins

1.4.1. Introduction

1.4.2. *rtxA1* regulation

1.4.3. MARTX toxin production and secretion

1.4.4. MARTX toxin domain organization

1.4.5. MARTX toxin effector delivery

1.5. MARTX toxin effector domains

1.5.1. MARTX toxins and heterologous protein transfer

1.6. Driving questions

CHAPTER 2 – The *Vibrio vulnificus* MARTX toxin effector domain region is not required for toxin expression, secretion, or delivery to host cells

2.1. Chapter-specific acknowledgements

2.2. Overview

2.3. Results

2.3.1. Strain generation and validation

2.3.2. Modification of *rtxA1* does not alter *in vitro* bacterial growth

2.3.3. Modified MARTX toxin secretion is secreted to culture media

2.3.4. Bla modification does not render strains resistant to current clinical antibiotic therapy

2.3.5. Modified MARTX toxin delivers the heterologous Bla effector to host cytosol

2.3.6. Toxin-dependent lysis of target cells does not require effector domains

2.3.7. MARTX effector domains are required for induction of cell rounding

2.4. Discussion

CHAPTER 3 – The MARTX toxin effector domain region confers biphasic epithelial dysfunction and is essential for systemic spread from the intestine

3.1. Overview

3.2. Results

3.2.1. Bacterial strain selection and verification

3.2.2. Effector domains are required for MARTX toxin-associated virulence

3.2.3. MARTX effector domain region is required for bacterial spread to distal organs

3.2.4. Neither overt intestinal tissue damage nor epithelial apoptosis is a prerequisite to *V. vulnificus* dissemination

3.2.5. Bacterial dissemination does not induce organ pathology

3.2.6. The MARTX toxin rapidly disrupts transepithelial resistance *in vitro*

3.2.7. MARTX toxin effector domains are essential for rapid loss of T84 monolayer TER

3.2.8. The MARTX toxin induces a biphasic disruption of paracellular epithelial permeability

3.2.9. Late, but not early, onset TER disruption coincides with cell lysis

3.3. Discussion

CHAPTER 4 – Individual MARTX effector domains share redundant functions but exhibit distinct virulence profiles

4.1. Overview

4.2. Results

4.2.1. Generation of a library of validated Δ*effector* strains in the CMCP6 *rtxA1* gene

4.2.2. *V. vulnificus* single effector mutants exhibit distinct virulence profiles during i.g. infection

4.2.3. No single MARTX effector domain required for bacterial survival in the gut at 6 hpi

4.2.4. No single MARTX effector domain is required for intestinal barrier disruption or bacterial dissemination

4.2.5. MARTX potently inhibits phagocytosis dependent upon the effector domain region, but no single effector is required

4.3. Discussion

CHAPTER 5 – Surface hypothermia predicts murine mortality in the intragastric *V. vulnificus* infection model

5.1. Overview

5.2. Results

5.2.1. Bacterial strain selection

5.2.2. V. vulnificus strains show distinct survival patterns

5.2.3. VST measurement profiles vary dependent upon survival outcome

5.2.4. VST of 23.5 is associated with lethality during *V. vulnificus* infection

5.2.5. VST ≤23.5 predicts live/dead survival outcomes and reduces infection hours

5.3. Discussion

CHAPTER 6 – Discussion

6.1. Summary

6.2. Discussion and future directions

6.3. Concluding statements

CHAPTER 7 – Materials and Methods

REFERENCES

APPENDIX I - MARTX toxin ability to inhibit phagocytosis does not extend to protozoan cells

APPENDIX II - Preliminary data on development of a seabass bacterial colonization model

LIST OF FIGURES

1. **Chapter 1** - Introduction

1.1. Expression at the *rtx* gene locus leads to MARTX toxin secretion

1.2. MARTX toxins deliver effector domains to target cell cytosol

1.3. MARTX toxins are capable of heterologous protein transfer

1.4. Current paradigm of MARTX toxin activity in pathogenesis

2. **Chapter 2** - Defining the *V. vulnificus* MARTX TOXIN regions involved in toxin production, secretion & delivery

2.1. Modified MARTX toxin schematics

2.2. Chromosomal modification of *rtxA1* gene does not alter bacterial growth *in vitro*

2.3. Strains expressing modified RtxA1::Bla toxins exhibit β-lactamase activity

2.4. The *rtxA1* effector domain region, N-terminus, and CPD catalytic activity are dispensable for MARTX toxin secretion

2.5. MARTX toxin C-terminal repeat regions are required for MARTX toxin secretion

2.6. Modified *rtxA1::bla* strain is not resistant to clinical antibiotic treatment for *V. vulnificus*

2.7. Modified MARTX toxin targets eukaryotic cells and delivers the heterologous Bla domain to eukaryotic cytosol

2.8. MARTX toxin N-terminus is required for Bla delivery to target cells

2.9. Effector domain region is not required for MARTX dependent lysis

2.10. Repeat-containing regions of $MARTX_{Vv}$ toxin are necessary and sufficient for host cell lysis

2.11. Rapid cell rounding induced by $MARTX_{Vv}$ requires effector domains

3. **Chapter 3 -** The MARTX toxin effector domain region confers biphasic epithelial dysfunction and is essential for systemic spread from the intestine
   - 3.1. Modified MARTX toxin composition and layout
   - 3.2. Elimination of *rtxA1* effector domain region does not impact gene expression
   - *3.3. V. vulnificus* MARTX toxin effector domains confer virulence *in vivo*
   - 3.4. *rtxA1* is not required for *V. vulnificus* intestinal survival at 6 hpi
   - 3.5. MARTX effector domain region is required for *V. vulnificus* dissemination from intestine to distal organs
   - 3.6. Intestinal tissue pathology is not a prerequisite to *V. vulnificus* dissemination
   - 3.7. MARTX toxin effector domains do not induce increased intestinal epithelial apoptosis
   - 3.8. Disseminated bacteria do not induce organ pathology at 6 hpi
   - 3.9. Polarized T84 monolayer for modeling the intestinal epithelium *in vitro*
   - 3.10. Epithelial dysfunction is observed with *V. vulnificus* MOI between 0.25 and 25
   - 3.11. *vvhA* is not required for epithelial disruption, while *rtxA1* is required for induction of early monolayer dysfunction
   - 3.12. MARTX toxin effector domains rapidly induce intestinal barrier dysfunction *in vitro*
   - 3.13. Initial polarized monolayer dysfunction does not correlate with unpolarized, *in vitro* lysis kinetics
   - 3.14. Cytoskeletal morphology is maintained during barrier dysfunction at 60 mins
   - 3.15. MARTX toxin induces a biphasic increase in epithelial paracellular permeability

3.16. Neither LDH nor viable bacteria are recovered from the basal T84 transwell media

3.17. Early, effector-dependent monolayer dysfunction is lysis-independent, while late, pore-dependent monolayer dysfunction corresponds to cell lysis

3.18. MOI increases over the course of T84 co-incubation experiments

3.19. *In vitro* necrosis does not predict *in vivo* virulence outcomes

4. **Chapter 4** – Individual MARTX effector domains share redundant functions but exhibit distinct virulence profiles

4.1. Identity and function of individual MARTX effector domains in C-type toxins including representative isolate CMCP6

4.2. Toxin schematics for single MARTX effector domain deletion strains

4.3. Modified MARTX toxins are generated and deliver their effector domain cargo to target eukaryotic cells

4.4. V. vulnificus strains lacking single MARTX toxin effector domains have altered virulence potential *in vivo*

4.5. No single MARTX effector is required for intestinal survival at 6 hpi

4.6. No single effector domain is required for induction of epithelial barrier dysfunction

4.7. No single MARTX effector is required for bacterial dissemination from the intestine

4.8. MARTX effector domain region is required for toxin-dependent disruption of phagocytosis

4.9. No single MARTX effector domain is required for toxin anti-phagocytic activity

4.10. Ectopic delivery of the RRSP domain is sufficient to inhibit phagocytosis

5. **Chapter 5** – Surface hypothermia predicts murine mortality in the intragastric *V. vulnificus* infection model
    5.1. Schematic depiction of the MARTX toxin variants produced by strains in this study
    5.2. V. vulnificus strains exhibit distinct survival patterns
    5.3. VST measurement profiles vary dependent upon survival outcome
    5.4. Minimum VST of infected imce is significantly different between survivors and non-survivors
    5.5. VST ≤ 23.5 °C predicts live/dead survival outcomes and reduces infection hours
6. **Chapter 6** – Discussion
    6.1. Summary and model figure

LIST OF TABLES

Chapter 1 - Introduction

Table 1.1 – Distribution of *rtxA* loci among bacterial species

Table 1.2 – MARTX toxin effector domains and their characteristics

Chapter 5 – Surface hypothermia predicts murine mortality in the intragastric *V. vulnificus* infection model

Table 5.1 – Statistical analyses of survival outcomes and curves

Chapter 7 – Materials and Methods

Table 7.1 – Strains used in this study

CHAPTER 1 – INTRODUCTION

Vibrio biology

The family Vibrionaceae (Domain Eubacteria, Kingdom Bacteria, Phylum Proteobacteria, Class Gammaproteobacteria, Order Vibrionales) currently consists of the genus *Vibrio* and the five additional genera *Photobacterium, Salinivibrio, Enterovibrio, Grimontia,* and *Allivibrio*. The Vibrionaceae are Gram-negative rod- or comma-shaped bacteria with polar, sheathed flagella (33, 34). Vibrionaceae taxonomy was originally based on phenotypic examination of metabolic and morphological parameters. Though metabolically versatile, members of the Vibrionaceae generally exhibit facultative anaerobic metabolism, the ability to ferment D-glucose, and growth at 20^{o}C (33). Today, DNA sequence is an integral part of Vibrionaceae phylogeny, though it has been noted that phenotypically-derived taxonomic clusters correlate to DNA sequence-based taxonomy when 80% similarity cutoffs for both phenotypic and DNA homology are observed (33).

While taxonomic organization for members of the Vibrionaceae is a matter of ongoing debate (33, 36, 37), recent phylogenetic analyses list approximately 85 species in the *Vibrio* genus (37). In the laboratory, most vibrios can be selectively isolated by growth on thiosulfate-citrate bile salts sucrose (TCBS) media (38). Notably, though, certain environmental conditions trigger vibrios to enter a viable but nonculturable (VBNC) state, from which they must be resuscitated in order to grow by conventional culture mechanisms (39-42).

Members of the *Vibrio* genus have been detected in the water column and in sediment, as well as in association with phytoplankton, zooplankton, macroalgae, amoebal protists, aquatic plants, macroinvertebrates (e.g. shellfish), and vertebrate fish. Long thought to associate

primarily/preferentially with such eukaryotic hosts, vibrios have more recently been shown to proliferate, even bloom, in host-free contexts. Thus, it remains unknown whether bacterial association with hosts are transient in nature, or constitute *bona fide* bacterial niches. For detail on *Vibrio* environmental dynamics, readers are directed to an expert meta-analysis and review by Takemura, Chien, and Polz (43). Generally, the strongest predictors of total *Vibrio* abundance are water temperature and salinity (43). Additional biotic and abiotic variables exhibit modest and/or inconsistent correlations with total *Vibrio* population size. The relationships among bulk-measurable environmental parameters and *Vibrio* populations further vary dependent on the species under study (43).

For members of the *Vibrio* genus that associate with eukaryotic organisms, bacterial:host relationships take on a variety of forms. In numerous cases, these relationships exhibit the properties of beneficial symbioses (mutualism). Now studied for approximately a quarter-century, the mutualistic relationship between *Vibrio fischeri* and the squid *Euprymna scolopes* is a model for symbiotic bacterial:host relationships (44, 45). Similarly, *Vibrio logei* is symbiotically associated with squids in the *Sepiola* genus (46). In each of these cases, the luminescent *Vibrio* occupies the squid light organ and provides counter-illumination as a means of protection from predation.

Vibrio halioticoli, also known as *Vibrio haliotis,* and related *Vibrio spp V. superstes, V. gallicus, V. ezurae,* and *V. neonates,* occupy the gut of various *Haliotis* abalone. Their metabolism of alginate likely contributes to algal digestion by the abalone host (47, 48). Metabolism of algal carbohydrates is probably also an evolved trait for *Vibrio* to engage in

symbioses with red, green, and brown algae, which in turn gain physiological and survival benefits from their bacterial associates (reviewed in (43)).

Diazotrophic *Vibrio spp.,* specifically *V. harveyi and V. alginolyticus,* associate with marine corals where they are thought to contribute metabolically accessible nitrogen products to their hosts (49). Diazotrophic *Vibrio spp,* including *V. porteresiae, V. alginolyticus, V. anguillarum, V. diazotrophicus*, and *V. parahaemolyticus*, have also been isolated from a variety of aquatic plants including grasses and rice. It is anticipated that these vibrios likewise form symbiotic associations with their plant hosts by virtue of the ability to fix atmospheric nitrogen (33, 50-54).

Other *Vibrio*:host relationships are commensal. *Vibrio cholerae* and *Vibrio mimicus* interact with amoebal protists. Bacteria access a replicative niche in amoebal vacuoles or cysts without apparent harm to the *Acanthamoeba* (55-58). *Vibrio splendidus* is an abundant colonizer of coral (59), and additional members of the genus have also been identified in healthy coral samples (60-63). In fact, *V. alginolyticus* and two *Vibrio* isolates closely related to *Vibrio shiloi* and *Vibrio proteolyticus* are capable of using coral mucus as their sole carbon source *in vitro* (62, 63, 65).

V. cholerae is regularly isolated in association with zooplankton (e.g. copepods) and phytoplankton (e.g. cyanobacteria), both of which are reported to enhance its growth (66-70). However, given that the quantity of planktonic *V. cholerae* is orders of magnitude higher than the number of attached *V. cholerae,* the impact of planktonic associations on the overall population size remains unclear (43). While not diazotrophic, *V. cholerae* associates with

freshwater plants, and plant attachment seems favorable for bacterial survival and numerical enrichment, relative to water (43, 71, 72).

In addition, an abundance of studies demonstrate *Vibrio* presence in healthy fish, shellfish, and seabird populations (73-76). In the case of the fish gut, host association provides bacterial access to proliferation-favorable environments that in turn promote transmission to the surrounding water (77-84). High concentrations of *Vibrio spp,* especially *V. cholerae, V. parahaemolyticus,* and *Vibrio vulnificus,* are well documented in shellfish (85-88). Whether their presence is a passive byproduct of shellfish filter feeding or a bacterially advantageous locale remains unclear, but very recent evidence suggests that genes encoding a tight adherence *(tad)* locus promotes *V. vulnificus* colonization in an experimental oyster model (89, 90).

Finally, the *Vibrio* genus includes numerous species that exhibit detrimental or pathogenic characteristics in certain host contexts. Collectively termed "vibrioses," the diseases resulting from pathogenic *Vibrio* exposures vary. *V. cholerae* colonizes egg masses of the insect *Chironomus,* leading to egg mass dissociation and hatching failure (91, 92). *Vibrio penaeicida,* causative agent of "Syndrome 93," and *Vibrio nigripulcritudo*, causative agent of "Summer Syndrome," are among the vibrios that act either opportunistically or as "true" pathogens to cause disease in shrimp (93, 94). Numerous *Vibrio spp,* including *V. alginolyticus, V. anguillarum, V. harveyi, V. ordalii, V. salmonicida, V. splendidus,* and *V. vulnificus,* are fish pathogens, and as such represent threats to aquaculture systems. Vibros have additionally been implicated in disease of scallops, clams, lobsters, and octopus (reviewed in (33)).

Among the best-studied vibrios are the species that are pathogenic to humans (reviewed in (33)). These include primarily *V. cholerae, V. parahaemolyticus,* and *V. vulnificus. V.*

cholerae is the etiologic agent of the diarrheal disease cholera, which is obtained through the consumption of contaminated water (70). Diseases with cholera-like characteristics are noted in ancient literature sources as early as 500 B.C., and seven global pandemics have been described between 1817 and present day (95, 96). The causative agent was not identified as *V. cholerae* until 1884, when Robert Koch linked "cholera and its bacillus" (97). *V. cholerae,* endemic to the Ganges Delta, eventually spread globally, and most recently caused a post-earthquake outbreak in Haiti (98). Though cholera remains devastating to the global community due to insufficient preventative infrastructure, the disease is actually relatively treatable with prompt rehydration therapy (sometimes coupled with antibiotic treatment) to ameliorate a patient's extensive fluid loss (99).

V. parahaemolyticus is a foodborne pathogen that causes gastroenteritis in individuals exposed to the bacteria, usually via raw or undercooked shellfish. Infections are reported globally, with the O3:K6 serotype appearing particularly problematic since its identification in 1996 (33, 100). In the United States (US), *V. parahaemolyticus* causes approximately 35,000 infections each year (101), but the disease is generally mild and self-limiting. As such, only four of the 35,000 annual *V. parahaemolyticus* infections are lethal (101).

In contrast to the vibrioses caused by *V. cholerae* or *V. parahaemolyticus, V. vulnificus* infections are generally neither readily treatable nor self-limiting. The USDA reports that 1 in 6 Americans fall ill with a foodborne infection every year, resulting in more than 3000 fatalities and an estimated $15 billion in economic burden due to combined medical costs, productivity loss, and death (101). Of the cited foodborne illnesses, the most economically costly on a per-case basis are those caused by *V. vulnificus* at $3.3 million per case. These foodborne *V.*

vulnificus infections result in hospitalization rates of more than 90% and fatality rates that exceed 50% (101-105).

V. vulnificus epidemiology

Vibrio infections in the US are monitored both actively, by the Foodborne Diseases Active Surveillance Network (FoodNet), and passively, by the Centers for Disease Control (CDC) Cholera and Other Vibrio Illness Surveillance (COVIS) network. Between 2012 and 2014, COVIS summaries reported an average of 127 *V. vulnificus* cases in the US each year (106-108). Analysis of reported cases reveals that they are almost evenly split between foodborne and non-foodborne routes of exposure (103, 105). However, estimates that account for under-reporting suggest that there are actually approximately 100 foodborne infections in the USA each year (101, 104). While infection incidence of *V. vulnificus* is much lower than that of related bacterial species, including *V. paraheamolyticus,* fatalities are disproportionately high (101). Illustratively, *V. vulnificus* accounts for 0.001% of acquired foodborne illnesses, yet nearly 3% of all deaths from foodborne infections (101).

Annual *V. vulnificus* case counts have increased over the past 15 years in the US, and the infection remains prevalent in endemic countries, including Japan, Taiwan, and South Korea (102, 109, 110). Moreover, growing risk of pathogen exposure in historically non-endemic areas is highlighted by locally-aquired case reports from countries including Sweden, Germany, France, and Denmark (111, 112). The rise in *V. vulnificus* infection incidence is in part attributable to improved reporting (102). Importantly, however, increased infection incidence likewise correlates with increasing sea surface temperature (102, 113). The global geographic

range of the bacterium is predicted to continue its expansion as water bodies warm (111, 112, 114, 115). In addition, the temporal range of *V. vulnificus* infections, currently heavily restricted to summer months, may likewise expand with permissive temperature (109, 114-118). Combined, these factors lead to models that predict *V. vulnificus* infection rates that grow over time (119).

V. vulnificus pathogenesis

Infection Progression

V. vulnificus is capable of infecting by two routes. The bacterium can cause wound infections when skin lesions are exposed to contaminated water, such as during recreational swimming or fishing (120, 121). These infections may progress to necrotizing fasciitis and septicemia (122). Much like *V. parahaemolyticus*, *V. vulnificus* also infects via an oral route when consumed in contaminated shellfish (123, 124). While transmission routes have thus been well studies in aquatic eel systems, transmission among humans has not been studied, as the terrestrial mammal is generally agreed to be an accidental and/or dead-end host.

While infections may occur via either the skin or i.g. route, two-thirds of septic *V. vulnificus* cases arise from foodborne infection. Moreover, fatality rates of foodborne infection exceed that of wound infection by 2-3 fold, likely because of the frequent development of sepsis (103, 105). Foodborne *V. vulnificus* infections are characterized by rapid disease progression. Time from hospitalization to death averages four to five days, though in some cases is less than 24 hours (116, 125-127). Disease appears to develop in successive stages characterized by: (i)

bacterial survival and/or outgrowth in the intestine; (ii) intestinal damage leading to systemic bacterial spread; and (iii) septic shock.

Ingested bacteria quickly outgrow in the gastrointestinal tract. In laboratory mouse models, the inoculated population steadily multiplies between 12 and 22 hours post-infection (hpi) (1). In a subset of clinically presenting cases, infection is restricted to the gut and bacteria are detectable only in the gastrointestinal tract or feces. Associated symptoms include diarrhea, abdominal pain, or vomiting. It has been speculated that *V. vulnificus* gastroenteritis is underreported, given that those with mild cases may not seek treatment (128). Still, gut-exclusive infections are in the vast minority of clinical presentation – on the order of five to eleven percent of total *V. vulnificus* cases (116, 122, 129, 130).

In the gut, *V. vulnificus* is capable of inducing fulminant necrotic damage and inflammation, as demonstrated in the small intestine of autopsied human patients (131) and experimentally infected mice (1, 132-134). *V. vulnificus* compromises the barrier that normally separates the intestinal lumen and its contents from bodily tissues. Such damage is thought to allow bacteria to flood from the gut to the bloodstream (135). In patients, intestinal damage is most frequently observed in the distal small intestine, specifically the ileum (131). At 16 hpi, orally inoculated mice have bacterial loads that are highest in the ileum compared to other intestinal subsections (134). Subsequently, *V. vulnificus* is capable of disseminating to the bloodstream following its injection into mouse ligated ileal loops (135-137). Together these data suggest the ileum is the primary site of bacterial egress from the intestine to the bloodstream.

The majority of clinical *V. vulnificus* patients present with primary septicemia, wherein bacteria can be cultured from blood samples (122). It is this systemic spread of bacteria that

distinguishes *V. vulnificus* from other vibrioses, both in the laboratory (137), and in the clinic (116). In mouse models, detection of viable bacteria in the spleen or liver correlates with lethal infection outcomes (138, 139).

V. vulnificus primary septicemia is associated with symptoms including fever, chills, hypotension, and change of mental status (122). In addition, *V. vulnificus* infection induces inflammatory cytokine production in mice (140), cells (141-143), and patients (144). On the whole, septic bacterial infections are notoriously difficult to treat regardless of the causative agent. Antibiotic efficacy is low and the body's inflammatory response challenging to combat. Thus in a high proportion of cases, sepsis culminates in lethal multi-organ failure (145-148). The same poor clinical outcomes generally associated with sepsis are likewise observed with septicemic *V. vulnificus* infections, for which the case fatality rate exceeds 50 percent (122).

Pre-disposing conditions

An association between *V. vulnificus* infection and pre-existing liver diseases has been well documented in individual case studies and retrospective analyses (105, 121, 122, 131, 149-156). Analyses of more than 1200 cases by Menon, et al. in 2013 concluded that individuals with liver disease are more likely to develop septic infections when exposed to *V. vulnificus* via contaminated food (103, 122). A diversity of diseases, including hepatitis infection, chronic alcoholism, and non-alcoholic fatty liver disease, can lead to the liver cirrhosis (scarring) and dysfunction that predisposes patients to bacterial infection, including infections by *V. vulnificus* (157).

The liver plays a key role in regulation of iron homeostasis, and liver dysfunction is associated with hemochromatosis (elevated circulating iron levels/iron overload) in up to 30

percent of patients (158, 159). Hematological disorders not arising from liver cirrhosis, specifically transient or hereditary hemochromatosis, are also identified as risk factors for bacterial infections, including *V. vulnificus* infection (103, 160-162). Survival of *V. vulnificus* in patient blood samples is positively correlated with serum ferritin levels (163), and iron overload in mice facilitates *V. vulnificus* outgrowth and depresses phagocytic clearance (164). Conversely, the iron-regulatory hormone hepcidin mediates resistance to Gram-negative bacteria, including *V. vulnificus,* by sequestering iron (165-167). Together, these data indicate that diverse physiological conditions leading to iron overload put individuals at increased risk of contracting severe *V. vulnificus* infections.

In addition to its role in iron homeostasis, the liver is likewise critically important for first-line clearance of microbes that transit the intestinal epithelial barrier or otherwise enter systemic circulation (168-171). Indeed, 90 percent of the fixed and circulating phagocytic cells that comprise the reticuloendothelial system (RES) are located in the liver (172). Patients with chronic liver disease demonstrate impaired bacterial clearance from the circulation and dysregulated cytokine response to microbes (173, 174). As such, bloodborne infections are both more common and more severe in patients with liver cirrhosis (175, 176). Consistent with these observations, neutrophils isolated from patients with chronic liver disease are less active against *V. vulnificus*, which exhibits significantly higher survival in the blood of diseased individuals compared to control (163). The predisposition of patients with liver disease to lethal *V. vulnificus* infection is likely due not only to increased iron loads, but also to impaired immune clearance in these individuals.

Though both liver and hematological diseases are identified as pre-disposing conditions of septic *V. vulnificus* infection, neither is an absolute risk factor. In a 1997 memo to the US Food and Drug Administration (FDA), Karl Klontz estimated that up to seven percent of the US adult population – that is, approximately 21 million people - are susceptible to infection (177). This is a generous estimate, including a wide range of putatively pre-disposing conditions and giving each the same relative risk weight. Nonetheless, the World Health Organization (WHO) highlights the inconsistency between the actual number of *V. vulnificus* cases and the number of *V. vulnificus*-exposed individuals, estimating that "less than one illness occurs per 10,000 meals of raw Gulf oysters served to the highest risk population, people with liver diseases" (177). Thus, there appears to be a relatively low attack rate on susceptible populations consuming seafood contaminated with *V. vulnificus* (177).

Conversely, neither liver disease nor hematological disorder is a necessary prerequisite to *V. vulnificus* infection. According to the 2013 analysis by Menon, et al. (103), only 40 percent of *V. vulnificus* patients have liver disease and less than 10 percent report hematological disease. Approximately 20 percent of total *V. vulnificus*-infected patients report no predisposing conditions at all (103). Estimates on the number of truly 'healthy individuals' that contract *V. vulnificus* infections decrease to five percent when considering cases of primary sepsis (122) (177). Nonetheless, the data suggest that *V. vulnificus* can infect individuals without pre-existing conditions.

The act of correlating risk factors and infection incidence often requires assumptions of homogeneity among populations. First, many analyses – e.g. the 2005 analyses by WHO – assume that all persons with a given condition (e.g. liver disease) are at equivalently increased

risk of infection (177). While other reports do adjust for variables including age, sex, and number of co-occurring disease conditions (103), there doubtless remains heterogeneity among populations with any identified risk factor.

Moreover, susceptibility analyses inherently assume homogeneity of the infecting bacterial population. However, the diversity of *V. vulnificus* isolates and their differing virulence potential (139) clearly indicate strain and isolate heterogeneity. Lethal potential is not predicted by a strain's "clinical" or "environmental" origin (178). Thus, the study of virulence determinants in *V. vulnificus* is an active area of investigation in the field, and one that is addressed in this study.

Experimental Models of Pathogenesis

Human studies Numerous bacterial diseases, including cholera infections by *V. cholerae,* are studied in controlled clinical trials. Such experiments provide human-specific insights into pathogenesis and treatment options. However, the high morbidity and mortality associated with *V. vulnificus*, coupled with a lack of treatment efficacy, render this method untenable for *V. vulnificus* studies. Therefore volunteer trials are not conducted for this organism.

Mouse models The first experimental animal studies of a novel lactose-positive *Vibrio* species (aka *Beneckea vulnifica* (179, 180), eventually *V. vulnificus* (181-184)) were published by Poole and Oliver in 1978 (137). Given the multiple clinically suspected infection routes, Poole and Oliver employed a variety of mouse models for *V. vulnificus* study: subcutaneous (s.c.) injection to mimic wound infection; intragastric (i.g.) inoculation to mimic gastrointestinal infection; and intraperitoneal (i.p.) and intravenous (i.v.) injections to simulate the systemic bacteremia that can result from either route of exposure (137). Due to the severe nature of human

V. vulnificus infections, virulence is most commonly monitored using death as an endpoint. In that way, genetic or treatment modifications that reduce lethality are quantified. In all the virulence models, it is assumed that mice ultimately die of multi-organ failure in a manner similar to humans. The cytokine induction reminiscent of sepsis has recently been profiled (140). However, there have not been post-mortem studies to confirm and/or parse the failure of specific organs upon *V. vulnificus* challenge and, as such, some elements of the physiological response to lethal *V. vulnificus* challenge in mice remain uncharacterized.

Each of the initial models – s.c., i.g., i.p., and i.v. – has persisted over the subsequent 40 years of *V. vulnificus* study, though with some modifications. While Poole and Oliver found *V. vulnificus* to be avirulent in adult mice exposed to the bacteria i.g. (137), reports of foodborne human disease have continually indicated that humans acquire *V. vulnificus* infections by ingestion (101). This discrepancy was first circumvented in 1984 using infant mice (185). Use of these immunologically immature animals continues today (135, 136, 186, 187). Subsequent work has adapted adult mouse models to render animals more susceptible to infection by either generalized immunosuppression (164, 178) or neutropenia (132). In contrast to i.g. infection models in other bacterial studies, antibiotic pre-treatment is generally not used. As such, these studies are conducted in the presence of the normal gut microflora.

Clinical data support that boht liver cirrhosis and hereditary hemochromatosis predispose individuals to lethal *V. vulnificus* infections. Both of these conditions are associated with elevated serum iron levels. Hence some pathogenesis research uses iron dextran pre-treatment to raise serum iron concentration in mice. Indeed, a study in 1981 demonstrated that iron overloaded mice are more susceptible to *V. vulnificus* (188). This conclusion became more

generalizable when a panel of 24 *V. vulnificus* isolates was tested in 1992 (178). Iron overload is now commonly used as a precursor to infection via i.g., i.p, and s.c. routes (11, 164, 187).

Iron administration in mice is optimal for mimicking transient hemochromatosis, such as that which occurs in patients having received blood transfusion (161). However, there remain differences between transient and chronic iron hemochromatosis. Notably, there currently exists a mouse model of genetic hemochromatosis which likely better recapitulates the multiple facets of chronic iron overload (189), but this mouse line has yet to be paired with *V. vulnificus* infection for study of pathogenesis.

Multiple approaches have attempted to mimic the multifaceted nature of liver dysfunction that characterizes many clinical cases of *V. vulnificus* (103, 183). Liver disorder was induced in mice by bile duct ligation, but these animals did not demonstrate increased susceptibility to disease (138). In contrast, a mouse model of liver cirrhosis induced by carbon tetrachloride injection does demonstrate increased mortality upon *V. vulnificus* infection (190).

However, administration of iron remains the most frequent modification to adult mouse models. The disadvantage of iron overload is a considerably accelerated infection course compared to iron-normal mice (11, 188). In addition, iron overload exacerbates the occasional lung contamination that occurs in *Vibrio* i.g. infection models (191), leading to bacterial outgrowth in the lung and death due to off-target pneumonic infection (Satchell lab, unpublished). Based on models for *V. cholerae* colonization in adult mice (192), our laboratory developed an adult mouse model of *V. vulnificus* infection that uses a combination of anesthetic pre-treatment (ketamine-xylazine) and stomach acid neutralization (sodium bicarbonante, $NaHCO_3$) to facilitate intestinal colonization (1, 35, 193). While the exact mechanisms of this

model's efficacy have not been determined, it is thought to be due to the combination of decreased acid stress ($NaHCO_3$) and transiently altered inflammatory response (ketamine) (194). This is the model employed in the current study, and its details are reported in Chapter 7 – Materials and Methods.

Other mammalian models *V. cholerae* researchers developed a model using ligated ileal loops of rabbits to examine the pathogenic effects of bacteria inoculated in a discrete intestinal segment (195). This method has since been modified to study *V. vulnificus* dissemination and lethality in rats, rabbits, and mice (136, 137, 187, 196).

Fish models A subset of *V. vulnificus* strains are capable of causing disease in eels owing to the presence of a plasmid that confers resistance to the bactericidal effects of fish serum (197). Pathogenesis in eels is studied using numerous models of infection, including exposure by patch contact, eel-eel contact, cohousing, bath challenge, i.g. inoculation, or direct injection (198, 199).

***C. elegans* model** *Caenorhabditis elegans* has been employed to study various host-pathogen interactions (summarized in (200)). Oral infection of *C. elegans* with *V. vulnificus* led to intestinal distension and death that was attenuated when known virulence genes were disrupted (200), suggesting that virulence determinants are shared between the *C. elegans* and mouse models. Studies using fluorescently tagged bacteria have since demonstrated with both *Escherichia coli* and *V. vulnificus* that live and dead microbes are not distinguishable by fluorescence intensity in the *C. elegans* gut (201). Therefore, future studies using this model must use an alternative method, such as plating for colony forming units (CFU), to make conclusions about *V. vulnificus* colonization ability.

Virulence determinants in *Vibrio vulnificus*

Virulence factors are generally defined as elements that "help bacteria to (i) invade, (ii) cause disease, and (iii) evade host defenses" (202). Because most *V. vulnificus* studies are designed to study lethal infection course, *V. vulnificus* virulence factors are further characterized by their contribution to lethal disease outcomes in model organisms. Multiple genes falling into these categories are implicated in *V. vulnificus* virulence. The majority of studies have used genetic manipulation to demonstrate necessity and/or sufficiency of specific genes.

Resistance to host

As many *V. vulnificus* infections are acquired gastrointestinally, resistance to acid stress in the stomach likely influences bacterial survival in the host. In *V. vulnificus*, low pH environments lead to increased bacterial superoxide levels (105, 203). Bacterial manganese superoxide dismutase (SOD) is used to neutralize acidic environments. Accordingly, mutations in *V. vulnificus sod* genes lead to increased pH sensitivity (203), and *sod* mutants have increased median lethal dose ($LD_{50,}$ (204)) in mouse models of infection (205).

The *cadBA* operon, which encodes a lysine/cadaverin antiporter and lysine decarboxylase, is also important for *V. vulnificus* acid tolerance *in vitro* (206). Interestingly, the role of *cadBA* is not obvious when bacteria are exposed to pH 4.4 immediately following growth at neutral pH (7.6). However, conditioning bacteria by pre-exposure to pH 5.8 before exposure to pH 4.4 improves survival dependent upon *cadBA* (206). According to the conclusions of Rhee, et al. (206), "it is apparent that the contribution of the *cadBA* genes for the acid tolerance of *V. vulnificus* is substantial, but dependent on prior exposure to acidic pH." Neutralization of animal stomach acid with $NaHCO_3$ is integral to some current mouse models of i.g. *V. vulnificus*

infection. This indicates that *V. vulnificus* grown in standard culture media, e.g. Luria Burtani (LB) broth, are not primed to resist the acidic stomach environment (1, 35, 193). However, these and other results on bacterial survival in the presence of oxidative stress indicate that conditions including low pH (206) or nutrient limitation (207), may prime *V. vulnificus* to deal with subsequent stressors. Environmentally stress-primed *V. vulnificus* that encounter the human host are therefore likely to exhibit conditionally increased virulence potential (206).

Evasion of the host immune response is an additional requirement of bacterial pathogenesis. The capsular polysaccharide (CPS) of *V. vulnificus* confers resistance to complement opsonization, reducing phagocytosis by host immune cells (208) and thereby contributing significantly to virulence potential in mice (208-210). In fact, according to Jones and Oliver (105), "expression of CPS is one of the few known virulence factors of *V. vulnificus* that is recognized to be absolutely required for pathogenicity."

Motility and adhesion

V. vulnificus expresses a polar flagellum that is integral to swimming motility (196). The *flg* operon encodes the *Vibrio* polar flagellum and its basal apparatus (34, 211). Disruption of the *flg* operon, both by transposon insertion and directed mutation, has resulted in decreased bacterial bloodstream invasion and decreased virulence in mouse models (196, 212, 213). Jones and Oliver point out that studies on the *flg* operons suffered from polar mutations and lack of successful complementation (105). Even if taken at face value, however, it remains unclear whether *flg*-mediated virulence phenotypes arise from motility itself, from attachment apparently mediated by *flg* components, or from the inflammation induced by immune recognition of bacterial flagellin.

A role for attachment in virulence is supported by Type IV pilin-associated phenotypes. Disruption of *pilA* (encoding a pilin subunit) or *pilD* (encoding a pre-pilin peptidase) leads to defective bacterial attachment *in vitro* and increased LD_{50} *in vivo* (214, 215). Mutants in the tight adherence (*tad*) genes encoding fibrils, or Flp pili, have recently been shown to have defective oyster colonization (90). The effect of Flp pili on mammalian pathogenesis, however, has not yet been tested. Mutants in the gene for outer membrane protein OmpU, which binds fibronectin in the mammalian extracellular matrix, demonstrate decreased attachment, cytotoxicity, and virulence compared to parent strains (216). Together these studies suggest that bacterial attachment to host cells is critical for cytotoxicity and bacterial virulence.

Iron acquisition

The importance of iron availability during *V. vulnificus* infection is highlighted by the correlations between liver disease/hemochromatosis and septic *V. vulnificus* infection, as discussed above in the section "Pre-disposing conditions" (103). Transcriptional responses of *V. vulnificus* to varied iron concentrations revealed global gene expression profiles involved in iron acquisition (217). The *V. vulnificus* chatechol siderophore, vulnibactin, and its receptor are required for full virulence in mice, while heme does not appear to be a vital iron source during infection (217-221). The TonB system, which actively transports iron-bound substrates across the outer membrane of Gram-negative bacteria, is also important for *V. vulnificus* pathogenesis (217). However, whether this is due directly to its role in iron acquisition, or indirectly to its regulation of virulence-related genes including flagella and secreted toxin remains to be de-convoluted (187).

Secreted factors

Bacteria encode a diverse array of secretion systems for export of proteins from the bacteria cytosol to either the extracellular space or directly into targeted cells. Thus far, six systems for secretion from Gram-negative bacteria have been characterized (222). Unlike many pathogenic bacteria, *V. vulnificus* does not possess complete loci for Type 3 or Type 4 secretion systems (T3SS, T4SS, respectively). However, the Type 1, Type 2, and Type 6 secretion systems have been functionally characterized in *V. vulnificus,* and secrete important virulence factors.

The *V. vulnificus* Type 6 secretion system (T6SS) encodes a molecular syringe that can deliver proteins from the bacteria to targeted bacterial or eukaryotic cells (222). The T6SS is important for intra-specific bacterial competition in *V. cholerae*, where it contributes to increased fitness by killing neighboring bacteria and facilitating horizontal gene transfer (223, 224). Although less well characterized, the *V. vulnificus* T6SS is also anti-bacterial and likely contributes to *V. vulnificus* population dynamics in the environment (225). The T6SS of related *V. cholerae* acts as an important modulator of host processes (226, 227). However, disruption of the T6SS in *V. vulnificus* does not alter infection outcomes in a mouse model, so it is thus far unclear whether *V. vulnificus* T6SS targets eukaryotic host cells (225).

V. vulnificus encodes structurally characterized components of a Type 2 secretion system (T2SS) (228, 229). Mutations in the T2SS significantly reduce overall protein secretion from *V. vulnificus* (230). T2SS disruption also significantly improves survival of *V. vulnificus* infected mice (230). A recent transposon mutagenesis screen suggests that the T2SS is important for *V. vulnificus* survival and proliferation in serum (231).

Two of the best-characterized T2SS products are the hemolysin VvhA and the metalloprotease VvpE (230). The 51-kD VvhA hemolysin/cytolysin encoded by *vvhA* is toxic to eukaryotic cells, and its activity against erythrocytes is thought to liberate iron for bacterial benefit (232, 233). Indeed, it is repressed under iron-rich conditions (234). Interestingly, however, *vvhA* mutants do not exhibit virulence defects when mice are inoculated i.p., (232). In addition to its lytic activities, VvhA promotes autophagic flux, reactive oxygen species (ROS) production, mitochondrial damage, and caspase3/7-dependent death in epithelial cells (235, 236). Relatedly, its actions are linked to increased intestinal epithelial permeability and damage (1, 236). Virulence defects are exhibited when *vvhA* mutants are inoculated i.g., suggesting that its activity on the intestinal epithelia may be more salient to its role during infection compared to its activity against erythrocytes.

The metalloprotease VvpE, which has a broad substrate range, causes severe phenotypes when injected to mice in its purified form (237, 238). Reports for a virulence role of VvpE have been conflicting, however. Multiple groups, each using i.p. injection of mice, have reported that *vvpE* is not required for virulence (239, 240). More recently, it was reported that mice infected i.g. with a *vvpE* mutant exhibited increased survival. As with *vvhA*, this emphasizes the role of VvpE in acting at the intestinal barrier to influence bacterial dissemination from the gut. Indeed, VvpE inhibits expression of mucin from intestinal goblet cells and disrupts intestinal tight junction integrity (241, 242). Relatedly, the mucin-binding protein GbpA was recently shown to promote bacterial virulence in i.g. infected mice (243).

Finally, *V. vulnificus* encodes a functional T1SS at the *rtx* locus. T1SS are fairly specific, and translocate only one or a few substrates (222). The *V. vulnificus rtx* locus also includes an

rtxA1 gene homologous to that originally discovered in *V. cholerae* (136, 244, 245), the product of which is the Multifunctional Autoprocessing Repeats-in-Toxins (MARTX) toxin (described in detail below). *rtxA1* has been linked to multiple forms of cell death including necrosis and apoptosis (246, 247). The importance of *vvhA* and *rtxA1* in virulence has been demonstrated across multiple infection models (136, 245, 248, 249). Compared to VvhA, however, RtxA1 exerts the dominant virulence role during i.g. infection and is considered the primary secreted virulence factor of *V. vulnificus* (1, 105).

Notably, reports that *rtxA1*-dependent cytotoxicity requires cell-cell contact implies that cytotoxicity and virulence phenotypes observed with adhesion-related genes, including *pil, flg,* and *omp*, are likely related to decreased MARTX toxin delivery (212, 214, 216). Moreover, there may be overlapping regulatory effects. For example, *tonB* mutants are defective in iron transport and motility. However, they also have decreased *rtxA1* expression (187). In the future, the contributions of each function could be tested using a variety of double mutants in the *pil, flg, omp,* and *rtxA1* loci. Still, these reports indicate an important role for *rtxA1* and its MARTX gene product in dictating *V. vulnificus* virulence potential during i.g. infection.

MARTX toxins

Introduction

Bacteria have evolved not only to exist in diverse habitats, but also to manipulate their respective niches to support microbial outcomes. For microorganisms that associate with single or multicellular hosts, the ability to deliver "effectors" to the eukaryotic cell cytosol is integral to strategic modulation of the environment. Bacterial effector delivery is typically accomplished in

one of two ways. In one method, a complex secretion machinery is expressed on the bacterial envelope through which a diverse array of protein cargos are delivered directly to host cell cytosol. This strategy is exemplified by T3SS, which deliver bacterial effector proteins across eukaryotic cell membranes through a bacterial injection needle complex (222). In the well-studied case of *Salmonella*, one system (T3SS1) facilitates bacterial invasion across the intestinal epithelial barrier and entry into host cells. A second system (T3SS2), helps establish the intracellular replication niche of the *Salmonella* containing vacuole by delivering bacterial effectors across the macrophage phagosomal membrane (250). T4SS, like T3SS, utilize a large protein complex that spans – in the case of Gram-negative bacteria – both bacterial membranes and the target host membrane (222). The *Legionella pneumophila* T4SS delivers >200 effector molecules across the endosomal membrane to manipulate macrophages for survival of the bacterium within the cell (251). Finally, T6SS deliver effectors to target cells by an injection strategy (222). For example, an actin crosslinking effector delivered by *V. cholerae* induces inflammation and accelerates gut motility to displace resident microbes and create an intestinal environment that favors *V. cholerae* (8, 226).

Alternatively, effectors can be delivered as extracellularly secreted toxins, where an "A" component is a single effector protein that bears an activity and the "B" component is important for binding the target cell and delivering the effector. The A and B components can be separate secreted proteins or distinct functional domains of a single protein. This strategy allows for a bacterial effector to be transported into the target cell without necessitating direct cytosolic injection. In some cases, several effector proteins share the same B component. The functional results of A-B toxins are similar to effectors of direct injection systems in that they often

modulate cell biological pathways. However, toxins are most frequently limited to a single effector or effector domain activity (252).

A unique hybrid of the two described approaches is the effector delivery mechanism of MARTX toxins. Almost exclusively expressed from organisms lacking T3SS or T4SS, MARTX toxins encompass all necessary components for both effector activity and delivery within a large, singular, extracellularly-secreted polypeptide. This single protein comprises the entire translocation machinery. However, more like direct injection systems, MARTX toxins can deliver not just one, but multiple cytopathic bacterial effectors to target host cells. Further, via horizontal gene acquisition and genetic recombination, diverse combinations of effector domains can arise within the single polypeptide. Thus, MARTX toxins are multifunctional translocation machinery, processing machinery, and bacterial effector cargo (2, 13, 253).

Similar to other effector delivery systems, MARTX toxins are key factors in the pathogenesis of numerous organisms. MARTX toxins act as accessory toxins during *V. cholerae* infections, supporting bacterial colonization of the intestine (192). During host infections with the pathogen *V. vulnificus*, MARTX toxins act as the primary virulence factor facilitating initial colonization, dissemination, and lethality in mammals and eels (1, 11, 197, 254). The fish pathogen *V. anguillarum* has also been shown to induce lethal infections in salmon dependent upon a MARTX toxin (255). Thus, MARTX toxins contribute significantly to disruption of human and aquatic health.

rtxA1 regulation

The histone-like nucleoid structuring (H-NS) protein that has predicted binding sites throughout the *rtxA1* gene (248, 256-258). Expression of the *rtxA1* gene in *V. vulnificus* is

positively regulated by HlyU, which acts as an antirepressor of H-NS. A comparable paradigm has been demonstrated for the regulation of *rtxA1* in *V. anguillarum* (259, 260). HlyU, in turn, is regulated by the quorum sensing regulator SmcR, a homolog of the regulator LuxR from *V. harveyi* (258).

Expression of *rtxA1,* as well as a portion of its secretion system, is up-regulated in response to eukaryotic cell exposure *in vitro* (136, 254, 261). This result is consistent with data that *rtxA1* is up-regulated during *in vivo* mouse infection (140).

MARTX toxin production and secretion

MARTX toxin *rtx* gene loci are present across multiple bacterial genera including *Aeromonas, Photorhabdus, Proteus, Vibrio,* and *Xenorhabdus,* and are best characterized in the *Vibrio* species *V. cholerae, V. vulnificus,* and *V. anguillarum* (Table 1.1). Each *rtx* locus consists of two divergently transcribed operons: *rtxHCA* and *rtxBDE* (244, 245, 255, 262). The first gene in the operon, *rtxH,* encodes a conserved hypothetical protein of as-yet unexplored function. The adjacent *rtxC* gene encodes for a putative acyltransferase (244). Fatty acid post-translational modification by homologous acyltransferases is a well-established mechanism of activation among other members of the repeats-in-toxins (RTX) toxin family (263, 264). Yet, the contribution of *rtxC* to MARTX-associated virulence is still debatable and the gene does not appear to be essential for cytotoxicity (248, 265, 266). Further, MARTX toxin acylation has not yet been reported. The last gene in the operon, *rtxA* (sometimes designated *rtxA1),* encodes the MARTX toxin itself. The *rtxA* open reading frame (ORF) can exceed 15 kilobases in the case of some toxin variants (2). An *rtxA* ORF is often the largest gene in the entire bacterial genome.

Table 1.1. Distribution of *rtxA* loci among bacterial species as of 2015

Cause disease in humans	**Cause disease in aquatic animals**	**Associate with insects or nematodes**	**Associate with aquatic animls**
Aeromonas hydrophila[2]	*Aeromonas hydrophila*[2] (fish)	*Photorhabdus asymbiotica*	*Vibrio caribbenthicus* (coral)
Proteus mirabilus	*Moritella viscosa* (fish)	*Photorhabdus luminescens*	*Vibrio nigripulchritudo* (shrimp)
Vibrio cholerae	*Vibrio anguillarum* (fish)	*Photorhabdus temperata*	*Vibrio splendidus* (seawater)
Vibrio vulnificus	*Vibrio ordalli* (fish)	*Xenorhabdus bovenii*	
	Vibrio vulnificus BT2 (eels)	*Xenorhabdus doucetiae*	
		Xenorhabdus nematophila	
		Xenorhabdus poinarii	

[1]Alphabetical list limited to MARTX toxins previously annotated (2, 13) or newly identified by TBLASTN search of 1544 representative or 3976 complete genomes deposited at National Center for Biotechnology Information (http://www.ncbi.nlm.nih.gov/) using *V. cholerae* MARTX toxin sequence without effector domains as query.
[2]Although early genomics supported that human clinical isolates lack the *rtxA* gene (17), a TBLASTN search of deposited draft genomes identified *rtxA* in at least 12 human clinical samples (unpublished) and four isolates from fish (20). Analyses conducted by Karla Satchell.

The genes in the adjacent *rtxBDE* operon are inverted relative to the *rtxHCA* operon (244). These genes, in cooperation with the unlinked *tolC* gene, form a dedicated MARTX toxin type 1 secretion system (T1SS) (Figure 1.1) (262, 267). In a manner analogous to the *hly*-encoded hemolysin secretion system of *E. coli,* RtxD is the presumed transmembrane protein linking with the outer membrane porin TolC to form a narrow "chunnel" through which each MARTX toxin is secreted. Unfolded protein is secreted directly from bacterial cytoplasm to extracellular environment without a periplasmic intermediate (268). Again similar to *E. coli* hemolysin, MARTX toxin secretion is energized by ATPases peripherally associated with the

inner membrane (Figure 1.1) (269). Atypically, the MARTX toxin secretion system requires two different ATPase proteins, RtxB and RtxE (254, 262). Both ATPases are essential for secretion and are proposed to work as a heterodimer, although the functional consequence of this unusual T1SS is not known (262)

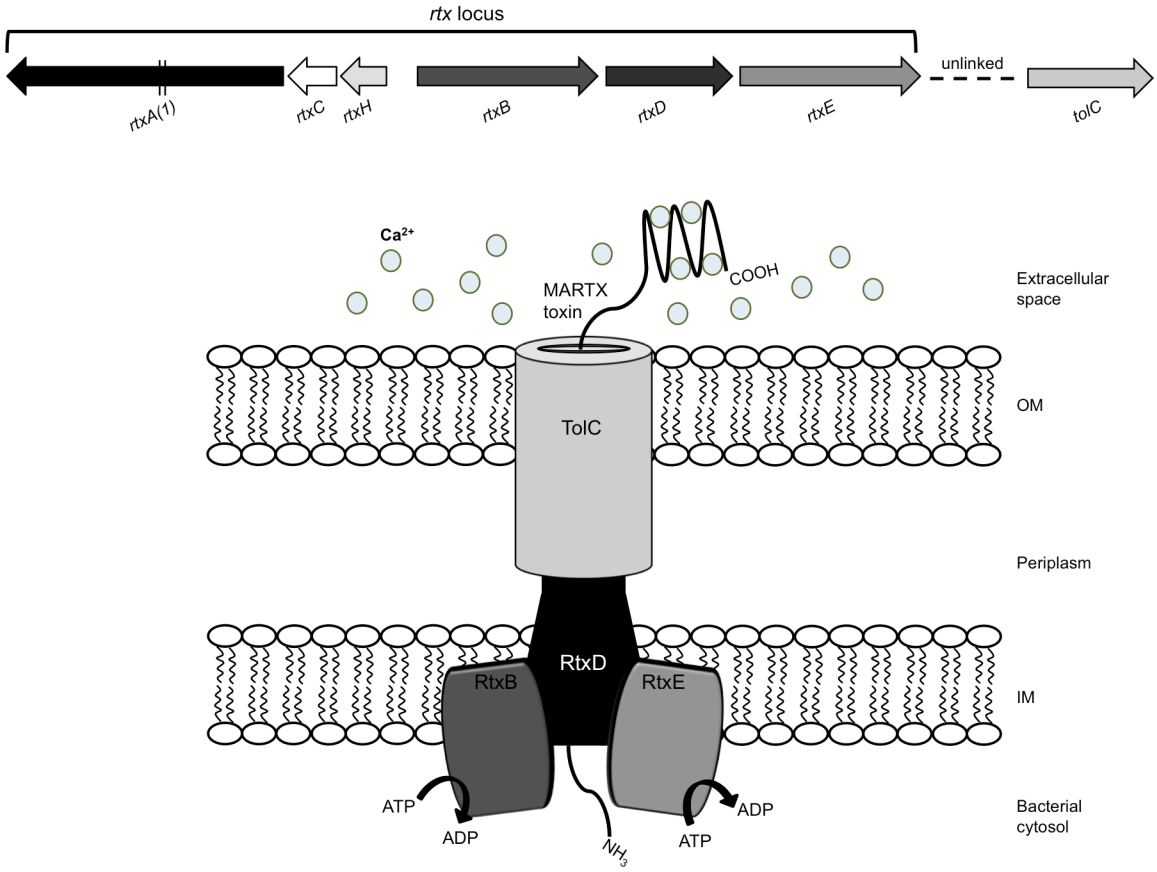

Figure 1.1. **Expression at the rtx gene locus leads to MARTX toxin secretion.** Expression of the *rtxBDE* operon and unlinked *tolC* genes results in formation of a T1SS 'chunnel' spanning the bacterial inner and outer membranes. The MARTX toxin, product of the *rtxA* (or *rtxA1*) gene, is secreted from bacterium to extracellular space without a periplasmic intermediate. Secretion requires calcium (Ca^{2+}), which likely participates in the folding of the RTX-like tandem aa repeats present in the MARTX C-terminus.

Secreted MARTX toxin-associated activity can be detected from supernatant fluids (3, 6, 30, 254, 255). This indicates that portions of the toxin can fold, at least transiently, in the extracellular space. However, observable toxin activity is short-lived due to degradation by secreted proteases (132, 270) and induction of toxin autoprocessing by bacterial culture media (246, 271). Moreover, *rtxA*-induced cytotoxicity requires contact between *V. vulnificus* and target cells (136, 261). This is somewhat surprising for a secreted virulence factor, and is likely observed for two reasons. First, *rtxA1* expression is induced by host cell exposure. Second, the relative instability of supernatant-borne MARTX toxins suggests that only freshly synthesized toxin is successfully delivered to host cells. This precedent has been demonstrated for adenylate cyclase (AC) toxin, an RTX toxin family member from *Bordetella pertussis.* In that case, bacterial-host proximity facilitates the delivery of freshly synthesized product from bacteria to target cells (272).

AC toxin is also captured in bacterial outer membrane vesicles (OMVs) (273). The MARTX toxin secreted by *V. cholerae* is stabilized by association with outer membranes and with OMVs. However this does not appear to be a universal phenomenon, as the same association between MARTX toxin and OMVs has not been observed with *V. vulnificus* (270, 274).

MARTX toxin domain organization

MARTX toxins, once expressed, are massive proteins with deduced primary sequences from 3500-5300 aa. The toxins are comprised of four distinct regions: the N-terminal arm, the effector domains, the cysteine protease domain (CPD), and the C-terminal arm (Figure 1.2). They are classified as members of the broader RTX protein family by virtue of characteristic

RTX tandem amino acid (aa) repeat sequences in the C-terminus (Figure 1.2). However, it is the presence of the N-terminal arm and the CPD that further define the core structures essential to be designated within the MARTX toxin subfamily (275).

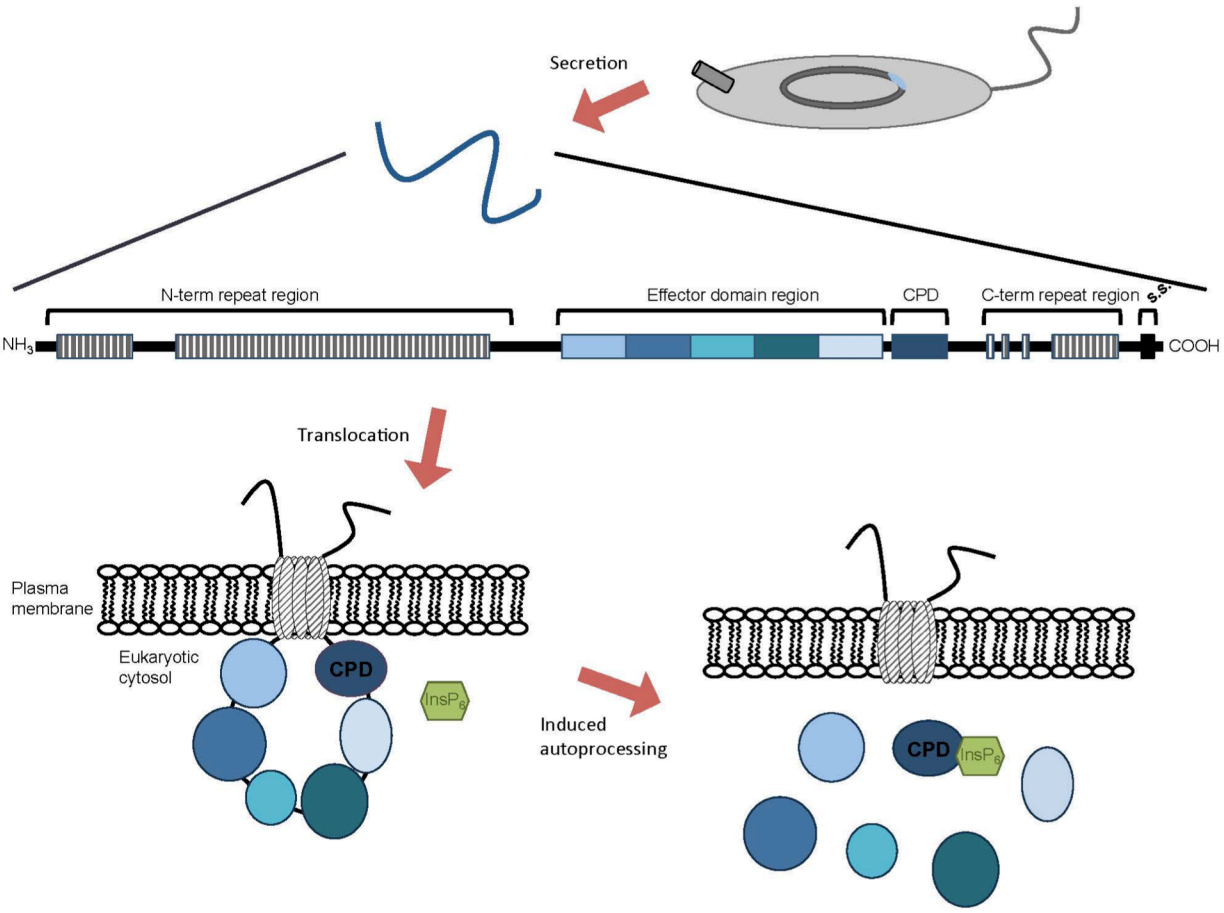

Figure 1.2. MARTX toxins deliver effector domains to target cell cytosol. MARTX toxins exhibit modular organization with characteristic N- and C-terminal repeat regions flanking a central core consisting of the CPD and arrayed effector domains. Following toxin expression and secretion from a bacterium, MARTX repeat regions facilitate pore formation in target cell membranes. Once translocated through the repeat region pore, the CPD is activated for autoproteolysis by inositol hexakisphosphate (InsP6). Cleavage at susceptible leucine converts the MARTX effector domain cargo to finite bacterial effectors in the eukaryotic cytosol.

The C-terminal region of a MARTX toxin harbors the repeats that classify these toxins as RTX famiy members. The C-terminal region is dominated by 15 tandem copies of a "C" repeat sequence. The first nine aa of each C repeat match classical glycine and aspartate-rich RTX sequences known to form a beta-barrel with calcium ions at the turn at the end of each beta strand. Each repeat also contains nine additional aa. Together these two portions comprise an 18-aa non-canonical RTX motif that comprises the C repeat sequence (2, 244).

Downstream of the RTX repeats is a small region of less than 200 aa. A stop codon just 13 aa from the end of the toxin entirely disrupts toxin function in *V. cholerae.* This is consistent with other RTX toxins where the C-terminus carries information for secretion by its designated T1SS (10, 276). MARTX toxin secretion (and, therefore, activity) is calcium dependent. Therefore it is proposed that MARTX C-repeats, similar to RTX calcium binding repeats, remain unstructured in the relatively low-calcium bacterial cytosol and fold upon reaching the calcium-rich extracellular environment (Figure 1.2) (30, 246). This transition might drive MARTX toxin export from C- to N- terminus by a calcium-dependent molecular ratchet mechanism, as has been shown for other RTX toxins (277-280).

Distinguishing MARTX toxins from all other RTX family proteins is the presence of conserved repeat sequences at the N-terminus of the protein (Figure 1.2). The ~1960 aa N-terminus is dominated by a total of 52 aa repeats sequences that fall into two groups: 14 copies of the 19-aa "A" repeats and 38 copies of the 20-aa "B" repeats. While still glycine-rich, these are not classified as RTX repeats and – lacking aspartate residues in key positions – are not thought to bind calcium ions. Nonetheless, each is predicted to form a beta-barrel structure consistent with a function in pore formation (2, 13).

The *V. vulnificus* MARTX causes necrotic cytotoxicity (30, 246). However, some MARTX toxins – such as that from *V. cholerae* – induce cytopathic effects in the absence of cell lysis (6, 255). While the pore-forming repeat regions of the MARTX toxins from *V. vulnificus* and from *V. cholerae*, for example, are identical in size and 93% identical in aa sequence, only the toxin from *V. vulnificus* induces cell lysis (3, 30). Though thus far unexplained, functional variances between MARTX toxins of different bacterial species may reflect differences in pore structure. Alternatively, *V. vulnificus* may simply produce much more toxin due to gene induction in the presence of cells (136, 254).

MARTX toxin effector delivery

Whether or not the toxin causes cell lysis, the Ca^{2+}-bound, folded MARTX repeat regions somehow form a pore in the target cell membrane. The MARTX repeat pore facilitates translocation of the central effector domain region (3). Very little is known about the mechanistic process of effector domain translocation. The membrane pore has been estimated at 1.63 nm (136). This diameter implies that the central MARTX toxin region must travel through the pore in an unfolded state. Thermodynamic studies of the central effector domain region suggests that natural structural instability – that is, the relatively easy transition between folded and unfolded state – allows for their translocation across the eukaryotic membrane (281, 282). Moreover, it has been suggested that a more stable folded state is possible in the eukaryotic cytosol compared to the extracellular space. As such, the energetic drive toward stability may provide impetus for effector domain translocation from extracellular space to cytosol (279, 281).

Within the translocated central portion of all MARTX toxins is the CPD that confers toxin autoprocessing activity (Figure 1.2) (283). After its translocation, this domain is activated

in the cell cytosol by the eukaryotic-specific small molecule inositol hexakisphosphate (InsP6). Upon activation, the CPD proteolytically cleaves the MARTX toxin at susceptible leucine residues. Cleavage releases discrete portions of the MARTX toxin into the target cell cytosol (271, 282, 284, 285). This CPD autocleavage is essential for full activity of the toxin to be observed, likely due to the role of subcellular localization in effector function (3, 283). CPD activity thus converts the large MARTX holotoxin into finite, *bona fide* bacterial effectors in a eukaryotic-specific context.

A unique feature of the MARTX toxins is the variety of observed effector domain compositions. The repeat regions and CPD are highly conserved in size and sequence across a multitude of Gram-negative bacteria. A given MARTX toxin, to current knowledge, delivers only the effectors present in its own polypeptide (i.e. no effectors encoded at other loci have been found to use the MARTX toxin pore as a delivery mechanism). But, the effector domain complement present in MARTX toxins is not always the same. Thus, while MARTX toxins are classified as large single polypeptide toxins, they function as effector delivery platforms (253).

MARTX toxin effector domains

Any singular MARTX toxin possesses a repertoire of one to five of ten defined effectors, organized in a characteristic modular fashion (Figure 1.2) (2, 13). Once translocated and autoprocessed by the CPD, MARTX effectors act on a variety of eukaryotic cellular targets (Table 1.2) via diverse biochemical mechanisms. Effector activity results in modulation of key cellular pathways regulating cellular energy balance, cytoskeletal integrity, and survival/proliferation.

Table 1.2. MARTX toxin effector domains and their characteristics			
Abbreviation	Description	Known characteristics	References
ABH	Alpha-beta hydrolase	PI3P-specific phospholipase Activation of small GTPase CDC42 Inhibits autophagy and endosomal trafficking	(2-4)
ACD	Actin crosslinking domain	Formation of isopeptide linkage between actin monomers resulting in cell rounding, inhibition of phagocytosis, and blocking actin filament elongation	(5-9)
DmX	Domain X (formerly PasyHD1)	Binds ADP ribosylation factors (ARFs) for activation of autoproteolysis	(10-12)
DUF1	Domain of unknown function in the first position	Binds prohibitin, increases prohibitin expression on cell surface	(14)
ExoY	Adenylate cyclase	Conversion of ATP to cyclic AMP similar to *Pseudomonas aeruginosa* ExoY	(11)
MCF	Makes caterpillars floppy-like	Cellular-induced cysteine autoprotease that induces the intrinsic pathway of apoptosis	(15, 16)
PasyHD2	*P. asymbiotica* homology domain 2	Domain of no known function with a predicted lipid raft localization motif	(13, 18, 19)
RID	Rho-inactivation domain	Inactivation of small GTPases by fatty acid acylation of the target's polybasic region; results in cellular actin depolymerization	(3, 21-23)
RRSP	Ras/Rap1 specific peptidase (formerly DUF5)	Site-specific processing of small GTPases Ras and Rap resulting in loss of phospho-ERK, cell rounding, and inhibition of cell proliferation	(26, 27)
VIP2	VIP2-like protein	Putative ADP-ribosylating activity with homology to *Bacillus cereus* VIP2 and other VIP2-like toxins	(10, 13, 28)

Specific modification of eukaryotic proteins is exemplified by the proteolytic activity of the Ras/Rap1-specific peptidase (RRSP). RRSP site-specifically cleaves the Ras and Rap1 GTPases to modulate mitogen activated kinases activity and thereby control cell survival. This highly potent toxic activity rapidly and completely abolishes proliferation of cells treated either with the toxic domain or with bacteria expressing a MARTX toxin (26, 27). Similarly, the Rho Inactivation Domain (RID) directly modifies target GTPases by acylation of the polybasic region of its substrates, leading to GTPase inactivation (3, 22, 23). Another example of direct modification is the MARTX-dependent catalysis of G-actin crosslinking by the actin crosslinking domain (ACD) (286, 287). The crosslinking of actin in the presence of bacteria is 100% efficient, resulting in crosslinking of all actin within 90 minutes (3, 6, 288). Dramatic cell rounding due to the ACD can also occur ahead of completion of crosslinking by the binding of crosslinked actin to formin on the growing end of actin filaments (9). The adenylate cyclase effector converts ATP to cyclic AMP (11), presumably affecting cell biological processes controlled by cytosolic levels of cyclic AMP. The alpha/beta hydrolase (ABH) effector domain is a phospholipase, which, by its cleavage of phosphoinositol-3-phosphate (PI3P), inhibits autophagic flux and endosomal trafficking in target cells (4). ABH is also reported to stimulate CDC42 activity, though this activity may be indirect (3).

Some MARTX effector domains are linked to cellular phenotypes but have as-yet unidentified biochemical mechanism. For example, MARTX toxin activity is linked to intrinsic apoptotic cell death (247, 289) through action of the Makes caterpillars floppy-like (MCF) effector domain (15, 16). The Domain X (PasyHD1 or DmX) binds host cell ADP-ribosylation factors (ARFs), inducing dysfunction and disrupting vesicle trafficking (12). In each of these two

cysteine proteases, catalytic residues have been identified as essential for autoproteolytic activity of MCF or DmX, but the role of the catalytic activity in downstream processes remains to be determined (12, 15). The DUF1 effector domain has recently been shown to bind and up-regulate host protein prohibitin 1 (PHB1) via the ERK pathway. The consequences of this binding are unknown and warrant further investigation (14).

Finally, the functions of at least two other uncharacterized effectors, *Photorhabdus asymbiotic* homology domain 2 (PasyHD2) and the vegetative insecticidal protein 2 homology domain (VIP2), remain to be investigated. Sequence analysis reveals little about the functions of DmX and PasyHD2, but similarities between VIP2 domain and other VIP2-like toxins and predicts this region could have ADP-ribosylation activity (3, 13).

MARTX toxins and heterologous protein transfer

As demonstrated by the variety of naturally occurring effector repertoires, MARTX toxins are capable of delivering cargo that ranges considerably in identity and size. This suggested that a MARTX toxin could also be capable of translocation of heterologous proteins.

Beta-lactamase (Bla) has served as a useful tool for study of protein transfer for many bacterial translocation systems because its presence can be monitored via enzymatic cleavage of fluorogenic and colorimetric lactam substrates (24). When a *bla* DNA sequence was cloned into *rtxA* in place of the native *V. cholerae rtxA* effector domain sequences, Bla activity was detectable in the supernatant of bacterial cultures. Thus, the heterologous MARTX proteins can be expressed and secreted from bacteria in the context of the MARTX toxin (Figure 1.3) (3). Moreover, Bla activity is detected after translocation into the target cell cytosol, indicating that the MARTX toxin is capable of transporting this heterologous protein across the eukaryotic

plasma membrane (Figure 1.3) (3, 16). This work in *V. cholerae* demonstrated that specific effector domains are not required for toxin secretion, for eukaryotic cell targeting, or for translocation. Moreover, cytosolic translocation of the heterologous Bla highlights the robustness of the MARTX toxin as a platform for effector delivery.

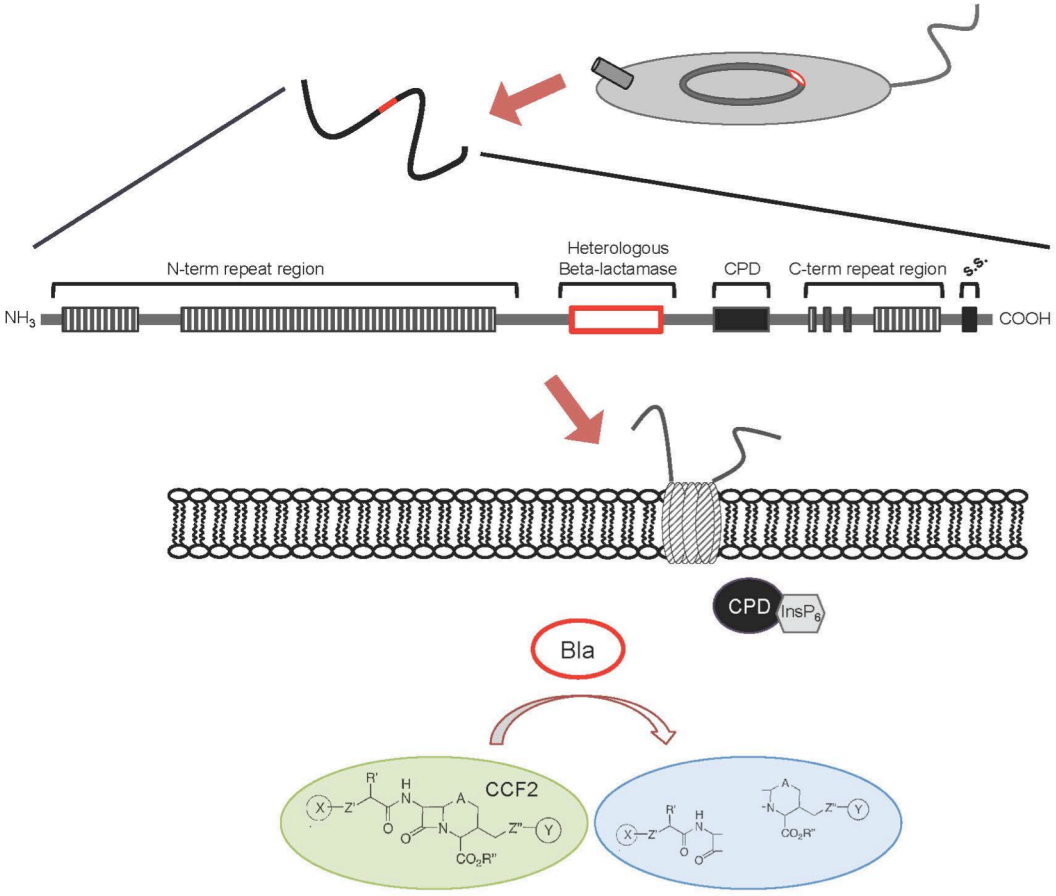

Figure 1.3. **MARTX toxins are capable of heterologous protein transfer.** Where a bla gene is cloned in place of *rtxA* effector domains, the heterologous protein is expressed, secreted and delivered to target cells in the context of the MARTX toxin. Bla activity can be detected by the cleavage of fluorogenic and colorimetric beta-lactam substrates, such as CCF2 (24). Heterologous protein transfer demonstrates the robustness of the MARTX toxin as a platform for effector delivery.

A major stumbling block in the study of MARTX toxin is that, likely due to a combination of traits including large size, inherent structural flexibility, and generally low expression, no MARTX toxin has been successfully purified in the two decades since its discovery (244). Thus, understanding its mechanism of action in many ways differs from traditional toxin biology approaches. Since the toxins are modular in nature, ectopic expression, intoxication, and microinjection have been productive in studying distinct domains in isolation. In addition, genetic manipulation of *rtxA1* on the chromosomes of genetically tractable bacteria has facilitated study by deletion, exchange, and insertion of effector domains. Indeed, the generation of the Bla system in *V. cholerae* MARTX was a major step toward a more fundamental understanding of these large and multifunctional proteins. Given the differences between the MARTX toxins of *V. cholerae* and *V. vulnificus* – namely, the lytic ability and diverse effector cargo of $MARTX_{Vv}$ as compared to the lack of lytic ability and relatively conserved effector cargo of $MARTX_{Vc}$ – experimental investigation is needed to determine whether results observed with *V. cholerae* toxin dynamics translate to our understanding of *V. vulnificus* toxin dynamics.

Driving Questions

The current model of *V. vulnificus* pathogenesis consists of three key stages: (i) bacterial outgrowth to high levels in the intestine, (ii) induction of widespread intestinal tissue damage, and (iii) bacterial flood to distal organs. In the current paradigm, the MARTX holotoxin promotes each of these stages by (i) enhancing bacterial survival in the intestine, (ii) causing lytic cell death, and (iii) promoting dissemination (Figure 1.4).

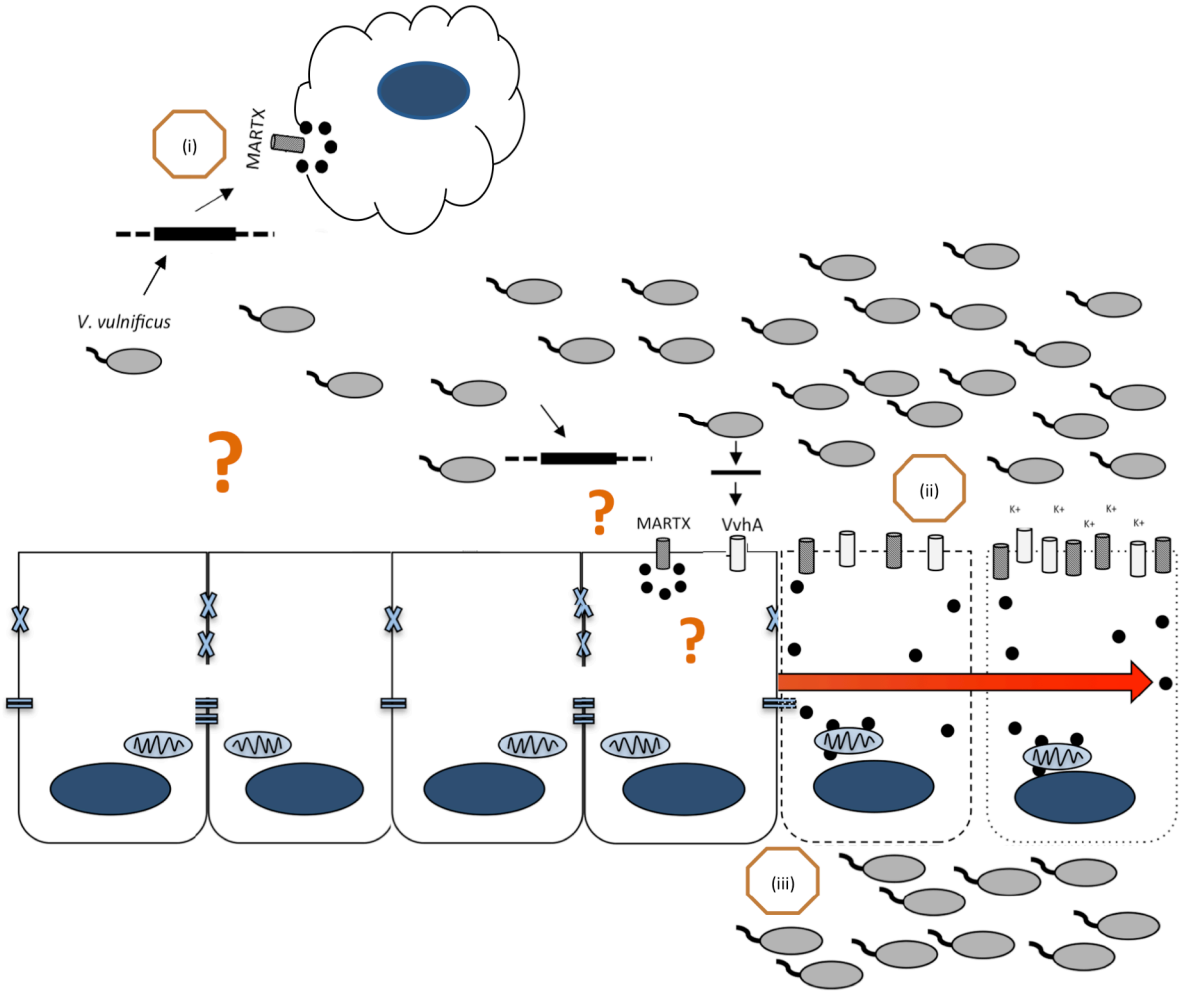

Figure 1.4. Current paradigm of MARTX-mediated functions in pathogenesis.
MARTX toxin (i) defends against phagocytosis and thereby promotes bacterial outgrowth in the intestinal lumen. (ii) When a critical bacterial level is reached in the intestine, toxin-mediated barrier dysfunction is induced by pore-forming toxins MARTX and VvhA. (iii) Widespread lytic necrosis in the intestine facilitates bacterial transit across the epithelial barrier and dissemination to distal organs.

From these facts arise numerous outstanding questions. Does the MARTX toxin interact with the epithelial barrier early during gastrointestinal infection? With such a large and dynamic protein, which are the MARTX toxin regions that functionally contribute to pathogenesis? And how are they doing so? Are critical MARTX functions attributable to specific toxin regions? Or, are MARTX phenotypes additive or synergystic from the activities of its component parts? Relatedly, why does a toxin that can cause necrotic cell lysis also initiate so many other cytopathic functions by virtue of its effector domain repertoire (Table 1.2)? Which of these functions are critical to its virulence role? These constitute the driving questions that will be addressed in this study.

The experiments presented in the following dissertation are the first to use modified Bla-containing MARTX toxins in *V. vulnificus* study. In Chapter 2, we investigate the interplay among MARTX toxin regions and toxin function to determine which toxin regions facilitate toxin expression, secretion, and delivery to target cells. In Chapter 3, the same powerful genetic platform is employed to address outstanding questions on the functional role of the MARTX toxin in *V. vulnificus* pathogenesis. In Chapter 4, the functional contributions of individual effector domains in the MARTX toxin repertoire are investigated. Finally, Chapter 5 outlines the novel application of mouse ventral surface temperature (VST) as a biomarker for lethal i.g. *V. vulnificus* infections. Together, a variety of *in vitro* and *in vivo* experiments are employed to advance the MARTX toxin and *V. vulnificus* pathogenesis fields by elucidating the functional relationships among MARTX toxin domains, cytopathic functions, and virulence.

CHAPTER 2

The *Vibrio vulnificus* MARTX toxin effector domain region is not required for toxin expression, secretion, or delivery to host cells

Chapter-specific acknowledgements

The work published in Kim, et al. 2015 was accomplished in collaboration with Satchell laboratory postdoctoral fellow Byoung Sik Kim, PhD (30). In this chapter, I describe my experimental contributions to this study. To ensure clarity about the validation of this system, which is used in all subsequent chapters, I also include data from a subset of Dr. Kim's experiments. Work by Dr. Kim is clearly designated as such in the text and figure legends. Any work not credited to Dr. Kim is my own.

Overview

The *V. vulnificus* gene *rtxA1* encodes a Multifunctional Autoprocessing Repeats-in-Toxins (MARTX) toxin, which is responsible for numerous cytopathic and cytotoxic functions. *rtxA1* is an important virulence factor of *V. vulnificus,* as defined by its significant contribution to lethal infection outcomes in mice. As such, its mechanisms of action are an area of active study. Processes induced by the *rtxA1* gene or its toxin product include: reactive oxygen species (ROS) stimulation, mitochondrial damage, inflammasome activation, cytoskeletal changes and cell rounding, and cell death via apoptosis or necrosis (136, 246, 247, 290).

MARTX toxins are large, multi-domain proteins that consist of N- and C-terminal amino acid repeat regions flanking a central effector domain repertoire (Figure 1.2) (13, 19). This organization is exemplified by the 5,206-amino-acid (aa) $MARTX_{Vv}$ toxin from representative

Korean clinical isolate CMCP6 (291) (Fig. 2.1). The N-terminal repeat-containing region includes an ~200-kDa amino-terminal arm, more than 50 percent of which consists of 19-to-20-aa glycine-rich repeats. At the carboxyl-terminal end of the protein are situated approximately ~100-kDa of glycine-rich repeats, and 15 copies of the atypically structured 18-aa repeats-in-toxin (RTX) repeat that classify this toxin as a member of the greater RTX protein family (2, 30).

Following secretion from the encoding bacterium, MARTX toxins undergo an extracellular intermediate prior to delivering their effector domains to targeted eukaryotic cells (6). The MARTX N- and C-terminal arms are then purported to together form a pore in the host cell membrane (2), though the structural basis of their role in pore formation has not been deduced. The MARTX pore, estimated at 1.6 nm (136), is thought to serve as the means of translocation for the unfolded central region of the MARTX protein to eukaryotic cytosol.

While the N- and C-terminal repeat regions are highly conserved, the effector domains vary in modular fashion. Thus the MARTX effector complement is variable across bacterial species, and even among isolates of *V. vulnificus* (reviewed in (13, 275)). Between the effector domains and the C-terminal repeat regions is the inositol hexakisphosphate (InsP6)-inducible cysteine protease domain (CPD). The CPD is responsible for autoprocessing activity that releases MARTX effectors to the eukaryotic cytosol (282-284).

The MARTX toxin has, to this point, never been successfully purified, likely owing to a combination of size, structural flexibility, and autoproteolytic activity. However, ectopic expression, alternative delivery, and microinjection have been successfully employed in MARTX toxin study. In this way, certain cytopathic activities have been attributed to the biochemical activities of discrete MARTX toxin effector domains (4, 12, 14, 27, 31). The

functionality of discrete MARTX effector domains suggests that the specific cytopathicities induced by a given toxin variant are dependent upon its effector domain composition. Effector variability across bacterial isolates makes it unlikely that any given portion of the effector repertoire is required for efficacious MARTX toxin expression, secretion, or translocation.

Conversely, conservation of the N- and C-terminal repeat region sequences suggests that these portions of the toxin are more likely to confer conserved toxin functions, specifically expression and delivery to host cells. In fact, the extreme C-terminus of the MARTX toxin encodes the characteristic T1SS secretion signal for RTX proteins (10, 13, 276). Studies suggest that a C-terminal portion of the toxin lacking the effector domains and N-terminal repeat region is sufficient to kill cells when it is ectopically expressed inside eukaryotic cells (246). However, a C-terminal toxin fragment is not cytotoxic when delivered as a purified protein from outside the cell (292).

Thus, data suggest important functions for both the repeat regions and the effector domain repertoire of the *V. vulnificus* MARTX toxin. However, studies have so far been limited to genetic disruption of the entire *rtxA1,* or to study of discrete expressed/purified toxin fragments.

This study employs a genetic approach to generate MARTX toxin variants to study toxin functionality in a manner that facilitates delivery of toxin variants in natural context from the bacterium to target cell. Specifically, genetic manipulation on the bacterial chromosome replaces the native MARTX effector repertoire with a heterologous beta-lactamase (*bla*) gene in a method comparable to that recently employed in the study of MARTX toxin in *Vibrio cholerae* (3).

This method allows the empirical testing of questions previously unanswered or unanswerable. Specifically: Which portions of the MARTX toxin are involved in its expression and secretion from bacteria? Which portions are necessary for delivery to host cells? What is the relationship between *rtxA1*-associated cytopathicities and toxin domains? To address these questions, the MARTX effector-free *V. vulnificus* strain and its derivative strains are tested for toxin dynamics in the context of natural toxin delivery from bacteria. The strains are likewise used to discern the portions of the MARTX toxin necessary for two ubiquitous toxin-associated phenotypes of cell rounding and cell lysis.

Indeed, these experiments reveal that the MARTX N- and C-terminal regions are each important for delivery of toxin domains from the bacteria to the eukaryotic cytosol. Likewise, these conserved regions are critical for cell lysis *in vitro*. However, the repeat regions cannot account for all activities of the toxin. Rather, the effector domains confer cytopathic activity separate from pore-induced necrosis.

Results

Strain generation and validation

To distinguish the function of independent portions of the MARTX toxin during natural intoxication of cells, a method is needed to ensure that genetic modification of the *rtxA1* toxin gene does not also disrupt protein synthesis, secretion from the bacterium, surface binding, or translocation. Kim and colleagues established a system in which the effector domains were replaced with the mature *Escherichia coli* TEM-1 Bla as an in-frame fusion (293-295), while the natural CPD autoprocessing site at aa 4090 (as mapped by Shen et al. (271)) and the putative

processing site in front of domain of unknown function in the first position (DUF1) (after aa 1959 based on alignment to the known processing site for *V. cholerae* MARTX [$MARTX_{Vc}$] (282)) were retained.

The modified gene arrangement was exchanged into the chromosome of *V. vulnificus*. These studies use a derivative of Korean clinical isolate CMCP6 generated by isolation of a spontaneous mutant resistant to rifampicin (Table 7.1, hereafter termed CMCP6). The *bla* gene was inserted into this CMCP6 strain background by double homologous recombination to create an *rtxA1*::*bla* strain. Additional modifications to the *rtxA1::bla* strain were also generated. These include strains deficient in the N- or C-terminal toxin coding regions; with a catalytically inactive CPD; or with a disruption in the *rtx* secretion apparatus. The MARTX toxins produced by these modified *rtxA1* genes are diagrammed in Figure 2.1 and the strains listed in Table 7.1. The *V. vulnificus* hemolysin also has a role in cytolysis (132, 296, 297) and virulence (1). The *vvhA* gene was deleted from all strains used in this study so as to focus on phenotypes arising from manipulation of the *rtxA1* locus.

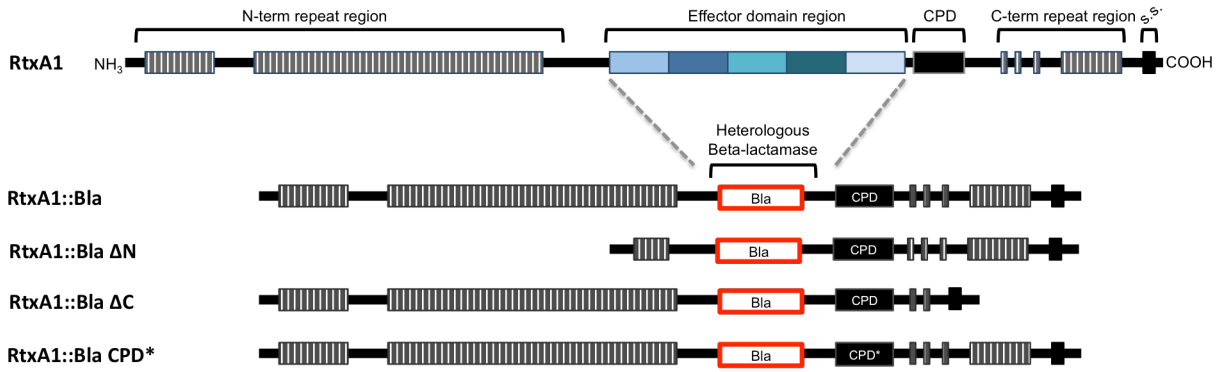

Figure 2.1. Modified MARTX toxin schematics. The RtxA1 protein (MARTX toxin) produced by the parental strain (top) was modified to replace the native effector domain region with a heterologous beta-lactamase (RtxA1::Bla). Subsequent strains were generated that product RtxA1::Bla toxins lacking N-terminal repeats (RtxA1::Bla ΔN), C-terminal repeats (RtxA1::Bla ΔC) or CPD activity (CPD*). CPD = cysteine protease domain; s.s. = secretion signal.

Modification of *rtxA1* does not alter *in vitro* bacterial growth

Once all strains were generated by Dr. Kim, I tested *in vitro* bacterial growth rates as measured by optical density (OD) in LB broth. Growth rates were unaltered by the modifications to the *rtxA1* gene (Figure 2.2).

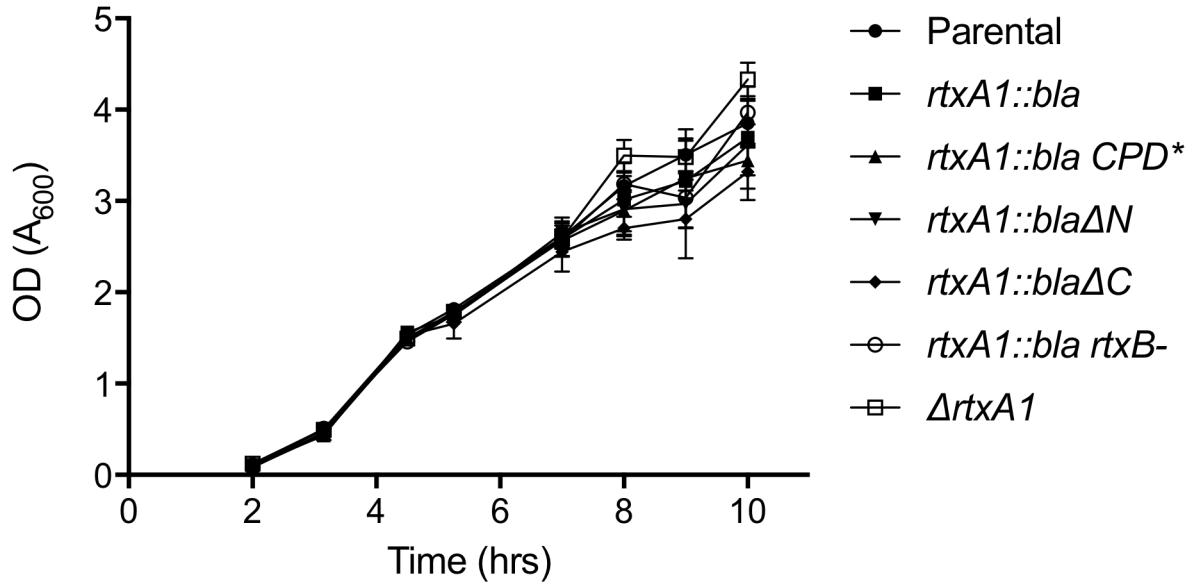

Figure 2.2. Chromosomal modification of *rtxA1* does not alter bacterial growth *in vitro*. Cultures grown in LB broth over ten hours show no growth defect for the strains with the modified rtxA1 gene as measured by optical density (OD) at 600nm (A_{600}). Three biological replicates per strain were used in a single growth experiment. Strains compared by two-way ANOVA.

Modified MARTX toxin is secreted to culture media

Because beta-lactamase protein possesses enzymatic activity, and MARTX toxins are secreted by a dedicated T1SS with no periplasmic intermediate, measuring cleavage of extracellular Bla substrates should serve as a measure of modified RtxA1::Bla toxin secretion.

This phenomenon was validated first via a semi-quantitative assay using ampicillin, a beta-lactam antibiotic substrate of Bla (Figure 2.3). On agar plates, ampicillin from an antibiotic-loaded disc diffuses in the media to generate a concentration gradient that decreases with increasing distance from the origin of the disc. Bacteria that are more sensitive to Amp (that is, inhibited for growth at lower concentrations) exhibit larger zones of growth inhibition, while those that are resistant to Amp (i.e. capable of tolerating higher concentrations of Amp) grow in closer proximity to the disc. This assay was utilized in development of the Bla system for study of the MARTX toxin in *Vibrio cholerae* (3).

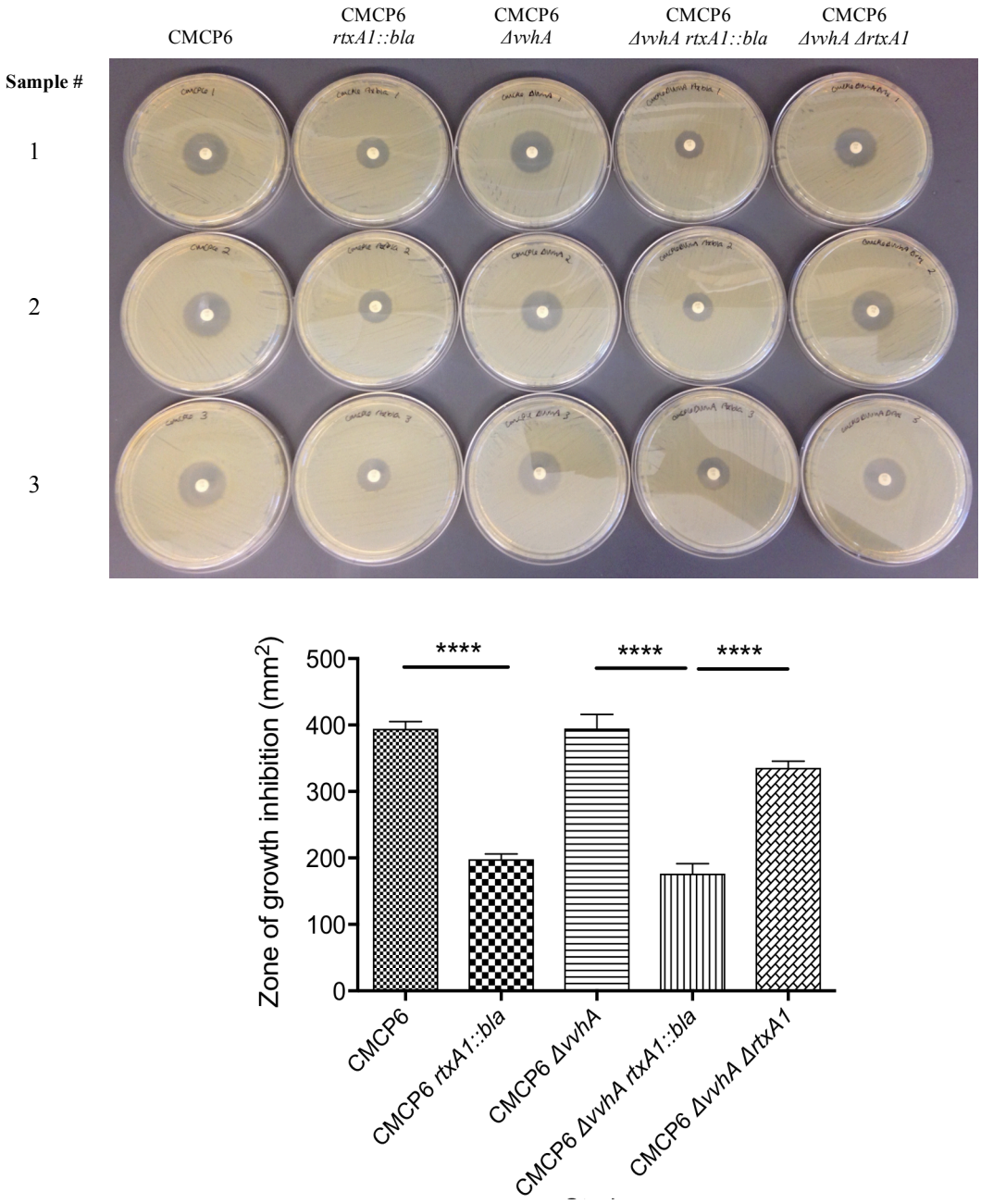

Figure 2.3. Strains expressing modified RtxA1::Bla toxins exhibit β-lactamase activity. Strains which contain the heterologous *bla* gene in the *rtxA1* coding region demonstrate secreted Bla activity with decreased zones of growth inhibition in the presence of ampicillin. Three biological replicates were used in a single experiment. The individual replicates are depicted above and the data quantified below. Results were compared by one-way ANOVA with Tukey post-test for multiple comparisons. **** $p<0.0001$

When strains of *V. vulnificus* with wild-type (WT) or modified MARTX toxins were grown as bacterial lawns in the presence of an ampicillin antibiotic disc (Figure 2.3), only those strains modified by introduction of the *bla* gene into the MARTX toxin were more resistant to ampicillin (smaller zone of growth inhibition). Strains with deletions in the *vvhA* or *rtxA1* locus had unmodified Amp resistance compared to the WT CMCP6 strain. These results confirm that cleavage of Bla substrates by *V. vulnificus* is dependent upon the presence of RtxA1::Bla.

Knowing that cleavage of Bla substrates by *V. vulnificus* could be used to specifically monitor RtxA1::Bla secretion, an assay of increased precision was desired. The compound nitrocefin undergoes a yellow-to-red color change upon cleavage of its beta-lactam ring, and quantitation of this color change has been previously used to track the secretion of modified T3SS substrates from *Pseudomonas aeruginosa* (298-300). Therefore we optimized a protocol for detection of RtxA1::Bla secretion from *V. vulnificus*. Because MARTX toxins are expressed at low levels prior to exposure to host cells (136), and because the toxin is degraded rapidly upon secretion (245, 246, 254), this protocol entails incubating nitrocefin directly with bacterial cultures rather than with culture supernatants. In this way, the Bla activity of MARTX secreted into the media can be captured directly upon its secretion.

As expected, whole cell cultures of *rtxA1::bla* were capable of hydrolyzing the chromogenic substrate (Figure 2.4) while strains lacking the *bla* modification in *rtxA1* (WT, *ΔrtxA1*) did not demonstrate any detectable nitrocefin cleavage (Figure 2.4). A mutant with a polar insertion in the *rtxB* gene of the associated T1SS exhibited significantly less nitrocefin cleavage compared to the *rtxA1::bla* strain. Thus nitrocefin cleavage is dependent upon secreted RtxA1::Bla toxin.

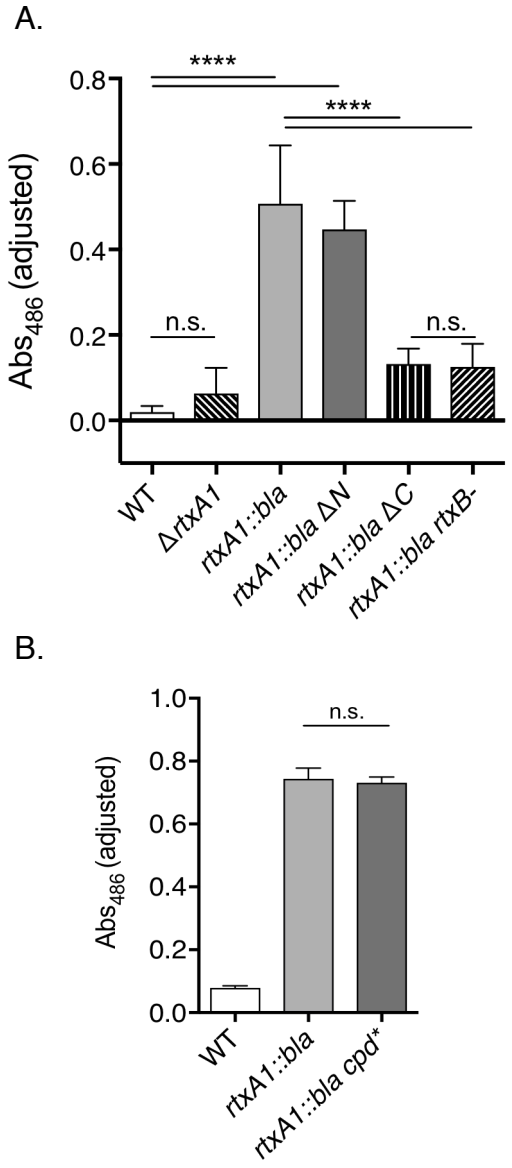

Figure 2.4. The *rtxA1* effector domain region, N-terminus, and CPD catalytic activity are dispensable for MARTX toxin secretion. Secretion of modified MARTXVv toxin from the indicated strain was examined by nitrocefin cleavage assay using whole bacterial culture. Three biological replicates were run for each experiment, and each was adjusted by subtracting background nitrocefin absorbance from a negative, media-only control. Panel (A) is pooled data from two independent experiments. Panel (B) is data from a single experiment. Results were compared by one-way ANOVA with Tukey post-test for multiple comparisons. **** $p<0.0001$

The N-terminal repeat region of RtxA1 is not required for toxin secretion (A), nor is CPD catalytic activity (B). Interestingly, Bla activity from the *rtxA1::bla ΔC* strain was only detectable at low levels, comparable to the non-secreting *rtxA1::bla rtxB-* strain. This result was novel, given the intentional conservation of the extreme C-terminal RtxA1 secretion sequence in *rtxA1::bla ΔC* (276, 301). The result indicate that the amino acid repeats at the C-terminus of the MARTX toxin might have a functional role in protein secretion.

To distinguish between defective toxin expression and defective toxin secretion, bacterial lysates were generated and subsequently co-incubated with nitrocefin. Lysates from *rtxA1::bla ΔC* exhibits nitrocefin cleavage activity at levels much greater than the corresponding intact bacterial cultures, and comparable to lysates from the *rtxA1::bla* and *rtxA1::bla rtxB-* strains (Figure 2.5). The *rtxA1::bla rtxB-* and *rtxA1::bla ΔC* strains also exhibit substrate cleavage when cultures are incubated with nitrocefin overnight. This result reiterated the fact that they generate functional, Bla-containing MARTX toxin, but its secretion dynamics differ from that of the *rtxA1::bla* strain. Together these data demonstrate that the C-terminal repeat regions of the *V. vulnificus* MARTX toxin are required for toxin secretion.

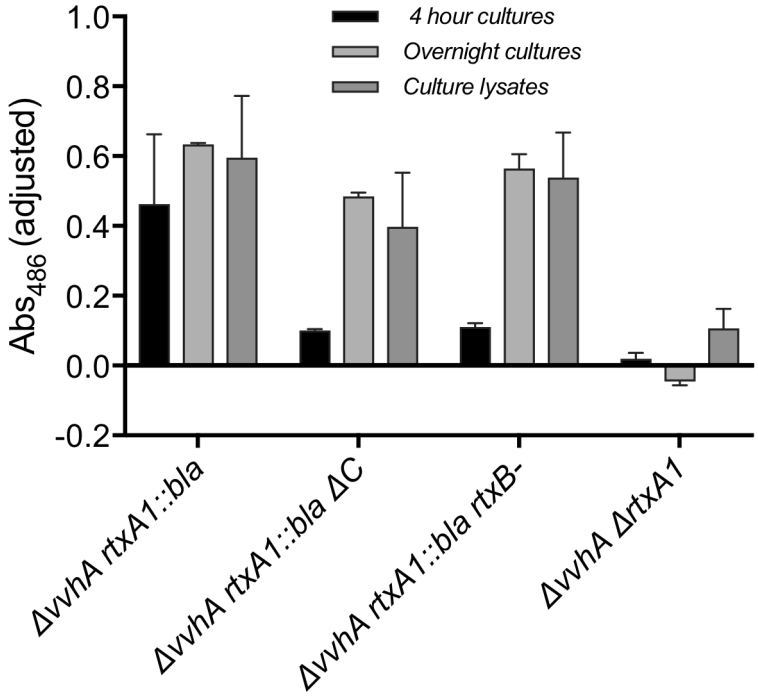

Figure 2.5. MARTX toxin C-terminal repeat regions are required for MARTX toxin secretion. Secretion of modified $MARTX_{Vv}$ toxin from the indicated strain was examined by nitrocefin cleavage assay using whole bacterial culture for duration of 4 hours (black) or 16 hours (light gray), or with culture lysates (dark gray). Data are three biological replicates per condition, each from a single experiment.

Bla modification does not render strains resistant to current clinical antibiotic therapy

One of the current clinical treatments for *V. vulnificus* infection is a beta-lactam antibiotic, ceftazidime (122). According to the literature, as a third-generation cephalosporin, ceftazidime should be impervious to the activity of the TEM-1 Bla utilized for modification of the *V. vulnificus* MARTX toxin (302). Nonetheless, we aimed to experimentally confirm that the MARTX Bla modification would not render *V. vulnificus* strains resistant to clinical antibiotic therapy. We tested ceftazidime resistance in the same manner as previous experiments for ampicillin resistance, using an antibiotic disc assay (Figure 2.6). The ceftazidime growth inhibition zones were indistinguishable in size amongst the tested strains, indicating that the modified *rtxA1::bla* strain is not resistant to this clinical antibiotic treatment regime.

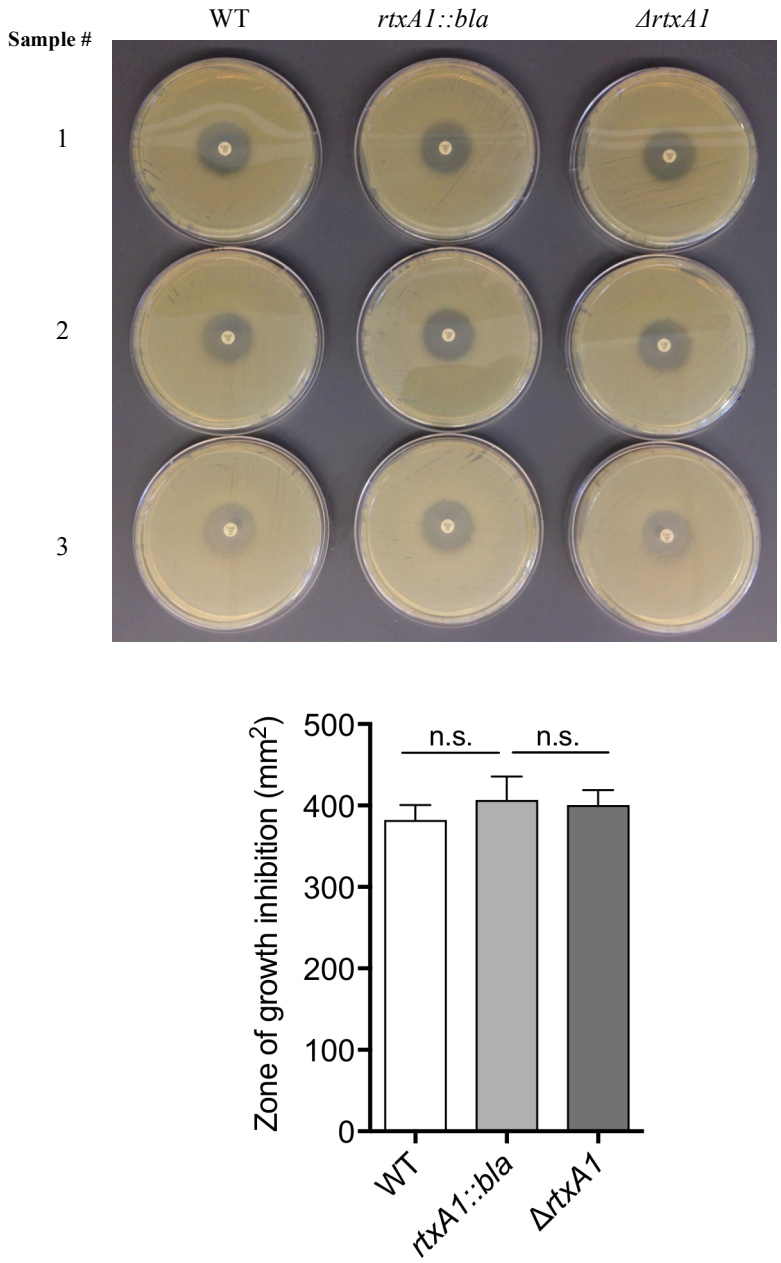

Figure 2.6. Modified *rtxA1::bla* strain is not resistant to clinical antibiotic treatment for *V. vulnificus*. Assessment of susceptibility of the indicated strains to ceftazidime using antibiotic disc assay. Results were compared by one-way ANOVA with Tukey post-test for multiple comparisons. n.s. = not significantly different. Data were collected from three biological replicates, depicted above and quantified below.

Modified MARTX toxin delivers the heterologous Bla effector to host cytosol

After I confirmed that MARTX toxin produced by *rtxA1::bla* was secreted, Dr. Kim next aimed to determine whether heterologous Bla was translocated to targeted eukaryotic cells via the MARTX toxin platform. To examine this question, a CCF2 assay was used in a manner comparable to previous studies on the delivery of T3SS substrates to eukaryotic cells by *P. aeruginosa* (303).

HeLa cells loaded with the fluorescent Bla substrate, CCF2 exhibited green fluorescence that is detectable by flow cytometry (stained, Figure 2.7). HeLa cells co-incubated with *V. vulnificus rtxA1::bla* exhibit a conversion of green to blue fluorescence, indicating successful delivery of Bla to the eukaryotic cytosol (Figure 2.7). The proportion of blue cells increases with increased co-incubation time and MOI. CCF2 cleavage is completely dependent upon RtxA1::Bla, as the *ΔrtxA1* strain is incapable of converting any cells from green to blue. Thus the modified RtxA1::Bla delivers a heterologous effector to targeted eukaryotic cytosol.

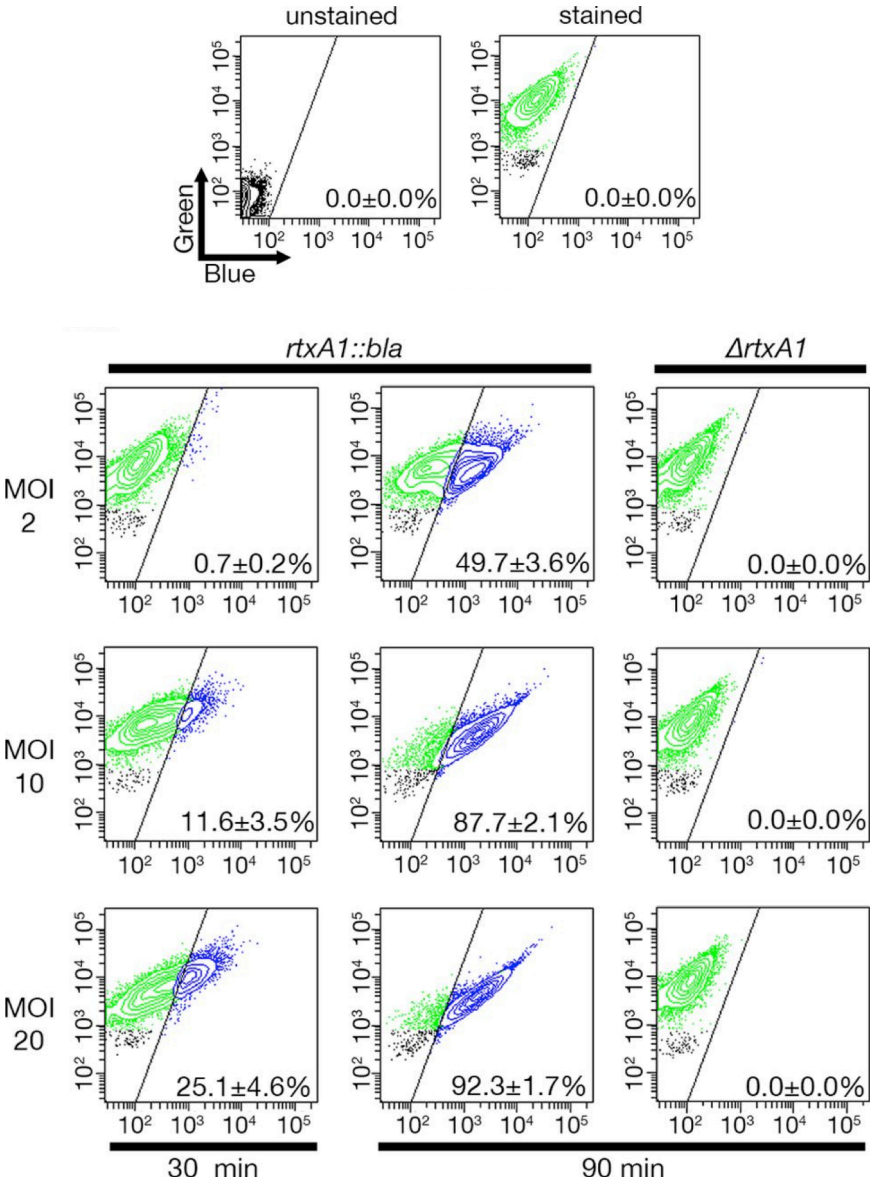

Figure 2.7. Modified MARTX toxin targets eukaryotic cells and delivers the heterologous Bla domain to eukaryotic cytosol. Translocation of Bla was detected by flow cytometry, where green fluorescence (518 nm; y axis) under conditions of violet laser excitation (409 nm) indicates the number of cells loaded with CCF2 and blue fluorescence (447 nm; x axis) indicates the number of cells with cleaved CCF2. Representative FACS analysis images from at least three biological replicates are shown, with means ± standard deviations of percentages of Bla-translocated cells shown within each panel. (30) This figure was generated by Dr. Byoung Sik Kim.

The lack of Bla translocation to cells co-incubated with *rtxA1::bla ΔC* is consistent with previous results that the C-terminus is required for toxin secretion. Interestingly, the lack of Bla translocation to cells co-incubated with *rtxA1::bla ΔN* indicates that MARTX effector translocation requires the protein's N-terminal repeat region (Figure 2.8). While the N- and C-terminal repeat regions had been previously predicted to work in concert for pore formation at the eukaryotic membrane (2), this is the first experimental evidence to directly support a model in which the N-terminal repeat regions are required for effector translocation. It has been previously reported that, when expressed ectopically, the MARTX C-terminus is sufficient for the toxin's cytopathic effects ((246)). However, the result of this study demonstrates the requirement of the MARTX N-terminus for delivering MARTX toxin effector domains in the toxin's native, bacterially derived context.

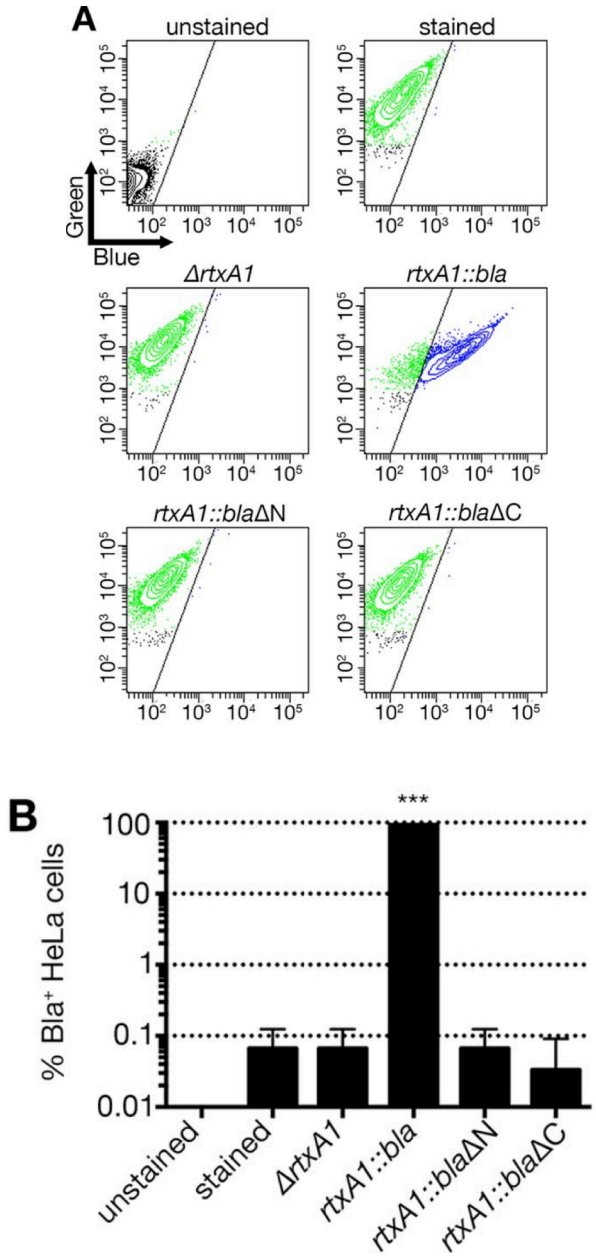

Figure 2.8. MARTX toxin N-terminus is required for Bla delivery to target cells. (A) HeLa cells were treated with the indicated *V. vulnificus* strain at an MOI of 10 for 60 min and then loaded with CCF2/AM. FACS analyses were done as described for Fig. 2, and representative images are shown. (B) Histograms show percentages of Bla-translocated, blue fluorescence-emitting cells as means ± standard deviations ($n \geq 3$). Results were compared by one-way ANOVA with Tukey post-test for multiple comparisons. ***$p<0.001$. This figure was generated by Dr. Byoung Sik Kim.

Toxin-dependent lysis of target cells does not require effector domains

The previous experiments demonstrate that effector-free RtxA1::Bla toxin is secreted from *V. vulnificus* and that the heterologous Bla domain is translocated to targeted eukaryotic cytosol. As such, the strain is validated as a tool for disentangling the role of MARTX toxin repeat regions and MARTX toxin effector domains in toxin-associated phenotypes. Specifically, the Bla system was used to test the role of the different toxin regions in cell lysis.

It is well documented that *V. vulnificus* induces necrotic lysis of eukaryotic cells when co-cultured *in vitro* (136, 246, 258). To test the role of the effector domain region in MARTX-induced lysis, HeLa cells were co-incubated with *V. vulnificus* strains at an MOI of 10 and cell lysis quantified by LDH release.

Compared to the strain making wild-type toxin, lysis by the *rtxA1::bla* strain was delayed, while the *ΔrtxA1* strain induces only background levels of lysis. (Figure 2.9). However, by 270 minutes of co-incubation, the lysis levels were indistinguishable at nearly 100 percent. Thus, MARTX effector domains influence the kinetics of cell lysis but ultimately are not required for toxin-dependent lysis of target cells. Rather, repeat region-mediated pore formation is sufficient for *V. vulnificus* MARTX-associated lysis of eukaryotic cells.

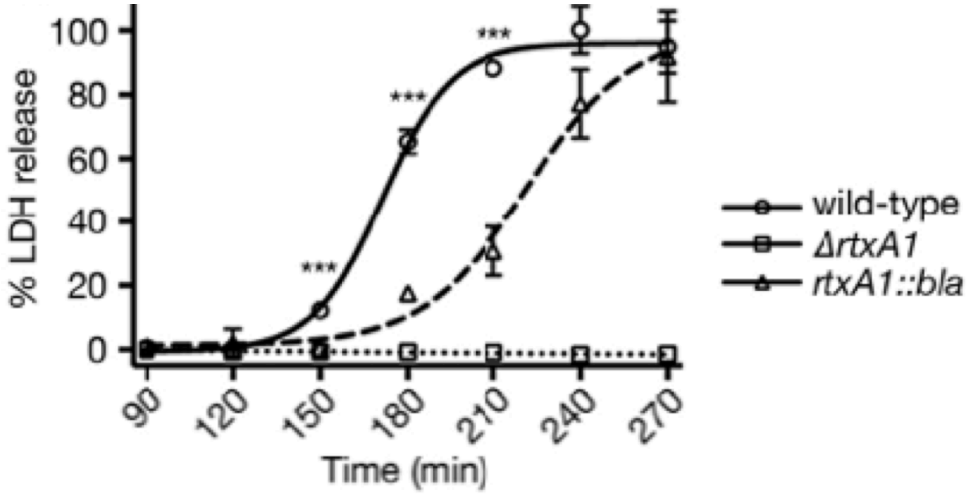

Figure 2.9. The MARTX effector domain region is not required for toxin-dependent lysis. HeLa cells were coincubated with the indicated *V. vulnificus* strains at an MOI of 10 and LDH release to supernatant fluids quantified at the indicated times. Samples were collected form the same three biological replicates at each time point. Results were compared by two-way ANOVA with Tukey post-test for multiple comparisons. *$p<0.05$, ***$p<0.001$. This figure was generated by Dr. Byoung Sik Kim.

In an endpoint assay of 270 minutes co-incubation, neither *rtxA1::bla ΔN* nor *rtxA1::bla ΔC* induced lysis beyond background levels. This result is consistent with previous data that *rtxA1::bla ΔC* is not secreted. Moreover, the requirement of the MARTX N-terminus for both Bla translocation and toxin-induced lysis indicates its role in formation of the MARTX pore, which is here demonstrated to be sufficient for induction of target cell lysis even in the absence of any native MARTX effector domains (Figure 2.10).

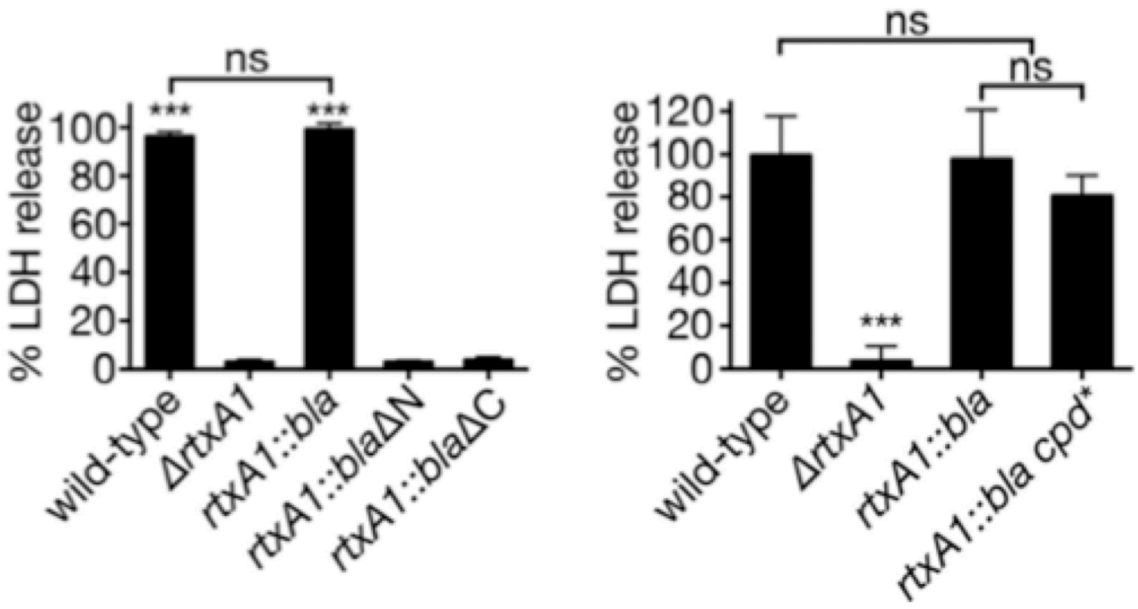

Figure 2.10. Repeat-containing regions of $MARTX_{Vv}$ toxin are necessary and sufficient for host cell lysis. Percent HeLa cell lysis at 270 min after coincubation with the indicated V. vulnificus strains at an MOI of 10 was determined by LDH release assay. Three biological replicates were used per experiment in two independent experiments. Results were compared by one-way ANOVA with Tukey post-test for multiple comparisons. ***$p<0.001$, n.s. = not significantly different. Panel A was generated by Dr. Byoung Sik Kim.

MARTX effector domains are required for induction of cell rounding

In addition to cell lysis, *rtxA1* induces cytoskeletal rearrangement and cell rounding (136). To characterize the region of the MARTX toxin responsible for this activity, HeLa cells were co-incubated at MOI=10 with strains making full-length or effector-free MARTX and cell rounding monitored at 30 minute intervals prior to the onset of detectable cell lysis (Figure 2.11). HeLa cells exposed to *V. vulnificus* making full length MARTX exhibited a rapid response, with nearly 50% of cells rounded in just 30 minutes of co-incubation and almost 100% of cells round by 120 minutes. In contrast, the effector-free *rtxA1::bla* strain did not induce cell rounding above the level of *ΔrtxA1* or PBS-inoculated negative controls, despite the eventual lysis of both cell subsets. These data reveal the novel insights that 1) the MARTX effector domain region is required for cell rounding, and 2) cell rounding is not a necessary prerequisite of necrotic lysis.

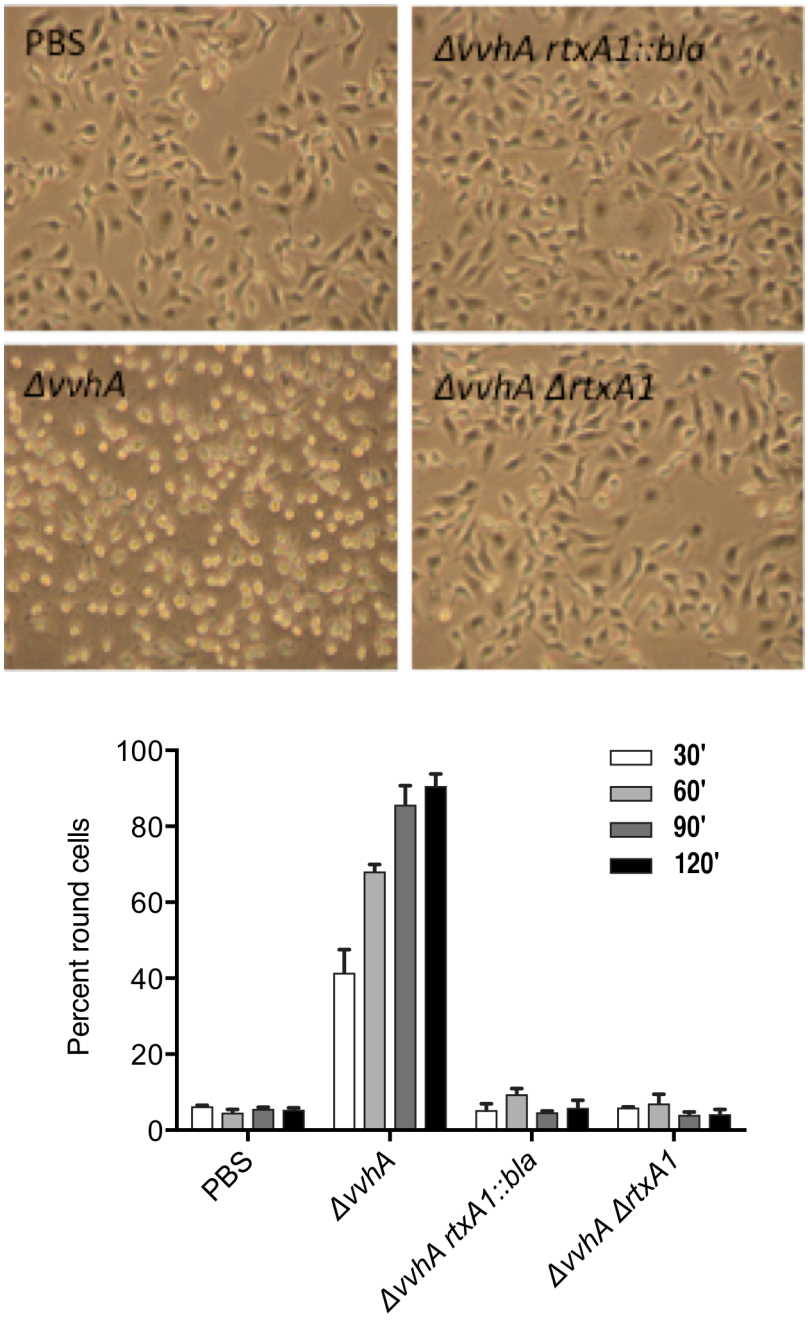

Figure 2.11. Rapid cell rounding induced by MARTX$_{Vv}$ requires effector domains. P Representative images of HeLa cells treated with PBS or indicated *V. vulnificus* strains for 120 min. Cell rounding was quantified every 30 min. Data are means ± standard deviations for n=3 images containing average 75 cells per image.

Discussion

The overall structural organization of MARTX toxins is consisten, and the N- and C-terminal portions of the encoding *rtxA1* genes are highly conserved (275). However, the total length of a given MARTX varies from 3500 to 5300 amino acids due to the variable number and identity of effector domains in the toxin's central region (2). How is it that certain toxin functionalities are conserved even with such variable effector composition?

For many years, models of MARTX toxin function have suggested that the N- and C-terminal repeat regions work in concert to form the 1.6-nm pore in targeted eukaryotic membranes, through which the central region of effector domains is translocated (275). However, this model had not been functionally tested for any MARTX toxin until 2015, when it was shown that the repeat regions of $MARTX_{Vc}$ are sufficient to deliver a heterologous effector to the eukaryotic cytosol (3).

Here is has been demonstrated that numerous characteristics of $MARTX_{Vc}$ are also true of $MARTX_{Vv}$, and thus are likely generalizable also to the entire MARTX family. Namely, the effector domain region is not required for MARTX toxin expression, secretion, or delivery to host cells. Moreover, the MARTX toxin is a sufficiently robust effector delivery platform that it can translocate not only its own diverse native effector repertoires, but also heterologous proteins.

This study expanded upon the work that had been completed in *V. cholerae* to further characterize toxin dynamics in *V. vulnificus*. Specifically, the novel use of quantitative nitrocefin cleavage assays for detection of MARTX secretion was used to determine that the toxin N-terminus is not required for toxin secretion, while the C-terminal repeats are required for

MARTX secretion from bacteria. Bacterial mutants were further employed to demonstrate that a toxin lacking N-terminal repeats could not translocate effectors to the eukaryotic cytosol. This result indicates the importance of the MARTX N-terminal repeats for eukaryotic membrane targeting and/or pore formation.

This study was also able to experimentally dissect questions about the MARTX toxin that are unique to *V. vulnificus*. While $MARTX_{Vc}$ does not induce necrosis of target cells, cell lysis is a well-documented phenotype of $MARTX_{Vv}$. Using bacterial mutants producing different versions of the MARTX toxin, we show that effector domains are not required for MARTX-induced cell lysis. The repeat region pore is sufficient not only for heterologous domain translocation, but also for lysis of target cells. The mechanisms of differences in lytic activity – that is, why the MARTX toxins of *V. vulnificus* but not those of *V. cholerae* or *Vibrio anguillarum* are lytic, despite 93 percent conservation of the repeat regions among strains – remain to be determined (6, 255).

Another outstanding question is the functional role of discrete MARTX toxin regions in bacterial virulence and pathogenesis. This study makes clear that *in vitro,* the MARTX toxin repeat regions are sufficient for a necrotic death of target cells. Moreover, effector domain-induced cell rounding is not a necessary prerequisite of toxin-induced necrosis. Still, the effector domains rapidly induce cytopathic effects that manifest in cytoskeletal re-arrangement and cell rounding well prior to the onset of necrosis, suggesting that translocation of effector domains is the primary function of the MARTX toxin pore. Such activity is reminiscent of the bifunctional *Bordetella pertussis* adenylate cyclase toxin that functions as both a hemolysin/cytolysin and for delivery of its adenylate cyclase effector domain (304). Whether one of these *in vitro* phenotypes

has a dominant role *in vivo,* or whether they each contribute to toxin-associated lethality, will be addressed in Chapter 3.

CHAPTER 3

The MARTX toxin effector domain region confers biphasic epithelial dysfunction and is essential for systemic spread from the intestine

Overview

Pathogenic bacteria are known for secreting virulence factors that promote infection of host organisms. In the case of *V. vulnificus,* the *rtxA1* gene encodes a multifunctional autoprocessing repeats-in-toxins (MARTX) toxin, which is the dominant secreted factor that determines lethality of intestinal infection (1). The 5206 a.a. MARTX toxin produced by *V. vulnificus* strain CMCP6 contains long regions of highly conserved tandem amino acid repeats at the N- and C-termini. These regions are required for toxin secretion and formation of the MARTX toxin pore, which has been estimated to have an inner diameter of 1.63 nm (30, 136). Between the repeat regions are situated a cysteine protease domain (CPD) and a region of modularly organized effector domains (13). The pore is thought to serve as the route for translocation of the central toxin region containing the CPD and effector domains across the eukaryotic plasma membrane from the extracellular space to the cytosol of target cells. Stimulated by the eukaryotic-specific molecule inositol hexakisphosphate (InsP6), the CPD is activated to cleave after leucine residues located between effector domains, thereby releasing bacterial effector proteins into the cytosol of the targeted eukaryotic cell (253).

The *V. vulnificus* MARTX toxin is associated with numerous cytopathic and cytotoxic functions *in vitro*. Specifically, the toxin plays a role in lysis of numerous eukyarotic cell types (246, 289), cytoskeletal dysfunction as illustrated by epithelial cell rounding (30), inflammasome

activation (290), inhibition of phagocytosis (163, 249, 305), and induction of apoptosis (247). Moreover, the discrete effector domains present in the inner region of MARTX toxins are being biochemically characterized to discern their enzymatic functions. Effector domains from various MARTX toxins are now known to inhibit Rho GTPases (3, 22), cleave Ras and Rap1 (27, 306), inhibit autophagy (4), induce apoptosis (31), and crosslink actin (19, 193, 288). Experiments suggest that different effector compositions confer different levels of MARTX toxin potentcy (193). Yet it has been challenging to discern functional relationships between discrete portions of the MARTX toxin and *V. vulnificus* virulence.

We have previously demonstrated that the MARTX toxin effector domain region is dispensable for toxin secretion from the bacterium and toxin translocation to target cells, indicating that secretion and translocation functions are conferred by the conserved repeat regions (30). In fact, the toxin repeat regions and the CPD comprise a sufficiently robust platform to deliver a heterologous beta-lactamase (Bla) in place of the native MARTX toxin effector repertoire (3, 30). Notably, the MARTX toxin pore is also sufficient to induce necrotic cytotoxicity of HeLa cells *in vitro,* even in the absence of effector domains (30, 136, 246). The intestinal tissue necrosis observed during *V. vulnificus* i.g. infection suggests that lytic toxin activity might be sufficient for MARTX-associated intestinal damage, bacterial dissemination, and lethality (1, 131, 132, 138, 139). In Chapter 2, we demonstrated that the MARTX toxin repeat regions are sufficient for cell lysis *in vitro.* Yet, the MARTX toxin effector domain region is retained across *V. vulnificus* isolates and is required for *in vitro* cell rounding and apoptosis induced by the bacterium (30, 31). Therefore, we hypothesized that the MARTX toxin effector

domain region is important for i.g. pathogenesis of *V. vulnificus,* despite the fact that it is dispensable for cell lysis.

In this study, we characterize the functional roles of MARTX toxin regions in *V. vulnificus* pathogenesis and virulence during i.g. infection. We find that the MARTX toxin effector domains collectively induce rapid loss of transepithelial resistance and increased paracellular permeability *in vitro* prior to the induction of intestinal epithelial cell lysis. Moreover, MARTX effector domains are required for bacterial dissemination from the intestines to the liver and spleen very early during i.g. infection. Surprisingly, overt intestinal epithelial necrosis is not a prerequisite to bacterial dissemination. Together these data indicate that the focus on the MARTX toxin as a virulence factor should de-emphasize its lytic function and emphasize toxic mechanisms of delivered effector domains that confer *V. vulnificus* virulence potential.

Results

Bacterial strain selection and verification

The MARTX cytotoxin product of *rtxA1* is established as a potent virulence factor of *V. vulnficus* infection (1, 249). The VvhA cytolysin/hemolysin product of the *vvhA* gene is also cytolytic and functions additively to virulence. However, the MARTX toxin exerts a more potent effect (1). To isolate MARTX-associated phenotypes from those of VvhA, we utilized a variant of *V. vulnificus* CMCP6 with an internal deletion in *vvhA* (30). In this strain, the wild-type version of the MARTX toxin (RtxA1, Figure 1A) is produced.

The *rtxA1* locus has then been manipulated in this *ΔvvhA* background. The *ΔvvhA rtxA1::bla* strain was previously generated by replacing the gene sequence encoding for the MARTX toxin effector domains with an in-frame sequence encoding TEM1 Bla to produce the modified RtxA1::Bla toxin (Figure 3.1). This effector-free strain expresses and secretes the modified Bla MARTX toxin, as previously characterized (30). An *rtxA1* null strain was also previously generated via internal deletion, resulting in the *ΔvvhA ΔrtxA1* strain (30).

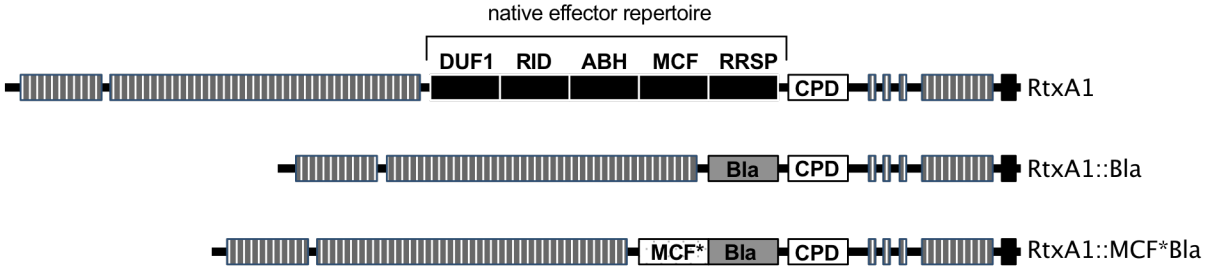

Figure 3.1 Modified MARTX toxin composition and layout. Schematic representation of toxins produced by *ΔvvhA, ΔvvhA rtxA1::bla,* and *ΔvvhA mcf*::bla* strains derived from *V. vulnificus* CMCP6. DUF1=domain of unknown function in the first position; RID=Rho Inactivation Domain; ABH=Alpha/Beta Hydrolase domain; MCF=Makes Caterpillars Floppy-like domain; RRSP=Ras/Rap1 Specific Protease domain; CPD=Cysteine Protease domain; striped boxes=repeat regions.

To verify that CMCP6 genetic manipulation did not compromise *rtxA1* gene expression, quantitative real-time PCR (qRT-PCR) was employed. mRNA transcript abundance from mutant strains was compared to that of the CMCP6 parent strain following growth in Luria Burtani (LB) broth. At the transcript level, there was no detectable difference of *rtxA1* gene expression between the *ΔvvhA* and *ΔvvhA rtxA1::bla* strains (Figure 3.2). Therefore, *rtxA1* mRNA expression is not affected by the presence or absence of the gene sequence encoding effector domains. Because RtxA1 protein level is extremely challenging to measure directly and because bacterial protein abundance is determined primarily by transcript level in *E. coli* (307), we moved forward on the assumption that equivalent transcript levels in the two strains results in equivalent protein production.

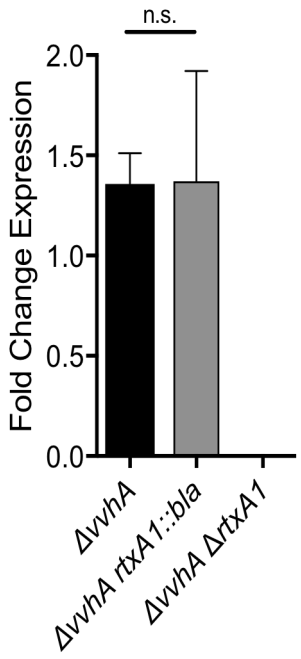

Figure 3.2. Elimination of *rtxA1* effector domain region does not impact transcript abundance. Expression of native and modified *rtxA1* gene measured by qRT-PCR relative to housekeeping *16s-rRNA* gene. Data were collected from three independent qRT-PCR runs, each with triplicate technical replicates. Statistical significance examined by one-way ANOVA using Tukey post-test for multiple comparisons. n.s. = not significant.

Effector domains are required for MARTX toxin-associated virulence

To examine the role of MARTX toxin effector domains in *V. vulnificus* virulence, mice were inoculated i.g. with either the parental *ΔvvhA* strain or the effector-free *ΔvvhA rtxA1::bla* strain (Figure 3.3A). The *ΔvvhA* strain caused fatality in 100% of mice by 24 hours post infection (hpi). In contrast, the *rtxA1::bla* was lethal to just 7% of infected mice (Figure 3.3). Thus, the *rtxA1::bla* strain is significantly attenuated, demonstrating that the MARTX toxin effector domains are instrumental to toxin-associated virulence.

To test for an association between *in vitro* cytolytic activity and virulence, mice were infected with either *ΔvvhA rtxA1::bla* – which causes *rtxA1*-mediated lysis *in vitro* – or *ΔvvhA ΔrtxA1* – which does not induce lysis *in* vitro – at a 100-fold higher dose. No significant differences in survival outcomes were observed between the two groups (Figure 1D). Notably, some *vvhA*- and *rtxA1*-independent lethality was observed at these high-doses. This could be due to bacterial components, such as LPS, and/or minor virulence factors, such as the VvpE metalloprotease, all of which may influence pathogenesis at very high dose in the absence of dominant virulence factors (241, 242). Nonetheless, the *ΔvvhA rtxA1::bla* strain does not confer additional virulence over the null mutant (30).

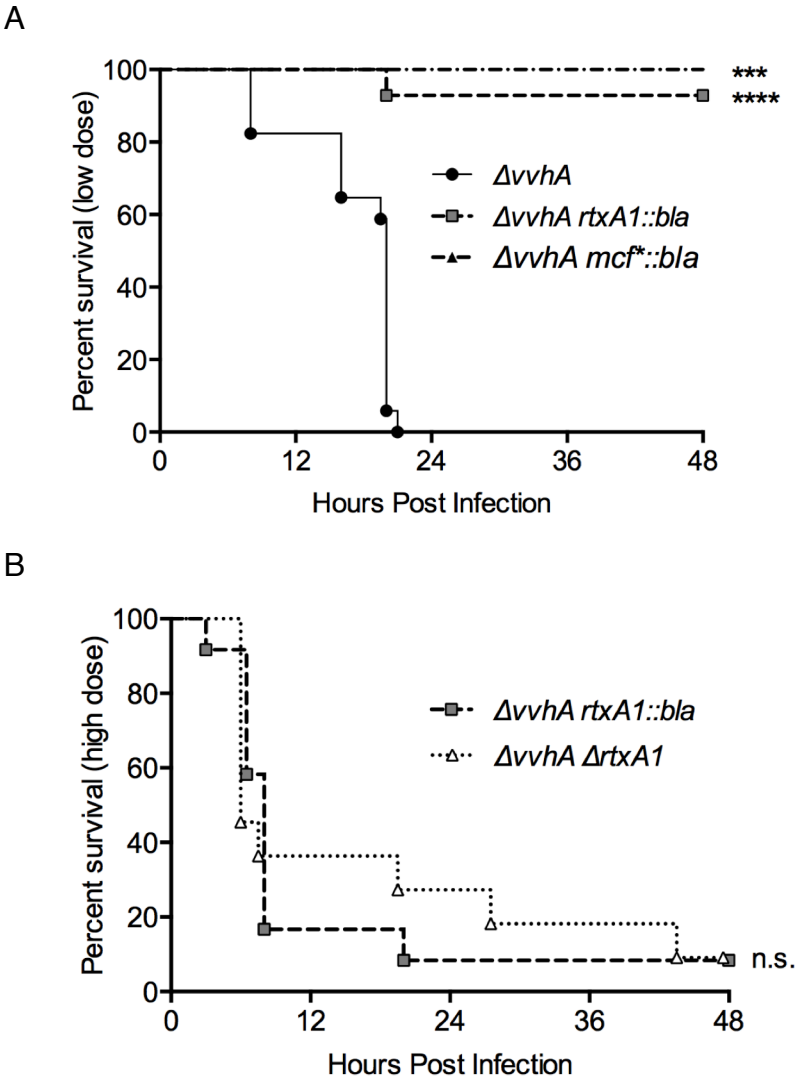

Figure 3.3. ***V. vulnificus*** **MARTX toxin effector domains confer virulence** ***in vivo.*** Mice infected i.g. with low dose (A, 2-5 x10^6 CFU) or high dose (B, 5-8 x 10^8 CFU) of the indicated strains were monitored over 48 hours for survival. Statistical significance was determined by log-rank test, ***p<0.001, ****p<0.0001, n.s. = not significant. For low dose survival experiments in (A), mice were inoculated in three independent experiments. Total mice inoculated with *ΔvvhA* number n = 17 and for *ΔvvhA rtxA1*::*bla* number n = 14. In one of those experiments, n = 5 mice were inoculated with *ΔvvhA mcf**::*bla*. For high dose survival experiments in (B), mice were inoculated in two independent experiments with *ΔvvhA rtxA1*::*bla* (total n = 12) and *ΔvvhA ΔrtxA1* (total n = 11).

Although the effector-free MARTX toxin expressed by *ΔvvhA rtxA1::bla* is sufficient to cause necrotic cytotoxicity *in vitro*, the kinetics of this process are delayed in the absence of MARTX toxin effector domains (Chapter 2) (30). Therefore, slower cell lysis kinetics could contribute to the observed virulence attenuation of *ΔvvhA rtxA1::bla* compared to *ΔvvhA*. If this correlation held true, it should then follow that a strain with intermediate MARTX-dependent lysis kinetics would exhibit intermediate virulence.

Our laboratory recently generated and described a *V. vulnificus* strain possessing a catalytically-inactive MCF-like effector domain integrated into the *rtxA1::bla* gene (31). This strain thus produces the toxin variant RtxA1::MCF*Bla (Figure 3.1) In this strain, the physical presence of the inactive effector domain stimulates the rate of *in vitro* cell lysis to a level intermediate that of *ΔvvhA rtxA1::bla* and *ΔvvhA* (31). However, the *ΔvvhA mcf*::bla* strain was completely attenuated during i.g. infection and showed no increased lethality above that of the *ΔvvhA rtxA1::bla* strain (Figure 3.3). Despite exhibiting intermediate *rtxA1*-dependent lysis kinetics *in vitro*, this strain does not exhibit intermediate virulence. Therefore, lysis kinetics do not correlate to strain virulence potential.

Collectively, these studies indicate that the ability of a given *V. vulnificus* strain to induce lysis *in vitro* does not correlate with bacterial virulence for i.g. inoculated mice. Rather, MARTX effector domains delivered by the holotoxin, while not required for cell lysis, are essential for MARTX toxin-associated virulence.

MARTX effector domain region is required for bacterial dissemination

It is known that detection of bacteria in the liver and spleen correlates with lethality in mouse models of *V. vulnificus* infection (138, 139). Clinically, outcomes of *V. vulnificus* human infection are considerably worse once the infection has become septic (103). Therefore, bacterial dissemination from the initial site of the infection constitutes a key step in *V. vulnificus* pathogenesis. Moreover, the *rtxA1* gene has been linked to the dissemination process (1, 136, 249).

To examine the role of MARTX toxin effector domains in *V. vulnificus* intestinal colonization and dissemination, we inoculated mice i.g. with *ΔvvhA*, *ΔvvhA rtxA1::bla,* or *ΔvvhA ΔrtxA1* at the same dose used to determine relative virulence of these strains. Knowing that initial lethality was observed approximately 8 hpi, we selected 6 hpi to euthanize mice and collect organs such that all mice could be examined prior to death. Isolated organs were homogenized and the resulting homogenate plated to determine the bacterial load per organ.

No differences in bacterial recovery from the intestine was detected across mice infected with *ΔvvhA, ΔvvhA rtxA1::bla* and *ΔvvhA ΔrtxA1* (Figure 3.4). Interestingly, this indicates that the bacterial load of the intestine at 6 hpi is independent not only of the MARTX toxin effector domains, but also of the entire toxin. Therefore, neither the MARTX toxin effector domain region nor the repeat regions influence intestinal bacterial load 6 hpi Moreover, early intestinal colonization does not account for virulence differences among the inoculated strains.

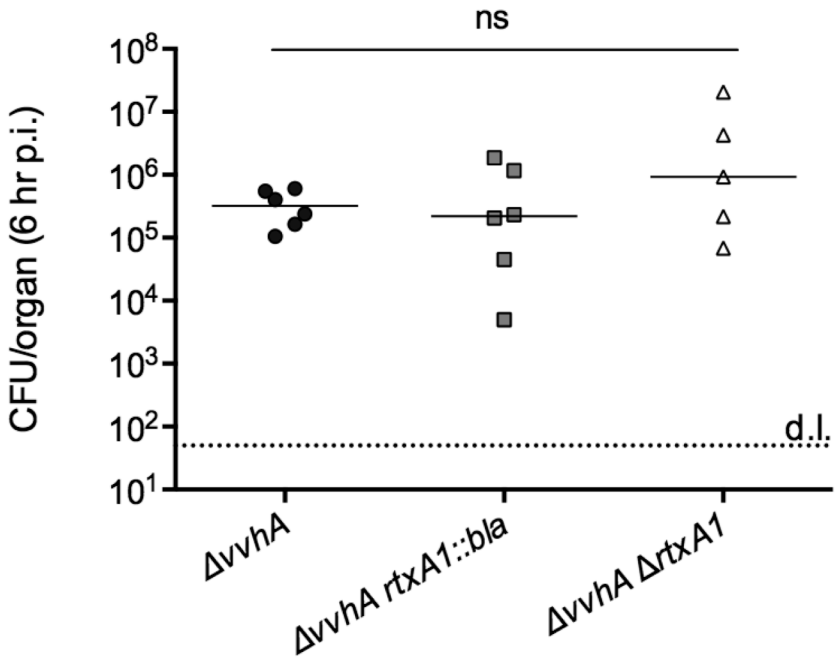

Figure 3.4. *rtxA1* is not required for *V. vulnificus* intestinal survival at 6 hpi Bacteria of the indicated strains recovered from plated tissue homogenate of the whole intestine at 6 hpi for 5-6 mice per group. Plot symbols represent CFU/organ for individual mice, lines represents mean. *d.l.,* detection limit. Data were analyzed by one-way ANOVA with Tukey post-test for multiple comparisons. n.s. = not significant. Total *n*=6 from data collected in two independent experiments.

Bacterial load in the liver and spleen of the same mice were also quantified at 6 hpi (Figure 3.5). While the *ΔvvhA* strain is detected in these organs at 2-5 x 10^4 CFU/organ, neither the *ΔvvhA rtxA1::bla* nor the *ΔvvhA ΔrtxA1* strain disseminated to this level. In fact, no colonies grew from the majority of liver and spleen homogenates from *ΔvvhA rtxA1::bla* or *ΔvvhA ΔrtxA1*-infected mice even when plated at a detection limit of 10 CFU/organ.

The inability to detect *V. vulnificus* in distal organs at a meaningful level in the absence of the MARTX toxin effector domain region reinforces the integral role of the MARTX toxin in *V. vulnificus* pathogenesis. In addition, this result indicates that lytic action conferred by MARTX toxin repeat regions is not sufficient to facilitate bacterial transit to distal organs. Rather, an intact MARTX toxin effector domain region is required for bacterial dissemination to, and/or survival in, distal organs including the liver and spleen.

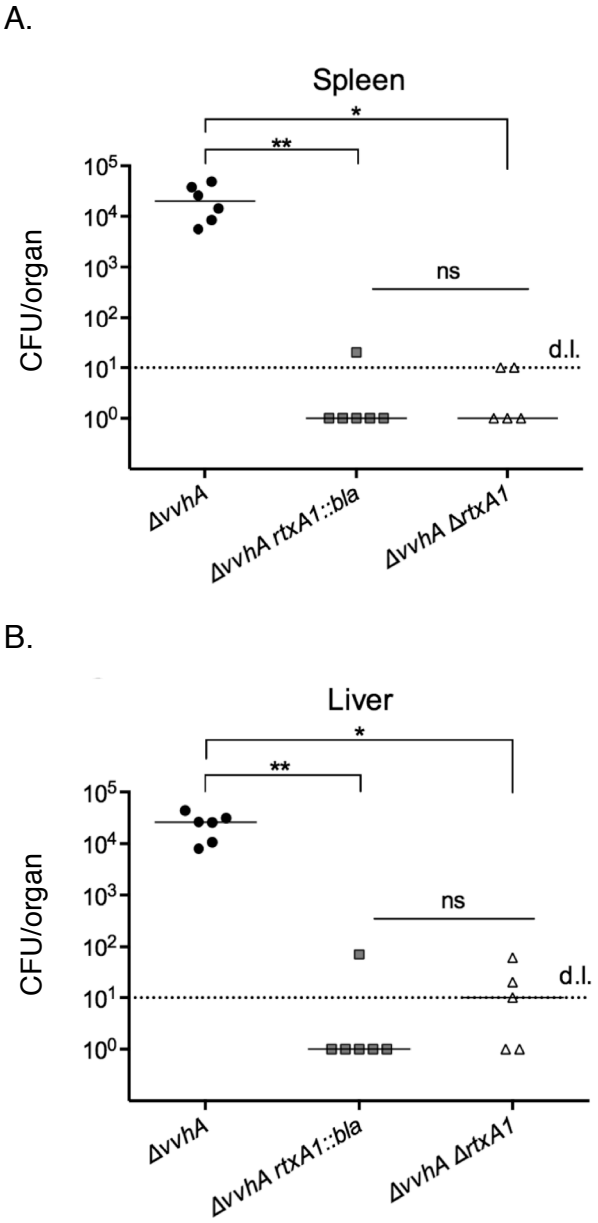

Figure 3.5. MARTX toxin effector domain region is required for bacterial dissemination from intestine to distal organs. Bacteria of the indicated strains recovered from plated tissue homogenate of the (A) spleen and (B) liver at 6 hpi for total 5-6 mice per group from two independent experiments. Plot symbols represent CFU/organ for individual mice, lines represents mean, and statistical significance was determined by one-way ANOVA followed by Tukey multiple comparison's test to determine *p* values. **p*<0.05, ***p*<0.01, ****p*<0.001, n.s. = not significant, d.l. = detection limit.

Neither overt intestinal tissue damage nor epithelial apoptosis is a prerequisite to *V. vulnificus* dissemination

Bacterial dissemination from the intestine to distal organs necessitates bacterial transit across the protective intestinal epithelial barrier from intestinal lumen to bloodstream, and resistance to immune defense mechanisms, particularly phagocytosis, encountered at each of these locations. While the MARTX toxin is known to facilitate bacterial resistance to phagocytosis (3, 163, 249), equivalent bacterial loads were observed in the intestines of mice at 6 hpi. Therefore at this time point, at least in the intestine, *V. vulnificus* are not differentially susceptible to immune clearance dependent upon *rtxA1,* though this occurs at later time points (1).

In previous studies, significant intestinal epithelial tissue damage has been observed in both mice and humans following i.g. *V. vulnificus* infection (1, 131, 132). This damage has subsequently been attributed to the additive function of secreted exotoxins VvhA and MARTX (1). To test the relationship between *ΔvvhA rtxA1::bla* lysis *in vitro,* intestinal epithelial damage during infection, and bacterial dissemination, mice were inoculated i.g. with the *ΔvvhA*, *ΔvvhA rtxA1::bla,* or *ΔvvhA ΔrtxA1* strains. At 6 hpi, the entire intestine was collected and analyzed with hemotoxalin and eosin (H/E) staining.

Surprisingly, no significant pathology was observed in any intestinal tissues at 6 hpi The epithelia remain intact in 4/4 *ΔvvhA*-infected mice, 3/4 *ΔvvhA rtxA1::bla*-infected mice, and 3/3 *ΔvvhA ΔrtxA1*-infected mice (Figure 3.6). In 1/4 *ΔvvhA rtxA1::bla*-infected mice, the intestine showed observable bacterial staining in the lumen and the small intestinal epithelium showed some damage at villous tips (Figure 3.6). This outlier sample demonstrates that rare events

resulting in rapid bacterial expansion can lead to epithelial damage and supports a model in which bacterial outgrowth in the intestine at later infection time points (8-12 hpi) indeed causes pathological changes, as previously shown (1). However, this event was not representative. Therefore, we conclude that *V. vulnificus* does not induce extensive intestinal epithelial necrosis by 6 hpi and the overt damage previously observed during later infection or in neutropenic mice is not solely responsible for dissemination (1, 132).

The intestine was imaged along the entire longitudinal axis, and no section-specific damage was observed anywhere from the proximal to distal gut. These results refute the idea that extensive necrosis and inflammation of the ileum is required for bacterial dissemination. With these methods, we cannot completely rule out the presence of localized foci of bacterial growth or epithelial damage. It remains possible that these exist and are either too small or too sporadic to be observed by histology. Nonetheless, we did not observe the same damage seen in previous mouse and human histology, despite known bacterial dissemination. This indicates that the MARTX toxin effector domain region facilitates bacterial dissemination even in the absence of such fulminant intestinal tissue damage.

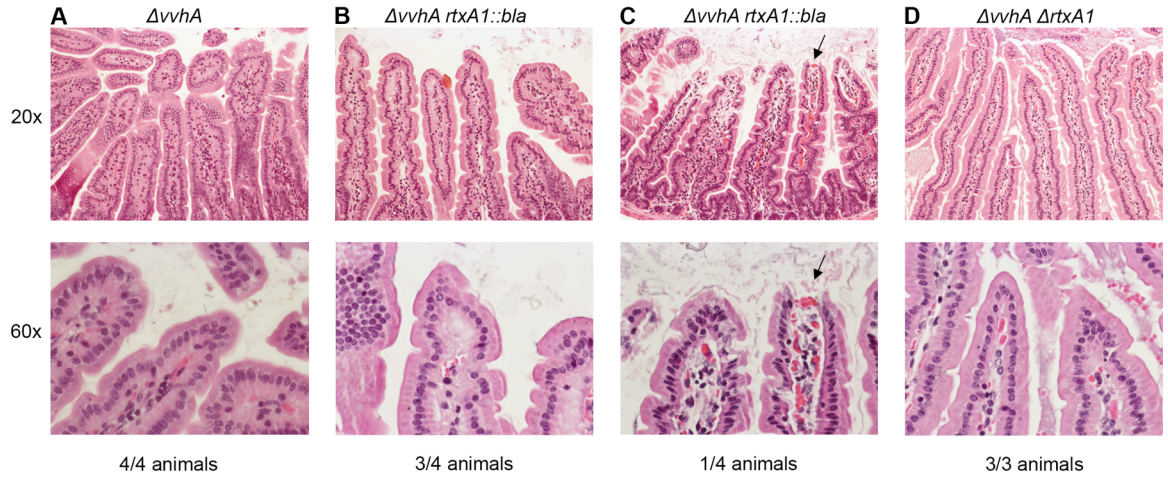

Figure 3.6. Intestinal tissue pathology is not a prerequisite to *V. vulnificus* dissemination. Histological cross sections at 20x (top row) and 60x (bottom row) from swiss-rolled, H&E-stained small intestines of 3-4 mice each inoculated i.g. with 2-5 x 10^6 CFU of bacterial strains as indicated at top. All samples were analyzed and photographs taken by Dr. Nike Beubier; representative images for each condition are shown.

The absence of fulminant intestinal tissue pathology during i.g. *V. vulnificus* infection suggested that the bacterium might instead be inducing localized apoptosis of intestinal epithelial cells rather than lysis. Indeed, it has been reported that *V. vulnificus* can induce mitochondrial-mediated apoptosis in an *rtxA1*-dependent manner (247). Apoptotic cells can be observed by an experienced pathologist in H&E stains tissue sections at high magnification. However, no major differences among tissue samples were observed in the examined H&E sections.

Nonetheless, this result was confirmed using an apoptosis-specific stain (Figure 3.7). The same embedded intestinal tissue used for H/E staining were also stained for cleaved caspase-3. Sporadic apoptosis is observed in the intestinal epithelial layer as indicated by positive staining for cleaved caspase-3 (Figure 3.7). However, no gross differences were observed dependent upon *rtxA1*. Therefore, differences in apoptosis do not account for differences in bacterial dissemination among *V. vulnificus* strains and do not provide a mechanism by which epithelial breach is occurring.

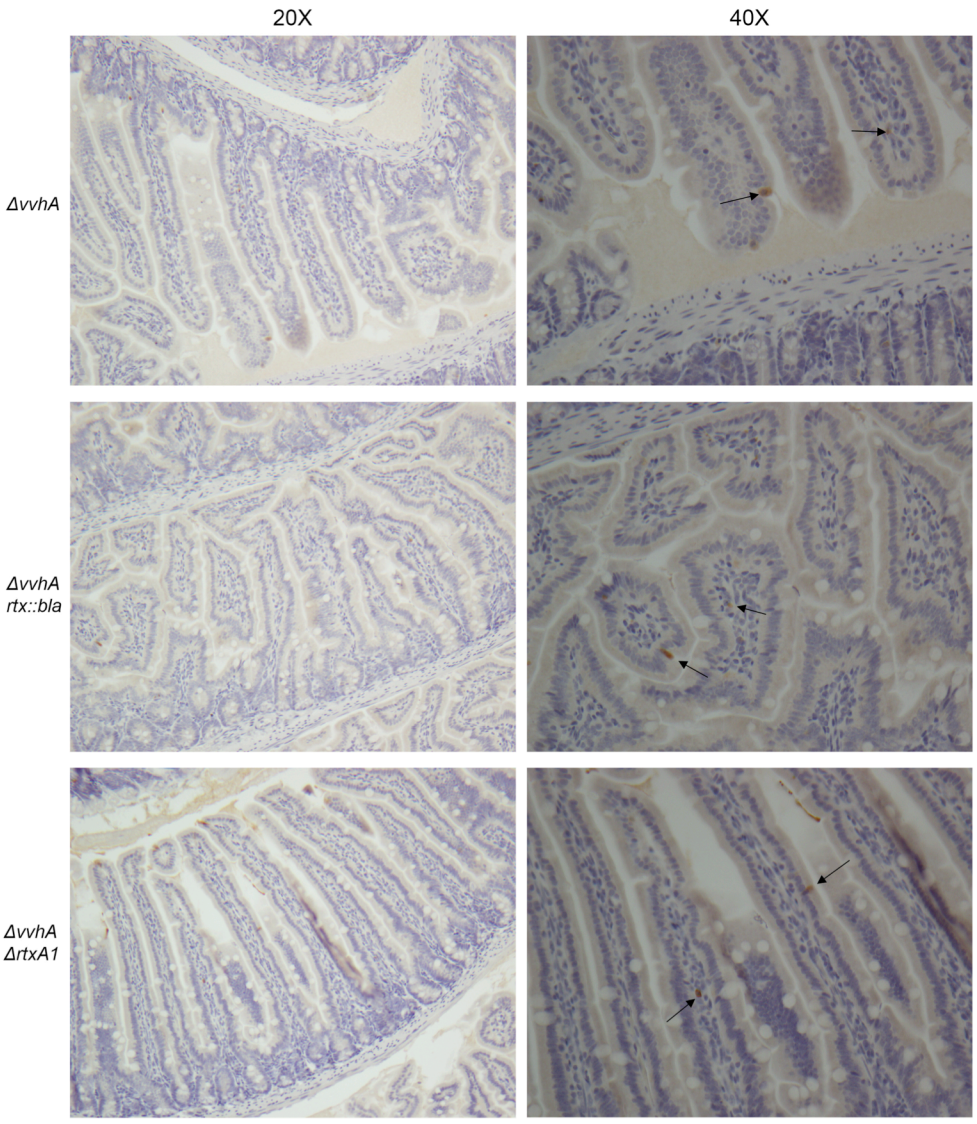

Figure 3.7. MARTX toxin effector domains do not induce increased intestinal epithelial apoptosis. Histological cross sections at 20x (left) and 40x (right) from swiss-rolled, cleaved-caspase-3 stained small intestines. Shown are representative images from a single mouse; in total 3-4 mice were each inoculated i.g. with 2-5 x 10^6 CFU of bacterial strains as indicated at left. Photographs taken by Dr. Nike Beubier.

Bacterial dissemination does not induce organ pathology

Previous studies have linked *V. vulnificus* dissemination from the intestine to the liver and spleen with lethal infection outcomes (138, 139). To assess organ damage, the spleen and liver were isolated from mice infected with *ΔvvhA*, *ΔvvhA rtxA1::bla,* or *ΔvvhA ΔrtxA1* at 6 hpi and assessed by histological examination. Despite the presence of $>10^4$ CFU *ΔvvhA* in the spleen and liver of infected mice (Figure 3.5), these organs retain their normal morphology at 6 hpi and tissues do not exhibit overt pathology (Figure 3.8). Therefore, disseminated *V. vulnificus ΔvvhA* do not induce direct spleen and liver organ damage at 6 hpi, despite the rapid onset of animal mortality beginning at 8 hpi Absent overt pathology in the form of either tissue necrosis or apoptosis, we reasoned that the changes induced by *V. vulnificus* MARTX to facilitate bacterial dissemination and associated lethality must be more subtle and not dependent on gross effects observable by pathology.

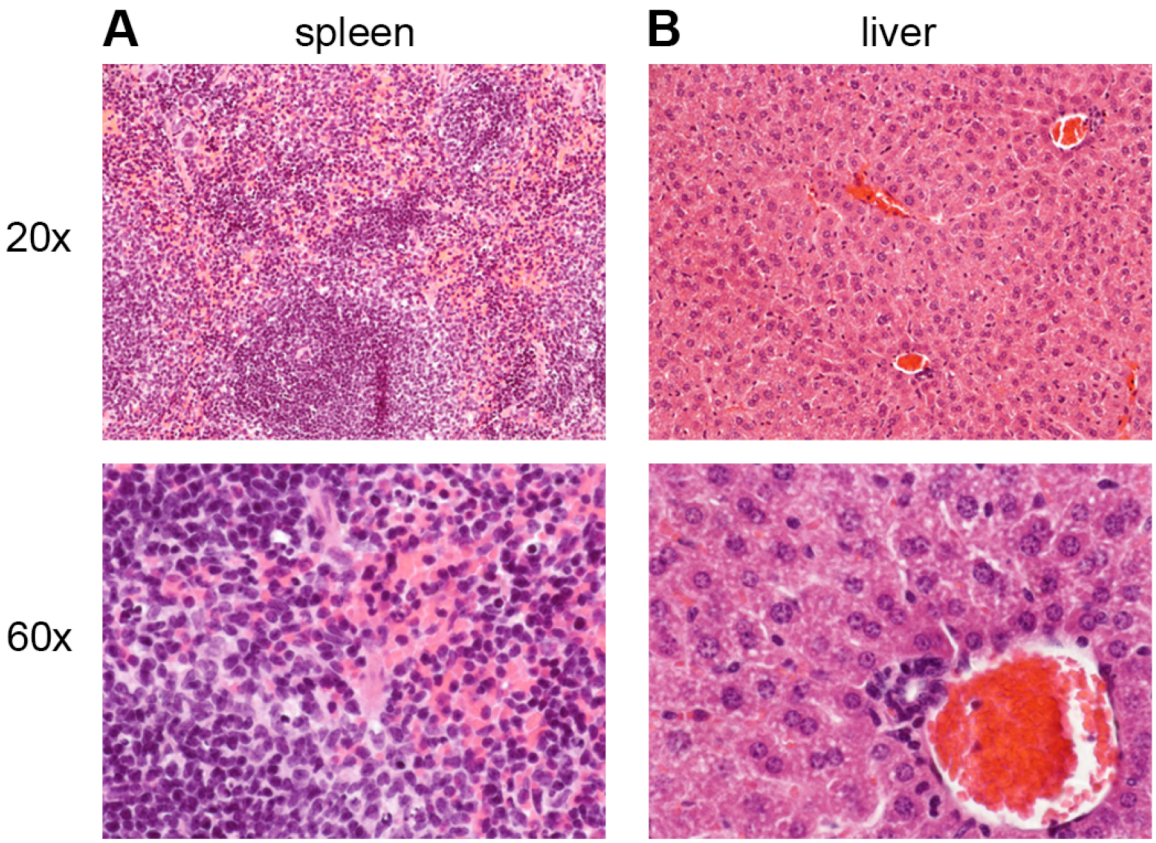

Figure 3.8. Disseminated bacteria do not induce organ pathology at 6 hpi
Histological cross sections at 20x (top row) and 60x (bottom row) from H&E-stained (A) spleen and (B) liver of mice inoculated i.g. with 5 x 10^6 CFU of *ΔvvhA* strain. Representative images from a single animal are shown. However, images from the total 3-4 mice per group were analyzed by pathologist Nike Beubier.

The MARTX toxin rapidly disrupts transepithelial resistance *in vitro*

Previous work that predominantly focused *V. vulnificus* research on cell lysis extensively used lactate dehydrogenase (LDH) release from nonconfluent, adherent epithelial cell monolayers as an *in vitro* system for MARTX-dependent cytotoxicity (Chapter 2) (1, 30, 136, 246, 305). For a more relevant three-dimensional culture model to monitor intestinal epithelial barrier breach events *in vitro*, the interaction between *V. vulnificus* and polarized confluent T84 colonic epithelial cells was studied (Figure 3.9). T84 cells were cultured as monolayers in transwells to transepithelial resistance (TER) of ≥1000 $\Omega*cm^2$. Log phase bacteria were added to the apical surface to mimic luminal i.g. bacterial exposure.

To determine appropriate MOI, a calculation of *in vivo* intestinal MOI was performed. These calculations assume homogenous distribution of bacteria along the length of the intestine, and use data from two separate experiments to capture a theoretical *in vivo* MOI range. Notably, localized differences in bacterial burden likely occur in the context of actual intestinal infection. Nonetheless, on average the numbers utilized in this study are supported by experimental colonization data, as outlined below. Together, the two *in vivo* studies used for calculations capture a theoretical MOI range of 0.001 – 12.5 CFU/cell.

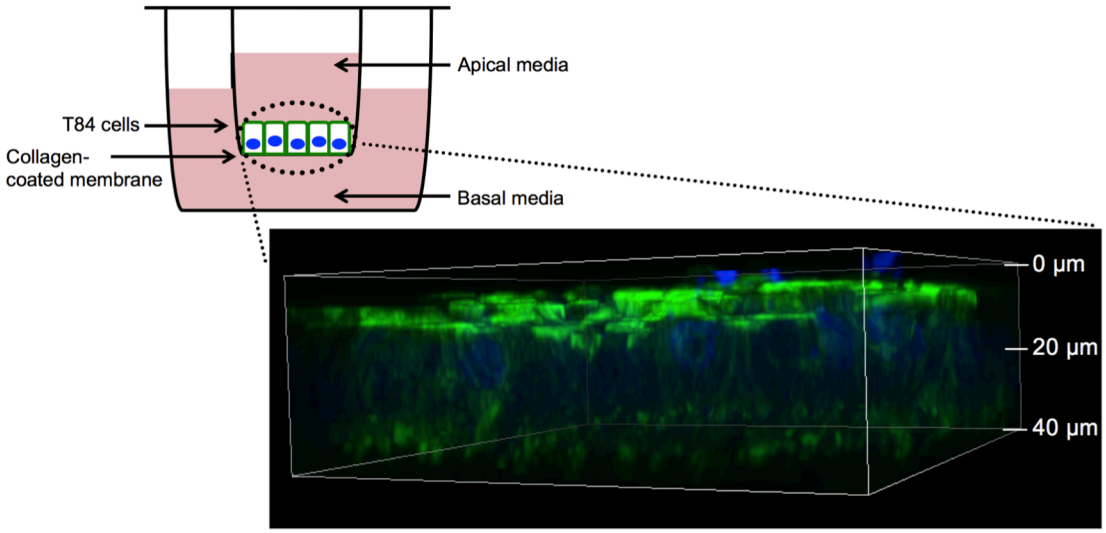

Figure 3.9. Polarized T84 monolayer for modeling the intestinal epithelium *in vitro*. Schematic representation and representative 3-D confocal microscopy image of untreated T84 monolayer stained for nuclei (DAPI, blue) and actin (phalloidin AlexaFluor 488, green).

Calculation A: MOI based upon 8 hpi bacterial burden in the mouse small intestine

The intestine of an average mouse of 35-45 grams has, in the jejunum (25):

$$Epithelial\ cell\ density: 1.90 * 10^7 \frac{cells}{cm^2}$$

Based upon the average of 4 and 6-week old age groups outlined in (29), the 32-38 day mice used in the current study (average 5-week) mice in this study should have an external intestinal epithelial surface area of:

$$Surface\ area = 21 \frac{cm^2}{small\ intestine}$$

Therefore, the total number of cells in the small intestinal epithelium is:

$$\begin{aligned} \#\ cells &= cell\ density * surface\ area \\ &= (1.90 * 10^7 \frac{cells}{cm^2}) * 22\ cm^2 \\ &= 40 * 10^7\ cells \end{aligned}$$

According to unpublished lab data from a previous study (1), the small intestinal bacterial burden of a mouse lethally infected with *V. vulnificus ΔvvhA* at 8 hpi is approximately:

$$Bacterial\ burden: 5 * 10^9\ CFU$$

To estimate small intestinal MOI *in vivo:*

$$\begin{aligned} MOI &= bacterial\ burden/\#\ of\ cells \\ &= (5 * 10^9\ CFU)/(40 * 10^7\ cells) \\ &= 12.5 \frac{CFU}{cell} \end{aligned}$$

Calculation B: MOI based upon 6 hpi bacterial burden in the whole intestine

This study examines bacterial burdens in the whole intestine, so the cells in the colon must be taken into account:

Surface area of the colon (29):

$$Surface\ area = 7.6 \frac{cm^2}{colon}$$

Epithelial cell density of colon (25):

$$Cell\ density = 8.98 * 10^6 \frac{cells}{cm^2}$$

Therefore, the total number of cells in the colon is:

$$\begin{gathered} \#\ cells = cell\ density * surface\ area \\ = (8.98 * 10^6 \frac{cells}{cm^2}) * 7.6\ cm^2 \\ = 6.8 * 10^7\ cells \end{gathered}$$

Total number of cells in the whole intestine:

$$\begin{gathered} Total\ cell\ \# = cell\ \#_{small\ intestine} + cell\ \#_{colon} \\ = (42 * 10^7 cells) + (6.8 * 10^7 cells) \\ = 49 * 10^7 cells \end{gathered}$$

Moreover, bacterial burden in this study is examined at an earlier time point:
Bacterial burden in the intestine at 6 hpi:

$$Bacterial\ burden = 5 * 10^5\ CFU$$

Thus the estimated MOI of whole intestine based on these colonization numbers is:

$$\begin{gathered} MOI = bacterial\ burden/\#\ of\ cell \\ = \frac{5 * 10^5\ CFU}{49 * 10^7\ cells} \\ = 0.001 \frac{CFU}{cell} \end{gathered}$$

The *in vivo* MOI range was then utilized to calculate *in vitro* MOI for different doses of bacteria applied apically. These bacterial doses were subsequently used for preliminary T84 dosing experiments (Figure 3.10). Noting that T84 dysfunction was induced *in vitro* at MOI=0.26, subsequent experiments were carried out at either MOI=0.26 or MOI=2.6, both within the reasonable calculated range for putative *in vitro* MOI.

Calculation C: *In vitro* MOI

To calculate MOI *in vitro,* the number of cells in a mature confluent monolayer was determined, using trypsin/ETDA to dissociate cells from the collagen-coated membrane. Subsequently, the MOI of a range of bacterial doses was determined:

T84 MOI at 10^1 CFU:

$$\frac{1 * 10^1\ CFU}{3.8 * 10^5 \pm 0.5\ cells} = 0.000026\ \frac{CFU}{cell} or\ 1\ CFU/38{,}461\ cells$$

T84 MOI at 10^7 CFU:

$$\frac{(1 * 10^7\ CFU)}{3.8 * 10^5 \pm 0.5\ cells} = 26\frac{CFU}{cell}$$

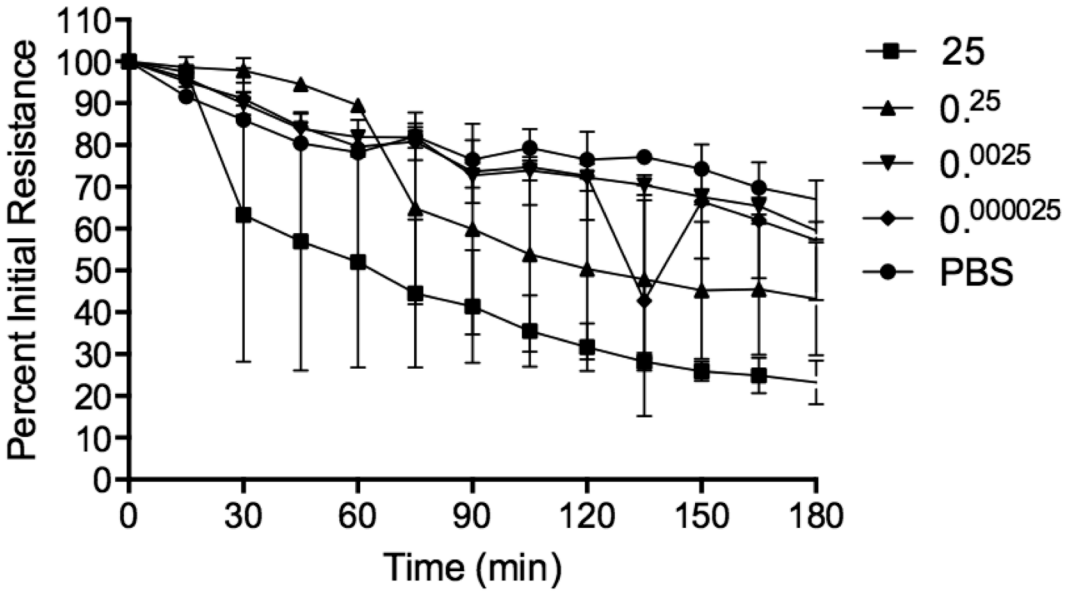

Figure 3.10. Epithelial dysfunction is observed with *V. vulnificus* MOI between 0.25 and 25. T84 monolayers (2/dose) exposed to CMCP6 over the indicated MOI range. Data represent mean percent initial resistance ± s.d. Data were not statistically analyzed due to insufficient replicate number.

Initial experiments examined the individual contributions of *vvhA* and *rtxA1* to characterize interactions between the epithelial monolayer and bacterial exotoxins *in vitro* (Figure 3.11). When applied to the apical surface of T84 monolayers, CMCP6 rapidly induced intestinal barrier dysfunction as demonstrated by a 50% decrease from initial TER after 60 minutes and more than 80% drop over 210 minutes. T84 monolayers exposed to *V. vulnificus ΔvvhA* exhibited a drop in TER identical to monolayers exposed to CMCP6. In contrast, T84 monolayers exposed to *ΔrtxA1* retained initial TER to nearly 90 minutes, exhibiting a significant delay and attenuation of TER disruption relative to CMCP6 and *ΔvvhA*-exposed monolayers. When monolayers were exposed to *ΔvvhA ΔrtxA1*, TER was maintained over the course of the experiment to the endpoint at 210 minutes and, over multiple experiments, often resulted in a rise in TER that may indicate a cellular response to bacteria in the absence of secreted toxin. Together these results reveal that both the VvhA hemolysin and MARTX toxin are sufficient for TER drop over a 3-hour time scale, but only the MARTX toxin accounts for the rapid loss of TER initiated shortly after addition of bacteria. Further, the contribution of VvhA that occurs after 120 min is not essential, additive or synergistic (Figure 3.11).

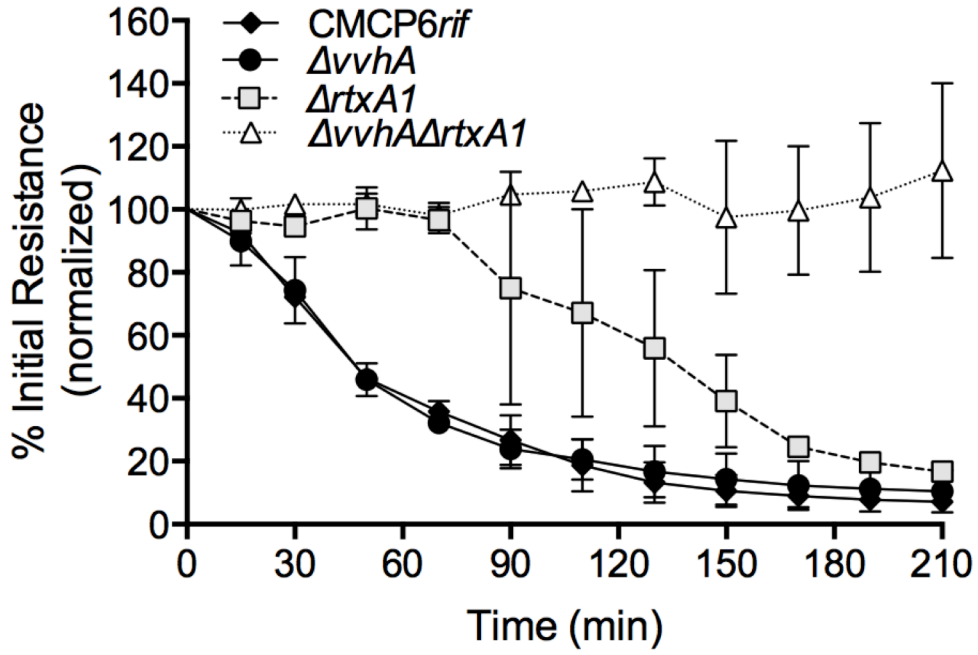

Figure 3.11. *vvhA* is not required for epithelial disruption, while *rtxA1* is required for induction of early monolayer dysfunction. TER of polarized monolayers (3 per condition) monitored over 180-210 minutes following apical exposure to the indicated strains of *V. vulnificus* at MOI≈2.6. Data expressed as percent initial resistance, relative to PBS-exposed monolayers.

MARTX toxin effector domains are essential for rapid loss of T84 monolayer TER

Having established the importance of the MARTX holotoxin in TER loss, the role of MARTX toxin regions was examined (Figure 3.12). T84 monolayers were co-incubated with *V. vulnificus ΔvvhA, ΔvvhA rtxA1::bla,* or *ΔvvhA ΔrtxA1*. Monolayers exposed to *ΔvvhA* dropped to 50% resistance in 60-75 minutes of co-incubation, as previously observed. However, the integrity of the monolayers exposed to *ΔvvhA rtxA1::bla* was maintained to approximately 100 minutes. Therefore, compared to the *ΔvvhA* strain, the *ΔvvhA rtxA1::bla* strain is significantly delayed in its ability to disrupt T84 monolayer integrity. T84 monolayers exposed to *ΔvvhA rtxA1::bla* for more than 100 minutes gradually exhibited a drop in TER, though TER loss induced by the *ΔvvhA rtxA1::bla* strain was attenuated throughout the duration of the experiment compared to that induced by *ΔvvhA*. Monolayers exposed to *ΔvvhA rtxA1::bla* strain were also distinct from the *ΔvvhA ΔrtxA1*-exposed monolayers, as the double mutant did not experience any disruption of TER. Thus, MARTX effector domains are necessary for rapid-onset monolayer disruption, but pore formation by the MARTX repeat regions is sufficient for T84 disruption past 100 minutes of co-incubation.

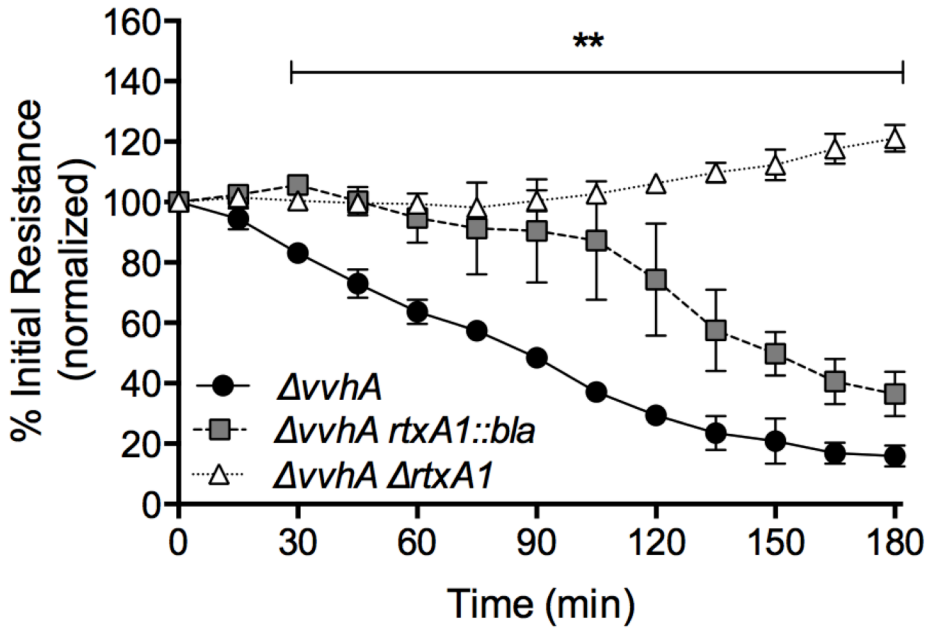

Figure 3.12. MARTX toxin effector domains rapidly induce intestinal barrier dysfunction *in vitro*. TER of polarized monolayers (3 per condition) monitored over 180 minutes following apical exposure to the indicated strains of *V. vulnificus* at MOI=2.6. Data expressed as percent initial resistance, relative to PBS-exposed monolayers. Data were analyzed by two-way ANOVA with statistically significant differences, as marked, compared for Δ*vvhA* to Δ*vvhA rtxA1*::*bla* across all the indicated time points, $^{**}p<0.01$

To test whether different toxin translocation and lysis kinetics previously observed in HeLa cells influenced bacterial interactions with T84 monolayers, the *ΔvvhA mcf*::bla* strain was again employed (Figure 3.13) (31). With the goal of observing even subtle differences between the strains, the applied dose was reduced 10-fold to MOI 0.25. However, even at this lower dose there was no detectable difference between the *ΔvvhA mcf*::bla* and *ΔvvhA rtxA1::bla*-exposed T84 monolayers. Both strains remained drastically attenuated in the ability to disrupt T84 TER compared to *ΔvvhA*. The *ΔvvhA* strain induced 50% TER loss by approximately 100 minutes – a delay relative to the 10-fold higher dose, but an increase relative to either of the strains lacking active MARTX effector domain regions. At the same 100-minute time point, monolayers exposed to *ΔvvhA mcf*::bla* or *ΔvvhA rtxA1::bla* retained approximately 90% initial resistance.

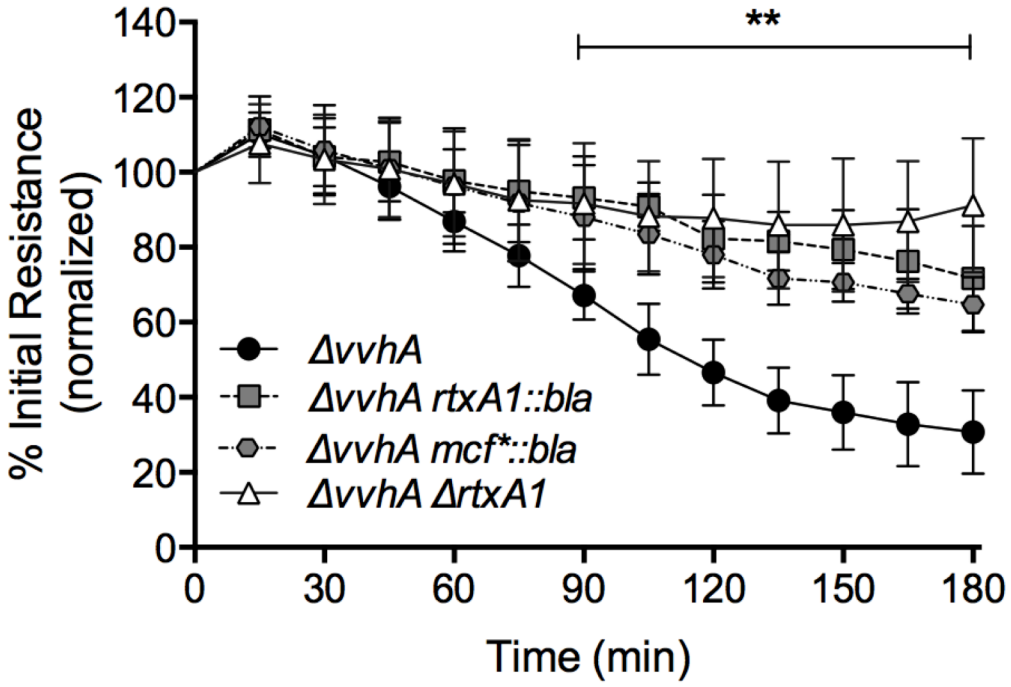

Figure 3.13. Initial polarized monolayer dysfunction does not correlate with unpolarized *in vitro* lysis kinetics. TER of polarized monolayers (3 per condition) monitored over 180 following apical exposure to the indicated strains of *V. vulnificus* at MOI=0.26. Data expressed as percent initial resistance, relative to PBS-exposed monolayers. Data were analyzed by two-way ANOVA with statistically significant differences, as marked, comparing for Δ*vvhA* to Δ*vvhA rtxA1*::*bla* or Δ*vvhA mcf**::*bla* across all the indicated time points, $^{**}p<0.01$

Surprisingly, this loss of TER by 60 mins was not due to overt actin depolymerization (Figure 3.14). Indeed, despite dropping to 45% initial resistance, the *ΔvvhA*-exposed monolayer exhibits actin morphology akin to the PBS control monolayers. Specifically, all samples retained characteristic honeycomb-like actin morphology in the *x*-*y* plane and columnar cellular structure in the monolayer *z*-plane. Therefore, the rapid initial loss of TER upon addition of *V. vulnificus* to T84 monolayers is not due to extensive loss of actin structure.

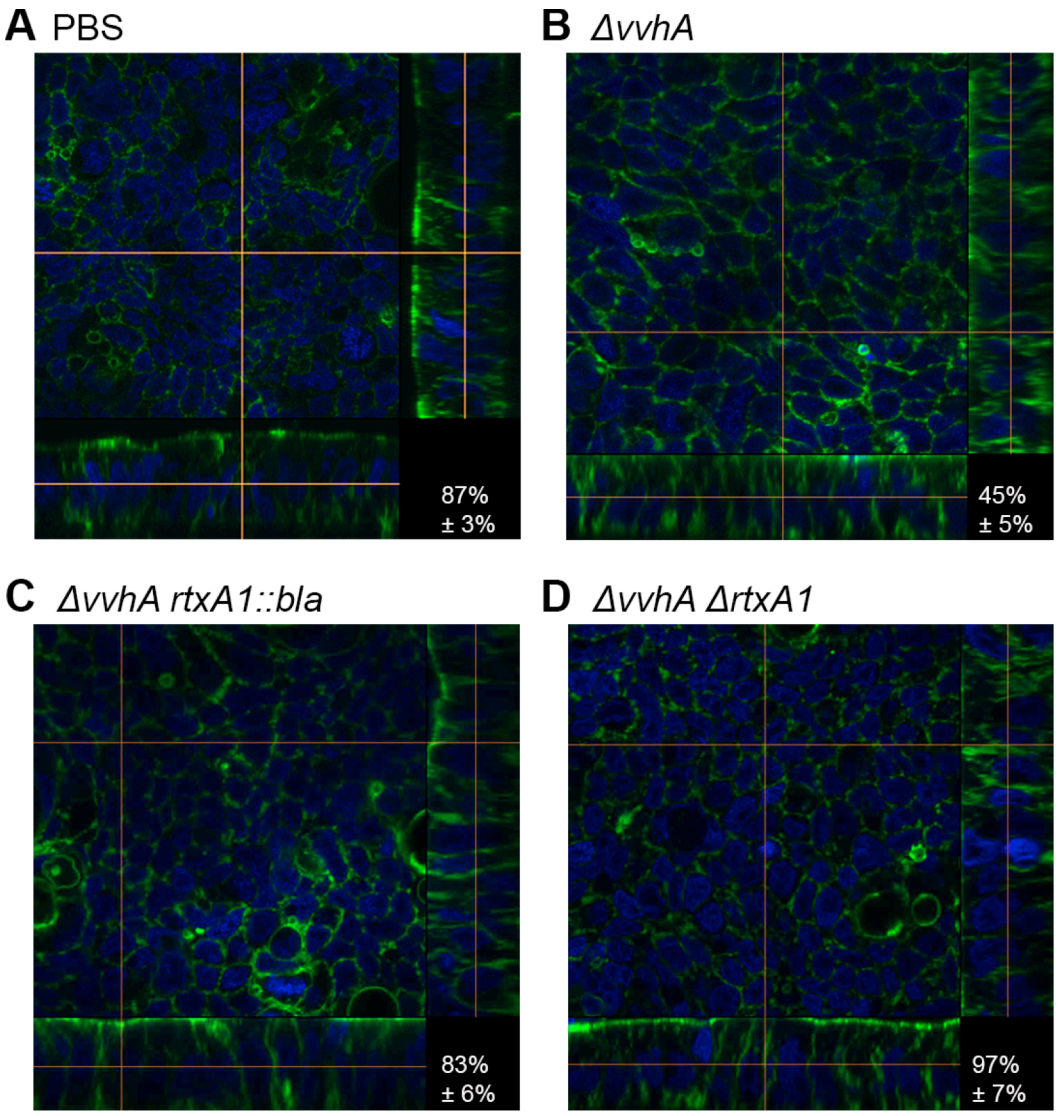

Figure 3.14. Cytoskeletal morphology is maintained during early barrier dysfunction at 60 mins. Confocal microscopy cross-section and *z*-stack images of T84 monolayers stained for nuclei (DAPI, blue) and actin (phalloidin AlexaFluor 488, green) following exposure to (A) PBS (negative control); (B) *ΔvvhA;* (C) *ΔvvhA rtxA1::bla;* or (D) *ΔvvhA ΔrtxA1*. Mean percent initial resistance ± s.d. for three monolayers per strain is indicated in the lower right corner of each panel.

The MARTX toxin induces a biphasic disruption of paracellular epithelial permeability

A common mechanism by which the integrity of a monolayer can be compromised is disruption of cell-cell junctions that results in increased paracellular permeability. To examine mechanisms of MARTX-induced barrier dysfunction, paracellular permeability to small molecules was examined with use of a fluorescently tagged, 3-kD dextran. The molecule cannot pass through cells and is likewise typically excluded from passing between cells by tight junctions. However, when intercellular junctions are disrupted, the dextran molecule gains passage between cells. Following application of dextran to the apical transwell chamber, PBS or bacteria were added to monolayers and basal media was sampled for dextran transit over time.

Appreciably greater amounts of dextran were sampled from the basal media of *ΔvvhA*-exposed monolayers compared to monolayers exposed to *ΔvvhA rtxA1::bla,* or *ΔvvhA ΔrtxA1* (Figure 3.15). Neither PBS mock-exposed nor *ΔvvhA ΔrtxA1*-exposed monolayers allowed more than 0.09 μg of dextran to cross from the apical to the basal compartment of the T84 transwells over the tested 180 minute timecourse. Similarly, a maximum of 0.15 μg of dextran was detected in *ΔvvhA rtxA1::bla*-exposed monolayers. However, the *ΔvvhA*-exposed monolayers allowed passage of 0.45 +/- 0.01 μg of fluorescent dextran (Figure 3.15, A).

A

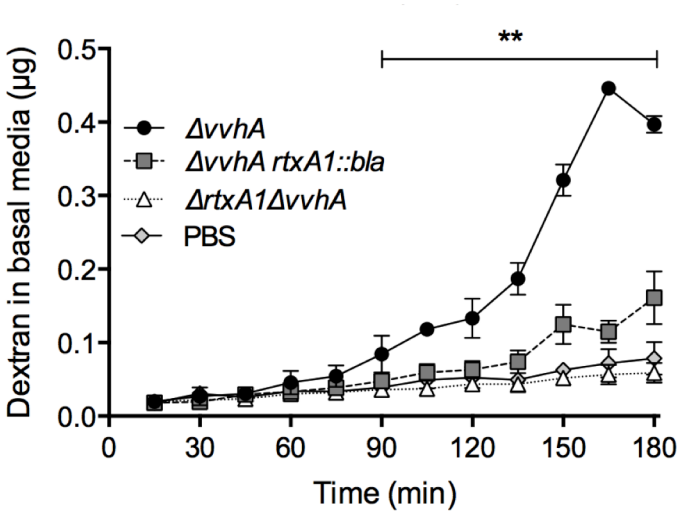

B

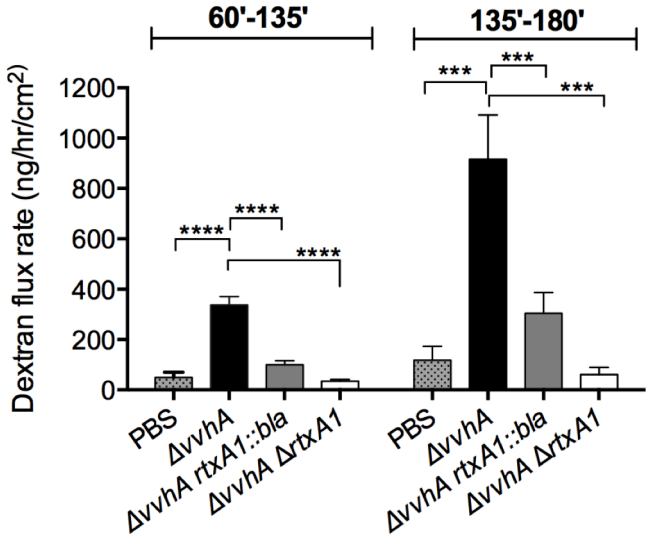

Figure 3.15. MARTX toxin induces a biphasic increase in epithelial paracellular permeability. (A) Amount of fluorescently labeled, 3-kD dextran in basal media of polarized T84 monolayers (3 per condition) following exposure to the indicated strains at MOI=2.6. Data analyzed by two-way ANOVA. (B) Biphasic dextran flux rates observed during *V. vulnificus* exposure, derived from the slope of the dextran curves displayed in panel A, from 60-135 minutes (left) or 135-180 minutes (right). Data were analyzed by one-way ANOVA followed by Tukey post-test test to determine *p* values; ***p*<0.01, ****p*<0.001, *****p*<0.0001.

In *ΔvvhA*-exposed transwells, an upward trend in basal dextran levels began between 45 and 60 minutes. By 90 minutes, significant differences in dextran transit between the *ΔvvhA* monolayers and all other monolayers were evident (Figure 3.15). In contrast, only basal levels were observed in *ΔvvhA rtxA1::bla* and *ΔvvhA ΔrtxA1*-exposed monolayers prior to 135 minutes. From 135-180 minutes, increased levels of dextran were sampled from the basal media of monolayers exposed to *ΔvvhA rtxA1::bla* compared to *ΔvvhA ΔrtxA1* or PBS-exposed monolayers, though these amounts were still considerably less than the basal dextran sampled from *ΔvvhA*-exposed monolayers.

These *in vitro* monolayer experiments revealed that both TER disruption and dextran flux exhibit biphasic characteristics. Specifically, the *ΔvvhA* strain caused rapid decay of TER, while *ΔrtxA1* and *ΔvvhA rtxA1::bla* (Figure 3.12) caused only late onset TER disruption. The *ΔvvhA* strain rapidly induced paracellular permeability, but the rate of dextran flux between 135 and 180 minutes (900 ng/hr/cm^2) was significantly greater than the flux rate from 60-135 minutes (350 ng/hr/cm^2) (Figure 3.15, B). In *ΔvvhA rtxA1::bla*-exposed monolayers, dextran flux rates were significantly greater in the 135-180 minute time frame (300 ng/hr/cm^2) compared to 60-135 minutes (100 ng/hr/cm^2). Overall, it was concluded that the MARTX toxin, when interacting with a polarized columnar monolayer, exerts two MARTX-dependent mechanisms of barrier disruption: one shortly after addition of bacteria and mediated by the effector domains and one later after addition of bacteria linked to the repeat regions.

Late, but not early, onset TER disruption coincides with cell lysis

Since the repeat regions are known to be sufficient for lysis of unpolarized cells, the contributions of this region to T84 cell lysis was explored as a mechanism for late vs early onset

loss of TER. Monolayers were exposed to *ΔvvhA, ΔvvhA rtxA1::bla,* or *ΔvvhA ΔrtxA1*. Sixty minutes following bacterial application, resistance of the *ΔvvhA*-exposed monolayers dropped to 50% of initial while *ΔvvhA rtxA1::bla,* or *ΔvvhA ΔrtxA1* monolayers retained TER >90%, as observed in previous independent experiments (Figure 3.12). Monolayer cell lysis was measured by sampling lactate dehydrogenase (LDH) release to media in both the apical and basal transwell chambers and expressed relative to LDH release from monolayers treated with 0.1% Triton X-100. LDH release to the basal transwell chamber was never detected (Figure 3.16) so monolayer lysis was quantified using media sampled from the apical chamber. The absence of LDH in the basolateral chamber may also explain the absence of bacteria in the same compartment, if the lower edge of the monolayer and appendages filling the filter pores do not provide a clear path across a partially lysed monolayer (Figure 3.16).

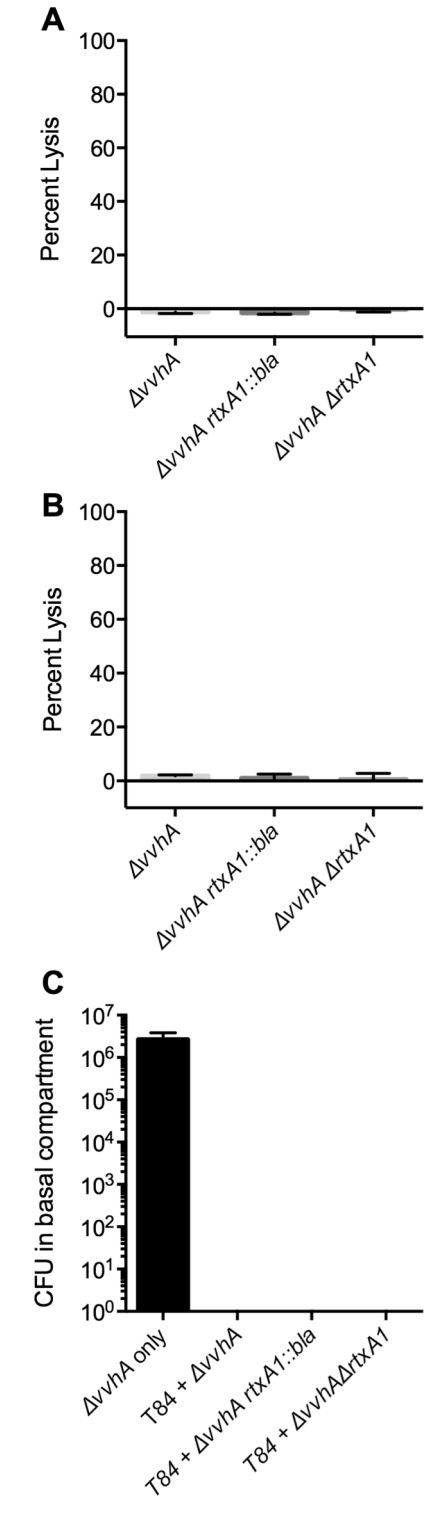

Figure 3.16. Neither LDH nor viable bacteria are recovered from the basal T84 transwell media. Percent lysis as measured by LDH release to the basal media of polarized T84 monolayers (3 per condition) at (A) 60 minutes or (B) 180 minutes. (C) Quantification of bacterial transmigration across transwell chamber membranes coated with collagen (marked *ΔvvhA* only) or collagen plus T84 cells. All data are reported as mean ± s.d.

Despite the large drop in TER in *ΔvvhA*-treated monolayers by 60 minutes, *ΔvvhA* cell lysis at 60 minutes averaged less than 10% and was no greater than the low levels likewise observed in PBS, *ΔvvhA rtxA1::bla,* or *ΔvvhA ΔrtxA1*-exposed monolayers (Figure 3.17). Therefore, rapid MARTX-dependent loss of TER by *ΔvvhA* occurs independent of cell lysis.

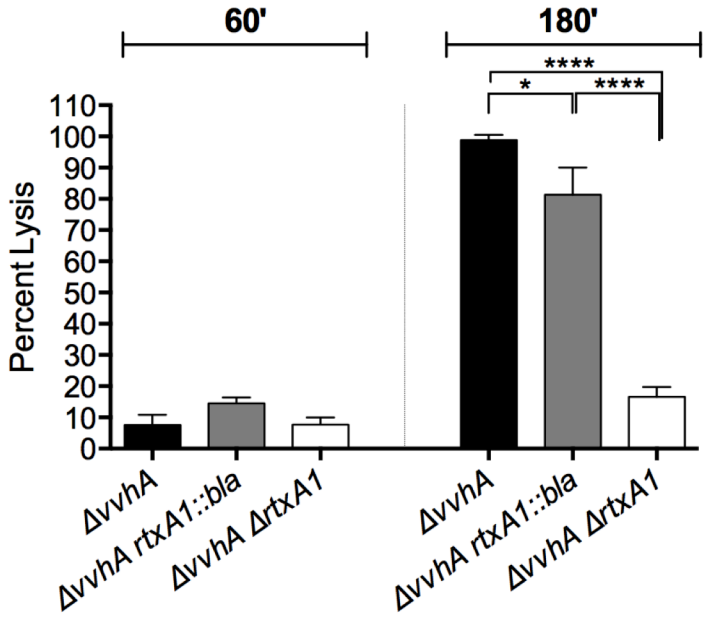

Figure 3.17. Early, effector-dependent monolayer dysfunction is lysis-independent while late, pore-dependent monolayer dysfunction corresponds to cell lysis. Lysis of polarized T84 monolayers, relative to samples treated with Triton X-100, at 60 minutes (left) and 180 minutes (right). Data were analyzed by one-way ANOVA followed by Tukey multiple comparison's test to determine *p* values; *$p<0.05$, ****$p<0.0001$.

By contrast, at 180 minutes following bacterial application, *ΔvvhA*-exposed monolayers retained just 10% initial resistance, *ΔvvhA rtxA1::bla*-exposed monolayers exhibited 50% initial resistance, and *ΔvvhA ΔrtxA1*-exposed monolayer resistance had increased to 180% initial. At this late timepoint, *ΔvvhA ΔrtxA1* lysis levels remained <20% while both *ΔvvhA* and *ΔvvhA rtxA1::bla* induced lysis exceeding 80% of cells in the monolayer. Therefore, T84 cell lysis occurred after prolonged monolayer exposure and corresponds to increased dextran flux and TER loss in both *ΔvvhA* and *ΔvvhA rtxA1::bla*-exposed monolayers.

At these later time points, bacterial MOI was increased 10-fold (135 minutes) or 25-fold (180 minutes) of the originally inoculated MOI (Figure 3.18), indicating that the lysis-dependent phase of monolayer disruption coincides with highly increased bacterial and toxin burden. Notably, the early phenotypes observed in this study were seen at doses 4-40-fold lower than previous studies using MOI in the 10-100 range. Combined, these observation support a model in which the MARTX effector domains induce cytopathic and physiological disruption rapidly and effectively at relatively low MOI (~0.25-2.5) while lytic effects of the MARTX pore are observable only at later time points because they require higher bacterial MOI and the accompanying higher toxin concentration.

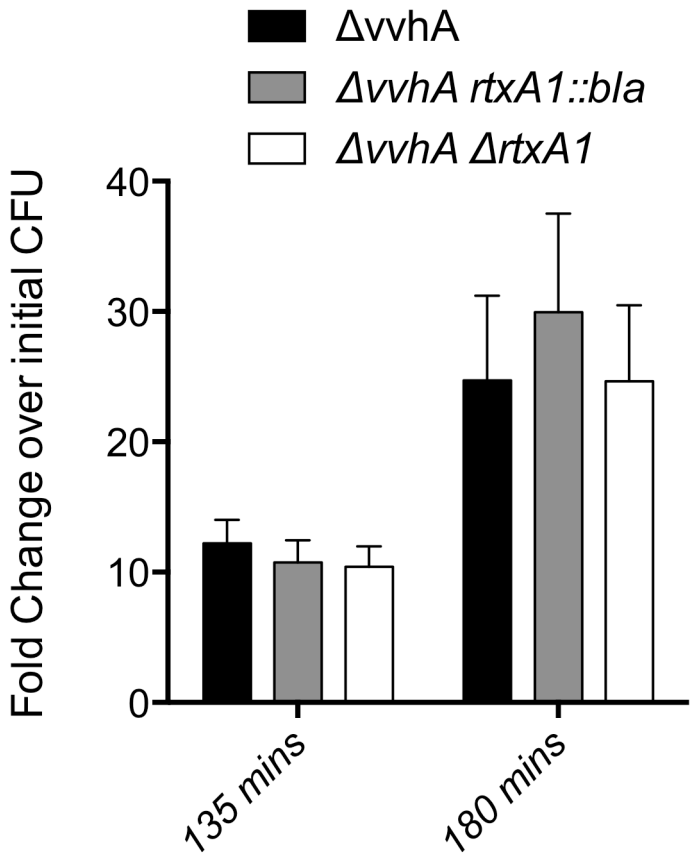

Figure 3.18. MOI increases over the course of T84 co-incubation experiments. Bacterial CFU were quantified by dilution and selective plating from the apical chamber of 3 independent T84 monolayers for each of the indicated strains at either 135 minues or 180 minutes into the co-incubation. Data at each timepoint were analyzed by one-way ANOVA with no resulting statistical differences.

Discussion

The important role of the MARTX toxin product of the *rtxA1* gene as a virulence factor during *V. vulnificus* infection has now been appreciated for nearly a decade (245). This potent cytotoxin has been linked to induction of multiple forms of cell death *in vitro* (136, 246, 247). During i.g. infection, fulminant intestinal tissue damage has been observed. Moreover, bacterial dissemination and sepsis are phenotypes intimately linked to lethal infection outcomes (103, 122, 132, 138, 139). Together, these data have led to a prevailing model that massive toxin-mediated destruction of the intestinal epithelial barrier is the key mechanism by which *V. vulnificus* exits the intestine culminating in lethal sepsis. The data presented here indicate a paradigm shift in our conceptual understanding of early *V. vulnificus* transmigration of the intestinal epithelial barrier. It was previously thought that secreted toxins must contribute to bacterial outgrowth in the intestine and fulminant intestinal damage that subsequently allowed for bacterial dissemination. Here, we have shown that the cytopathic activities of the MARTX toxin initiate dissemination earlier than previously appreciated and the early mechanisms involved are far more subtle in nature.

In studying the contribution of MARTX toxin regions to holotoxin function, we previously identified the MARTX repeat regions as sufficient for cellular necrosis (Chapter 2) (30). Yet, during intestinal infection of mice, bacteria that produce the effector-free MARTX toxin were more akin to an *rtxA1*-null mutant than the strain making lytic MARTX holotoxin (Figure 3.3). Thus, it is the effector domains that, when delivered in the MARTX toxin context, confer MARTX-mediated virulence during i.g. *V. vulnificus* infection (Figure 3.19). Notably, genetic and biochemical functional characterization of MARTX toxin complexity previously lent

hypothetical support to this result. Yet, these data represent the first direct experimental evidence that non-lytic functions previously attributed to the MARTX toxin (such as cytoskeleton disassembly, induction of apoptosis, inhibition of autophagy, and modulation of stress signaling (4, 21, 27, 31, 247, 308)) must play an important role in pathogenesis (Figure 3.19).

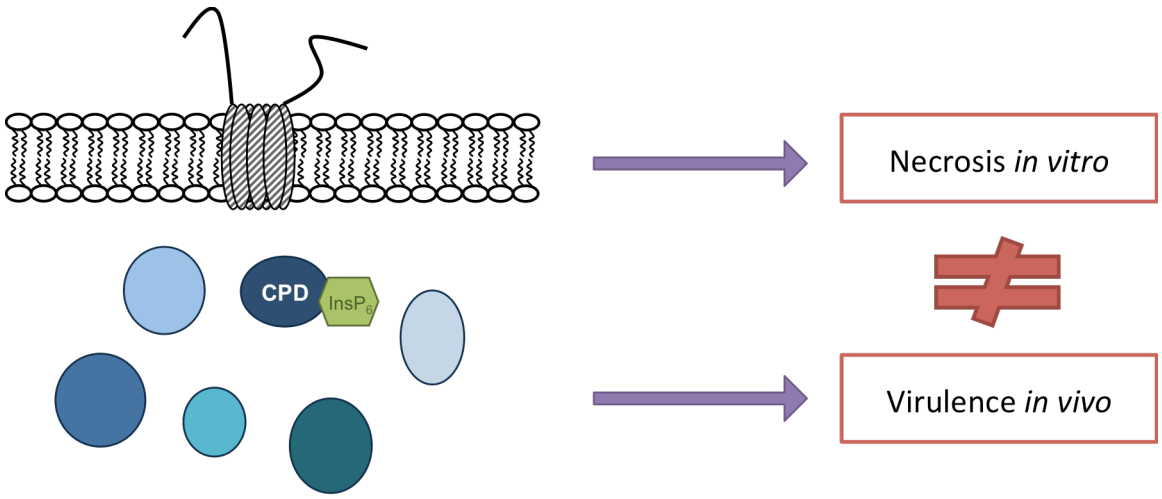

Figure 3.19. *In vitro* necrosis does not predict *in vivo* virulence outcomes. The MARTX toxin repeat regions are sufficient for pore formation in target eukaryotic membranes and induction of necrotic cytotoxicity. However, effector domains delivered by the MARTX toxin platform are required for MARTX-associated toxicity during i.g. bacterial infection. Thus the necrotic phenotype frequently associated with MARTX function does not predict virulence outcomes *in vivo*.

To further understand how the toxin contributes to virulence, a more physiologically relevant *in vitro* model system using polarized T84 cells was optimized for use with *V. vulnificus*. These studies demonstrated that the MARTX toxin induces biphasic intestinal epithelial dysfunction in the form of early-onset increases in paracellular permeability, followed by late-onset cell lysis. The effector domain region of the MARTX toxin is responsible for the rapid loss barrier function, Yet, studies with bacteria that express toxins lacking individual effector domains reveal that no single effector domain is essential for this rapid intestinal epithelial disruption. Rather there must be an additive or synergistic function from multiple effector domains in loss of epithelial barrier function, a mechanism by which effector domains may contribute to bacterial translocation from the intestine to the liver and spleen following i.g. infection in mice resulting in *V. vulnificus* sepsis.

The dissociation between MARTX-associated virulence, epithelial barrier breach, and lysis is further reflected in results from study of animal histopathology. The MARTX holotoxin does not induce overt intestinal tissue damage or excess apoptosis during early infection. This finding is consistent with the T84 experiments where rapid loss of TER was not linked to dramatic loss of cytoskeleton structure. Paracellular permeability increase in the absence of major changes to cytoskeletal morphology suggests that more delicate modulation of cellular dynamics, such as those at intercellular junctions, is occurring.

By contrast, the second phase of TER loss was linked to cell damage resulting in release of LDH. Notably, the second, lytic phase of TER loss also corresponded to increased bacterial MOI. As bacteria outgrow, MARTX toxin concentration presumably increases. These combined results suggest that eukaryotic membranes could be overwhelmed by quantity of toxin delivered,

regardless of the effector domain repertoire contained therein, and thus succumb to lysis in a pore-dependent manner. This is also supported by the observation of VvhA-dependent TER loss, where the kinetics of TER disruption by this lytic toxin were reminiscent of the effector-free RtxA1::Bla toxin kinetics.

The second-phase, lytic events at high bacterial MOI likely account also for the outlier pathology sample that showed observable bacterial staining in the intestinal lumen as well as epithelial damage at villous tips, suggesting that stochastic events leading to rare bacterial outgrowth at this early stage facilitate epithelial damage. However, the absence of significant necrotic or apoptotic phenotypes in all other *ΔvvhA*-infected mice indicates that the MARTX effector domain region is necessary for dissemination not because it causes or induces overt tissue damage, but because it induces early bacterial transit from the intestine via other mechanisms.

It was recently observed that another *V. vulnificus* secreted factor, the elastase VvpE, modulates paracellular permeability by altering tight junction protein dynamics (242). However no significant dysfunction is observed in monolayers exposed to *ΔvvhA ΔrtxA1* in the studies presented here. This indicates that *vvpE* does not increase permeability or intestinal damage in this context. The apparent discrepancy is likely due to differences both in bacterial MOI. *vvpE* was shown to increase intestinal permeability *in vivo* when mice were inoculated i.g. with a high dose of $1.1x10^9$ CFU. However, the *in vitro* MOI used in the present study corresponds to intestinal bacterial loads following inoculation with $5x10^6$ CFU, nearly 200-fold lower dose. Interestingly, observed *rtxA1* and *vvhA*-independent virulence at high-dose (Figure 3.3, B) does indicate a role for either bacterial components, such as LPS, or for minor virulence factors in the

absence of the two major cytotoxins. These combined data suggest that *vvpE* may play a functional role at the intestinal epithelial barrier and in virulence at high bacterial MOI.

An important caveat of these experiments is that events in the intestine are studied during an early phase of infection, at 6 hpi, in the mouse. At this time point, the number of bacteria in the gut does not yet depend upon *rtxA1*, and toxin-mediated epithelial destruction has not yet occurred. Nonetheless, previous studies have demonstrated that these *rtxA1*-mediated phenomena certainly occur at later time points (1, 132). This indicates that when known effects on *rtxA1*-dependent immune clearance (3, 249, 305) are not yet impacting intestinal bacterial load, strains producing the MARTX holotoxin are already detectable in the spleen and liver. We postulate that within the bloodstream and at tissue sites, *rtxA1* and its various regions may also play a critical role in resistance to immune clearance promoting bacterial outgrowth at these sites. In human cases where *V. vulnificus* infection progresses to septic shock and multi-organ failure, this rise in bacterial loads in the liver and spleen may predict dissemination-associated fatality. However, direct damage to the spleen or liver by bacteria may not be essential for death, given that mice exhibit no organ damage at 6 hpi yet begin to die by 8 hpi

Overall, the results presented in this study support a model in which *V. vulnificus* bacteria expressing the MARTX holotoxin rapidly induce intestinal epithelial dysfunction in the form of increased paracellular permeability and transmigration. These early steps are sufficient to facilitate bacterial dissemination and associated virulence potential. Our evidence suggests that initial translocation of bacteria out of the intestine is mediated by the MARTX effector domains and occurs in the absence of overt tissue damage in the intestine, spleen or liver tissues. Subsequent bacterial outgrowth – or a sporatic event resulting in higher bacterial burden – can

lead to intestinal tissue necrosis *in vivo*. Continued generation of MARTX toxins and subsequent expression of *vvhA* hemolysin genes contribute to later-stage tissue damage (1, 140). However, in the absence of MARTX effector domain functions, the early breach of the barrier and early arrival of bacteria at distal organs does not occur, resulting in dramatically reduced virulence potential.

CHAPTER 4

Discrete MARTX toxin effector domains modulate *V. vulnificus* virulence potential

Overview

Vibrio vulnificus is an aquatic bacterium that, like other *Vibrio* species, is routinely detected in the marine or estuarine microflora (43). Unfortunately, the bacterium is also a potential human pathogen when ingested, usually in raw oysters (105). Once consumed via the foodborne route, *V. vulnificus* is adept at crossing epithelial barriers to spread systemically, causing primary septicemia that is lethal in more than 50 percent of cases (105, 309).

The Multifunctional Autoprocessing Repeats-in-Toxins (MARTX) toxin, product of the *rtxA1* gene, is a potent secreted virulence factor of *Vibrio vulnificus* (2, 245). The MARTX toxin promotes rapid bacterial dissemination from the gastrointestinal tract into the bloodstream and distal organs, leading to the sepsis characteristic of *V. vulnificus* infections (Chapter 3) (35, 138, 140). In addition, the MARTX toxin confers resistance to phagocytosis, suggesting that *rtxA1*-expressing *V. vulnificus* are better at resisting clearance by the host immune system (249, 310).

The *V. vulnificus* MARTX toxin is composed of N- and C-terminal amino acid repeats that form a pore in target eukaryotic cells. Pore formation results in translocation of a central region of MARTX effector domains to the eukaryotic cytosol (Chapter 2) (30). Despite the fact that the MARTX repeat region pore, absent effector domains, is sufficient for toxin-induced necrosis *in vitro*, we have previously shown that the effector domains are absolutely required for toxin-dependent virulence *in vivo* (Chapter 3) (30, 35). The MARTX pore, absent its effector domains, does not render any virulence advantage over a MARTX-null mutant, despite the fact

that the MARTX effector-free strain induces necrotic cell death *in vitro*. The effector domain region induces rapid increases in paracellular intestinal permeability. Moreover, the rapid induction of epithelial dysfunction by effectors is thought to facilitate bacterial spread from the intestine, because the effector domain region is also required for dissemination to distal organs (Chapter 3) (35).(35).

Thus, the MARTX toxin has been shown to act as a delivery platform for the region of bacterial effector domains encoded between its N- and C-termini, which in turn confer toxin-associated virulence *in vivo* (Chapter 3) (35, 253). In previous studies, we examined the effector domain region in its entirety (Chapters 2 and 3) (30, 35). The effector domain region, however, is in fact composed of multiple discrete effector domains, the bounds of which have been defined by protein cleavage assays or genetic analyses (13, 282, 283). Further, the identity and function of many discrete effector domains have been elucidated after extensive biochemical investigation (reviewed in (253) and in Table 1.2). Thus, we aimed to expand upon our previous studies of the entire MARTX toxin region by performing a detailed analysis of individual effector domains and their contributions to *V. vulnificus* pathogenesis.

The *V. vulnificus* strain CMCP6 possesses a "C-type *rtxA1"* (193). CMCP6 is an optimal strain choice for studying individual MARTX effector functions for numerous reasons. First, each of the effectors in CMCP6 is unique, unlike other toxins which host duplicates of the same effector (e.g. strain CECT4999 (13, 19). Second, with five effectors, C-type toxin effector repertoires contain the maximal number of effector domains observed in any individual MARTX toxin (range, 1-5 (2)). Finally, C-type toxins are found in approximately 25 percent of clinically

derived *V. vulnificus* isolates and >85 percent of oyster-derived isolates (193), indicating their abundance in the environment and their virulence potential in humans.

The CMCP6 MARTX toxin has effectors in the repertoire, listed in the order of their position from N- to C-terminus: Domain of Unknown Function in the first position (DUF1), Rho Inactivation Domain (RID), Alpha-Beta Hydrolase domain (ABH), Makes Caterpillars Floppy-like domain (MCF), and Ras/Rap1 Specific Peptidase (RRSP) (Table 1.2, Figure 4.1). DUF1 binds and up-regulates the host protein prohibitin (14). RID targets GTPases including RhoA and CDC42 with acylation in the protein polybasic region. This modification leads to disruption of GTPase signaling and cytoskeletal dysfunction that manifests as cell rounding (3, 22, 23). The Alpha-Beta Hydrolase domain (ABH) is a phosphatidylinositol-3-phosphate (PI3P) phospholipase that inhibits autophagy and endosomal trafficking (3, 4). The Makes Caterpillars Floppy-like domain (MCF), undergoes auto-proteolytic cleavage and subsequently induces the intrinsic pathway of mitochondrial-mediated apoptosis (31). Finally, RRSP cleaves its target proteins, Ras and Rap1, and disrupts downstream ERK signaling (27, 32).

In the following experiments, the role of each effector domain in *V. vulnificus* pathogen:host interaction is investigated. A library of bacterial mutants, each deficient in a single effector domain, is generated and subsequently used to test the necessity of individual effector domains in MARTX-associated processes. We find that the MARTX effector domains of *V. vulnificus* exhibit functional redundancy for many MARTX-associated phenotypes *in vitro*, yet confer distinct virulence outcomes *in vivo*. This suggests the importance of elements of host response that are not captured in our *in vitro* assays (e.g. cytokine production) and likewise suggests interplay among co-delivered effector domains.

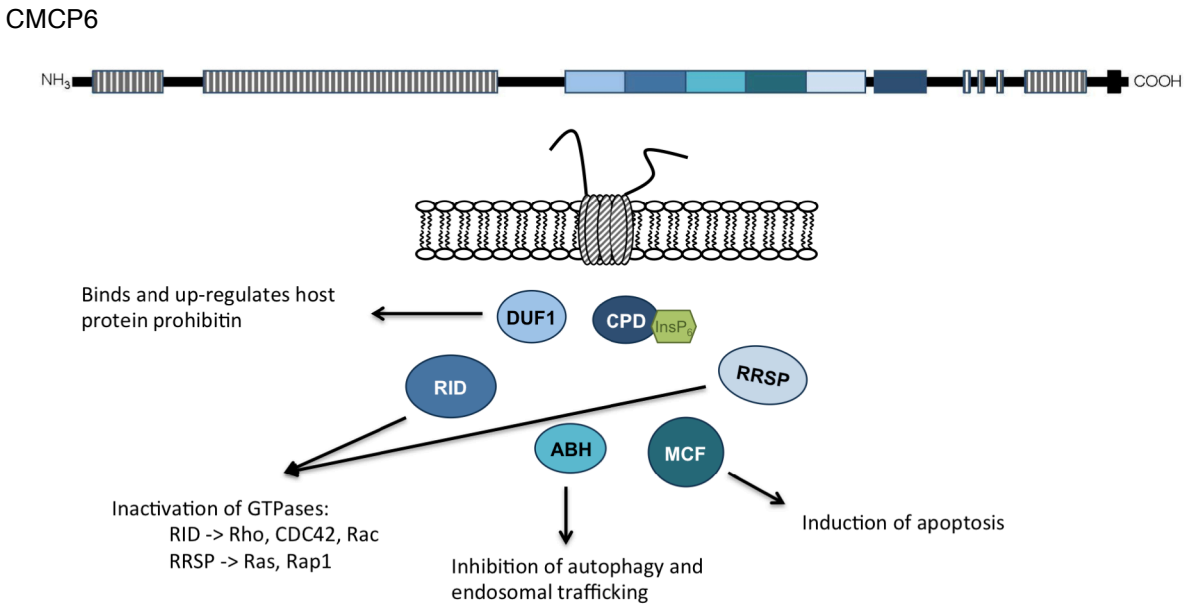

Figure 4.1. Identity and function of individual MARTX effector domains in C-type toxins including representative isolate CMCP6 (13). The Domain of Unknown Function in the first position (DUF1) binds and up-regulates the host protein prohibitin (14). The Rho Inactivation Domain (RID) inactivates target GTPases including RhoA and CDC42, by acylation of the target protein (3, 22, 23). The Alpha-Beta Hydrolase domain (ABH) is a phospholipase that inhibits autophagy and endosomal trafficking (3, 4). The Makes Caterpillars Floppy-like domain (MCF) auto-processes itself and subsequently induces mitochondrial-mediated apoptosis(31). In the fifth position, the Ras/Rap1 Specific Peptidase (RRSP) cleaves its target proteins and disrupts downstream ERK signaling (27, 32).

Results

Generation of a library of validated Δ*effector* strains in the CMCP6 *rtxA1* gene.

Knowing the important role of the MARTX effector domain repertoire in its entirety, the role of individual domains within the region was explored. Ideally, this experiment would have been conducted using strains with point mutations in the active sites of each MARTX effector domain so as to generate catalytically inactive effector domains in the context of the MARTX holotoxin. However, the catalytic residues of numerous domains have not as yet been identified, and some catalytic point mutants are known to exert intermediate effects when target-binding activity is retained (12, 15, 22, 31). Therefore, a library of strains was generated in the *ΔvvhA* background in which each strain harbors an in-frame deletion in the *rtxA1* coding region to eliminate a single effector domain from the otherwise functional toxin (Figure 4.2).

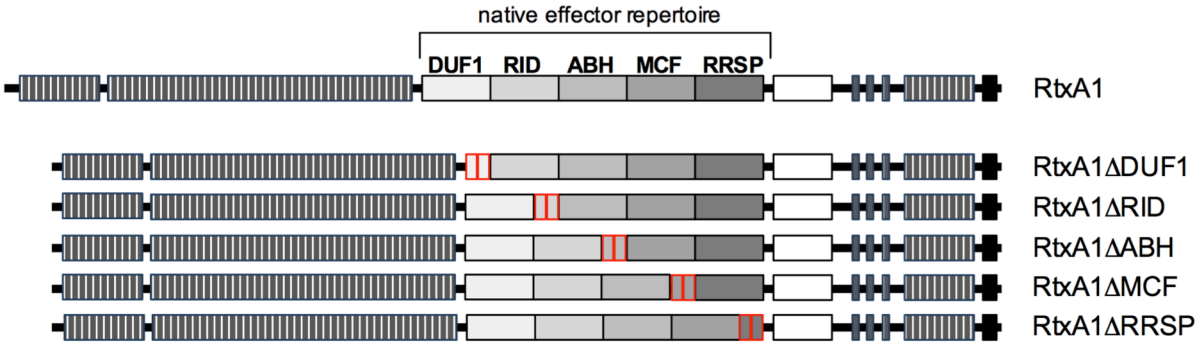

Figure 4.2. Toxin schematics for single MARTX effector domain deletion strains. Schematic representation of the *Δeffector* strain library. Effectors as indicated; striped boxes=repeat regions.

MARTX-dependent lysis is a well documented toxin phenotype (Chapters 2 and 3). Accordingly, all *Δeffector* strains were first validated as inducing release of LDH from polarized T84 monolayers at 180 minutes (Figure 4.3, A), demonstrating that the modified *rtxA1* genes expressed toxin that retained the cell lysis activity linked to the repeat regions. In addition, *Δduf1, Δrid, Δabh,* and *Δmcf* were confirmed to the induce loss of detectable Ras from HeLa cells when co-incubated with the target cells for 1 hour at MOI=100 (Figure 4.3, B). Ras was detected in cells incubated with the *Δrrsp* strain as expected due to loss of the RRSP-dependent cleavage of Ras (27). Cytopathic epithelial cell rounding in response to *V. vulnificus* has also been previously attributed to the MARTX effector domain repertoire (Chapter 2) (30). A strain expressing the wild-type MARTX toxin induces rounding of more than 90% of HeLa cells in 120 minutes (*ΔvvhA,* Figure 4.3, C) while a *ΔvvhAΔrtxA1* strain does not induce any effect above the background. The *Δduf1, Δabh, Δmcf,* and Δ*rrsp* strains similarly induced cell rounding, independently validating these strains are producing functional MARTX toxins. As expected, due to the disruption of its Rho-inactivated domain linked to cytoskeleton disassembly, epithelial cell rounding was significantly reduced in HeLa cells incubated with the Δ*rid* strain. These three assays together validate each Δ*effector* strain as retaining the ability to lyse cells and retain or lose activity specifically linked to two effector activities.

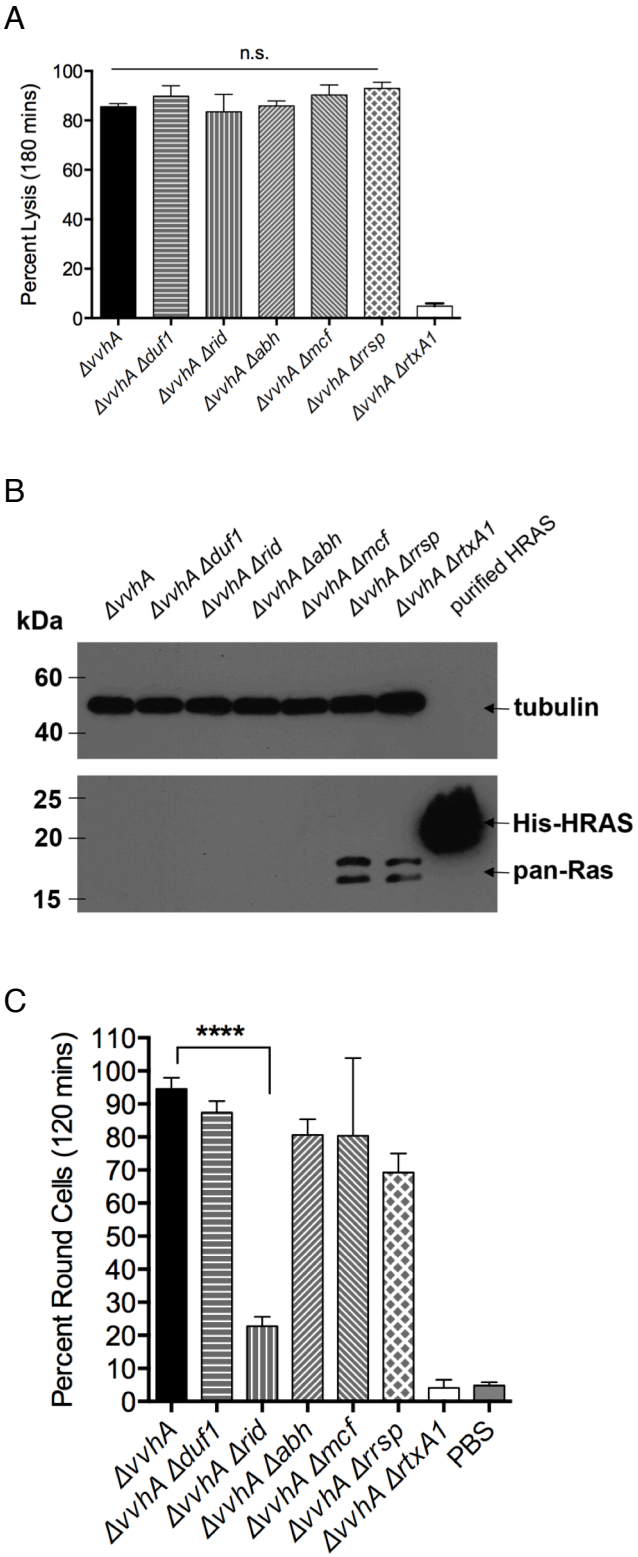

Figure 4.3. Modified MARTX toxins are generated and deliver their effector domain cargo to target eukaryotic cells. (A) Lysis of T84 monolayers exposed to the indicated bacterial strains for 180 minutes, expressed relative to Triton X-100 treated monolayers. (B) Western blot using lysates from HeLa cells exposed to the indicated strains for 60 minutes at MOI=100, probed with anti-Ras10 antibody (bottom) and anti-tubulin (top) (C) Percent of rounded HeLa cells observed upon exposure to the indicated bacterial strains for 120 minutes at MOI=10. In all cases experiments were conducted in triplicate Data were analyzed by one-way ANOVA followed by Tukey multiple comparison's test to determine *p* values; ****$p<0.0001$.

V. vulnificus single effector mutants exhibited distinct virulence profiles during i.g. infection

It has been previously demonstrated that the MARTX effector domain region is required for toxin-associated virulence during intragastric infection. Therefore we speculated that depletion of any individual MARTX effectors would reduce virulence compared to a strain producing MARTX holotoxin. In the event that MARTX toxin virulence function is additive, each of the five *Δeffector* strains should exhibit an equivalent, and relatively minor, virulence attenuation. Alternatively, one or more effectors may exert dominant effects. In that case, deletion of the dominants effector(s) would significantly attenuate bacterial virulence while deletion of secondary effectors would not considerably reduce *V. vulnificus* virulence potential. In a final hypothetical model, each single effector deletion could be highly attenuated, which would indicate cooperative or synergistic properties of the simultaneously delivered MARTX effector domains.

To test the role of individual MARTX toxin domains in *V. vulnificus* virulence, female CD1 mice were intragastrically inoculated with 6-8 x 10^6 CFU of the parental *ΔvvhA* strain, which produces the MARTX holotoxin, or the derivative strains *ΔvvhA Δduf1, ΔvvhA Δrid, ΔvvhA Δabh, ΔvvhA Δmcf,* or *ΔvvhA Δrrsp* each deficient in a single effector domain. Survival of the infected animals was monitored over 48 hours.

The mutant strains exhibited a variety of virulence profiles, which could be categorized into three groups. One mutant, *ΔvvhA Δmcf,* showed no virulence phenotype (Figure 4.4 D, dashed line). Compared to its parental *ΔvvhA* strain, the *ΔvvhA Δmcf* strain did not exhibit significantly different virulence potential.

In other cases, *Δeffector* strains exhibited attenuated virulence, as predicted (Figure 4.4. B and E, green lines). Mice infected with the *Δrid* mutant exhibited significantly delayed infection kinetics compared to the *ΔvvhA*-infected animals. The *ΔvvhA Δrrsp* mutant was also significantly attenuated in its virulence potential. In fact, the dose that is lethal in 100 percent of infected animals is, in the *ΔvvhA Δrrsp* mutant, closer to the median lethal dose (LD_{50}) (Figure 4.4, E). Thus deletion of either *rid* or *rrsp* from the MARTX toxin attenuates bacterial virulence potential and improves *V. vulnificus* infection outcomes in i.g. inoculated mice.

Surprisingly, an unexpected group showed accelerated kinetics (Figure 4.4, A and C). Mice infected with the *ΔvvhA Δduf1* or *ΔvvhA Δabh* strains died at a significantly faster rate than those infected with *ΔvvhA*. Deletion of *duf1* or *abh* from the MARTX coding region thus increased bacterial virulence potential. This result suggests that, in the context of the MARTX holotoxin, these effector domains actually negatively modulate lethality. Taken together, these survival data demonstrate that single MARTX effector domains modulate *V. vulnificus* virulence potential during i.g. infection.

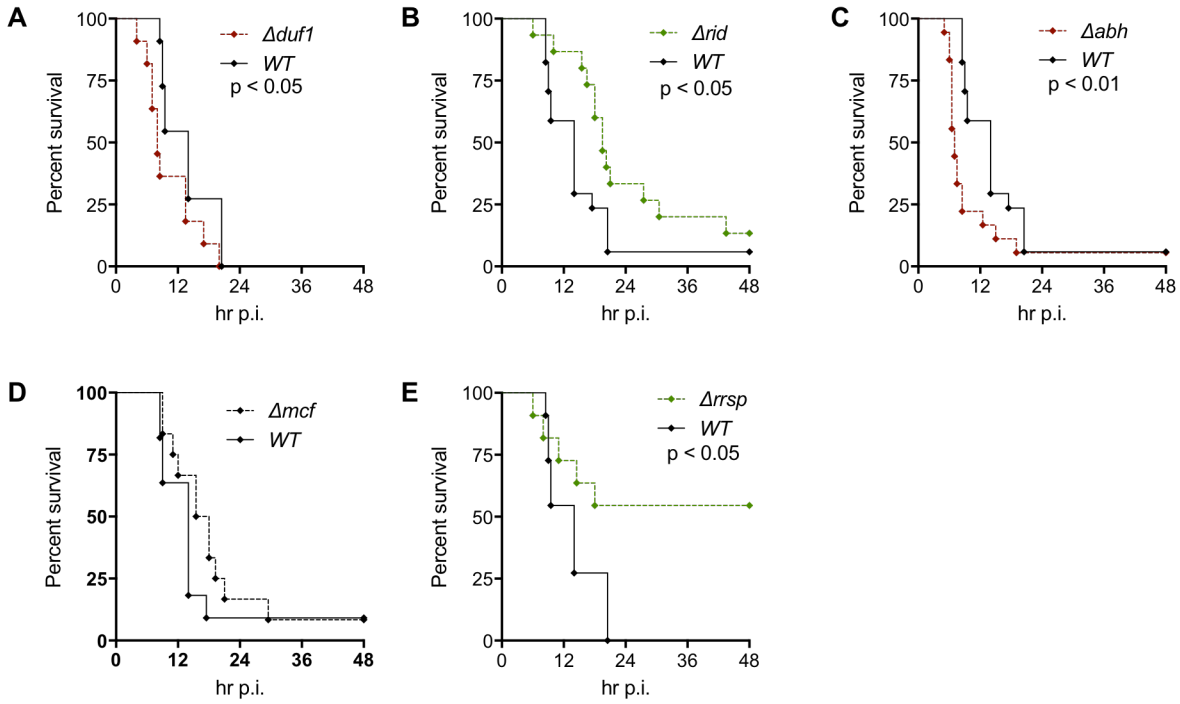

Figure 4.4. *V. vulnificus* strains lacking single MARTX toxin effector domains have altered virulence potential *in vivo.* Survival of mice (10-15 per group) inoculated with the indicated strains. Note that the data for control strains producing WT toxin is shared among panels (B/C, A/E); data were separated for each mutant strain for optimal visualization. Curves were compared by log-rank test and, where found to be significantly different, p-values given in each panel.

No single MARTX effector is required for bacterial survival in the gut at 6 hpi

To elucidate the mechanisms by which individual MARTX effector domains modulate virulence potential, key steps in the pathogenic process were investigated. The role of the MARTX toxin effector domain region in *V. vulnificus* virulence has been previously demonstrated by survival challenge experiments (Chapter 3). It was subsequently shown that the MARTX effector domain region's role as a virulence factor relates to its induction of epithelial barrier dysfunction and promotion of bacterial dissemination. Given the diverse virulence profiles of *V. vulnificus* strains lacking single MARTX toxin effectors, and the importance of epithelial barrier breach in *V. vulnificus* disease pathogenesis, we posited that individual effector domains could likewise be influencing systemic bacterial spread.

First, bacterial burden in the intestine was examined. At 6 hours post infection (hpi) (or upon natural death, if it preceded 6 hpi), mice were euthanized and the intestine isolated. Organ homogenates were generated, serially diluted, and plated to enumerate bacterial CFU. Quantification of bacterial load in the intestine demonstrated that no single effector domain is required for *V. vulnificus* survival in the gut at 6 hpi, as none of the strains lacking single effector domains demonstrating a survival defect relative to the parental strain making MARTX holotoxin (Figure 4.5). This is consistent with previous results (Chapter 3) showing that *rtxA1* is not required for intestinal survival at 6 hpi.

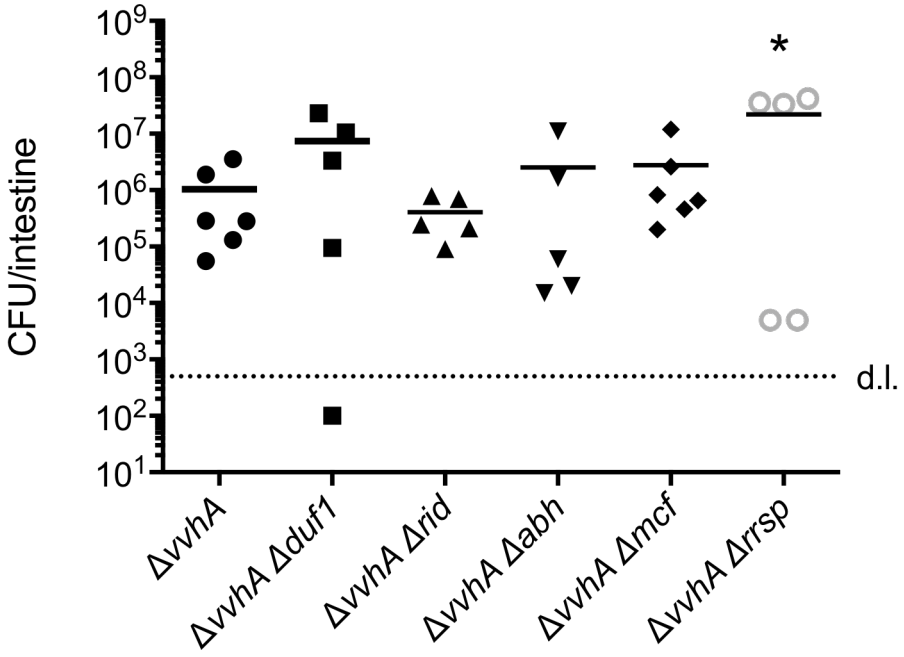

Figure 4.5. No single MARTX effector domain is required for intestinal survival at 6hpi. Bacteria of the indicated strains were quantified from intestinal homogenates (5-6 mice per group) by selective plating at 6 hpi. Data were analyzed by one-way ANOVA and Tukey's post-test to compare each *Δeffector* mutant to the parental *ΔvvhA*. *$p<0.05$

Interestingly, the *ΔvvhA Δrrsp* strain sustained a significantly higher average intestinal load at 6 hpi. However, the data exhibits a bifurcated distribution in which two of five mice have intestinal bacterial burdens three to four log units lower than the remaining three mice inoculated with the same strain. Thus approximately 40 percent of the *ΔvvhA Δrrsp*-infected mice have bacterial burdens below *ΔvvhA*-infected mice, while 60 percent have higher burdens relative to *ΔvvhA*-infected mice. Similar bifurcation patterns, though less pronounced, are observed in mice infected with either *ΔvvhA Δduf1* or *ΔvvhA Δrrsp*. In contrast, the individual data points for mice infected with *ΔvvhA, ΔvvhA Δrid,*and *ΔvvhA Δmcf* are more tightly clustered around the mean value.

No single MARTX effector domain is required for intestinal barrier disruption or bacterial dissemination

Previous experiments (Chapter 3, (35)) demonstrated the importance of the MARTX effector domain repertoire in disrupting intestinal epithelial barrier function and promoting bacterial dissemination from the gut to distal organs. Therefore, the library of MARTX effector mutants was used to define the effector domains essential for rapid loss of TER in polarized T84 monolayers. For this experiment, polarized T84 monolayers were exposed apically to *Δeffector* strains at MOI 2.5. TER was measured at 60 minutes, when early, effector-depedent loss of TER is most pronounced. TER was measured again at 120 minutes, when effector-independent barrier dysfunction begins (Figure 4.6).

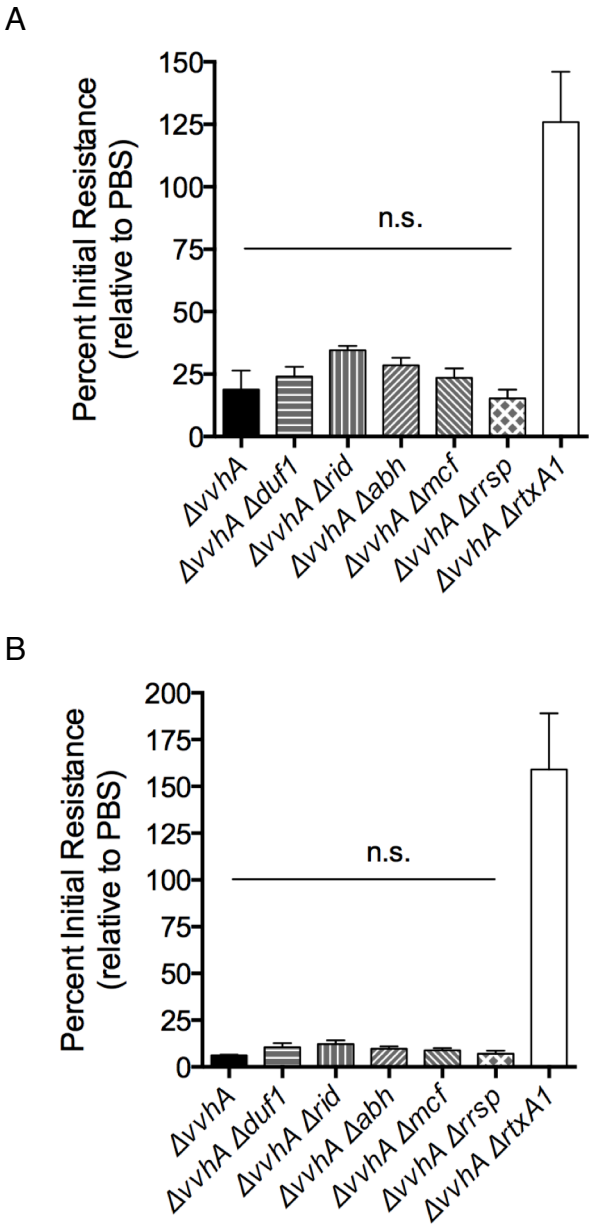

Figure 4.6. No single MARTX effector domain is required for induction of epithelial barrier dysfunction. TER of polarized monolayers measured at 60 mins (A) or 120 mins (B) minutes following apical exposure to the indicated strains of *V. vulnificus* at MOI=2.6. Data analyzed by one-way ANOVA and Tukey post-test, with no significant differences found among groups.

When applied to the apical side of polared T84 monolayers *in vitro,* each of the *Δeffector* strains induced loss of TER at a level comparable to the strain expressing the entire effector domain repertoire (Figure 4.6). Thus, no single MARTX effector is essential for induction of epithelial barrier dysfunction *in vitro*. In addition, this result indicates that despite its requirement for induction of cell rounding in nonconfluent HeLa epithelial cells, Rho inactivation induced by RID does not alone account for TER loss at 60 minutes. This suggests that MARTX effectors function redundantly or synergistically with regard to epithelial barrier disruption.

As no single MARTX effector domain was required for the MARTX toxin to induce intestinal epithelial barrier dysfunction in the *in vitro* T84 system, intestinal epithelial barrier breach was next examined *in vivo*. At 6 hpi, the liver and spleen of i.g.-infected, female CD1 mice were isolated. Organ homogenates were generated, serially diluted, and plated to enumerate bacterial CFU in these target organs.

Quantification of bacterial dissemination revealed indistinguishable bacterial loads in the liver of mice inoculated with the various mutant strains (Figure 4.7, A). The same was true of bacterial burdens examined in the spleen (Figure 4.7, B). These experiments demonstrate that no single MARTX effector domain is required for bacterial dissemination from the intestine and, as seen in *vitro*, suggests that there is redundancy in effector contribution to intestinal barrier breach.

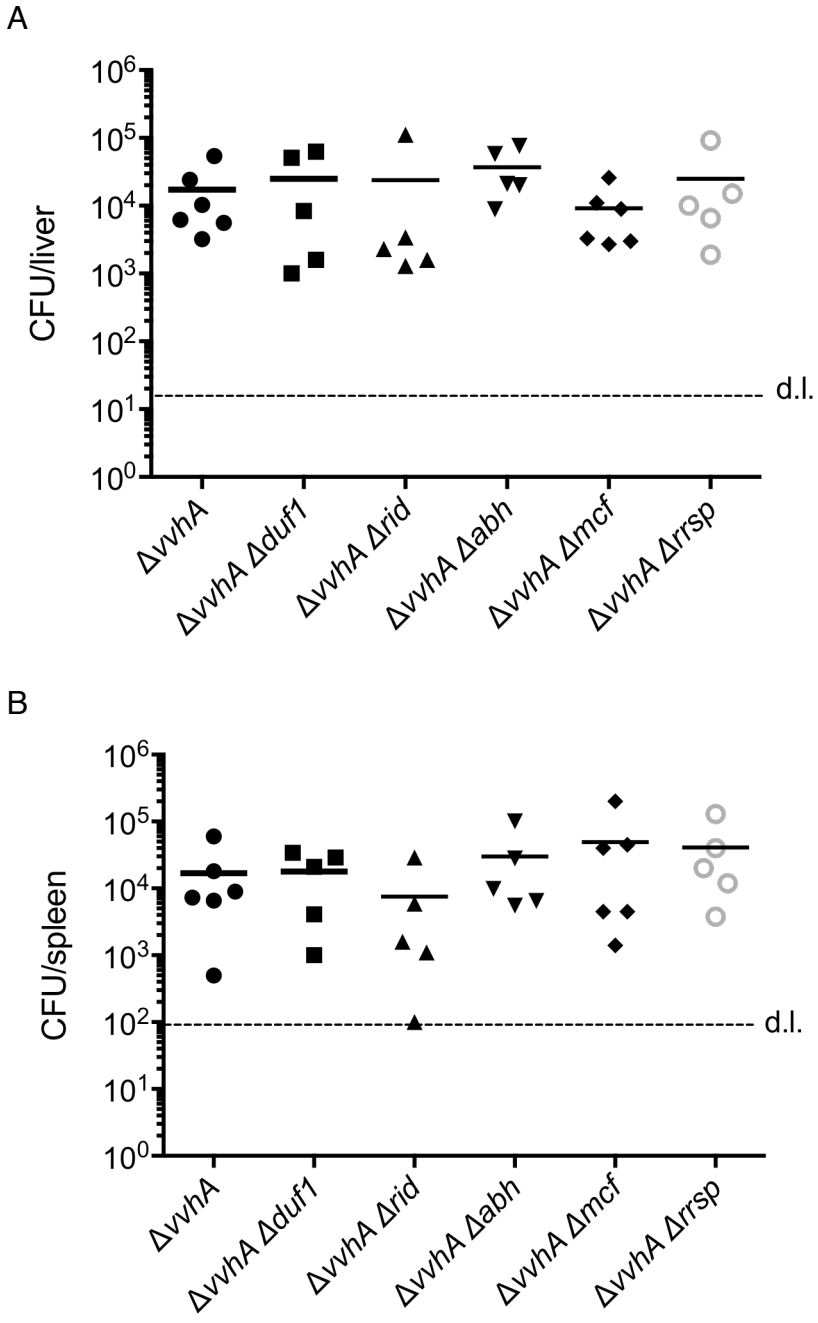

Figure 4.7. No single MARTX effector domain is required for bacterial dissemination from the intestine. Bacteria of the indicated strains were quantified from organ homogenates of the liver (A) or spleen (B) by selective plating at 6 hpi (5-6 mice per group). Data were analyzed by one-way ANOVA comparing each *Δeffector* mutant to the parental *ΔvvhA* with no significant differences found.

MARTX potently inhibits phagocytosis dependent upon the effector domain region, but no single effector is required

Since bacterial egress from the intestine does not depend upon individual MARTX toxin effector domains, and bacteria were found at equivalent doses in distal organs, we asked whether the disseminated bacteria exhibit differential susceptibility to immune-mediated clearance mechanisms. Both the liver and spleen have resident macrophage populations (in the liver also known as Kupffer cells) that play important roles during systemic bacterial infection (311, 312). As such, it is logical to deduce that disseminated *V. vulnificus* will interact with macrophages at these sites, and *rtxA1* has been linked to *V. vulnificus* defense against phagocytosis (249, 310).

To examine the role of the MARTX toxin and its effector domains in phagocytic inhibition, an assay that measures uptake of pH-sensitive, fluorescent beads was employed. This method has previously been published for study of anti-phagocytosis activity by *V. cholerae* (3), and the approach was modified for study of *V. vulnificus*. Specifically, the bacterial co-incubation time and MOI were decreased for *V. vulnificus* as compared to *V. cholerae,* to ensure that phagocytosis could be assessed prior to onset of any lytic killing by *V. vulnificus.*

In this assay, J774 murine macrophages were exposed to bacteria for 30 minutes at MOI=1 (Figure 4.8, A), then cells were washed, and the media replaced with a solution containing gentamicin and pHrodo beads coated with *Eschericia coli* lysate. The bacterially pre-treated J774 cells were co-incubated with pHrodo beads for one hour to allow phagocytosis to progress. Fluorescence, which is achieved only in the low-pH environment experienced in the acidified phagocytic vacuole, was quantified using a plate reader. J774 cells are not lysing under

these assay conditions, as measured by LDH release (Figure 4.8, B). This confirms that changes in phagocytic activity are being induced in live cells.

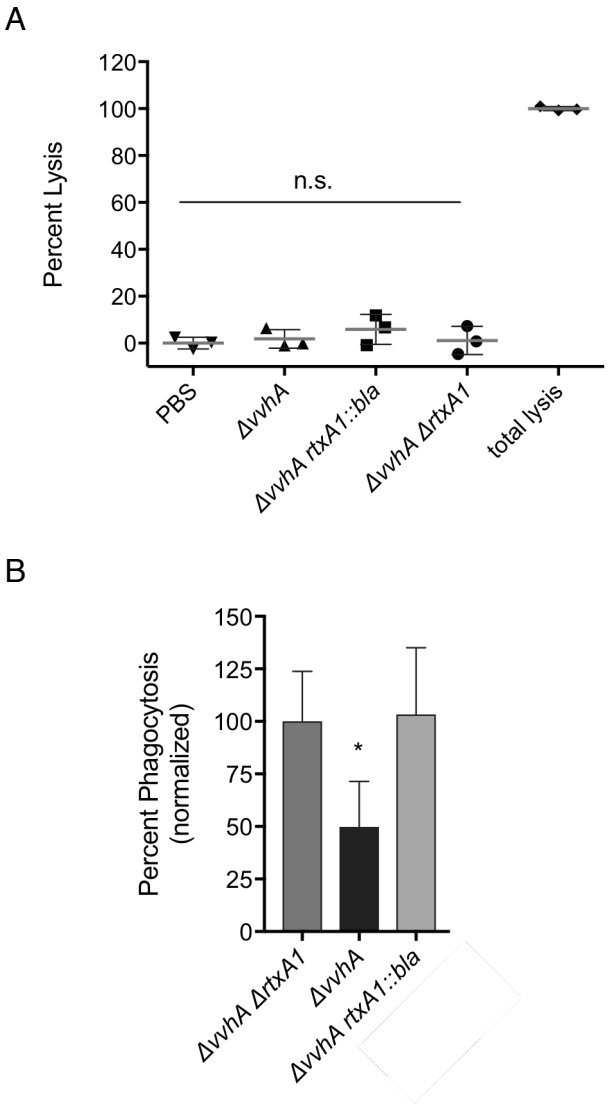

Figure 4.8. MARTX effector domain region is required for toxin-dependent disruption of phagocytosis. J774 cells were co-incubated with *V. vulnificus* of the indicated strains at MOI=1 for 30 minutes and gentamicin-containing media for a subsequent 60 minutes. Lysis was measured by relative LDH release (A) and percent phagocytosis of pHrodo beads measured relative to *ΔvvhA ΔrtxA1* (B). Phagocytosis results in (B) is data pooled from two independent experiments, each with three replicates per experiment. Data were analyzed by one-way ANOVA with Tukey post-test. *$p<0.05$, n.s. = not significantly different

Consistent with previous data, a *V. vulnificus* strain making the MARTX toxin inhibits J774 phagocytic activity (Figure 4.8B), confirming the efficacy of the pHrodo assay for these purposes. Under the conditions tested, J774 cells exposed to *ΔvvhA* were inhibited to 50 percent of their phagocytic activity as compared to cells co-incubated with *ΔvvhA ΔrtxA1*. When cells were exposed to *ΔvvhA rtxA1::bla,* they exhibited levels of phagocytosis equivalent to cells co-incubated with *ΔvvhA ΔrtxA1*. As the *ΔvvhA rtxA1::bla* strain was not capable of inhibiting phagocytosis, the MARTX effector domain region is required for the toxin's anti-phagocytic activity.

Though the effector domain region is required, no single MARTX effector domain is necessary for the MARTX toxin's antiphagocytic activity (Figure 4.9). Each of the *Δeffector* mutant *V. vulnificus* strains was capable of inhibiting J774 phagocytosis to the 50 percent levels exhibited with production of the MARTX holotoxin. This reveals that no one MARTX effector is responsible for phagocytic inhibition, and suggests functional redundancy among effectors.

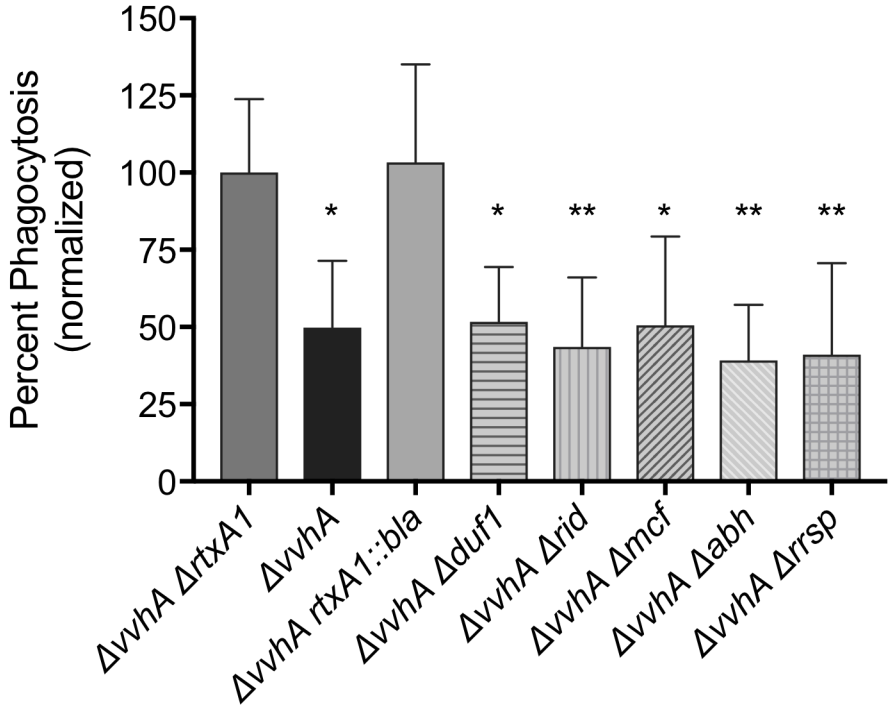

Figure 4.9. No single MARTX effector domain is required for toxin anti-phagocytic activity. Phagocytic activity was determined using the pHrodo bead assay and quantified relative to *ΔvvhAΔrtxA1*. Note that data in the first three columns (*ΔvvhAΔrtxA1, ΔvvhA, ΔvvhArtxA1::bla)* is derived from the same experiments presented in Figure 4.8. Experiments used three biological replicates per experiment, and data is pooled from two independent experiments. Statistical significance was determined using one-way ANOVA with Tukey post-test. *$p<0.05$ **$p<0.01$

To test whether anti-phagocytic activity is additive, synergistic, or redundant, the MARTX effector protein RRSP was delivered to J774 cytosol by an alternative mechanism. This experiment employed the *Bacillus anthracis* anthrax toxin system, which has been leveraged as a bioporter for delivery of exogenous proteins to eukaryotic cells (26, 27, 313, 314). In this system, RRSP was fused to the N-terminal region of *B. anthracis* lethal factor (LF_N). When delivered to cells with protective antigen (PA), the fusion RRSP protein is translocated to the eukaryotic cytosol, where it can assert its functions including cleavage of target proteins (26, 27, 32).

J774 cells were pre-treated with PA and LF_N-RRSP for 120 minutes prior to bacterial exposure, in a modification of the phagocytosis assay protocol used for experiments in Figure 4.8. The phagocytic activity of RRSP-treated cells was inhibited to approximately 50 percent. (Figure 4.10). J774 cells pre-treated with LF_N-RRSP are impaired in their phagocytic capacity at comparable levels to cells intoxicated with the MARTX holotoxin via *ΔvvhA* exposure. Therefore, the MARTX toxin domain RRSP alone is sufficient to inhibit phagocytosis *in vitro.*

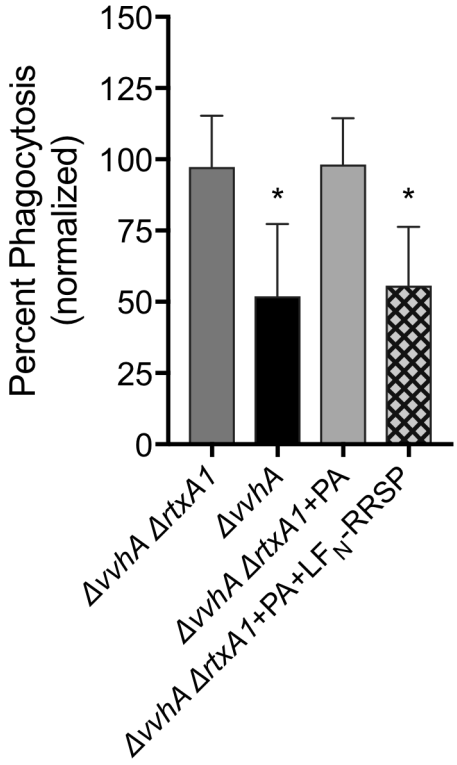

Figure 4.10. MARTX RRSP is sufficient to inhibit phagocytosis *in vitro.* J774 cells pre-treated with LF_N-RRSP are impaired in their phagocytic capacity at levels comparable to cells exposed to full length toxin via bacterial delivery. Experiments used three biological replicates per experiment, and data is pooled from two independent experiments. Results were compared by one-way ANOVA with Tukey post-test. *$p<0.05$

Discussion

The MARTX toxin and its effector domain repertoire are critical virulence determinants during i.g. *V. vulnificus* infection (Chapter 3) (1, 35). We have previously linked the MARTX effector repertoire to disruption of the intestinal epithelial barrier and bacterial egress from the gut to the bloodstream. These critical MARTX functions, carried out by the effector domain region, influence virulence by facilitating bacterial dissemination to the liver and spleen. It is generally agreed that the presence of bacteria in these distal organs correlates to lethal outcomes in mouse models of *V. vulnificus* infection and mimics septic infection in humans (138, 139).

However, data in this study reveal that strains with equivalent dissemination ability, as calculated by bacterial CFU in the liver and spleen at 6 hpi (Figure 4.7), exhibit different lethal potential (Figure 4.4). Indeed, studies on *V. vulnificus* wound infection showed that "mice did not die unless significant liver infection occurred." Yet the same study demonstrated the presence of $\geq 10^4$ CFU of bacteria in the liver of mice that did not succumb to infection (139). Therefore, bacterial dissemination to the liver is a necessary correlate, but not sufficient cause, of lethal *V. vulnificus* infection.

Our dissemination results are also highly reminiscent of a study conducted in fish, wherein equivalent levels of systemic *V. vulnificus* exhibited different virulence potential dependent upon *rtxA1* (305)**.** In the fish experiments, *V. vulnificus* was equivalently capable of colonizing and invading eel tissues whether or not it possessed *rtxA1*. However, eels infected with *rtxA1*-positive bacteria died, while those infected with an isogenic *rtxA1*-negative strain survived. Thus the virulence outcomes were different, with *rtxA1* acting as a significant virulence factor promoting lethal infection despite equivalent bacterial burden.

These prior results suggest that bacterial dissemination from the intestine following i.g. infection is necessary, but not sufficient, for lethal infection. This is consistent with results from the current study's *ΔvvhA Δrrsp*-infected mice. These mice each had $>10^3$ bacteria present in the liver or spleen at 6 hpi (Figure 4.7). Yet when the bacterial infection was allowed to run its full course (Figure 4.4), only fifty percent of mice died.

This discrepancy could be due to different bacterial susceptibility to phagocytosis. Indeed, anti-phagocytic activity of the MARTX toxin is another key toxin characteristic that can now be attributed specifically to the effector domain region. However, no single effector is required for phagocytic inhibition. *In vitro* each of the *V. vulnificus* mutants is equally capable of inhibiting phagocytosis. This result is also supported by a recent study demonstrating that only the deletion of multiple individual MARTX effector domains, but not single domains, lessened MARTX anti-phagocytic activity (310). Therefore an alternative explanation is needed for the distinct virulence phenotypes observed with single effector deletion mutants.

The fact that all strains appear equivalently susceptible to phagocytic clearance *in vitro* suggests that continued bacterial egress from the intestine could be required for full *V. vulnificus* virulence. Such a model is supported by the intestinal colonization data of mice infected with the *ΔvvhA Δrrsp* strain, wherein three of five animals exhibited very high intestinal bacterial burden at 6 hpi, but two of the five animals appeared to be clearing bacteria from the intestine. Relatedly, previous studies by Thiaville in a *V. vulnificus* wound infection model showed that bacterial infection of the liver required a certain minimum CFU threshold in the skin. In the case of wound infection, "*V. vulnificus* appears to require a strong base of infection of the skin before breaking through to the rest of the body" (139).

The data presented in Chapter 3 clearly demonstrate that extensive bacterial outgrowth in the intestine is not, in fact, required for early bacterial dissemination to the distal organs. At 6 hpi, bacterial counts in the liver are comparable to the delivered inoculum, and are equivalent across all strains (Figure 3.4). Still, results from Thiaville in combination with the data presented here support a model in which sustained bacterial load in the intestine is important for continuous translocation and systemic spread throughout the infection course. This would suggest that the animals clearing intestinal bacterial loads quickly have a better chance of surviving infection, even when bacteria have already disseminated.

In addition, we hypothesize that the physiological response to the disseminated bacteria differs among mice infected with different strains. Specifically, the cytokine response of mice with systemic *V. vulnificus* infection has very recently been characterized (140). This study revealed that the MARTX toxin stimulates production of numerous cytokines and chemokines not induced during infection with a *ΔrtxA1* mutant. Given the pivotal role that the MARTX toxin effector domains play in all investigated toxin-associated function (namely: intestinal barrier disruption, dissemination, and phagocytic inhibition), it is logical to extrapolate that effector domains and/or their associated functions induce the murine inflammatory response.

Moreover, the balance among pathways induced by the MARTX toxin effector domains likely dictates immune response of the host. Disrupting this balance could well lead to altered cytokine/chemokine production in infected mice. For example, under uninfected conditions, autophagy is important for both positive and negative regulation of cytokine production (315). The MARTX effector domain ABH inhibits autophagy and endosomal trafficking when delivered to the target cell cytosol (4). ABH could actually serve to down-regulate the production

of cytokines including IL-1α, IL-1β, and IL-18 in the context of *V. vulnificus* infection. If so, increased cytokine production and increased organ failure in *ΔvvhA Δabh*-infected mice as compared to *ΔvvhA*-infected mice could provide a mechanism for the exacerbated virulence seen upon infection with this mutant.

Conversely, Rho GTPase activity is vital for cellular signal transduction and NF-kappaB activation in response to extracellular signals (316). Thus inactivation of these signals in RID or RRSP-targeted cells should interfere with host immune response. The phagocytosis studies undertaken in this study used controlled *in vitro* systems. Under these conditions, bacterial MOI is tightly controlled and macrophage cells, being outside their physiological context, are not receiving the same signals that would be present from other eukaryotic cells in the context of *in vivo* infection. Thus, another putative explanation for distinct virulence profiles observed with MARTX effector mutants is that immune cells targeted by MARTX effectors are affected in their signaling capacity (310), leading to differences in cell-cell communication, differences in immune cell recruitment to infection sites, and/or altered systemic cytokine response. Based on the infection outcomes observed with *ΔvvhA Δrid* and *ΔvvhA Δrrsp* strains of *V. vulnificus,* the inhibition of GTPase signaling in the host renders the bacterium more virulent, and is conversely detrimental to the host.

Together these results support a model in which it is not only the presence of bacteria in the liver and spleen that is important. In fact, the genetic properties of the disseminated organism also critically influence lethal outcomes. This discovery is consistent with models of sepsis that suggest the infecting organism and its characteristics should be of central consideration in treating the systemic inflammatory response that results from bloodborne bacteria (145).

With regards to specific MARTX effector domains, some individual effectors positively regulate *V. vulnificus* virulence potential. The virulence deficiency of the *ΔvvhA Δrid* and *ΔvvhA Δrrsp* strains suggest that inactivation of GTPase signaling is critical to *V. vulnificus* virulence following i.g. infection. Surprisingly, the the *ΔvvhA Δduf1* and *ΔvvhA Δabh* strains exhibit increased virulence relative to the parental strain. Therefore, MARTX toxin potency is not simply an additive effect of multiple effector domains that positively contribute to virulence. Instead, there exist domains that each exert cytopathic effects *in vitro* but in the context of the MARTX holotoxin (that is, when delivered in concert with the other four effector domains) negatively regulate bacterial virulence potential. Both the mechanism, and the reason, for a MARTX effector domain to attenuate *V. vulnificus* virulence potential remain to be determined. However, it suggests the interplay and crosstalk of effectors simultaneously delivered to host cells via the MARTX toxin platform. It also likewise suggests that maximizing virulence potential may not be advantageous for *V. vulnificus* in the context of its natural environment.

CHAPTER 5

Surface hypothermia predicts murine mortality in the intragastric *Vibrio vulnificus* infection model

Overview

Vibrio vulnificus is a Gram-negative bacterium found in aquatic environments. It has the potential to cause disease in humans who encounter the bacterium (105, 125). Wound infections occur when open skin lesions are exposed to bacteria, usually during wading or swimming (122). Gastrointestinal infections arise when humans consume raw or undercooked seafood – most frequently, shellfish – that contains the microbe (124). In severe situations, these infections progress to necrotizing fasciitis and primary sepsis, respectively (317). Survival outcomes are particularly poor for gastrointestinal *V. vulnificus* infections with mortality rates exceeding 50% of infected individuals (101). In light of this infection severity, improved understanding of *V. vulnificus* pathogenesis is increasingly critical.

Controlled human case studies cannot be conducted due to low *V. vulnificus* treatment efficacy, and retrospective clinical analyses lack much of the detailed information necessary to obtain full comprehension of disease course (103, 109, 120, 318, 319). Therefore, to study *V. vulnificus* foodborne infection, a mouse model is routinely employed (1, 193). Following intragastric inoculation with a bacterial suspension, infected animals are monitored, usually over the course of 48-60 hpi, by which point they either succumb to or resolve the infection. In lethal cases, bacteria can be isolated from distal organs pre- and post-mortem, indicating this model

recapitulates the bacterial dissemination observed in septic human disease (Chapter 3) (1, 35, 138).

While laboratory mouse experiments provide invaluable data on infectious diseases, animal distress is, in many cases, an inherent component of animal experimentation. For this reason, scientists as well as regulatory bodies have sought methods to limit suffering of murine research subjects (320). Current data indicate that hypothermia is efficacious for predicting death due to late-stage infectious disease (321-324). In addition, contact-free, infrared surface thermometers – as an alternative to rectal probe or implanted telemetric thermometers – are ideal for use in studies of acute gastrointestinal pathogenesis. Yet, notably, the specific temperature boundaries that predict infection lethality, and the utility of these boundaries, depend heavily upon the model system in question (321, 325). Therefore, this study was conducted to test the efficacy of hypothermia as a predictor of *V. vulnificus* mortality after oro-gastric inoculation, and to define the specific temperature parameters for implementation of hypothermia as a humane endpoint in *V. vulnificus* intragastric virulence studies.

Results

Bacterial strain selection

These experiments were conducted using four strains of *V. vulnificus* that differ in the gene *rtxA1*, which encodes the primary virulence toxin, the Multifunctional Autoprocessing Repeats-in-Toxins (MARTX) toxin. All strains are detailed in Figure 5.1.

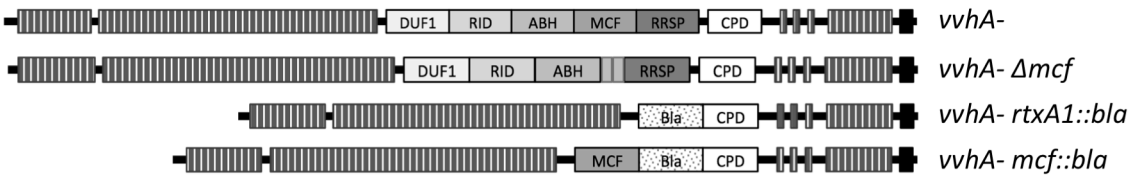

Figure 5.1. Schematic depiction of the MARTX toxin variants produced by strains in this study. DUF1=domain of unknown function in the first position; RID=Rho Inactivation Domain; ABH=Alpha/Beta Hydrolase domain; MCF=Makes Caterpillars Floppy-like domain; RRSP=Ras/Rap1 Specific Protease domain; CPD=Cysteine Protease domain; striped boxes=repeat regions.

V. vulnificus strain *vvhA- rtxA1::bla* was generated from the Korean clinical isolate *V. vulnificus* CMCP6 (Table 7.1). Although originally described as a genetic deletion of *vvhBA* (1), subsequent gene mapping revealed disruption of only *vvhA* by the stable integration of a portion of ampicillin-resistant plasmid pHGJ4. This strain was then further modified. Plasmids for alteration of *rtxA1* to *rtxA1::bla*, *mcf::bla,* or *Δmcf* have been described previously (Chapters 2 and 3) (30, 31, 35). Each plasmid was transferred from *Escherichia coli* SM10 λ *pir* or S17 λ *pir* to *V. vulnificus ΔvvhA-* by conjugation. Selection for double homologous recombination was conducted using sucrose counterselection to isolate recombinants as previously described (326). Genetic modification was confirmed by polymerase chain reaction (PCR).

V. vulnificus strains show distinct survival patterns

For pooled data across both experiments, all ten of the mock-infected animals survived to 48 hpi (Figure 5.2, A). In contrast, 90% of mice inoculated with the parental *V. vulnificus vvhA-* strain succumbed to infection within 24 hpi, an outcome consistent with previous experiments (Chapters 3 and 4) (1, 35)**.** In *vvhA- rtxA1::bla*, the *rtxA1* gene is altered to replace MARTX toxin effector domains with a heterologous beta-lactamase coding region. All mice infected with *vvhA- rtxA1::bla* survived to 48 hpi demonstrating significant virulence attenuation (Figure 5.2, A). These results are consistent with previous data demonstrating that elimination of the MARTX effector domains attenuated virulence equivalent to an *rtxA1*-null mutant (Chapter 3) (35).(35). By contrast, deletion of only the *mcf* coding region (*vvhA- Δmcf*) did not significantly attenuate virulence compared to *vvhA-*. This is consistent with the results observed in Chapter 4. Similarly, the addition of *mcf* into *vvhA- rtxA1::bla* did not significantly enhance virulence of the

attenuated strain (Figure 5.2B). Therefore, the MCF domain alone is neither necessary nor sufficient for MARTX toxin-associated virulence in *V. vulnificus*.

A

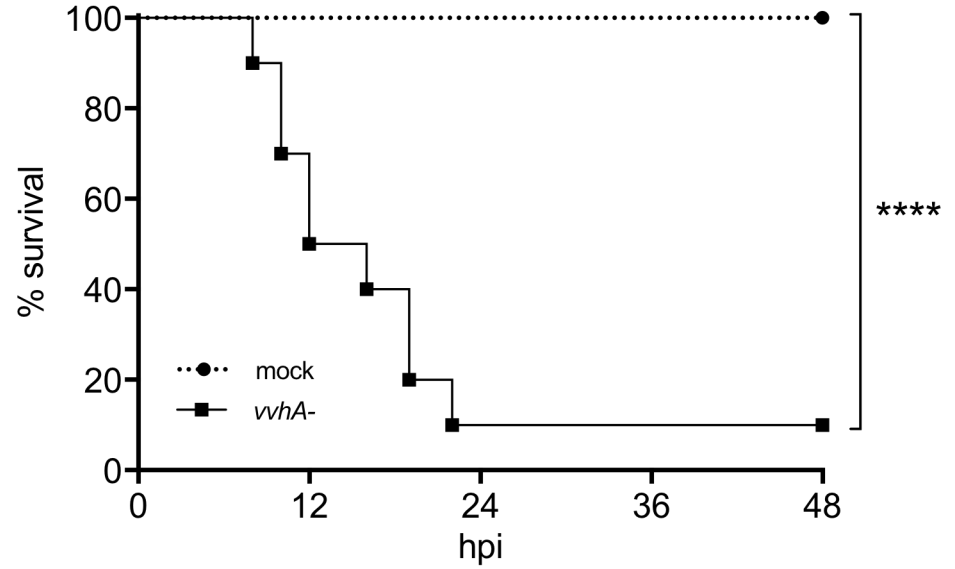

B

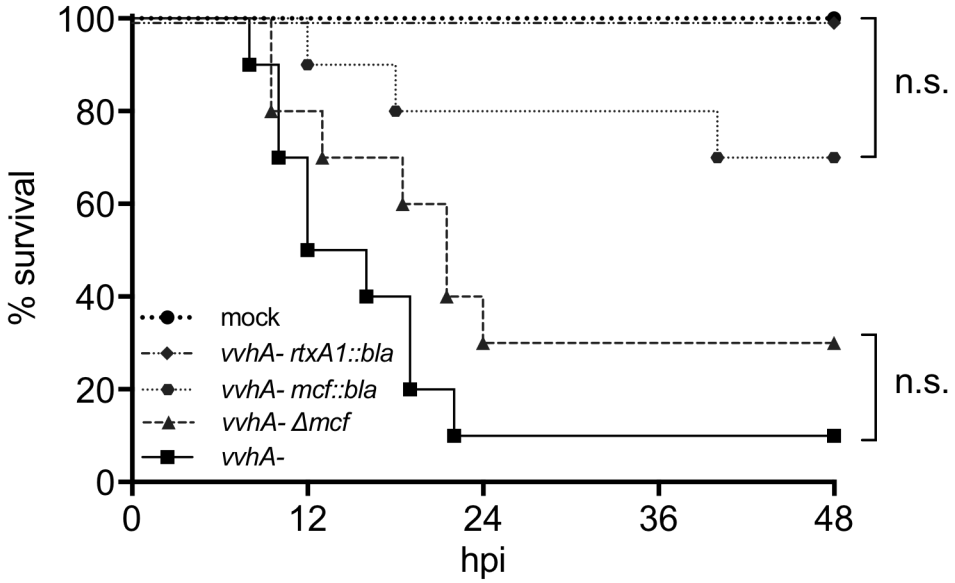

Figure 5.2. *V. vulnificus* strains exhibit distinct survival patterns. (A) Survival of mice infected with *vvhA*- compared to mock-infected mice, n=10/group. (B) Survival of mice infected with the indicated strains, n=10/group (note that mock and *vvhA*- curves are repeated from A). Survival curves were compared by log-rank test. ****$p \leq 0.0001$

Ventral surface temperature measurement profiles vary dependent upon survival outcome

Data were first analyzed pooling results for all *V. vulnificus* groups tested. Of 40 mice inoculated with any strain of *V. vulnificus*, 21 mice survived and 19 mice died. For non-survivors, the mean time-to-death (TTD) was 17 hpi (S.D. ± 8 hpi) with a range of 8 to 40 hpi. In the course of these experiments, ventral surface temperature (VST) was also measured (Figure 5.3). Among all mice, the minimum VST (VST_{min}) reading during the experiment was 21.1°C and the maximum VST (VST_{max}) was 33.7°C for a total measurement range of 12.6°C.

During the first 0 to 4 hpi, the majority (46 of 50) of tested animals exhibited a drop in VST relative to initial (VST_0). This drop was measured in both infected and mock-treated animals (Figure 5.3 A-C, grey zones). The temperature decrease at this initial stage is attributed to anesthetic-induced hypothermia (327) as it occurred independent of infection status. For mock-treated animals, VST rebounded to match or exceed VST_0, usually by 4 hpi and in all cases by 6 hpi (Fig. 2A). VST of mock-infected mice then generally remained stable after recovery from the initial drop (6-48 hpi).

Among *V. vulnificus* inoculated animals, measured VST of mice that survived spanned a wide range of more than 11°C (Figure 5.3, B). Survivors most frequently exhibited VST_{min} at 6 or 8 hpi. Subsequent VST readings in survivors were characterized by a period of temperature recovery (8-14 hpi) and finally a period of temperature stability (16-48 hpi).

In contrast, measured VST of mice that succumbed to infection generally did not recover after the anesthetic period of 0-4 hpi (Figure 5.3, C). Instead, VST of non-survivors continued to decrease, spanned a much smaller range of less than 4°C, and exhibited VST_{min} readings at 8-12 hpi (Fig. 2C). In many cases, VST of non-survivors increased in the span between 12 and 18 hpi,

despite the fact that these animals succumbed to infection by 24 hpi. This pattern is distinct both from the mock-treated group and infected animals that survive inoculation. Thus, VST measurement profiles vary depending upon both *V. vulnificus* infection status, and infection survival outcomes.

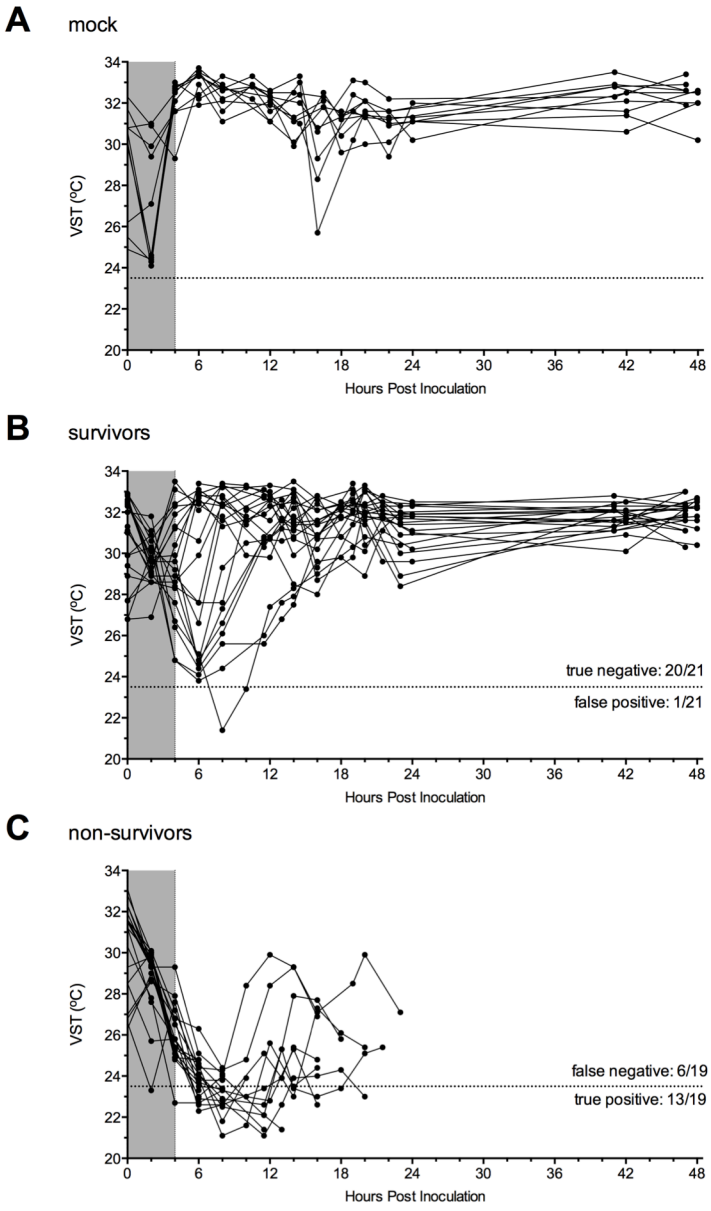

Figure 5.3 VST measurement profiles vary dependent upon survival outcome. Ventral surface temperature (VST) readings over time for: (A) mock infected mice, (B) mice that survived infection and (C) mice that did not survive infection. Each dot represents a single VST reading, and a continuous line connects VST readings from the same mouse. VST measurement ends either at 48 hpi or at time of death.

VST of 23.5°C is associated with lethality during *V. vulnificus* infection.

Comparing VST between 6 and 48 hpi across groups, mean VST_{min} of surviving mice (27.9±3.2^{o}C, Fig. 5.4) was not significantly different from mean VST_{min} of mock-infected mice (29.4±1.5^{o}C, Fig. 5.4). However, mice that later succumbed to infection exhibited significantly reduced VST_{min} compared to either survivors or mock-treated animals (22.9±1.2^{o}C Fig. 5.4). Detailed analysis suggests that 23.5°C delineates between lethally and non-lethally infected mice.

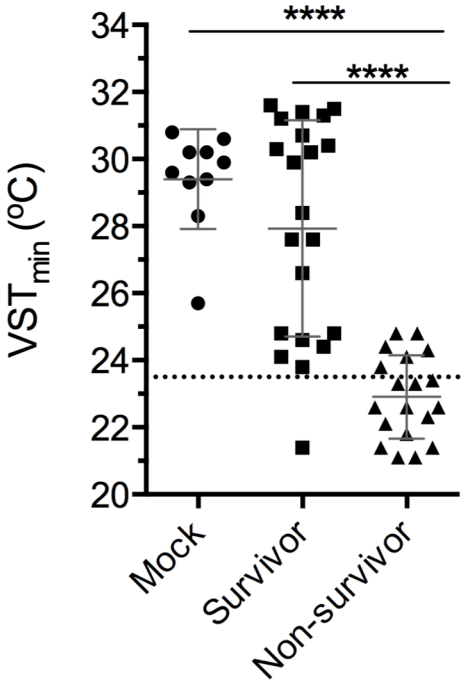

Figure 5.4. Minimum VST of infected mice is significantly different between survivors and non-survivors. Scatter plot of VST_{min} measured between 6 and 48 hpi. Lines indicate mean with error bars for standard deviation and temperature cutoff of 23.5°C is indicated with a dashed line. Results analyzed by one-way ANOVA with Tukey post test for multiple comparisons. ****p≤0.0001

Only 1 of 21 survivors exhibited VST≤23.5°C (false positive, Figure 5.3B). In diagnostic terms, a test's specificity is its ability to correctly identify individuals that are not affected by a condition. In other words, specificity measures the test's true negative rate as a ratio of true negatives calls to total negative outcomes. In this case, where survival is the experiment negative outcome, 21 mice survived infection and 20 of those mice had VST_{min}>23.5. Thus, the endpoint of VST≤23.5°C exhibits specificity of 95%. This high specificity result is important because it indicates only 5% of VST-indicated euthanizations will result in a mouse being counted as a non-survivor that otherwise would have survived infection.

Conversely, 13 of 19 non-survivors reached VST≤23.5°C (true positive, Figure 5.3C). The sensitivity of a diagnostic test indicates its ability to correctly identify those individuals affected by a condition in question. Sensitivity measures true positive rate by taking a ratio of true positive calls to total positive outcomes. In the case of VST endpoints applied to *V. vulnificus* infections, where death is the test's positive outcome, 13 non-survivor mice were predicted by their VST_{min} to have lethal infection, while a total of 19 mice were ultimately non-survivors. Therefore, VST≤23.5°C has a sensitivity of 68% in predicting *V. vulnificus* infection outcome. This result means that 68% of mice that spontaneously died were indicated by VST≤23.5°C. Moreover, because the remaining mice with lethal infections still proceed to death, the sensitivity of the overall experiment is actually unchanged; eventually all non-survivor outcomes are captured within the experimental context. Thus, with essentially no loss of experimental efficacy, nearly 70% of mice could have been humanely euthanized for a reduction of suffering prior to the onset of death.

Two additional measures are used to assess the diagnostic efficacy of VST≤23.5°C. Positive predictive value (PPV) is the proportion of positive diagnostic calls that are, indeed, true positives. In this case, 14 mice reached VST≤23.5°C. 13 of these 14 mice were non-survivors. Therefore, the hypothermia endpoint has a PPV of 93%. Conversely, the negative predictive value (NPV) is the proportion of negative test calls that are true negatives outcomes. Twenty of the 26 mice that had temperatures above the cutoff were survivors, while 6 were non-survivors. Therefore, the hypothermia endpoint VST≤23.5°C has a NPV of 77%. This analysis supports the conclusion that reduction in VST is predictive of subsequent death.

VST≤23.5°C predicts live/dead survival outcomes and reduces infection hours

The survival data were next analyzed comparing temperature-predicted outcomes to actual outcomes. To assess the efficacy of hypothermia as an experimental endpoint when comparing different infecting bacterial strains, time-to-death and time-to-VST≤23.5°C were compared for each infecting strain in this study (Figure 5.5). In the retrospective analysis (dotted lines), animals were plotted as non-survivors if either (1) the mouse exhibited VST≤23.5°C or (2) if the mouse died even if it never reached ≤23.5°C.

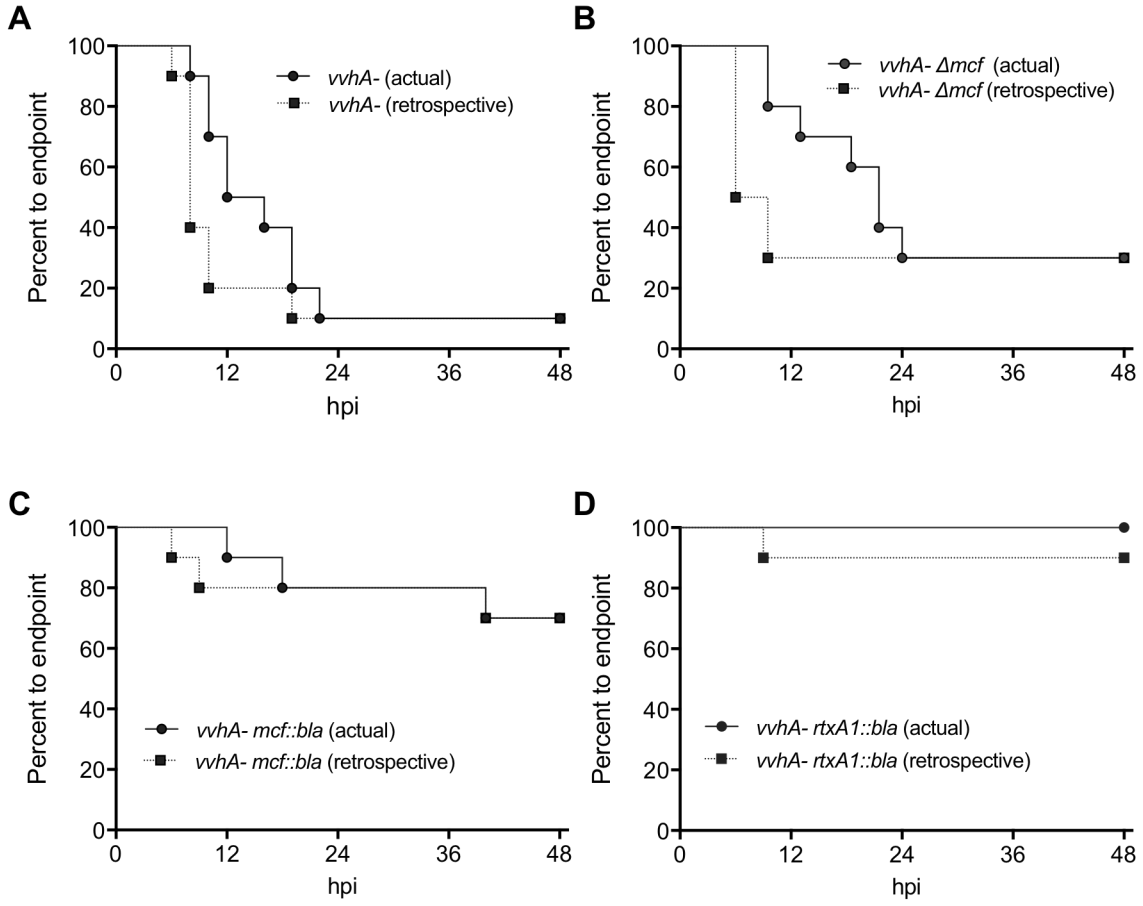

Figure 5.5. VST ≤ 23.5 °C predicts live/dead survival outcomes and reduces infection hours. Comparison of survival time for each of the *V. vulnificus* strains: (A) *vvhA*-; (B) *vvhA-Δmcf*; (C) *vvhA- mcf::bla*; (D) *vvhA- rtxA1::bla*. Actual curves (circles connected by solid line) use death as endpoint; retrospective curves (squares connected by dotted line) use VST≤23.5°C, or death if an animal died without reaching VST≤23.5°C. Statistical analyses are summarized in Table 2.

Statistical variation of binary outcomes (survival vs. death) was analyzed by chi-square test (χ^2, Table 2). The χ^2 analysis revealed no significant differences between binary survival outcomes when the hypothermia plus actual death endpoint was applied (Fig. 4, Table 2). In fact, in most cases the survival outcomes were identical (Figure 5.5A-C), but even in the case of a numerically different outcome the results were not significantly different (Figure 5.5, Table 5.2).

Table 5.2. Statistical analyses of survival outcomes and curves.

Strain	**Binary X^2 Analysis (actual vs. retro)**		**Log-rank curve comparison (actual vs. retro)**	
	χ^2	*p*	χ^2	*p*
vvhA-	0.0	1.0	1.8	0.18
vvhA- Δmcf	0.0	1.0	0.82	0.36
vvhA- mcf::bla	0.0	1.0	0.0085	0.92
vvhA- rtxA1::bla	1.05	0.30	1.0	0.32

VST≤23.5°C in some cases correlated with imminent death, although many animals lived for hours prior to succumbing to infection (Figure 5.3C). In non-survivors, TTD after VST≤23.5°C had a range of 15 h, mean of 10 h, and S.D. of 5 h. Therefore, while this endpoint is capable of predicting a lethal outcome, there is notable variability in the TTD. To illustrate this point, the endpoint curves (Figure 5.5) were compared using the log-rank test with 95% confidence, $p<0.05$. Interestingly, there were no statistical differences between endpoint curves when analyzed by log-rank test (Table 5.2). Nonetheless, detailed information on the kinetics of death were lost in the hypothermia-derived curves due to time discrepancies between VST≤23.5°C and actual death (Fig. 5.5). While this renders the VST endpoint unsuitable for survival curve comparison, the differences in area under the survival curves (Figure 5.5) illustrates the power of the alternative VST endpoint to perform its intended function: predict non-survivor outcomes, such that animals involved in the experiments can be euthanized prior to the onset of death. In the experiments illustrated in Figure 5.5, the hypothermia endpoint VST≤23.5°C would have eliminated 135 unnecessary infection hours for mice that would eventually succumb to infection (dotted vs solid lines).

Discussion

Measurement of virulence in animal models is central to studies of bacterial pathogenesis. In lieu of death, the 'moribund condition' – generally characterized by markers such as piloerection, hunching, and respiratory irregularity – is often utilized in animal protocols as an experimental endpoint, considered more humane than death. However, moribund status can be biased due to subjectivity and inconsistency of observers, and inaccurate if there is disconnect

between observed characteristics and imminent death (325, 328). In our research group, we have noted anecdotally that there is a lack of correlation between moribund status and imminent death during *V. vulnificus* experiments. In the past 25 years, temperature monitoring has been successfully utilized to develop more refined endpoints for fungal, bacterial, and viral infection studies (323, 329-332). Retrospective analysis of additional infectious disease experiments found hypothermia to be "the most valuable characteristic for distinguishing mice that survive or succumb to infection" (321).

Core body temperature can be measured by rectal thermometry (323, 324). However, this method is time consuming for research staff and is thought to increase animal distress due to extensive handling (325, 333). Moreover, intestinal probing has the potential to adversely affect experimental outcomes of a gastrointestinal pathogen due to the risk of lesion introduction (334). The alternative method of microchip implants for thermal telemetry facilitates rapid, contact-free measurement by researchers, but requires front-end time and monetary output that is not justifiable for the acute time scale of *V. vulnificus* infections (322, 325, 335). In addition, lesions generated at the microchip injection site are susceptible to unintentional infection (333). Since *V. vulnificus* infects open wounds (122), the risk of subcutaneous infection is a confounding factor that renders microchip thermometry untenable for *V. vulnificus* studies.

With the advent of new technology, body surface temperature can now be measured using an external infrared thermometer (331-333). Compared to other methods, use of a surface probe reduces animal stress, experimental complication, and initial cost (336). Importantly, measured core and surface temperatures are correlated (336). Correlations are particularly strong when core body temperatures are below normal, as is the case during infection-induced

hypothermia (321, 336). In the current study, infrared surface thermometry demonstrated utility in predicting disease severity during *V. vulnificus* infection and was utilized to identify a hypothermic temperature endpoint for these studies.

This study was conducted using four strains of *V. vulnificus* that differ in their known or predicted lethality. Predicted or realized differences in virulence were derived from modification of the virulence associated gene *rtxA1*. Indeed, when the central portion of the toxin – collectively termed the effector domain region – was deleted and replaced by a heterologous beta-lactamase coding sequence, *V. vulnificus* was significantly less virulent (Fig. 1C, *vvhA*- vs *vvhA- rtxA1::bla*, (35)). To examine the necessity of a single effector domain in virulence we tested a strain *vvhA- Δmcf* that harbors an in-frame deletion of the *mcf* effector domain (Fig. 1A) (31) and another that carries only the *mcf* effector domain region. These experiments support the conclusion that the *mcf* coding region is neither necessary nor sufficient to change the virulence potential of *V. vulnificus*. These data provided a virulence data set as a baseline for assessing the use of VST as an endpoint for V. vulnificus intestinal infections.

In many cases, differences in pathogen virulence are best defined by median lethal dose (LD_{50}) determination. These studies need not take experimental kinetics into account, because LD_{50} is determined by the number of survivors and non-survivors at a given pathogen dose. In the current study, 68% of mice that spontaneously died could have been euthanized on average 10 h prior to death using the defined VST endpoint. At 95% sensitivity, application of this endpoint did not compromise experimental efficacy. Thus, applying an endpoint of VST≤23.5°C during *V. vulnificus* infection has potential to considerably reduce animal suffering in studies where binary data is desired. Our finding that binary live vs. dead outcomes are predictable by

hypothermia suggests that the VST alternative endpoint is appropriate for LD_{50} determination and should be applied to LD_{50} studies to reduce suffering of animals in these experiments.

LD_{50} measurements require large numbers of mice to test an appropriate range of doses at a level that allows for statistical power. As such, many research groups use an alternative method for determining relative virulence: infecting different groups of mice with different strains at a set dose (as in Fig. 1C) and reporting differences in the survival curves. Unlike binary LD_{50} studies, these curves account for time-to-death, which allows for greater statistical power with lower numbers of mice. Yet, survival curves are also considered less sensitive in their ability to detect virulence differences among strains. This study reveals that the observed lag between the VST endpoint and death renders application of a VST endpoint a poor choice for these types of studies (Fig. 4, actual vs. retrospective) due to loss of death kinetics. The curve shift actually emphasizes the utility of VST≤23.5°C in predicting lethal outcomes well before the onset of death to the experimental animals. Yet, this result likewise indicates that a VST-based endpoint does not have the same cost-free benefit in survival curve experiments that it offers to LD_{50}.

Interestingly, these results leave researchers to determine whether it is more ethical to: (A) use larger numbers of mice and perform LD_{50} studies, with the ability to apply a humane experimental endpoint; or (B) use smaller numbers of mice in a survival curve analysis without the option of a humane endpoint, a decision that will depend largely on the specific experimental goals of the research group in question.

While hypothermia has been demonstrated as a key marker of death due to infectious disease, its relationship to survival of *V. vulnificus* infections had not previously been examined. It was here determined that surviving and non-surviving *V. vulnificus* infected mice demonstrate

distinct temperature responses. Non-surviving infected mice have significantly lower VST_{min} as compared to surviving mice. From these data, a temperature endpoint of 23.5°C was empirically determined and retrospectively applied to the survival results. When used as an experimental endpoint, VST≤23.5°C exhibited sensitivity of 68% and specificity of 95%. The temperature cutoff of 23.5°C demonstrates 93% PPV and 77% NPV. Given the outcomes of this study, a hypothermia-based humane endpoint can be applied to LD_{50} studies without concern of reducing the efficacy of the experiment. Binary (live vs. dead) survival outcomes are almost always numerically identical and in all cases statistically indistinguishable from survival data using death as an endpoint (Fig. 4, Table 2). As such, many hours of undue suffering would be eliminated from infection experiments.

By its very nature, an alternative endpoint aims to predict death early such that animal research subjects can be euthanized prior to death. VST≤23.5°C predicts non-survival outcomes an average of 10 hours in advance of the event. This allows for a considerable reduction in unnecessary mouse infection hours. Nonetheless, given that a hypothermia endpoint alters experimental kinetics, these kinetic changes suggest that VST endpoint should not be applied to survival curve experiments.

CHAPTER 6 – DISCUSSION

Summary

The studies outlined here elucidated the role of discrete MARTX toxin regions during intragastric (i.g.) pathogenesis of the bacterium *Vibrio vulnificus*. Genetic manipulation was used to generate bacterial strains capable of delivering novel MARTX toxin variants to target cells during *in vitro* co-incubation or *in vivo* infection. In this way, novel insights into *V. vulnificus* pathogen:host interaction were revealed.

First, study of toxin dynamics *in vitro* demonstrated that the MARTX toxin N- and C-terminal repeat regions form a pore in target eukaryotic cells that is sufficient for induction of lysis. The MARTX effector domains are not required for lysis *in vitro*. However, they are responsible for early induction of cytopathic effects that phenotypically manifest as cell rounding.

Combined, these data led to two contrasting hypotheses. Perhaps the conserved MARTX pore and its associated necrotic activity are sufficient for toxin-induced phenotypes *in vivo*, as is the paradigm with many lytic toxins. Alternatively, perhaps the effector domains, which induce cytopathic effect prior to lysis, are important for conferring toxicity and virulence during bacterial infection.

These dual hypotheses were experimentally investigated. In animal models, a *V. vulnificus* strain lacking the MARTX effector domains exhibits the same virulence and pathogenesis profiles as a MARTX-null mutant, indicating that it is the MARTX effector domains which confer toxicity *in vivo*. The effector domains are required for rapid induction of epithelial barrier dysfunction *in vitro* and for bacterial dissemination from the intestine *in vivo*.

Additionally, these experiments reveal the biphasic nature of MARTX toxin activity, in which the early lysis-independent phase relies upon effector domain activity, but the late lytic phase is effector-independent.

Because the effector domain region of the MARTX protein is in fact a repertoire of discrete effector domains, the next logical inquiry concerned the role of individual effector domains. Again, multiple outcomes were possible. No single effector domain is observed across all strains of *V. vulnificus* or across all MARTX toxin variants (13). This suggests that no single effector domain is required for MARTX toxicity. However, the modular composition of MARTX effector repertoires could simultaneously consist of some effectors that confer dominant virulence phenotypes and some effectors with secondary, additive, or redundant roles.

When tested, no single MARTX effector domain was required for the phenotypes attributed to the effector domain repertoire as a whole. Effector domains exhibit functional redundancy in *in vitro* models of intestinal barrier disruption and phagocytic inhibition. However, these same mutant strains have distinct virulence profiles *in vivo*. While some aspects of MARTX effector function are redundant, different effector repertoires do confer different toxicity profiles, indicating that changes in effector composition have functional consequences during infection.

Together these studies experimentally demonstrate the role of the MARTX toxin as an effector delivery platform, wherein the composition of the delivered effector domains plays a defining role in bacterial virulence. Though the toxin can undoubtedly cause lysis, the experiments presented here should shift the focus of the MARTX field away from its lytic function and toward its role in delivering bacterial effectors capable of modulating target cells. In

this way, the MARTX can be conceptualized as an alternative bacterial effector delivery mechanism, which is especially interesting in light of a bacterium like *V. vulnificus*, which lacks the Type 3 and Type 4 secretion systems characteristic of many pathogenic bacteria.

Discussion and Outstanding Question

The overall structural organization of MARTX toxins is predictable, and the N- and C-terminal portions of the encoding *rtxA1* genes are highly conserved (275) However, the total length of a given MARTX varies from 3500-5300 amino acids due to the variable number and identity of effector domains in the toxin's central region (2). The role of the MARTX toxin as a system for bacterial effector delivery had previously been hypothesized (13). Yet, the functional roles of the effector domains and repeat regions had not been previously investigated in the context of *V. vulnificus*.

In the study described here, we found that numerous characteristics of $MARTX_{Vc}$ are also true of $MARTX_{Vv}$. Namely, the MARTX effector domain region is not required for MARTX toxin expression, secretion, or delivery to host cells. Moreover, in both cases the MARTX toxin is a sufficiently robust effector delivery platform that it can translocate not only its own diverse native effector repertoires, but also heterologous proteins. So far this has been demonstrated in both *Vibrio cholerae* and *V. vulnificus* using beta-lactamase, which exhibits its functional enzyme characteristics both extracellularly and in the eukaryotic cytosol (Chapter 2) (3, 30). Bla must undergo an unfolded transition between these two folded states in order to be translocated through the MARTX pore, the diameter of which has been estimated at 1.6 nm (136). We posit that this MARTX platform can be modified to deliver any heterologous effector possessing

protein dynamics that allow for an unfolded state during membrane translocation and proper re-folding in the eukaryotic cytosol (281).

We hypothesize that these characteristics found to be shared by $MARTX_{Vc}$ and $MARTX_{Vv}$ - that is, the sufficiency of the N- and C-terminal domains to deliver centrally encoded domains to eukaryotic cytosols – are likely generalizable also to the entire MARTX family. *rtxA1* loci have been identified across numerous *Vibrio* species as well as other bacterial genera including *Photorhabdus, Xenorhabdus,* and *Aeromonas* (253). Still, functional characterization of *rtxA1* genes in these organisms remains an open, and potentially fruitful, area of investigation.

The experiments described in Chapter 2 also gave insight to *V. vulnificus*-specific aspects of the MARTX toxin. Using bacterial mutants producing different versions of the MARTX toxin, we show that the repeat region pore is sufficient not only for heterologous domain translocation, but also for lysis of target cells. Of the three organisms in which MARTX toxins have been functionally characterized, *V. vulnificus* is the only bacterium that causes MARTX-dependent cell lysis. Neither *V. cholerae* nor *Vibrio anguillarum* induce MARTX-dependent necrosis of target cells, yet cell lysis remains one of the best-documented phenotypes of $MARTX_{Vv.}$ activity (Chapter 2) (22, 30, 136, 246, 305).

The mechanisms of differences in lysis – that is, why $MARTX_{Vv,}$ but not $MARTX_{Vc}$ or $MARTX_{Va}$, is lytic – is a key outstanding question (6, 255). The N- and C-terminal repeat regions of $MARTX_{Vv,}$ and $MARTX_{Vc}$ share 93 percent homology (30). While highly conserved, the two are not identical. Thus it is possible that differences in repeat region sequence make one

pore more conducive for lysis. The size of the *V. vulnificus* MARTX toxin pore has been estimated at 1.63 nm, but the MARTX toxin pore size has not been estimated for *V. cholerae.*

The differences between MARTX toxin repeat regions could influence toxin multimerization. MARTX toxins are thought to function monomerically, with the N- and C-terminal regions of each polypeptide forming a translocation-conducive pore. However, it is possible that MARTX toxins could oligomerize. There is a precedent for RTX toxin oligomerization in the case of the adenylate cyclase (AC) toxin, CyaA, from *Bordatella pertussis,* where

> "translocation of the [enzymatic] adenylate cyclase domain and oligomerization into cation-selective pores appear to represent two independent and parallel/competing activities of the membrane-inserted form of CyaA. Either activity can be upmodulated at the expense of the other by specific substitutions of key glutamate residues forming pairs in the predicted transmembrane segments […] (276)"

These two alternative conformers permit flux of different ions and induce different reactions in their target cells (337, 338). If the same is true of MARTX toxins, changes promoting MARTX toxin oligomerization could favor formation of larger-diameter, lytic pores.

Alternatively, toxin expression and delivery levels may differ among MARTX-producing species. Indeed, the bacterial toxin literature reveals a precedent for time and dose-dependent effects of pore-forming toxins (PFT) on their target cells. Eukaryotic cells are capable of recovering from short-term exposure to many PFTs, as demonstrated for nine of ten PFTs tested by Thelestam and Möllby in 1983 (339). In fact, the transient membrane permeability induced by exposure to the *Streptococcus* PFT streptolysin-O has been leveraged as a tool for exogenous

protein delivery to living cells (340). Generally, it is accepted that a cell's recovery from PFTs entails isolating the affected membrane segment by endo-, exo-, and/or ecto-cytosis. Depending on the recovery pathway, an intoxicated membrane section is either repaired (e.g. via degradation of the PFT) and recycled, or irreversibly released to the extracellular milieu (341-343).

However, there are limits on recovery and "excessive pore formation indeed leads to target cell death" (341). The same streptolysin-O that has been used in protein delivery strategies is characterized (and named) as a "potent cytolytic agent"(344). An abundance of studies report necrosis of erythrocytes and nucleated cells upon exposure to PFTs. A small subset of examples includes: the *Clostridium septicum* alpha toxin (345, 346), *Staphylococcus aureus* Panton-Valentine leukocidin (PVT), *Escherichia coli* hemolysin A (HlyA) (347), and the hemolysins from *V. cholerae* (HlyA) and *V. vulnificus* (VvhA) (296, 297).

The idea of differing toxin expression is supported by *in vitro* evidence in which the cellular reaction to *V. vulnificus* MARTX toxin is biphasic. The first phase of activity, attributed to the MARTX effector domains, is lysis-independent. This is exhibited by rounding of unpolarized cells (Chapter 2) (30) and by the induction of paracellular permeability and barrier dysfunction in polarized intestinal epithelial cell monolayers (Chapter 3) (35). The onset of lytic MARTX toxin activity occurs after longer periods of bacterial:cell co-incubation. In the case of experiments where a set number bacteria are inoculated and then allowed to outgrow, the onset of lysis likewise coincides with MOIs that have increased up to 30-fold relative to the inoculum ratios (Figure 3.12). Assuming continued toxin production, bacterial outgrowth almost certainly means that the rate of toxin delivery to eukaryotic cells increases over time in co-incubation

experiments. We anticipate that lysis occurs after target cell intoxication has reached a threshold beyond which cells cannot ameliorate the effects of the PFT on the membrane.

Unfortunately, dose-dependent lysis experiments cannot be conducted directly for MARTX toxins in the absence of purified MARTX toxin. For reasons including low expression in broth culture, extremely large size, and rapid degradation, the MARTX toxin has thus far never been purified. However, it is possible that the relatively novel effector-free RtxA1::Bla toxin (Chapters 2 and 3) could be purified. This protein is much reduced in size compared to its holotoxin counterpart. Moreover, highly specific Bla antibodies make it feasible to use that domain as a target for protein pull-down. Working in *Vibrio* strains lacking both CPD activity (*cpd**) and the extracellular protease VvpE (*vvpE*) would minimize extracellular MARTX toxin cleavage and thereby maximize the amount of protein available for purification. It would likewise be possible to first expose bacteria to eukaryotic cells so as to increase *rtxA1* exposure. Combining the above conditions would likely make protein purification and, therefore, dose-dependent MARTX toxin experiments, feasible.

Alternatively, relative *rtxA1* expression could be tested across MARTX-producing strains as a starting point for addressing dosing questions. While expression from the *rtx* operons has been tested for single species under different conditions (e.g. in broth culture vs. in contact with eukaryotic cells or during mouse infection (136, 140, 254, 261)), no study has yet compared *rtxA* expression across bacterial species. This could be accomplished using either traditional qRT-PCR, or even using the modified Bla strains in conjunction with the nitrocefin-based secretion assays outlined in Chapter 2. Alternatively, modification of the RtxA1::Bla system could putatively yield toxins delivering fluorophore (e.g. super-folder GFP (348)) quantifiable using a

high-resolution microscopy method (349, 350). In theory, one could use genetic manipulation to exchange MARTX toxins (or portions thereof) among various *Vibrio* species, testing the same toxin in different genetic/strain contexts. However, this would almost surely meet with biosafety concerns for gene swapping in pathogens. One or more of these genetic methods might suggest whether cell lysis arises from dose-dependent effects that are higher in *V. vulnificus* as compared to other *Vibrios* delivering MARTX toxins.

With that said, *in vivo* data from the study of MARTX toxins highlight its non-lytic roles as vital for pathogenesis. Bischofberger, et al, posited the importance of non-lytic PFT effects during infection in a 2012 review on pathogenic pore-forming toxins:

> "During the course of infection, most cells are probably exposed to rather low concentration of PFTs, which would not necessarily lead to cell death. The toxin-triggered changes in cytoplasmic ion composition in these cells will however lead to a panel of secondary events, whose contribution to pathogenesis requires further investigation." (341)

Indeed, some deleterious effects of the MARTX toxin – namely, inflammasome activation – have been ameliorated by stopping potassium (K+) efflux (290), indicating a putative role for ion-based responses in target cells.

Even more relevant to MARTX study, however, is the research on other toxins that form pores in the service of effector delivery. Such is the case with the AC toxin, which encodes functionally independent regions that confer AC activity and hemolysis (304). Mutants lacking adenylate cyclase activity, but retaining the hemolytic (HLY) domain, exhibit median lethal doses (LD_{50}) that are 1000-fold higher than their parental strains. Strains lacking the HLY

domain are attenuated at levels comparable to the AC mutants, which – given that the HLY domain is required for AC domain delivery – lends credence to the idea that HLY domain is functioning to deliver AC to host cells and not additively with AC activity (351, 352).

During intestinal infection of mice, bacteria that produce a MARTX toxin able to lyse cells, but absent the effector domain region, were indistinguishable from bacteria that did not produce the toxin at all (Figure 3.3). Thus the effector domain region is required for MARTX-associated virulence. Whether the effector domain region is sufficient for MARTX activity was not directly tested, given that these domains necessitate delivery via the MARTX platform. Still, their requirement for virulence and bacterial dissemination, and the lack of distinction between the *rtxA1::bla* strain and an *rtxA1*- strain, together strongly suggest that delivery of effectors is the mechanism of MARTX toxicity *in vivo*.

Notably, genetic and biochemical characterization of MARTX toxin complexity previously lent hypothetical support to this result. Yet, these data represent the first direct experimental evidence that non-lytic functions previously attributed to the MARTX toxin (such as cytoskeleton disassembly, induction of apoptosis, inhibition of autophagy, and modulation of stress signaling (4, 21, 27, 31, 247, 308)) play an important – indeed, central – role in pathogenesis. We have here presented data that should shift the focus of the MARTX field away from lytic necrosis and toward the myriad other functions associated with *rtxA1* or its effector domains.

Specifically, the discrepancy between lytic toxin phenotypes and *in vivo* function has been highlighted. Fulminant intestinal tissue damage has been observed in previous mouse experiments and clinical cases. Moreover, bacterial dissemination and sepsis are phenotypes

intimately linked to lethal infection outcomes (103, 122, 132, 138, 139). The importance of *rtxA1* in dissemination (136, 249), combined with its known lytic properties (11, 136, 246, 305), naturally led to a prevailing model that toxin-mediated necrosis of the intestinal epithelial barrier is the key mechanism by which *V. vulnificus* exits the intestine culminating in lethal sepsis (1).

However, we have now shown in histology of infected mice that the MARTX holotoxin does not induce overt intestinal tissue damage or excess apoptosis during early infection – even in animals that have already experienced epithelial barrier breach and bacterial dissemination to distal organs. First, this demonstrates that fulminant intestinal damage, though seen after lethal *V. vulnificus* infections in humans and mice, is not a necessary prerequisite to bacterial egress to the bloodstream. This finding is consistent with the *in vitro* T84 experiments where rapid loss of TER was not linked to dramatic loss of cytoskeleton structure or cell lysis. Paracellular permeability increases in the absence of major changes to cytoskeletal morphology suggests that more delicate modulation of cytoskeletal dynamics, such as those at intercellular junctions, is occurring.

Another outstanding question now is how *V. vulnificus* bacteria are moving across the epithelial barrier *in vivo*. Modulation of paracellular permeability by the MARTX effector domain region may act to directly facilitate paracellular bacterial transit between epithelial enterocytes for subsequent transport to the lymphatics or blood stream in the intestinal lamina propria. Indeed, *V. vulnificus* transmission across a polarized *in vitro* epithelial monolayer has been previously observed (187). Interestingly, it was not observed in our experiments (Figure 3.16), despite application of comparably scaled MOI (MOI=5 in previous study and 2.5 in this study). This discrepancy was likely due to technical differences (8 μm pore in previous study

compared to 3μm pore in our study), though there could also be differences in physiological attributes between the cell lines (HCA-7 versus T84, both of human colonic epithelial origin) that facilitate different resistance to translocation.

As an alternative or additional mechanism to bacterial translocation between cells, the same mechanisms by which the MARTX effector domain repertoire dysregulates enterocytes may also dysregulate the function of other specialized cell subsets in the intestinal epithelial monolayer. M cells, responsible for luminal antigen sampling, are present in the epithelial layer that covers lymphoid nodules and Peyer's patches. The so-called "weak point of the intestinal epithelial barrier" (353), M cells are known to provide a route for transepithelial migration of viable bacteria, including *V. cholerae,* from the intestinal lumen to the underlying Peyer's patches (354, 355). While M cell luminal sampling is integral to proper antigen presentation and immune responsiveness, pathogens such as *Salmonella, Shigella,* and *Yersinia* exploit the properties of M cells to access the mucosa and spread systemically (355, 356). Goblet cells have been implicated in transcytosis of *Listeria* and thus represent another putative route by which *V. vulnificus* is breaching the intestinal barrier (357).

Whether by paracellular transit, misregulated transcytosis, or a combination of both, *V. vulnificus* are capable of rapid dissemination from the intestine following i.g. infection, dependent upon the MARTX effector domain region. In this study, we detected bacterial dissemination to the liver and spleen of infected mice. A high proportion of the mononuclear phagocytes that comprise the reticuloendothelial system reside in the liver and spleen. As such, disseminated *V. vulnificus* are surely encountering phagocytes attempting to clear the bacteria. Previous studies on *rtxA1* in *V. vulnificus* demonstrated its importance in resisting the activity of

phagocytes (249, 358). This study is the first to demonstrate that anti-phagocytic activity conferred by the MARTX toxin is completely dependent upon its effector domains. this is another key piece of evidence highlighting the MARTX function as an effector delivery platform.

The *V. vulnificus* strain making RtxA1::Bla is thus deficient in multiple cellular activities. Lacking effector domain, *V. vulnificus rtxA1::bla* does not induce rapid intestinal barrier dysfunction *in vitro* nor disseminate from the intestine *in vivo.* Moreover, even in the rare occasion that the bacteria disseminate (see points above the detection limit in Figure 3.5) they cannot inhibit phagocytic activity in a manner akin to strains making full MARTX. Thus the bacteria are likely cleared effectively by monocytes/macrophages in the circulation, liver, and spleen. In contrast, *V. vulnificus* making the full MARTX – or any derivative strain containing four of the five effectors from the native complement – rapidly induces epithelial barrier dysfunction *in vitro,* disseminates *in vivo*, and confers potent antiphagocytic activity *in vitro*. Thus these strains are both better at becoming systemic, and better at resisting clearance once reaching these typically sterile locations.

Interestingly, though, there is still more to be understood about the mechanisms of *V. vulnificus* i.g. pathogenesis and sepsis, because strain equivalent in the aforementioned measures of barrier disruption, dissemination, and anti-phagocytic activity do not exhibit the same virulence potential (Figure 4.4). These results demonstrate that single MARTX toxin effector domains significantly alter bacterial virulence potential, despite exhibiting functional redundancy in many measures of pathogenesis. This raises the question: what are the uncharacterized aspects

of the host response to disseminated *V. vulnificus,* and how do they change among strains making different MARTX toxin variants?

A recent publication characterized the cytokine response of mice to *V. vulnificus* infection (140). Prior cell-culture based studies on both human and mouse cells demonstrated the production of inflammatory cytokines in response to *V. vulnificus* (141, 142, 144, 289), and one study demonstrated the importance of the MARTX secretion gene *rtxE* in (359) the production of IL-8 following exposure to *V. vulnificus*. However, the 2017 study by Murciano, et al. was the first to characterize cytokine profiles *in vivo* in response to various *V. vulnificus* mutants. In so doing, the role of *rtxA1* in modulation of the murine immune response to *V. vulnificus* is revealed. In the background of clinical strain YJ016, a *V. vulnificus* mutant deficient in *rtxA1* stimulated less production of chemokines: Ccl2, Ccl3, Cxcl1, Cxcl2, Cxcl3, and cytokines: IL-1alpha, IL-6, TNF (140). Thus, the MARTX toxin and its associated activities are stimulating a response in the mouse host, resulting in production of inflammatory factors, and contributing to lethal infection observed in infected mice and humans. While the role of individual MARTX effector domains in cytokine/chemokine stimulation was not tested, we can postulate the relationships among known effector functions, inflammation, and the observed virulence profiles of single MARTX effector mutants that exhibited many comparable phenotypes *in vitro*.

The pathology of sepsis is a complex one, but "the currently accepted immunologic paradigm suggests that sepsis is present when systemic activation of inflammatory pathways (i.e. systemic inflammatory response syndrome [SIRS]) is triggered by infection" (145, 146, 360). Given this paradigm, it could be extrapolated that conditions promoting increased cytokine production would be pathogenic.

Such a framework aids in forming putative explanations about the surprising enhancement of virulence in the mutant lacking the MARTX toxin alpha-beta hydrolase (ABH) domain. This Δ*abh* strain showed accelerated virulence outcomes relative to the strain making MARTX holotoxin. ABH has been shown to inhibit autophagy and endosomal trafficking (4). Autophagy negatively regulates IL-1 and IL-18 production (315, 361), so exposure to the MARTX holotoxin would likely increase IL-1 and IL-18 production by ABH-mediated alleviation of autophagic control on their production. Infection with the Δ*abh* mutant, in contrast, would not cause any ABH-mediated inhibition, and autophagy would continue its control on the levels of these interleukins.

Prohibitin, a binding partner of the MARTX domain of unknown function (DUF1), is thought to suppress inflammation during sepsis (362). DUF1 has been reported to up-regulate prohibitin in host cells upon intoxication (14), which could in turn provide such protection. This would explain the hypervirulent phenotype of the Δ*duf1* mutant, which would lack prohibitin-mediated protection putatively induced by the MARTX holotoxin.

Each of the above hypotheses has considered cytokine induction as detrimental to host infection outcomes. However, Hotchkiss et al. point out that, “although cytokines are considered to be culprits, they also have beneficial effects in sepsis” (148). This has been particularly well-supported by evidence that TNF antagonization leads to worsened outcomes in sepsis mouse models and in human patients (reviewed in (148)). The results with some of the MARTX single-deletion strains seem to fall in support of a beneficial role for cytokines.

The deletion of RRSP had the most beneficial impact on *V. vulnificus* infection virulence outcomes. While the delivery of ~5 x 10^6 parental *V. vulnificus* killed nearly all mice in 24 hours,

the same dose was lethal in approximately 50 percent of mice infected with the Δ*rrsp* mutant. RRSP, or Ras/Rap1 Specific Peptidase, cleaves the target GTPases to render them inactive. Rap1 induces pro-inflammatory cytokine production in the pro-inflammatory (M1) macrophage population (363). Similarly, Ras has previously been shown to positively regulate production of the inflammatory cytokines IL6 and IL8 (364, 365). RRSP-mediated inactivation of Ras and Rap1 would likely decrease cytokine production. The drastically improved outcome of animals infected with Δ*rrsp* indicates that its activities *in vivo* are generally detrimental to the host. Perhaps the cytokines produced by Ras and Rap1 are beneficial for the defense against *V. vulnificus* infection.

A similar premise can be outlined in connection to the Rho Inactivation Domain (RID). RID also inactivates target GTPases, but by acylation modification rather than cleavage (23). Rho GTPases, including RhoA, Rac1, and CDC42, are integral to NF-kappaB activation (366, 367). NF-kappaB, in turn, "has long been considered a prototypical proinflammatory signaling pathway, largely based on the role of NF-kappaB in the expression of proinflammatory genes including cytokines, chemokines, and adhesion molecules" (316). Inactivating Rho GTPases would thereby inhibit NF-kappaB mediated signal transduction, apparently to negative effect (given the improved infection outcomes of mice inoculated with Δ*rid* relative to the parental strain).

In reality, of course, none of these signaling events occur in isolation. Bacteria alone – i.e. a strain lacking *rtxA1* – stimulate a physiological and immunological response in the host (140). Moreover, in the presence of *rtxA1*, a battery of five MARTX effectors is simultaneously set upon the eukaryotic cytosol of any given target cell. In turn, interrelated signaling pathways

are modulated by these MARTX effectors. Indeed, there is evidence for crosstalk among MARTX effector domains and the pathways they induce in target cells (368). The most concrete example of this is the modulation of GTPase CDC42 by the *V. cholerae* MARTX toxin (3). In that system, an ABH domain stimulates CDC42 activation, while RID suppresses CDC42 activation, the net result of which is no change to CDC42 activation in cells exposed to MARTX holotoxin.

In that example, two effects ameliorate one another – a negative and positive coming to a net zero sum. Yet "coordinated crosstalk of effector function suggests that MARTX toxins are not simply a sum of all their parts" (368). The studies presented here certainly support such a model. While the MARTX toxin effector domain region is completely required for MARTX-associated virulence, its individual effector domains do not additively contribute to this requirement. Two effector domains – RID and RRSP – positively contribute to virulence. In contrast, the DUF1 and ABH domains appear to reduce virulence in the context of the MARTX holotoxin.

Ten total effector domains have been characterized (Table 1.2). Thus a variety of effector domain compositions are found across MARTX toxins (13, 253). As no single effector is the same across all MARTX toxin variants, this suggests no single domain is crucial for toxin function. Such a paradigm might be evolutionarily advantageous as the loss of a single effector is not overly deleterious. Here we demonstrated that strains lacking single effector domains were equally capable of disrupting the intestinal barrier, disseminating, and inhibiting phagocytes. Doubtless, single effectors dictate toxin potency – as was demonstrated by virulence data here and has been previously shown (193).

Still, it is now becoming evident that MARTX toxin generally disrupt three key cellular processes: GTPase activity, cytoskeletal dynamics, and vesicular trafficking {Woida, 2018 #921}. Based on studies of MARTX toxin effector domain biochemistry, there are numerous toxic mechanisms employed that ultimately result in these deleterious effects. The ACD directly crosslinks actin to disrupt the cytoskeleton, while RID-mediated disruption of GTPases results in cytoskeletal changes that lead to cell rounding. RID GTPase disruption occurs by fatty acid modification, while RRSP targets GTPases for proteolysis. The DmX domain disrupts cellular Golgi organization, while ABH also impacts endocytic trafficking. Thus, a hypothetical MARTX toxin possessing ACD, RID, and DmX ultimately induces the same toxicity as a MARTX toxin variant carrying RID, RRSP, and ABH, albeit by different biochemical mechanism. Thus MARTX purposes can theoretically be conducted by a number of different effector domain configurations. Such a theory is backed by the abundant variety of MARTX toxin effector domain compositions observed in sequenced isolates (13). Together, these data lead to the hypothesis that a "successful" MARTX toxin is much more likely to be defined by a functional signature than a specific complement of effector domains.

This observation leads to a final outstanding question: What selects for MARTX toxin in the environment? In other words, from where does evolutionary pressure upon MARTX toxin and its effector composition arise? The MARTX toxin is characterized as a potent virulence factor based on experiments in mice as a surrogate for human infection. *V. cholerae* is transmitted in high number from infected humans back to the environment, However, as with many other pathogenic bacteria, the human represents an evolutionary dead-end to *V. vulnificus*.

The coincidental evolution hypothesis proposes that, where it is not directly beneficial to between- or in-host survival, virulence is a coincidental by-product of the adaptation to other ecological niches (369). One can imagine that aquatic bacteria such as *V. vulnificus* encounter myriad environments and organisms for which it must be prepared. In the marine environment, *V. vulnificus* is co-existing with predatory phages and competing bacteria. While these surely exert pressures on *V. vulnificus,* there is no evidence for the MARTX toxin to serve in phage defense nor in interbacterial competition. These seem unlikely purposes primarily because: (i) the MARTX CPD is activated by inositol hexakisphosphate, found in the eukaryotic cytosol; and (ii) the targets of MARTX toxin effector activity are generally conserved in eukaryotes but not prokaryotes. Thus, the MARTX toxin must confer some benefit to *V. vulnificus* in its interaction either with single-celled eukaryotes (protists) or multicellular eukaryotes, both categories which have abundant representation in the temperate estuarine environments preferred by *V. vulnificus*. It is likely that *V. vulnificus* employs the MARTX toxin to promote its habitation in a favorable niche. However, given that the environmental niche of *V. vulnificus* remains unknown, so too does the role of the MARTX toxin in its environmental life cycle.

CONCLUDING REMARKS

Overall, the results presented in this study support a model in which *V. vulnificus* bacteria expressing the MARTX holotoxin rapidly induce intestinal epithelial dysfunction in the form of increased paracellular permeability and transmigration (Figure 6.1). These early steps are sufficient to facilitate bacterial dissemination and associated virulence potential. Our evidence suggests that initial translocation of bacteria out of the intestine is mediated by the MARTX

effector domains and occurs in the absence of overt tissue damage in the intestine, spleen or liver tissues. Subsequent bacterial outgrowth – or a sporatic event resulting in higher bacterial burden – eventually leads to intestinal tissue necrosis *in vivo* (Figure 6.1). Continued generation of MARTX toxins, and subsequent expression of *vvhA* hemolysin genes, contributes to this tissue damage (1, 140). MARTX toxin effector domains delivered to phagocytes render immune cells less capable of phagocytic bacterial clearance. However, in the absence of MARTX effector domain functions, the early breach of the barrier and early arrival of bacteria at distal organs does not occur, and phagocytic activity is not inhibited, resulting in dramatically reduced virulence potential.

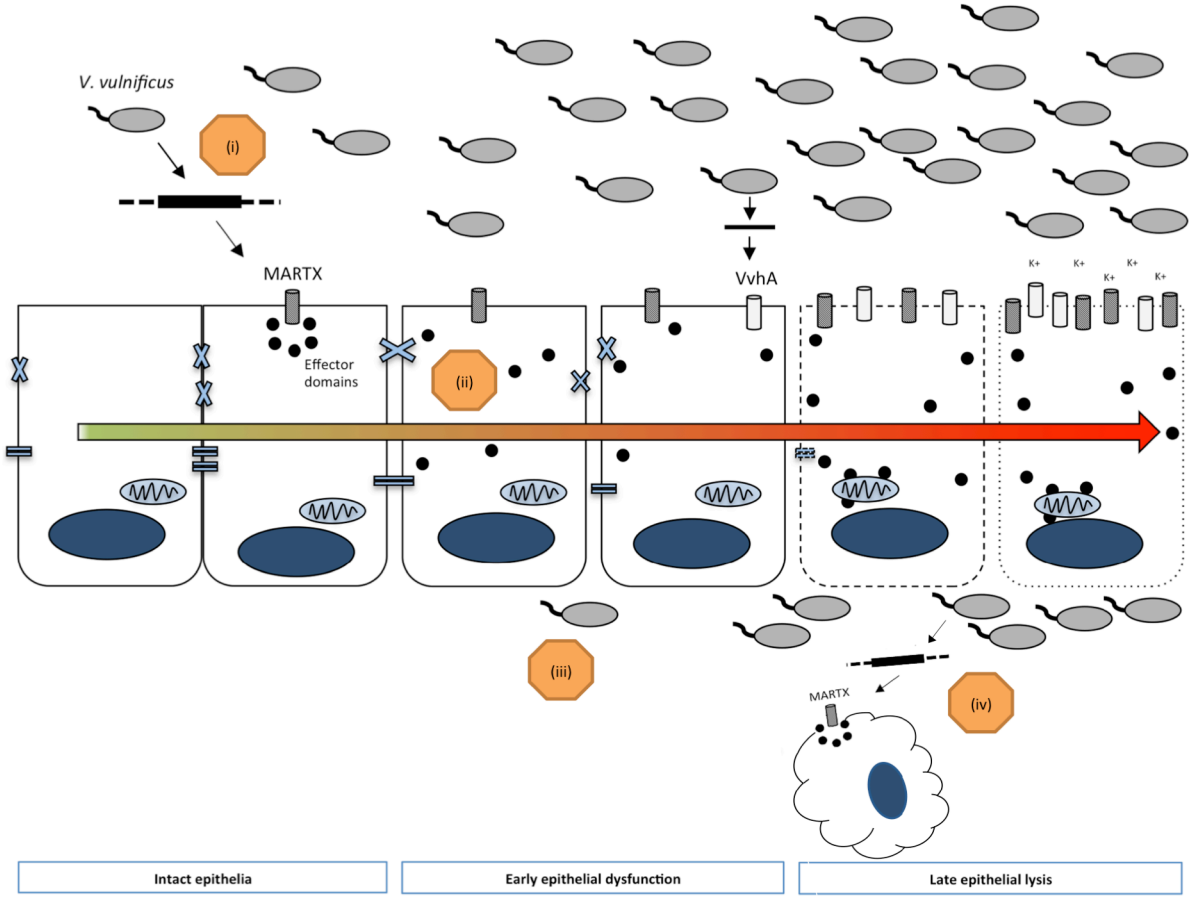

Figure 6.1. Summary model of MARTX effector-mediated functions.
The studies outlined in this dissertation revealed novel insights about *V. vulnificus* pathogenesis, particularly early i.g. infection, and the role of MARTX toxin effector domains in these early steps. (i) Epithelia exposed to *V. vulnificus* exhibit rapid monolayer dysfunction mediated by the MARTX toxin effector domain region. (ii) Monolayer dysfunction is characterized by increased paracellular permeability in the absence of lysis. (iii) MARTX-mediated barrier dysfunction facilitates early bacterial dissemination from the intestinal lumen to distal organs, prior to the onset of overt intestinal tissue damage. As intestinal bacterial burdens increase, lysis-mediated barrier dysfunction is mediated by pore-forming toxins and does not require the MARTX effector domain region *in vitro*. Notably, however, early barrier dysfunction events mediated by the MARTX toxin effector domain region are required for bacterial virulence potential conferred by the MARTX toxin. (iv) The MARTX toxin effector domains are also responsible for the anti-phagocytic activity of the MARTX toxin. and can act upon macrophages to inhibit phagocytosis. They are not necessary for early intestinal survival but confer resistance to phagocytic activity. Individual domains contribute to distinct virulence outcomes, indicating that as-yet uninvestigated aspects of the infection process impact *V. vulnificus* virulence potential during i.g. infection.

Collectively these ideas support the role of the MARTX toxin as an effector delivery platform akin to that of bacterial T3SS and T4SS in its ability to simultaneously deliver multiple effectors to target cells (253). In this understanding, the repeat region pore is functionally analogous to the secretion apparatus and the MARTX effector domains are analogous to T3S or T4S effectors. The major distinction between the pathogenic effector delivery systems is the generation of the MARTX toxin from a single gene locus that encodes the entire virulence factor, which is functionally distinct from the separate loci that encode T3S or T4S apparatuses and their respective secreted effectors (253). In that regard, the MARTX toxin shares more similarity to A-B toxins (352).

Interestingly, the horizontal gene transfer observed at the *rtxA1* locus to generate a variety of MARTX effector domain compositions indicates a mechanism by which distinct bacterial effector repertoires can be delivered to targeted eukaryotic cells in the context of a singular secreted toxin, with direct consequences to virulence (193). In fact, the effector domain repertoire is inextricably linked to MARTX toxin functional identity, as it has here been illuminated that the effector domain region itself dictates MARTX-linked bacterial virulence potential.

CHAPTER 7 – Materials and Methods

Bacterial strains and growth conditions

Bacteria were routinely grown in Luria-Burtani (LB) broth (10 g tryptone, 5 g yeast extract, 5 g NaCl per 1L dH_2O) containing 50 μg/mL rifampin or 10 μg/ml chloramphenicol as needed. For all experiments, *V. vulnificus* was streaked from frozen glycerol stocks onto LB plates. The following day, single colonies were grown in 2 mL of antibiotic-containing LB broth overnight at 30°C and then subcultured 1:100 into LB without antibiotic and grown to mid-log phase. Cultures were pelleted and resuspended in sterile phosphate buffered saline (PBS, 10mM sodium phosphate, 140 mM NaCl, pH 7.4) to indicated concentrations based on optical density (A_{600}) in Beckman DU530 spectrophotometer or ThermoFisher NanoDrop.

Generation of *V. vulnificus* strains with modified *rtxA1*

All novel *V. vulnificus* strains listed in Table 7.1 were generated from the Korean clinical isolate *V. vulnificus* CMCP6. (Methods for construction of previously strains generated by others and used in this study have been published in (30) and (31)). *Escherichia* coli strains DH5 α*λpir*, SM10*λpir*, and S17*λpir* were used for new strain construction (370, 371).

The CMCP6 MARTX toxin CPD processing sites have not been precisely mapped although the boundaries of each effector domain have been defined based on extensive sequence alignment (13). To ensure that processing of neighboring effectors was not negatively impacted by the deletion, the predicted processing sites were preserved along with 15% of the effector domain itself. The designed deletions correspond to the following nucleotides based on the CMCP6 sequence of Kim *et al*., (372) (National Center for Biotechnology Information

Reference #NC_004460.2): *Δduf1 (Δ*5890–6699); *Δrid (Δ*6814–8688); *Δabh (Δ*8794–9279); *Δmcf* (*Δ*9490–10,722); and *Δrrsp* (*Δ*10,753–12,252).

Fragments corresponding to regions upstream and downstream of the desired deletion were either commercially synthesized (Integrated DNA Technologies, Coralville, IA) or amplified from the CMCP6 genome. The two fragments corresponding to each strain were assembled into digested pDS132 (373) either using Gibson Assembly according to the manufacturer's protocols (New England Biolabs, Ipswich, MA) or by standard ligation using T4 DNA ligase. The resulting plasmids were confirmed by sequencing and transformed to SM10λ*pir* (370), and S17λ*pir* (371). The Δ*effector* deletion plasmids were transferred to *V. vulnificus ΔvvhA* by conjugation followed by selection for double homologous recombination using sucrose counterselection to isolate recombinants as previously described (326). Deletions in the *rtxA1* gene were confirmed by amplification of DNA across the deletion junction.

To generate the rtxA1::bla::cpd* strain, one 500-bp double-stranded synthetic gBlock was assembled into SphI-SacI-digested pDS132 vector using Gibson Assembly master mix at 50°C. This gBlock insertion was designed to include a codon change of the catalytic C4230 residue of CPD to Ala. The resulting pHEG1401 plasmid was sequenced for accuracy and then transformed to SM10λpir.

Table 7.1. Strains used in this study.

Strain name	Description	Antibiotic resistance	Source
CMCP6	Derivative of Korean clinical isolate CMCP6 generated by isolation of a spontaneous mutant resistant to rifampicin	Rifampicin 50µg/mL	HeeGon Jeong, PhD (1)
ΔvvhA	CMCP6 with in-frame removal of 972 base pairs from *vvhA* coding region	Rifampicin 50µg/mL	Byoung Sik Kim, PhD (30)
rtxA1::bla	CMCP6 *vvhA-*, heterologous *bla* replaces native effector repertoire	Rifampicin 50µg/mL	Byoung Sik Kim, PhD (30)
*rtxA1::bla cpd**	*rtxA1::bla* with alanine point mutation in catalytic C4230 residue of cysteine protease domain	Rifampicin 50µg/mL	HEG (30)
rtxA1::blaΔN	*rtxA1::bla* with deletion of N terminal repeat region corresponding to base pairs 217 to 5655	Rifampicin 50µg/mL	Byoung Sik Kim, PhD (30)
rtxA1::blaΔC	*rtxA1::bla* with deletion of C terminal repeat regions corresponding to base pairs 7597 to 9879	Rifampicin 50µg/mL	Byoung Sik Kim, PhD (30)
rtxA1::bla rtxB-	rtxA1::bla with *nptII* insertion in *rtxB* for disruption of *rtx* secretion machinery	Rifampicin 50µg/mL	Byoung Sik Kim, PhD (30)
ΔrtxA1	CMCP6, *vvhA-* with 9635 base pair deletion in *rtxA1* coding region	Rifampicin 50µg/mL	Byoung Sik Kim, PhD (30)
ΔvvhA Δduf1	*ΔvvhA* background; deletion of base pairs 5890–6699 in *rtxA1*	Rifampicin 50µg/mL	HEG (35)
ΔvvhA Δrid	ΔvvhA background; deletion of base pairs 6814–8688 in rtxA1	Rifampicin 50µg/mL	HEG (35)
ΔvvhA Δabh	ΔvvhA background; deletion of base pairs8794–9279 in rtxA1	Rifampicin 50µg/mL	HEG (35)
ΔvvhA Δmcf	ΔvvhA background; deletion of base pairs 9490–10,722 in rtxA1	Rifampicin 50µg/mL	Shivangi Agarwal, PhD (35)
ΔvvhA Δrrsp	ΔvvhA background; deletion of base pairs 10,753–12,252 in rtxA1	Rifampicin 50µg/mL	HEG (35)
vvhA-	CMCP6 with disruptive plasmid integration in *vvhA (ΩvvhA::bla)*	Rifampicin 50µg/mL	HeeGon Jeong, PhD (1)
vvhA- Δmcf	*vvhA-*with *mcf* deletion in *rtxA1*	Rifampicin 50µg/mL	HEG (64)
vvhA- rtxA1::bla	*vvhA-* with heterologous *bla* replaceing native *rtxA1* effector repertoire	Rifampicin 50µg/mL	HeeGon Jeong, PhD (1)
vvhA- mcf::bla	*vvhA- rtxA1::bla* with *mcf* reintroduced	Rifampicin 50µg/mL	Shivangi Agarwal, PhD (64)

Nitrocefin cleavage assay

V. vulnificus strains were grown in triplicate cultures in LB to the exponential phase, and 90 µl of whole bacterial cultures was incubated with 10 µl of nitrocefin (1 mg/ml in PBS) for 3-4 h at room temperature. Absorbance (A_{486}) of cleaved nitrocefin was measured at the indicated time points using a SpectraMax M5 plate reader (Molecular Devices).

For assays requiring bacterial lysates, *V. vulnificus* were grown until cultures reached the exponential phase (optical density at 600 nm [OD_{600}] = 0.5), at which point bacteria were pelleted by centrifugation at 15,000 × *g* in 4°C for two minutes. Cell pellets were washed with resuspended in ice-cold water and sonicated. Lysates were centrifuged at 20,000 × *g* in 4°C for 30 min to remove cell debris. The supernatant from these lysates was the collected and assayed as described for whole bacterial culture.

Antibiotic disk assays

Fresh LB agar plates of controlled 25-mL volume were swabbed with exponential-phase cultures of the indicated strains, and a 6.5-mm-diameter antibiotic disk containing either ceftazidime (CAZ) or ampicilling (amp) (Thermo Scientific) was placed in the center of each plate using sterilized tweezers. Plates were incubated inverted at 30°C overnight. The area (A) of the clear zone of inhibition around the disk was quantified as $A = \pi(0.5d)^2 - A_{\text{disk}}$, where d is the measured diameter of the zone and A_{disk} is 33.18 mm^2.

qRT-PCR

Bacteria were grown as described above. RNA was extracted using Qiagen RNeasy Kit (Qiagen, 74104) and RNA Protect Bacteria Reagent (Qiagen, 76506) according to the manufacturer's instructions. Isolated RNA was quantified using a Nano-Drop spectrophotometer. RNA was DNase treated using Turbo DNA Free Kit (Life Tech, AM1907). RNA was reversed transcribed using random hexamers (Roche, 11034731001) and Superscript III Reverse Transcriptase (Life Tech 18080–093) in the presence of RNasin (Promega N2611). qRT-PCR was carried out using iQ SYBR Green Supermix (BioRad 170–8880) and the BioRad iQ5 Multicolor RealTime PCR Detection System. Efficiency testing established primer efficiency of 83% and 87% for *rtxA1* and *16s rRNA* primer pairs, respectively. Primers used were: qRT-RTXF (5'AATACCGCTCTTCACAACC3'); qRT-RTXR (5'GCTTTCTGGGTGCTTACC3'); qRT-16srRNA_F (5'CTTGACATCCAGAGAATCTA3'); qRT-16srRNA_R (5'GACTTAACCCAACATTTCAC 3')

Three separate qRT-PCR analyses were performed and data pooled following analysis. The *16s rRNA* gene served as internal housekeeping control. Fold change was calculated relative to parental CMCP6.

Ethics statement

These studies were carried out in strict accordance with the recommendations in the United States Public Health Service (USPHS) regulations and applicable federal and local laws. The protocol (Protocol No. IS00000905) was approved by the Northwestern University

Institutional Animal Care and Use Committee (IACUC) as detailed in methods. All efforts were made to minimize suffering

Mouse i.g. infection in Chapter 3 and 4

Female ICR mice were obtained from Charles River at age 32–38 days. Mice were anesthetized via intraperitoneal injection with 100 µL of anaesthetic cocktail containing 60–70 µg/kg ketamine and 12–14 µg/kg xylazine in PBS. Mice were inoculated i.g. using a 1-cm animal feeding needle attached to a 1-mL syringe. Mice were administered 50 µL of 8.5% aqueous sodium bicarbonate, followed immediately by 50 µL of bacterial culture containing the CFU indicated for a given experiment. Mice were monitored every 2 hours for the first 28 hours of the experiment and subsequently every 4–8 hours for a total experimental duration of 48 hpi For low dose survival experiments, mice were inoculated with *V. vulnificus* strains *ΔvvhA* (n = 17), *ΔvvhA rtxA1*::*bla* (n = 14) and *ΔvvhA mcf**::*bla* (n = 5) For high dose survival experiments, mice were inoculated with *ΔvvhA rtxA1*::*bla* (n = 12) and *ΔvvhA ΔrtxA1* (n = 11).

For bacterial recovery from organs, 5–6 mice per group were inoculated and then euthanized 6 hpi The whole intestine (less the cecum) was excised and homogenized in 5 mL PBS. The liver and spleen were excised and each homogenized in 1 mL PBS. CFU/organ was calculated by plating serially diluted homogenates to LB agar containing rifampin to select for *V. vulnificus*.

For histopathology, 3–4 mice per group were inoculated and euthanized 6 hpi The liver and spleen were dissected. A 1-cm sample was isolated from the proximal end of each segment of the small and large intestine (duodenum, jejunum, ileum, colon) for cross-sectional sampling.

The remaining portions of each segment were opened along the longitudinal axis, rolled from proximal to distal, and sectioned to obtain samples in a "swiss roll" orientation. After 24–48 hours fixation in 10%-buffered formalin, all tissues were paraffin-embedded, processed, and stained with H&E. For immunohistochemistry, 4 μm of the same embedded tissues were sectioned, mounted on slides, and stained for apoptotic marker cleaved caspase-3 using the CP229C antibody from Biocare Medical, Concord, CA. All pathology slides were viewed and scored by NU Pathologist Nike Beaubier, MD, who was blinded to treatment groups.

Mouse i.g. infection in Chapter 5

Fifty female C57BL/6 mice were obtained from Jackson Laboratories (Bar Harbor, ME). Animals were housed 5 per cage in wood shavings with disposable paper huts and cotton bedding squares as nesting material. Water and food were provided *ad libitum.* Experiments were conducted when mice were 5-6 weeks of age. For each of the two independent experiments, 25 mice were divided into 5 groups of 5 mice each to be either mock-inoculated with PBS, or inoculated with one of the four *V. vulnificus* strains.

Each mouse was transiently anaesthetized using isoflurane and then inoculated intragastrically (i.g.) with 50 μL of PBS or $1x10^8$ colony-forming units (CFU) *V. vulnificus* suspended in PBS using a 1-cm animal feeding needle attached to a 1-mL syringe. Mice were then injected intraperitoneally with 100 μL of a cocktail containing 10 μg/ml ketamine and 2 μg/ml xylazine in PBS to facilitate bacterial infection (192).

Mice were monitored hourly for the first 24 hour (h) and subsequently every 4-8 h until 48 h post-infection (hpi). Ventral surface temperature (VST) was measured every 2 h during the

first 24 h then once at 40-42 h and once at 47-48 h. Temperature was measured using the non-contact infrared TW2 thermometer (ThermoWorks, Alpine, UT) as recommended by the manufacturer. Thermometer emissivity maintained at the manufacturer's default setting of 0.95. The TW2 thermometer is accurate +/- 1.0°C when the object of interest is between 15 and 35°C.

To obtain temperature measurements, mice were restrained by scruffing. The thermometer was held approximately 6 cm from the mouse ventral side and the beam aimed below the base of the sternum, according to procedures that have previously described practices for obtaining consistent temperature readings (333). Because mouse temperature can change rapidly upon handling, efforts were made to minimize and standardize handling methods across all mice (333, 374, 375). As such, a temperature stabilization time of 5-10 seconds was employed prior to temperature recording.

HeLa cells studies

For cell rounding assay, HeLa cells were seeded into 6-well dishes to a density of 10^5 cells per well overnight. The media were exchanged for 3 ml of phenol-red free DMEM without FBS and penicillin-streptomycin, and PBS or the indicated *V. vulnificus* strains were added at an MOI of 10. Images for random spots of the culture wells were taken through a microscope every 30 min using a digital camera (Nikon Eclipse TS100; ×10 magnification). Percentages of round cells were calculated as the number of round cells in an image/the total number of cells in an image × 100. Results were determined counting at least 50 (average, 75) cells per image for 3 images per group. Only the cells showing a spherical shape were counted as positive.

For cell lysis assays, HeLa cells were seeded into 12-well dishes to a density of 10^5 cells per well overnight. The media were exchanged for 1 ml of phenol-red free or calcium-free DMEM, without FBS and penicillin-streptomycin, and *V. vulnificus* strains were added at MOI according to the experimental protocol. At the indicated timepoints, supernatant media was extracted at centrifuged at 15,000xg for one minute. A 100µL-aliquot was extracted for assay, to which 1µL of 100 mg/ml gentamicin was added to kill any remaining bacteria in the sample. LDH present in the sampled media was measured using a CytoTox 96 nonradioactive cytotoxicity assay kit (Promega, Madison, WI) according to the manufacturer's instructions. Percent cell lysis was calculated as A_{490} (sample)/A_{490} (100% lysis control) × 100.

For western blotting, cells were seeded at 5 x 10^5 cells/well in a 12-well dish and treated with a given *V. vulnificus* strain (in biological triplicate) at MOI=100 for one hour. Supernatant was collected and centrifuged at 15,000xg for two minutes to collect any un-attached cells. After spinning, the supernatant was aspirated away. 100µL of 2X SDS-page buffer was added to each well and cells were collected by scraping. This volume was used to resuspend the pellet from the spun supernatant, and the total sample was boiled for 10 minutes. Twenty microlitres of lysate were separated by SDS–PAGE and transferred to nitrocellulose (Amersham) using the Bio Rad Trans-Blot Turbo system. Nitrocellulose membranes were blocked overnight at 4 °C in 5% (w/v) powdered milk diluted in Tris-buffered saline containing 0.001% Tween-20 (TBS-T). Immunodetection of proteins was conducted by western blotting for Ras proteolysis using the pan-Ras RAS10 (EMD Millipore, 05–516, 1:500) and tubulin (Sigma-Alrich, T6074, (1:10,000) monoclonal antibodies as previously described (27).

T84 cell studies

T84 cells obtained from American Type Culture Collection (#CCL-248) were routinely grown in T84 media (1:1 DMEM/F12 Nutrient Mix (Gibco 11320–033)) supplemented with 10% fetal bovine serum (FBS) and 1% penicillin-streptomycin) to no more than 30 passages. For cell polarization, Costar Transwell Permeable Supports (6.5mm insert, 24-well plate, 3.0 μm polycarbonate membrane, Reference #3415) were coated with collagen and dried in a laminar flow hood overnight. Transwells were incubated with T84 media for 1 hour prior to the addition of 10^6 T84 cells to the apical chamber of the transwell. Media was changed every 2–3 days for 10–14 days until monolayers reached $\geq 1000 \Omega/cm^2$ (376) as measured using an EVOM (World Precision Instruments). A minimum of three monolayers were prepared per assay condition.

One hour prior to bacterial co-incubation, monolayers were washed twice with warm Hanks Balanced Salt Solution (HBSS, Sigma-Aldrich) and media was replaced with 1:1 phenol-red free T84 media without FBS or antibiotic. Ten μL of PBS or the appropriate concentration of bacteria were applied drop-wise to the apical media. Monolayers were maintained at 37°C using a plate warmer. TER was measured in 15–20 minute intervals or as indicated in legends.

For confocal imaging, following 60 minutes of bacterial co-incubation, cells were fixed in 4% paraformaldehyde for 20 minutes. Monolayers were permeabalized using 0.1% TritonX-100. Actin was stained using AlexaFluor 488 phalloidin (ThermoFisher A12379) and nuclei were stained with 4′-6′-diamidino-2-phenylindole (DAPI, Life D1306), each according to manufacturer's recommendations. Entire monolayers affixed to membrane were excised, mounted in Pro-Long Gold Antifade (Life Technologies, P36930) under a cover slip, and imaged using a Nikon A1R Spectral microscope.

For dextran flux studies, 200 μg fluorescein dextran (3-kD, ThermoFisher D3305) was added to the apical chamber immediately following application of PBS or bacteria to the apical chamber of transwells. Dextran transit across the monolayer was measured by sampling 20 μL media from the basal transwell chamber, after which the extracted volume was replaced with 20 μL fresh media. Sample fluorescence was measured using a Tecan Safire 2 fluorescence plate reader (excitation: 494 nm, emission: 521 nm) and amount of dextran (in pg) was calculated against a standard curve, accounting for volume differences due to sampling. Flux rates were reported as μg dextran/hr/cm^2 from the slope of the plotted linear curve.

For LDH release assays, 100 μL of media was extracted from either the apical or basal chambers of PBS, bacterial, or Triton X-100 incubated monolayers. One μL 100 mg/ml gentamicin was added and samples were centrifuged at 15,000*xg* for 1 minute. 50 μL of the resulting supernatant was transferred to a 96-well culture plate. LDH activity was measured using the Promega CytoTox Non-Radioactive Cytotoxicity Assay kit according to manufacturer's instructions. The apical and basal samples were processed separately with data reported adjusting for volume.

J774 cell studies

J774 cells were routinely maintained at 37 °C with 5% CO2 in DMEM medium (Life Technologies) with 10% fetal bovine serum (Gemini Bio-Products, West Sacramento, CA) and 1% penicillin-streptomycin. For phagocytosis assays, J774 cells were seeded on the day of the experiment (>2 hour in advance to allow attachment) at 10^5 cells/well into a 96-well dish. Just prior to the experiment, cells were washed once with warmed Roswell Park Memorial Institute

(RPMI, Life Technologies) medium without phenol red or any supplementation. Ninty µL of the phenol red-free RPMI was then added to each well, and 10µL of resuspended *V. vulnificus* containing 10^5 CFU added to the cells to accomplish MOI=1. Plates were incubated at 37°C/ 5%CO2 for 30 min. Cells were washed once with RPMI, then 100 µl pHrodo Green *E.coli* Bioparticles (Life Technologies) – suspended in RPMI with 100 µg/ml gentamicin – added to each well. Plates were incubated on a 37% plate warmer for one hour, then read in the SpectraMax M5 plate reader with excitation at 509 nm and emission at 533 nm. Percent phagocytosis was calculated as A533(sample)/A533(untreated control) × 100.

For LF_N-RRSP intoxication studies, the media was exchanged for fresh media to which 7 nM PA and 3 nM LF_N-RRSP (courtesy were added to the media and incubated for two hours at 37 °C with 5% CO2. Phagocytosis assays then proceeded as described above.

For cell lysis studies, J774 cells were seeded on the day of the experiment (>2 hour in advance to allow attachment) at 10^5 cells/well into a 96-well dish. Just prior to the experiment, cells were washed once with warmed Roswell Park Memorial Institute (RPMI, Life Technologies) medium without phenol red or any supplementation. Ninty µL of the phenol red-free RPMI was then added to each well, and 10µL of resuspended *V. vulnificus* containing 10^5 CFU added to the cells to accomplish MOI=1. Plates were incubated at 37°C/ 5%CO2 for 30 min. Cells were washed once with RPMI, then 100 µl RPMI with 100 µg/ml gentamicin was added to each well. To three wells, 0.1% TritonX-100s was added to lyse cells as a positive control. Plates were incubated on a 37% plate warmer for one hour. After co-incubation, the 100 µL volume of media from each well was transferred to a 1.5-mL Eppendorf tube and centrifuged at 15,000xg for two minutes. A 50-µL aliquot of supernatant was removed from each sample and

transferred to a 96-well flat clear-bottom plate. LDH activity was measured using the Promega CytoTox Non-Radioactive Cytotoxicity Assay kit according to manufacturer's instructions.

Statistical analyses

Statistical analyses were performed as indicated in figure legends using GraphPad Prism 6.0 software.

REFERENCES

1. Jeong HG, Satchell KJ. 2012. Additive function of Vibrio vulnificus MARTX(Vv) and VvhA cytolysins promotes rapid growth and epithelial tissue necrosis during intestinal infection. PLoS Pathog 8:e1002581.
2. Satchell KJ. 2011. Structure and function of MARTX toxins and other large repetitive RTX proteins. Annu Rev Microbiol 65:71-90.
3. Dolores JS, Agarwal S, Egerer M, Satchell KJ. 2015. Vibrio cholerae MARTX toxin heterologous translocation of beta-lactamase and roles of individual effector domains on cytoskeleton dynamics. Mol Microbiol 95:590-604.
4. Agarwal S, Kim H, Chan RB, Agarwal S, Williamson R, Cho W, Paolo GD, Satchell KJ. 2015. Autophagy and endosomal trafficking inhibition by Vibrio cholerae MARTX toxin phosphatidylinositol-3-phosphate-specific phospholipase A1 activity. Nat Commun 6:8745.
5. Kudryashov DS, Cordero CL, Reisler E, Satchell KJ. 2008. Characterization of the enzymatic activity of the actin cross-linking domain from the Vibrio cholerae MARTX Vc toxin. J Biol Chem 283:445-52.
6. Fullner KJ, Mekalanos JJ. 2000. In vivo covalent cross-linking of cellular actin by the Vibrio cholerae RTX toxin. EMBO J 19:5315-23.
7. Fullner KJ, Lencer WI, Mekalanos JJ. 2001. Vibrio cholerae-induced cellular responses of polarized T84 intestinal epithelial cells are dependent on production of cholera toxin and the RTX toxin. Infect Immun 69:6310-7.
8. Ma AT, Mekalanos JJ. 2010. In vivo actin cross-linking induced by Vibrio cholerae type VI secretion system is associated with intestinal inflammation. Proc Natl Acad Sci U S A 107:4365-70.
9. Heisler DB, Kudryashova E, Grinevich DO, Suarez C, Winkelman JD, Birukov KG, Kotha SR, Parinandi NL, Vavylonis D, Kovar DR, Kudryashov DS. 2015. ACTIN-DIRECTED TOXIN. ACD toxin-produced actin oligomers poison formin-controlled actin polymerization. Science 349:535-9.
10. Dolores J, Satchell KJ. 2013. Analysis of Vibrio cholerae genome sequences reveals unique rtxA variants in environmental strains and an rtxA-null mutation in recent altered El Tor isolates. MBio 4:e00624.
11. Ziolo KJ, Jeong HG, Kwak JS, Yang S, Lavker RM, Satchell KJ. 2014. Vibrio vulnificus biotype 3 multifunctional autoprocessing RTX toxin is an adenylate cyclase toxin essential for virulence in mice. Infect Immun 82:2148-57.
12. Kim BS, Satchell KJ. 2016. MARTX effector cross kingdom activation by Golgi-associated ADP-ribosylation factors. Cell Microbiol 18:1078-93.
13. Satchell KJ. 2015. Multifunctional-autoprocessing repeats-in-toxin (MARTX) Toxins of Vibrios. Microbiol Spectr 3.
14. Kim BA, Lim JY, Rhee JH, Kim YR. 2015. Characterization of Prohibitin 1 as a Host Partner of Vibrio vulnificus RtxA1 Toxin. J Infect Dis doi:10.1093/infdis/jiv362.

15. Agarwal S, Agarwal S, Biancucci M, Satchell KJ. 2015. Induced autoprocessing of the cytopathic Makes caterpillars floppy-like effector domain of the Vibrio vulnificus MARTX toxin. Cell Microbiol doi:10.1111/cmi.12451.
16. Agarwal S, Zhu Y, Gius D, Satchell KJ. 2015. Makes Caterpillars Floppy (MCFVv)-like domain of Vibrio vulnificus induces mitochondrial-mediated apoptosis. Infection and Immunity in press.
17. Grim CJ, Kozlova EV, Ponnusamy D, Fitts EC, Sha J, Kirtley ML, van Lier CJ, Tiner BL, Erova TE, Joseph SJ, Read TD, Shak JR, Joseph SW, Singletary E, Felland T, Baze WB, Horneman AJ, Chopra AK. 2014. Functional genomic characterization of virulence factors from necrotizing fasciitis-causing strains of Aeromonas hydrophila. Appl Environ Microbiol 80:4162-83.
18. French CT, Panina EM, Yeh SH, Griffith N, Arambula DG, Miller JF. 2009. The Bordetella type III secretion system effector BteA contains a conserved N-terminal motif that guides bacterial virulence factors to lipid rafts. Cell Microbiol 11:1735-49.
19. Roig FJ, Gonzalez-Candelas F, Amaro C. 2011. Domain organization and evolution of multifunctional autoprocessing repeats-in-toxin (MARTX) toxin in Vibrio vulnificus. Appl Environ Microbiol 77:657-68.
20. Pang M, Jiang J, Xie X, Wu Y, Dong Y, Kwok AH, Zhang W, Yao H, Lu C, Leung FC, Liu Y. 2015. Novel insights into the pathogenicity of epidemic Aeromonas hydrophila ST251 clones from comparative genomics. Sci Rep 5:9833.
21. Sheahan KL, Satchell KJ. 2007. Inactivation of small Rho GTPases by the multifunctional RTX toxin from Vibrio cholerae. Cell Microbiol 9:1324-35.
22. Ahrens S, Geissler B, Satchell KJ. 2013. Identification of a His-Asp-Cys catalytic triad essential for function of the Rho inactivation domain (RID) of Vibrio cholerae MARTX toxin. J Biol Chem 288:1397-408.
23. Zhou Y, Huang C, Yin L, Wan M, Wang X, Li L, Liu Y, Wang Z, Fu P, Zhang N, Chen S, Liu X, Shao F, Zhu Y. 2017. N(epsilon)-Fatty acylation of Rho GTPases by a MARTX toxin effector. Science 358:528-531.
24. Pechous RD, Goldman WE. 2015. Illuminating Targets of Bacterial Secretion. PLoS Pathog 11:e1004981.
25. Cheng H, Bjerknes M. 1983. Cell production in mouse intestinal epithelium measured by stathmokinetic flow cytometry and Coulter particle counting. Anat Rec 207:427-34.
26. Antic I, Biancucci M, Satchell KJ. 2014. Cytotoxicity of the Vibrio vulnificus MARTX toxin Effector DUF5 is linked to the C2A Subdomain. Proteins 82:2643-56.
27. Antic I, Biancucci M, Zhu Y, Gius DR, Satchell KJ. 2015. Site-specific processing of Ras and Rap1 Switch I by a MARTX toxin effector domain. Nat Commun 6:7396.
28. Stiles BG, Pradhan K, Fleming JM, Samy RP, Barth H, Popoff MR. 2014. Clostridium and bacillus binary enterotoxins: bad for the bowels, and eukaryotic being. Toxins (Basel) 6:2626-56.
29. Wolczuk K, Wilczynska B, Jaroszewska M, Kobak J. 2011. Morphometric characteristics of the small and large intestines of Mus musculus during postnatal development. Folia Morphol (Warsz) 70:252-9.

30. Kim BS, Gavin HE, Satchell KJ. 2015. Distinct roles of the repeat-containing regions and effector domains of the Vibrio vulnificus multifunctional-autoprocessing repeats-in-toxin (MARTX) toxin. MBio 6.
31. Agarwal S, Zhu Y, Gius DR, Satchell KJ. 2015. The Makes Caterpillars Floppy (MCF)-Like Domain of Vibrio vulnificus Induces Mitochondrion-Mediated Apoptosis. Infect Immun 83:4392-403.
32. Biancucci M, Rabideau AE, Lu Z, Loftis AR, Pentelute BL, Satchell KJF. 2017. Substrate Recognition of MARTX Ras/Rap1-Specific Endopeptidase. Biochemistry 56:2747-2757.
33. Gomez-Gil B, Thompson, C.C., Matsumura, Y., Sawabe, T., Iida, T., Christen, R., Thompson, F., Sawabe, T. 2014. The Family *Vibrionaceae*, p 659-747. *In* Rosenberg E, DeLong, E.F., Lory, S., Stackebrandt, E., Thompson, F. (ed), The Prokaryotes, Fourth Edition ed. Springer.
34. McCarter LL. 2001. Polar flagellar motility of the Vibrionaceae. Microbiol Mol Biol Rev 65:445-62, table of contents.
35. Gavin HE, Beubier NT, Satchell KJ. 2017. The Effector Domain Region of the Vibrio vulnificus MARTX Toxin Confers Biphasic Epithelial Barrier Disruption and Is Essential for Systemic Spread from the Intestine. PLoS Pathog 13:e1006119.
36. Thompson CC, Vicente AC, Souza RC, Vasconcelos AT, Vesth T, Alves N, Jr., Ussery DW, Iida T, Thompson FL. 2009. Genomic taxonomy of Vibrios. BMC Evol Biol 9:258.
37. Sawabe T, Ogura Y, Matsumura Y, Feng G, Amin AR, Mino S, Nakagawa S, Sawabe T, Kumar R, Fukui Y, Satomi M, Matsushima R, Thompson FL, Gomez-Gil B, Christen R, Maruyama F, Kurokawa K, Hayashi T. 2013. Updating the Vibrio clades defined by multilocus sequence phylogeny: proposal of eight new clades, and the description of Vibrio tritonius sp. nov. Front Microbiol 4:414.
38. Pfeffer C, Oliver JD. 2003. A comparison of thiosulphate-citrate-bile salts-sucrose (TCBS) agar and thiosulphate-chloride-iodide (TCI) agar for the isolation of Vibrio species from estuarine environments. Lett Appl Microbiol 36:150-1.
39. Oliver JD, Hite F, McDougald D, Andon NL, Simpson LM. 1995. Entry into, and resuscitation from, the viable but nonculturable state by Vibrio vulnificus in an estuarine environment. Appl Environ Microbiol 61:2624-30.
40. Ramamurthy T, Ghosh A, Pazhani GP, Shinoda S. 2014. Current Perspectives on Viable but Non-Culturable (VBNC) Pathogenic Bacteria. Front Public Health 2:103.
41. Xu HS, Roberts N, Singleton FL, Attwell RW, Grimes DJ, Colwell RR. 1982. Survival and viability of nonculturableEscherichia coli andVibrio cholerae in the estuarine and marine environment. Microb Ecol 8:313-23.
42. Pinto D, Santos MA, Chambel L. 2015. Thirty years of viable but nonculturable state research: unsolved molecular mechanisms. Crit Rev Microbiol 41:61-76.
43. Takemura AF, Chien DM, Polz MF. 2014. Associations and dynamics of Vibrionaceae in the environment, from the genus to the population level. Front Microbiol 5:38.
44. Ruby EG, Lee KH. 1998. The Vibrio fischeri-Euprymna scolopes Light Organ Association: Current Ecological Paradigms. Appl Environ Microbiol 64:805-12.

45. McFall-Ngai M. 2014. Divining the essence of symbiosis: insights from the squid-vibrio model. PLoS Biol 12:e1001783.
46. Fidopiastis PM, von Boletzky S, Ruby EG. 1998. A new niche for Vibrio logei, the predominant light organ symbiont of squids in the genus Sepiola. J Bacteriol 180:59-64.
47. Sawabe T, Setoguchi N, Inoue S, Tanaka R, Ootsubo M, Yoshimizu M, Ezura Y. 2003. Acetic acid production of Vibrio halioticoli from alginate: a possible role for establishment of abalone-V-halioticoli association. Aquaculture 219:671-679.
48. Sawabe T. 2006. The Mutual Partnership between Vibrio halioticoli and Abalones. Biology of Vibrios:219-230.
49. Chimetto LA, Brocchi M, Thompson CC, Martins RCR, Ramos HR, Thompson FL. 2008. Vibrios dominate as culturable nitrogen-fixing bacteria of the Brazilian coral Mussismilia hispida. Systematic and Applied Microbiology 31:312-319.
50. Rameshkumar N, Fukui Y, Sawabe T, Nair S. 2008. Vibrio porteresiae sp. nov., a diazotrophic bacterium isolated from a mangrove-associated wild rice (Porteresia coarctata Tateoka). Int J Syst Evol Microbiol 58:1608-15.
51. Bagwell CE, Piceno YM, Ashburne-Lucas A, Lovell CR. 1998. Physiological diversity of the rhizosphere diazotroph assemblages of selected salt marsh grasses. Appl Environ Microbiol 64:4276-82.
52. Lovell CR, Decker PV, Bagwell CE, Thompson S, Matsui GY. 2008. Analysis of a diverse assemblage of diazotrophic bacteria from Spartina alterniflora using DGGE and clone library screening. J Microbiol Methods 73:160-71.
53. Gamble MD, Bagwell CE, LaRocque J, Bergholz PW, Lovell CR. 2010. Seasonal variability of diazotroph assemblages associated with the rhizosphere of the salt marsh cordgrass, Spartina alterniflora. Microb Ecol 59:253-65.
54. Urdaci MC, Marchand M, Grimont PA. 1988. [Species of the genus Vibrio associated with marine products from Arachon Bay]. Ann Inst Pasteur Microbiol 139:351-62.
55. Abd H, Saeed A, Weintraub A, Nair GB, Sandstrom G. 2007. Vibrio cholerae O1 strains are facultative intracellular bacteria, able to survive and multiply symbiotically inside the aquatic free-living amoeba Acanthamoeba castellanii. FEMS Microbiol Ecol 60:33-9.
56. Abd H, Valeru SP, Sami SM, Saeed A, Raychaudhuri S, Sandstrom G. 2010. Interaction between Vibrio mimicus and Acanthamoeba castellanii. Environ Microbiol Rep 2:166-171.
57. Abd H, Weintraub A, Sandstrom G. 2005. Intracellular survival and replication of Vibrio cholerae O139 in aquatic free-living amoebae. Environ Microbiol 7:1003-8.
58. Sandstrom G, Saeed A, Abd H. 2010. Acanthamoeba polyphaga is a possible host for Vibrio cholerae in aquatic environments. Exp Parasitol 126:65-8.
59. Koren O, Rosenberg E. 2006. Bacteria associated with mucus and tissues of the coral Oculina patagonica in summer and winter. Appl Environ Microbiol 72:5254-9.
60. Bourne DG, Munn CB. 2005. Diversity of bacteria associated with the coral Pocillopora damicornis from the Great Barrier Reef. Environ Microbiol 7:1162-74.
61. Kvennefors EC, Sampayo E, Ridgway T, Barnes AC, Hoegh-Guldberg O. 2010. Bacterial communities of two ubiquitous Great Barrier Reef corals reveals both site- and species-specificity of common bacterial associates. PLoS One 5:e10401.

62. Ducklow HW, Mitchell R. 1979. Bacterial-Populations and Adaptations in the Mucus Layers on Living Corals. Limnology and Oceanography 24:715-725.
63. Sharon G, Rosenberg E. 2008. Bacterial growth on coral mucus. Current Microbiology 56:481-488.
64. Gavin HE, Satchell KJF. 2017. Surface hypothermia predicts murine mortality in the intragastric Vibrio vulnificus infection model. BMC Microbiol 17:136.
65. Bordas MA, Balebona MC, Rodriguez-Maroto JM, Borrego JJ, Morinigo MA. 1998. Chemotaxis of pathogenic Vibrio strains towards mucus surfaces of gilt-head sea bream (Sparus aurata L.). Appl Environ Microbiol 64:1573-5.
66. Mueller RS, McDougald D, Cusumano D, Sodhi N, Kjelleberg S, Azam F, Bartlett DH. 2007. Vibrio cholerae strains possess multiple strategies for abiotic and biotic surface colonization. J Bacteriol 189:5348-60.
67. Huq A, Small EB, West PA, Huq MI, Rahman R, Colwell RR. 1983. Ecological relationships between Vibrio cholerae and planktonic crustacean copepods. Appl Environ Microbiol 45:275-83.
68. Islam MS, Drasar BS, Bradley DJ. 1990. Long-term persistence of toxigenic Vibrio cholerae 01 in the mucilaginous sheath of a blue-green alga, Anabaena variabilis. J Trop Med Hyg 93:133-9.
69. Islam MS, Mahmuda S, Morshed MG, Bakht HB, Khan MN, Sack RB, Sack DA. 2004. Role of cyanobacteria in the persistence of Vibrio cholerae O139 in saline microcosms. Can J Microbiol 50:127-31.
70. Colwell RR. 1996. Global climate and infectious disease: the cholera paradigm. Science 274:2025-31.
71. Spira WM, Huq A, Ahmed QS, Saeed YA. 1981. Uptake of Vibrio cholerae biotype eltor from contaminated water by water hyacinth (eichornia crassipes). Appl Environ Microbiol 42:550-3.
72. Islam MS, Drasar BS, Bradley DJ. 1990. Survival of toxigenic Vibrio cholerae O1 with a common duckweed, Lemna minor, in artificial aquatic ecosystems. Trans R Soc Trop Med Hyg 84:422-4.
73. Cardoso MD, Lemos LS, Roges EM, de Moura JF, Tavares DC, Matias CAR, Rodrigues DP, Siciliano S. 2018. A comprehensive survey of Aeromonas sp. and Vibrio sp. in seabirds from southeastern Brazil: outcomes for public health. J Appl Microbiol doi:10.1111/jam.13705.
74. Hossain ZZ, Farhana I, Tulsiani SM, Begum A, Jensen PKM. 2018. Transmission and Toxigenic Potential of Vibrio cholerae in Hilsha Fish (Tenualosa ilisha) for Human Consumption in Bangladesh. Front Microbiol 9:222.
75. Tesfaye S, Kasye, M., Chane, M., Bogale, B. Agere, Z.A. 2018. Preliminary Survey of Gram-Negative Bacterial Pathogens from Commonly Caught Fish Species (*Orochromis niloticus, Cyprinus carpio* and *Clarias gariepinus*) in Lake Hayiq, Ethiopia. Fisheries and Aquaculture Journal 9:238.
76. Miyasaka J, Yahiro S, Arahira Y, Tokunaga H, Katsuki K, Hara-Kudo Y. 2006. Isolation of Vibrio parahaemolyticus and Vibrio vulnificus from wild aquatic birds in Japan. Epidemiol Infect 134:780-5.

77. Sugita H, Ushioka S, Kihara D, Deguchi Y. 1985. Changes in the Bacterial Composition of Water in a Carp Rearing Tank. Aquaculture 44:243-247.
78. Liston J. 1957. The Occurrence and Distribution of Bacterial Types on Flatfish. Journal of General Microbiology 16:205-216.
79. Xing MX, Hou ZH, Yuan JB, Liu Y, Qu YM, Liu B. 2013. Taxonomic and functional metagenomic profiling of gastrointestinal tract microbiome of the farmed adult turbot (Scophthalmus maximus). Fems Microbiology Ecology 86:432-443.
80. Aiso K, Simidu U, Hasuo K. 1968. Microflora in Digestive Tract of Inshore Fish in Japan. Journal of General Microbiology 52:361-&.
81. Newman JT, Cosenza BJ, Buck JD. 1972. Aerobic Microflora of Bluefish (Pomatomus-Saltatrix) Intestine. Journal of the Fisheries Research Board of Canada 29:333-&.
82. Yoshimizu M, Kimura T. 1976. Study on the Intestinal Microflora of Salmonids. Fish Pathology 10:243-259.
83. Muroga K, Higashi M, Keitoku H. 1987. The Isolation of Intestinal Microflora of Farmed Red Seabream (Pagrus-Major) and Black Seabream (Acanthopagrus-Schlegeli) at Larval and Juvenile Stages. Aquaculture 65:79-88.
84. Smriga S, Sandin SA, Azam F. 2010. Abundance, diversity, and activity of microbial assemblages associated with coral reef fish guts and feces. FEMS Microbiol Ecol 73:31-42.
85. Froelich B, Ayrapetyan M, Oliver JD. 2013. Integration of Vibrio vulnificus into marine aggregates and its subsequent uptake by Crassostrea virginica oysters. Appl Environ Microbiol 79:1454-8.
86. Froelich B, Oliver JD. 2013. The interactions of Vibrio vulnificus and the oyster Crassostrea virginica. Microb Ecol 65:807-16.
87. Murphree RL, Tamplin ML. 1995. Uptake and Retention of Vibrio-Cholerae O1 in the Eastern Oyster, Crassostrea-Virginica. Applied and Environmental Microbiology 61:3656-3660.
88. Froelich BA, Phippen B, Fowler P, Noble RT, Oliver JD. 2017. Differences in Abundances of Total Vibrio spp., V. vulnificus, and V. parahaemolyticus in Clams and Oysters in North Carolina. Appl Environ Microbiol 83.
89. Froelich BA, Noble RT. 2014. Factors affecting the uptake and retention of Vibrio vulnificus in oysters. Appl Environ Microbiol 80:7454-9.
90. Pu M, Duriez P, Arazi M, Rowe-Magnus DA. 2018. A conserved tad pilus promotes Vibrio vulnificus oyster colonization. Environ Microbiol 20:828-841.
91. Halpern M, Broza YB, Mittler S, Arakawa E, Broza M. 2004. Chironomid egg masses as a natural reservoir of Vibrio cholerae non-O1 and non-O139 in freshwater habitats. Microb Ecol 47:341-9.
92. Halpern M, Gancz H, Broza M, Kashi Y. 2003. Vibrio cholerae hemagglutinin/protease degrades chironomid egg masses. Appl Environ Microbiol 69:4200-4.
93. Goarant C, Ansquer D, Herlin J, Domalain D, Imbert F, De Decker S. 2006. "Summer Syndrome" in Litopenaeus stylirostris in New Caledonia: Pathology and epidemiology of the etiological agent, Vibrio nigripulchritudo. Aquaculture 253:105-113.

94. Costa R, Mermoud I, Koblavi S, Morlet B, Haffner P, Berthe F, Legroumellec M, Grimont P. 1998. Isolation and characterization of bacteria associated with a Penaeus stylirostris disease (Syndrome 93) in New Caledonia. Aquaculture 164:297-309.
95. Barua D. 1992. History of Cholera, p 1-36. *In* Baria D, Greenough, W.B. (ed), Cholera Current Topics in Infectious Disease. Springer, Boston, MA.
96. Sack DA, Sack RB, Nair GB, Siddique AK. 2004. Cholera. Lancet 363:223-33.
97. Koch R. 1884. An Address on Cholera and its Bacillus. The British Medical Journal 2:453-459.
98. Lantagne D, Balakrish Nair G, Lanata CF, Cravioto A. 2014. The cholera outbreak in Haiti: where and how did it begin? Curr Top Microbiol Immunol 379:145-64.
99. WHO. 2017. Cholera Fact Sheet. http://www.who.int/mediacentre/factsheets/fs107/en/. Accessed
100. Nair GB, Ramamurthy T, Bhattacharya SK, Dutta B, Takeda Y, Sack DA. 2007. Global dissemination of Vibrio parahaemolyticus serotype O3:K6 and its serovariants. Clin Microbiol Rev 20:39-48.
101. Sandra Hoffman BM, Michael Batz. 2015. Economic Burden of Major Foodborne Illnesses Acquired in the United States. USDA,
102. Newton A, Kendall M, Vugia DJ, Henao OL, Mahon BE. 2012. Increasing rates of vibriosis in the United States, 1996-2010: review of surveillance data from 2 systems. Clin Infect Dis 54 Suppl 5:S391-5.
103. Menon MP, Yu PA, Iwamoto M, Painter J. 2013. Pre-existing medical conditions associated with Vibrio vulnificus septicaemia. Epidemiol Infect doi:10.1017/S0950268813001593:1-4.
104. Scallan E, Hoekstra RM, Angulo FJ, Tauxe RV, Widdowson MA, Roy SL, Jones JL, Griffin PM. 2011. Foodborne illness acquired in the United States--major pathogens. Emerg Infect Dis 17:7-15.
105. Jones MK, Oliver JD. 2009. Vibrio vulnificus: disease and pathogenesis. Infect Immun 77:1723-33.
106. CDC. 2014. National Enteric Disease Surveillance: COVIS Annual Summary, 2012. Diseases CNCfEaZI,
107. CDC. 2016. National Enteric Disease Surveillance: COVIS Annual Summary, 2014. Diseases CNCfEaZI,
108. CDC. 2015. National Enteric Disease Surveillance: COVIS Annual Summary, 2013. Diseases CNCfEaZI,
109. Lee SH, Chung BH, Lee WC. 2013. Retrospective analysis of epidemiological aspects of Vibrio vulnificus infections in Korea in 2001-2010. Jpn J Infect Dis 66:331-3.
110. Kubota K, Kasuga F, Iwasaki E, Inagaki S, Sakurai Y, Komatsu M, Toyofuku H, Angulo FJ, Scallan E, Morikawa K. 2011. Estimating the burden of acute gastroenteritis and foodborne illness caused by Campylobacter, Salmonella, and Vibrio parahaemolyticus by using population-based telephone survey data, Miyagi Prefecture, Japan, 2005 to 2006. J Food Prot 74:1592-8.
111. Le Roux F, Wegner KM, Baker-Austin C, Vezzulli L, Osorio CR, Amaro C, Ritchie JM, Defoirdt T, Destoumieux-Garzon D, Blokesch M, Mazel D, Jacq A, Cava F, Gram L,

Wendling CC, Strauch E, Kirschner A, Huehn S. 2015. The emergence of Vibrio pathogens in Europe: ecology, evolution, and pathogenesis (Paris, 11-12th March 2015). Front Microbiol 6:830.
112. Baker-Austin C, Trinanes, J.A., Taylor, N.G.H., Hartnell, R. Siitonen, A., Martinez-Urtaza, J. 2012. Emerging *Vibrio* risk at high latitudes in response to ocean warming. Nature Climate Change 3:73-77.
113. Kaspar CW, Tamplin ML. 1993. Effects of temperature and salinity on the survival of Vibrio vulnificus in seawater and shellfish. Appl Environ Microbiol 59:2425-9.
114. Vezzulli L, Colwell RR, Pruzzo C. 2013. Ocean warming and spread of pathogenic vibrios in the aquatic environment. Microb Ecol 65:817-25.
115. Vezzulli L, Pezzati E, Brettar I, Hofle M, Pruzzo C. 2015. Effects of Global Warming on Vibrio Ecology. Microbiol Spectr 3.
116. Hlady WG, Klontz KC. 1996. The epidemiology of Vibrio infections in Florida, 1981-1993. Journal of Infectious Diseases 173:1176-1183.
117. O'Neill KR, Jones SH, Grimes DJ. 1992. Seasonal incidence of Vibrio vulnificus in the Great Bay estuary of New Hampshire and Maine. Appl Environ Microbiol 58:3257-62.
118. CDC. 2012. National Enteric Disease Surveillance: Cholera and Other Vibrio Illness Surveillance (COVIS). Diseases CNCfEaZI,
119. Chu C, Do Y, Kim Y, Saito Y, Lee SD, Park H, Lee JK. 2011. Mathematical Modeling of Vibrio vulnificus Infection in Korea and the Influence of Global Warming. Osong Public Health Res Perspect 2:51-8.
120. Bisharat N, Agmon V, Finkelstein R, Raz R, Ben-Dror G, Lerner L, Soboh S, Colodner R, Cameron DN, Wykstra DL, Swerdlow DL, Farmer JJ, 3rd. 1999. Clinical, epidemiological, and microbiological features of Vibrio vulnificus biogroup 3 causing outbreaks of wound infection and bacteraemia in Israel. Israel Vibrio Study Group. Lancet 354:1421-4.
121. Dechet AM, Yu PA, Koram N, Painter J. 2008. Nonfoodborne Vibrio infections: an important cause of morbidity and mortality in the United States, 1997-2006. Clin Infect Dis 46:970-6.
122. Horseman MA, Surani S. 2011. A comprehensive review of Vibrio vulnificus: an important cause of severe sepsis and skin and soft-tissue infection. Int J Infect Dis 15:e157-66.
123. do Nascimento SM, dos Fernandes Vieira RH, Theophilo GN, Dos Prazeres Rodrigues D, Vieira GH. 2001. Vibrio vulnificus as a health hazard for shrimp consumers. Rev Inst Med Trop Sao Paulo 43:263-6.
124. Froelich BA, Noble RT. 2016. Vibrio bacteria in raw oysters: managing risks to human health. Philos Trans R Soc Lond B Biol Sci 371:pii 20150209.
125. Oliver JD. 2015. The Biology of Vibrio vulnificus. Microbiol Spectr 3.
126. Vollberg CM, Herrera JL. 1997. Vibrio vulnificus infection: an important cause of septicemia in patients with cirrhosis. South Med J 90:1040-2.
127. Hlady WG. 1997. Vibrio infections associated with raw oyster consumption in Florida, 1981-1994. Journal of Food Protection 60:353-357.

128. Strom MS, Paranjpye RN. 2000. Epidemiology and pathogenesis of Vibrio vulnificus. Microbes Infect 2:177-88.
129. Shapiro RL, Altekruse S, Hutwagner L, Bishop R, Hammond R, Wilson S, Ray B, Thompson S, Tauxe RV, Griffin PM. 1998. The role of Gulf Coast oysters harvested in warmer months in Vibrio vulnificus infections in the United States, 1988-1996. Vibrio Working Group. J Infect Dis 178:752-9.
130. Klontz KC, Lieb S, Schreiber M, Janowski HT, Baldy LM, Gunn RA. 1988. Syndromes of Vibrio vulnificus infections. Clinical and epidemiologic features in Florida cases, 1981-1987. Ann Intern Med 109:318-23.
131. Chen Y, Satoh T, Tokunaga O. 2002. Vibrio vulnificus infection in patients with liver disease: report of five autopsy cases. Virchows Arch 441:88-92.
132. Fan JJ, Shao CP, Ho YC, Yu CK, Hor LI. 2001. Isolation and characterization of a Vibrio vulnificus mutant deficient in both extracellular metalloprotease and cytolysin. Infect Immun 69:5943-8.
133. Lee SJ, Jung YH, Kim JS, Lee HJ, Lee SH, Lee KH, Jang KK, Choi SH, Han HJ. 2017. A Vibrio vulnificus VvpM Induces IL-1beta Production Coupled with Necrotic Macrophage Death via Distinct Spatial Targeting by ANXA2. Front Cell Infect Microbiol 7:352.
134. Han GY, Jung, Y.H., Jang, K.K., Choi, S.H., Lee, S.J. 2014. *Vibrio vulnificus* Induces the Inflammation of Mouse Ileal Epithelium: Involvement of Protein Kinase C adn Nuclear Factor-Kappa B. Journal of Life Science 24:664-670.
135. Hong SHJ, K.; Park, M.J.; Lee, Y.S.; Duong Nu, T.M.; Kim, S.Y.; Rhee, J.H.; Lee, S.E. 2013. Destructive Intestinal Translocation of *Vibrio vulnificus* Determines Successful Oral Infection. Journal of Bacteriology and Virology 43:262-269.
136. Kim YR, Lee SE, Kook H, Yeom JA, Na HS, Kim SY, Chung SS, Choy HE, Rhee JH. 2008. Vibrio vulnificus RTX toxin kills host cells only after contact of the bacteria with host cells. Cell Microbiol 10:848-62.
137. Poole MD, Oliver JD. 1978. Experimental pathogenicity and mortality in ligated ileal loop studies of the newly reported halophilic lactose-positive Vibrio sp. Infect Immun 20:126-9.
138. Kashimoto T, Iwasaki C, Gojo M, Sugiyama H, Yoshioka K, Yamamoto Y, Okamura M, Susa N, Ueno S. 2015. Vibrio vulnificus detected in the spleen leads to fatal outcome in a mouse oral infection model. FEMS Microbiol Lett 362:fnv0005.
139. Thiaville PC, Bourdage KL, Wright AC, Farrell-Evans M, Garvan CW, Gulig PA. 2011. Genotype is correlated with but does not predict virulence of Vibrio vulnificus biotype 1 in subcutaneously inoculated, iron dextran-treated mice. Infect Immun 79:1194-207.
140. Murciano C, Lee CT, Fernandez-Bravo A, Hsieh TH, Fouz B, Hor LI, Amaro C. 2017. MARTX Toxin in the Zoonotic Serovar of Vibrio vulnificus Triggers an Early Cytokine Storm in Mice. Front Cell Infect Microbiol 7:332.
141. Powell JL, Wright AC, Wasserman SS, Hone DM, Morris JG, Jr. 1997. Release of tumor necrosis factor alpha in response to Vibrio vulnificus capsular polysaccharide in in vivo and in vitro models. Infect Immun 65:3713-8.

142. Powell JL, Strauss KA, Wiley C, Zhan M, Morris JG, Jr. 2003. Inflammatory cytokine response to Vibrio vulnificus elicited by peripheral blood mononuclear cells from chronic alcohol users is associated with biomarkers of cellular oxidative stress. Infect Immun 71:4212-6.
143. Xie DL, Zheng MM, Zheng Y, Gao H, Zhang J, Zhang T, Guo JC, Yang XF, Zhong XP, Lou YL. 2017. Vibrio vulnificus induces mTOR activation and inflammatory responses in macrophages. PLoS One 12:e0181454.
144. Shin SH, Shin DH, Ryu PY, Chung SS, Rhee JH. 2002. Proinflammatory cytokine profile in Vibrio vulnificus septicemic patients' sera. FEMS Immunol Med Microbiol 33:133-8.
145. Kumar A. 2013. An alternate pathophysiologic paradigm of sepsis and septic shock: Implications for optimizing antimicrobial therapy. Virulence 5.
146. Bone RC, Balk RA, Cerra FB, Dellinger RP, Fein AM, Knaus WA, Schein RM, Sibbald WJ. 1992. Definitions for sepsis and organ failure and guidelines for the use of innovative therapies in sepsis. The ACCP/SCCM Consensus Conference Committee. American College of Chest Physicians/Society of Critical Care Medicine. Chest 101:1644-55.
147. Freeman BD, Natanson C. 2000. Anti-inflammatory therapies in sepsis and septic shock. Expert Opin Investig Drugs 9:1651-63.
148. Hotchkiss RS, Karl IE. 2003. The pathophysiology and treatment of sepsis. N Engl J Med 348:138-50.
149. Daniels NA. 2011. Vibrio vulnificus oysters: pearls and perils. Clin Infect Dis 52:788-92.
150. Weis KE, Hammond RM, Hutchinson R, Blackmore CG. 2011. Vibrio illness in Florida, 1998-2007. Epidemiol Infect 139:591-8.
151. Turiño-Luque JD, Garrido Rasco, R., González Galán, V., de Alarcón, A. 2007. Sepsis and cellulitis by *VIbrio vulnificus* in cirrhotic patient. Anales de medicina interna 24:4560457.
152. Nazir S, Brown K, Shin AK, Donato AA. 2016. Vibrio vulnificus infection and liver cirrhosis: a potentially lethal combination. BMJ Case Rep 2016.
153. Chong Y, Park MY, Lee SY, Kim KS, Lee SI. 1982. Vibrio vulnificus septicemia in a patient with liver cirrhosis. Yonsei Med J 23:146-52.
154. Haq SM, Dayal HH. 2005. Chronic liver disease and consumption of raw oysters: A potentially lethal combination - A review of Vibrio vulnificus septicemia. American Journal of Gastroenterology 100:1195-1199.
155. Kizer KW. 1994. Vibrio vulnificus hazard in patients with liver disease. West J Med 161:64-5.
156. Park SD, Shon HS, Joh NJ. 1991. Vibrio vulnificus septicemia in Korea: clinical and epidemiologic findings in seventy patients. J Am Acad Dermatol 24:397-403.
157. MayoClinic. 10 January 2018 2018. Cirrhosis. https://www.mayoclinic.org/diseases-conditions/cirrhosis/symptoms-causes/syc-20351487. Accessed 9 April 2018.
158. Kowdley KV. 2016. Iron Overload in Patients With Chronic Liver Disease. Gastroenterol Hepatol (N Y) 12:695-698.

159. Milic S, Mikolasevic I, Orlic L, Devcic E, Starcevic-Cizmarevic N, Stimac D, Kapovic M, Ristic S. 2016. The Role of Iron and Iron Overload in Chronic Liver Disease. Med Sci Monit 22:2144-51.
160. Chart H, Griffiths E. 1985. The Availability of Iron and the Growth of Vibrio-Vulnificus in Sera from Patients with Hemochromatosis. Fems Microbiology Letters 26:227-231.
161. Yoshida S, Tanabe T, Yamamoto S, Chiba S, Mizuguchi Y. 1983. [Fatal Vibrio vulnificus infection in a patient with aplastic anemia]. J UOEH 5:95-100.
162. Bullen JJ, Spalding PB, Ward CG, Gutteridge JMC. 1991. Hemochromatosis, Iron, and Septicemia Caused by Vibrio-Vulnificus. Archives of Internal Medicine 151:1606-1609.
163. Hor LI, Chang TT, Wang ST. 1999. Survival of Vibrio vulnificus in whole blood from patients with chronic liver diseases: association with phagocytosis by neutrophils and serum ferritin levels. J Infect Dis 179:275-8.
164. Hor LI, Chang YK, Chang CC, Lei HY, Ou JT. 2000. Mechanism of high susceptibility of iron-overloaded mouse to Vibrio vulnificus infection. Microbiol Immunol 44:871-8.
165. Stefanova D, Raychev A, Arezes J, Michels K, Dillon B, Horwitz M, Mehrad B, Ganz T, Nemeth E, Bulut Y. 2017. Hepcidin Mediates Host Defense against Gram-Negative Pathogens by Controlling Non-Transferrin-Bound Iron. American Journal of Hematology 92:E207-E207.
166. Stefanova D, Raychev A, Arezes J, Ruchala P, Gabayan V, Skurnik M, Dillon BJ, Horwitz MA, Ganz T, Bulut Y, Nemeth E. 2017. Endogenous hepcidin and its agonist mediate resistance to selected infections by clearing non-transferrin-bound iron. Blood 130:245-257.
167. Arezes J, Jung G, Gabayan V, Valore E, Ruchala P, Gulig PA, Ganz T, Nemeth E, Bulut Y. 2015. Hepcidin-Induced Hypoferremia Is a Critical Host Defense Mechanism against the Siderophilic Bacterium Vibrio vulnificus. Cell Host & Microbe 17:47-57.
168. Llorente C, Schnabl B. 2016. Fast-Track Clearance of Bacteria from the Liver. Cell Host & Microbe 20:1-2.
169. Balmer ML, Slack E, de Gottardi A, Lawson MAE, Hapfelmeier S, Miele L, Grieco A, Van Vlierberghe H, Fahrner R, Patuto N, Bernsmeier C, Ronchi F, Wyss M, Stroka D, Dickgreber N, Heim MH, Mccoy KD, Macpherson AJ. 2014. The Liver May Act as a Firewall Mediating Mutualism Between the Host and Its Gut Commensal Microbiota. Science Translational Medicine 6.
170. Seki E, Schnabl B. 2012. Role of innate immunity and the microbiota in liver fibrosis: crosstalk between the liver and gut. Journal of Physiology-London 590:447-458.
171. Benacerraf B, Sebestyen MM, Schlossman S. 1959. A quantitative study of the kinetics of blood clearance of P32-labelled Escherichia coli and Staphylococci by the reticuloendothelial system. J Exp Med 110:27-48.
172. Baas J, Senninger N, Elser H. 1994. The Reticuloendothelial System - an Overview of Function, Pathology and Newer Methods of Measurement. Zeitschrift Fur Gastroenterologie 32:117-123.
173. Ashare A, Stanford C, Hancock P, Stark D, Lilli K, Birrer E, Nymon A, Doerschug KC, Hunninghake GW. 2009. Chronic liver disease impairs bacterial clearance in a human model of induced bacteremia. Clin Transl Sci 2:199-205.

174. Bunchorntavakul C, Chamroonkul N, Chavalitdhamrong D. 2016. Bacterial infections in cirrhosis: A critical review and practical guidance. World J Hepatol 8:307-21.
175. Bartoletti M, Giannella M, Lewis RE, Viale P. 2016. Bloodstream infections in patients with liver cirrhosis. Virulence 7:309-19.
176. Ashare A, Monick MM, Powers LS, Yarovinsky T, Hunninghake GW. 2006. Severe bacteremia results in a loss of hepatic bacterial clearance. Am J Respir Crit Care Med 173:644-52.
177. WHO. 2005. Risk assessment of *Vibrio vulnificus* in raw oysters: Interpretive summary and technical report. World Health Organization FaAOotUN,
178. Stelma GN, Jr., Reyes AL, Peeler JT, Johnson CH, Spaulding PL. 1992. Virulence characteristics of clinical and environmental isolates of Vibrio vulnificus. Appl Environ Microbiol 58:2776-82.
179. Reichelt JL, Baumann P, Baumann L. 1976. Study of genetic relationships among marine species of the genera Beneckea and Photobacterium by means of in vitro DNA/DNA hybridization. Arch Microbiol 110:101-20.
180. Baumann P, Baumann L, Mandel M. 1971. Taxonomy of marine bacteria: the genus Beneckea. J Bacteriol 107:268-94.
181. Hollis DG, Weaver RE, Baker CN, Thornsberry C. 1976. Halophilic Vibrio species isolated from blood cultures. J Clin Microbiol 3:425-31.
182. Farmer JJ. 1979. Vibrio ("Beneckea") vulnificus, the bacterium associated with sepsis, septicaemia, and the sea. The Lancet 2:903.
183. Blake PA, Merson MH, Weaver RE, Hollis DG, Heublein PC. 1979. Disease caused by a marine Vibrio. Clinical characteristics and epidemiology. N Engl J Med 300:1-5.
184. Clark WAS, A.G. 1977. Deoxyribonucleic Adic Reassociation Experiments with a Halophilic, Lactos-Fermenting Vibrio Isolated from Blood Cultures. International Journal of Systematic Bacteriology 27:194-199.
185. Johnson DE, Calia FM, Musher DM, Goree A. 1984. Resistance of Vibrio vulnificus to serum bactericidal and opsonizing factors: relation to virulence in suckling mice and humans. J Infect Dis 150:413-8.
186. Kim YR, Lee SE, Kim JR, Rhee JH. 2015. Safety and vaccine efficacy of an attenuated Vibrio vulnificus strain with deletions in major cytotoxin genes. FEMS Microbiol Lett 362:fnv169.
187. Duong-Nu TM, Jeong K, Hong SH, Nguyen HV, Ngo VH, Min JJ, Lee SE, Rhee JH. 2015. All Three TonB Systems Are Required for Vibrio vulnificus CMCP6 Tissue Invasiveness by Controlling Flagellum Expression. Infect Immun 84:254-65.
188. Wright AC, Simpson LM, Oliver JD. 1981. Role of iron in the pathogenesis of Vibrio vulnificus infections. Infect Immun 34:503-7.
189. Zhou XY, Tomatsu S, Fleming RE, Parkkila S, Waheed A, Jiang J, Fei Y, Brunt EM, Ruddy DA, Prass CE, Schatzman RC, O'Neill R, Britton RS, Bacon BR, Sly WS. 1998. HFE gene knockout produces mouse model of hereditary hemochromatosis. Proc Natl Acad Sci U S A 95:2492-7.

190. Espat NJ, Auffenberg T, Abouhamze A, Baumhofer J, Moldawer LL, Howard RJ. 1996. A role for tumor necrosis factor-alpha in the increased mortality associated with Vibrio vulnificus infection in the presence of hepatic dysfunction. Ann Surg 223:428-33.
191. Pineyro P, Zhou X, Orfe LH, Friel PJ, Lahmers K, Call DR. 2010. Development of two animal models to study the function of Vibrio parahaemolyticus type III secretion systems. Infect Immun 78:4551-9.
192. Olivier V, Queen J, Satchell KJ. 2009. Successful small intestine colonization of adult mice by Vibrio cholerae requires ketamine anesthesia and accessory toxins. PLoS One 4:e7352.
193. Kwak JS, Jeong HG, Satchell KJ. 2011. Vibrio vulnificus rtxA1 gene recombination generates toxin variants with altered potency during intestinal infection. Proc Natl Acad Sci U S A 108:1645-50.
194. Fuentes JM, Talamini MA, Fulton WB, Hanly EJ, Aurora AR, De Maio A. 2006. General anesthesia delays the inflammatory response and increases survival for mice with endotoxic shock. Clin Vaccine Immunol 13:281-8.
195. De SN, Chatterje DN. 1953. An experimental study of the mechanism of action of Vibriod cholerae on the intestinal mucous membrane. J Pathol Bacteriol 66:559-62.
196. Kim SY, Thanh XT, Jeong K, Kim SB, Pan SO, Jung CH, Hong SH, Lee SE, Rhee JH. 2014. Contribution of six flagellin genes to the flagellum biogenesis of Vibrio vulnificus and in vivo invasion. Infect Immun 82:29-42.
197. Amaro C, Sanjuan E, Fouz B, Pajuelo D, Lee CT, Hor LI, Barrera R. 2015. The Fish Pathogen Vibrio vulnificus Biotype 2: Epidemiology, Phylogeny, and Virulence Factors Involved in Warm-Water Vibriosis. Microbiol Spectr 3.
198. Amaro C, Biosca EG, Esteve C, Fouz B, Toranzo AE. 1992. Comparative-Study of Phenotypic and Virulence Properties in Vibrio-Vulnificus Biotype-1 and Biotype-2 Obtained from a European Eel Farm Experiencing Mortalities. Diseases of Aquatic Organisms 13:29-35.
199. Marco-Noales E, Milan M, Fouz B, Sanjuan E, Amaro C. 2001. Transmission to eels, portals of entry, and putative reservoirs of Vibrio vulnificus serovar E (biotype 2). Applied and Environmental Microbiology 67:4717-4725.
200. Dhakal BK, Lee W, Kim YR, Choy HE, Ahnn J, Rhee JH. 2006. Caenorhabditis elegans as a simple model host for Vibrio vulnificus infection. Biochem Biophys Res Commun 346:751-7.
201. Hsiao JY, Chen CY, Yang MJ, Ho HC. 2013. Live and dead GFP-tagged bacteria showed indistinguishable fluorescence in Caenorhabditis elegans gut. J Microbiol 51:367-72.
202. Peterson JW. 1996. Bacterial Pathogenesis. *In* th, Baron S (ed), Medical Microbiology, Galveston (TX).
203. Kim JS, Sung MH, Kho DH, Lee JK. 2005. Induction of manganese-containing superoxide dismutase is required for acid tolerance in Vibrio vulnificus. J Bacteriol 187:5984-95.
204. Reed LJ, Muench, H. 1938. A simple method of estimating fifty per cent endpoints. American Journal of Hygiene 27:4930497.

205. Kang IH, Kim JS, Lee JK. 2007. The virulence of Vibrio vulnificus is affected by the cellular level of superoxide dismutase activity. J Microbiol Biotechnol 17:1399-402.
206. Rhee JE, Rhee JH, Ryu PY, Choi SH. 2002. Identification of the cadBA operon from Vibrio vulnificus and its influence on survival to acid stress. Fems Microbiology Letters 208:245-251.
207. Rosche TM, Smith DJ, Parker EE, Oliver JD. 2005. RpoS involvement and requirement for exogenous nutrient for osmotically induced cross protection in Vibrio vulnificus. FEMS Microbiol Ecol 53:455-62.
208. Yoshida SI, Ogawa M, Mizuguchi Y. 1985. Relation of Capsular Materials and Colony Opacity to Virulence of Vibrio-Vulnificus. Infection and Immunity 47:446-451.
209. Wright AC, Simpson LM, Oliver JD, Morris JG. 1990. Phenotypic Evaluation of Acapsular Transposon Mutants of Vibrio-Vulnificus. Infection and Immunity 58:1769-1773.
210. Wright AC, Powell JL, Kaper JB, Morris JG. 2001. Identification of a group 1-like capsular polysaccharide operon for Vibrio vulnificus. Infection and Immunity 69:6893-6901.
211. Kim YK, McCarter LL. 2000. Analysis of the polar flagellar gene system of Vibrio parahaemolyticus. J Bacteriol 182:3693-704.
212. Lee JH, Rho JB, Park KJ, Kim CB, Han YS, Choi SH, Lee KH, Park SJ. 2004. Role of flagellum and motility in pathogenesis of Vibrio vulnificus. Infect Immun 72:4905-10.
213. Kim YR, Rhee JH. 2003. Flagellar basal body flg operon as a virulence determinant of Vibrio vulnificus. Biochemical and Biophysical Research Communications 304:405-410.
214. Paranjpye RN, Strom MS. 2005. A Vibrio vulnificus type IV pilin contributes to biofilm formation, adherence to epithelial cells, and virulence. Infect Immun 73:1411-22.
215. Paranjpye RN, Lara JC, Pepe JC, Pepe CM, Strom MS. 1998. The type IV leader peptidase/N-methyltransferase of Vibrio vulnificus controls factors required for adherence to HEp-2 cells and virulence in iron-overloaded mice. Infect Immun 66:5659-68.
216. Goo SY, Lee HJ, Kim WH, Han KL, Park DK, Lee HJ, Kim SM, Kim KS, Lee KH, Park SJ. 2006. Identification of OmpU of Vibrio vulnificus as a fibronectin-binding protein and its role in bacterial pathogenesis. Infect Immun 74:5586-94.
217. Alice AF, Naka H, Crosa JH. 2008. Global gene expression as a function of the iron status of the bacterial cell: influence of differentially expressed genes in the virulence of the human pathogen Vibrio vulnificus. Infect Immun 76:4019-37.
218. Kim IH, Shim JI, Lee KE, Hwang W, Kim IJ, Choi SH, Kim KS. 2008. Nonribosomal peptide synthase is responsible for the biosynthesis of siderophore in Vibrio vulnificus MO6-24/O. J Microbiol Biotechnol 18:35-42.
219. Simpson LM, Oliver JD. 1983. Siderophore production by Vibrio vulnificus. Infect Immun 41:644-9.
220. Litwin CM, Rayback TW, Skinner J. 1996. Role of catechol siderophore synthesis in Vibrio vulnificus virulence. Infect Immun 64:2834-8.
221. Webster AC, Litwin CM. 2000. Cloning and characterization of vuuA, a gene encoding the Vibrio vulnificus ferric vulnibactin receptor. Infect Immun 68:526-34.

222. Green ER, Mecsas J. 2016. Bacterial Secretion Systems: An Overview. Microbiol Spectr 4.
223. Borgeaud S, Metzger LC, Scrignari T, Blokesch M. 2015. The type VI secretion system of Vibrio cholerae fosters horizontal gene transfer. Science 347:63-7.
224. Unterweger D, Miyata ST, Bachmann V, Brooks TM, Mullins T, Kostiuk B, Provenzano D, Pukatzki S. 2014. The Vibrio cholerae type VI secretion system employs diverse effector modules for intraspecific competition. Nat Commun 5:3549.
225. Church SR, Lux T, Baker-Austin C, Buddington SP, Michell SL. 2016. Vibrio vulnificus Type 6 Secretion System 1 Contains Anti-Bacterial Properties. PLoS One 11:e0165500.
226. Logan SL, Thomas J, Yan J, Baker RP, Shields DS, Xavier JB, Hammer BK, Parthasarathy R. 2018. The Vibrio cholerae type VI secretion system can modulate host intestinal mechanics to displace gut bacterial symbionts. Proc Natl Acad Sci U S A doi:10.1073/pnas.1720133115.
227. Miyata ST, Kitaoka M, Brooks TM, McAuley SB, Pukatzki S. 2011. Vibrio cholerae requires the type VI secretion system virulence factor VasX to kill Dictyostelium discoideum. Infect Immun 79:2941-9.
228. Yanez ME, Korotkov KV, Abendroth J, Hol WG. 2008. The crystal structure of a binary complex of two pseudopilins: EpsI and EpsJ from the type 2 secretion system of Vibrio vulnificus. J Mol Biol 375:471-86.
229. Korotkov KV, Gray MD, Kreger A, Turley S, Sandkvist M, Hol WG. 2009. Calcium is essential for the major pseudopilin in the type 2 secretion system. J Biol Chem 284:25466-70.
230. Hwang W, Lee NY, Kim J, Lee MA, Kim KS, Lee KH, Park SJ. 2011. Functional characterization of EpsC, a component of the type II secretion system, in the pathogenicity of Vibrio vulnificus. Infect Immun 79:4068-80.
231. Carda-Dieguez M, Silva-Hernandez FX, Hubbard TP, Chao MC, Waldor MK, Amaro C. 2018. Comprehensive identification of Vibrio vulnificus genes required for growth in human serum. Virulence doi:10.1080/21505594.2018.1455464:1-41.
232. Wright AC, Morris JG. 1991. The Extracellular Cytolysin of Vibrio-Vulnificus - Inactivation and Relationship to Virulence in Mice. Infection and Immunity 59:192-197.
233. Helms SD, Oliver JD, Travis JC. 1984. Role of Heme Compounds and Haptoglobin in Vibrio-Vulnificus Pathogenicity. Infection and Immunity 45:345-349.
234. Kim IH, Wen Y, Son JS, Lee KH, Kim KS. 2013. The Fur-Iron Complex Modulates Expression of the Quorum-Sensing Master Regulator, SmcR, To Control Expression of Virulence Factors in Vibrio vulnificus. Infection and Immunity 81:2888-2898.
235. Lee SJ, Jung YH, Oh SY, Song EJ, Choi SH, Han HJ. 2015. Vibrio vulnificus VvhA induces NF-kappa B-dependent mitochondrial cell death via lipid raft-mediated ROS production in intestinal epithelial cells. Cell Death & Disease 6.
236. Song EJ, Lee SJ, Lim HS, Kim JS, Jang KK, Choi SH, Han HJ. 2016. Vibrio vulnificus VvhA induces autophagy-related cell death through the lipid raft-dependent c-Src/NOX signaling pathway. Scientific Reports 6.
237. Chang AK, Kim HY, Park JE, Acharya P, Park IS, Yoon SM, You HJ, Hahm KS, Park JK, Lee JS. 2005. Vibrio vulnificus secretes a broad-specificity metalloprotease capable

of interfering with blood homeostasis through prothrombin activation and fibrinolysis. J Bacteriol 187:6909-16.
238. Kothary MH, Kreger AS. 1987. Purification and characterization of an elastolytic protease of Vibrio vulnificus. J Gen Microbiol 133:1783-91.
239. Jeong KC, Jeong HS, Rhee JH, Lee SE, Chung SS, Starks AM, Escudero GM, Gulig PA, Choi SH. 2000. Construction and phenotypic evaluation of a Vibrio vulnificus vvpE mutant for elastolytic protease. Infect Immun 68:5096-106.
240. Shao CP, Hor LI. 2000. Metalloprotease is not essential for Vibrio vulnificus virulence in mice. Infect Immun 68:3569-73.
241. Lee SJ, Jung YH, Oh SY, Jang KK, Lee HS, Choi SH, Han HJ. 2015. Vibrio vulnificus VvpE inhibits mucin 2 expression by hypermethylation via lipid raft-mediated ROS signaling in intestinal epithelial cells. Cell Death Dis 6:e1787.
242. Lee SJ, Jung YH, Ryu JM, Jang KK, Choi SH, Han HJ. 2016. VvpE mediates the intestinal colonization of Vibrio vulnificus by the disruption of tight junctions. Int J Med Microbiol 306:10-9.
243. Jang KK, Gil SY, Lim JG, Choi SH. 2016. Regulatory Characteristics of Vibrio vulnificus gbpA Gene Encoding a Mucin-binding Protein Essential for Pathogenesis. J Biol Chem 291:5774-87.
244. Lin W, Fullner KJ, Clayton R, Sexton JA, Rogers MB, Calia KE, Calderwood SB, Fraser C, Mekalanos JJ. 1999. Identification of a *Vibrio cholerae* RTX toxin gene cluster that is tightly linked to the cholera toxin prophage. Proc Natl Acad Sci USA 96:1071-1076.
245. Lee JH, Kim MW, Kim BS, Kim SM, Lee BC, Kim TS, Choi SH. 2007. Identification and characterization of the Vibrio vulnificus rtxA essential for cytotoxicity in vitro and virulence in mice. J Microbiol 45:146-52.
246. Kim YR, Lee SE, Kang IC, Nam KI, Choy HE, Rhee JH. 2013. A bacterial RTX toxin causes programmed necrotic cell death through calcium-mediated mitochondrial dysfunction. J Infect Dis 207:1406-15.
247. Lee BC, Choi SH, Kim TS. 2008. Vibrio vulnificus RTX toxin plays an important role in the apoptotic death of human intestinal epithelial cells exposed to Vibrio vulnificus. Microbes Infect 10:1504-13.
248. Liu M, Alice AF, Naka H, Crosa JH. 2007. The HlyU protein is a positive regulator of rtxA1, a gene responsible for cytotoxicity and virulence in the human pathogen Vibrio vulnificus. Infect Immun 75:3282-9.
249. Lo HR, Lin JH, Chen YH, Chen CL, Shao CP, Lai YC, Hor LI. 2011. RTX toxin enhances the survival of Vibrio vulnificus during infection by protecting the organism from phagocytosis. J Infect Dis 203:1866-74.
250. Moest TP, Meresse S. 2013. Salmonella T3SSs: successful mission of the secret(ion) agents. Curr Opin Microbiol 16:38-44.
251. So EC, Mattheis C, Tate EW, Frankel G, Schroeder GN. 2015. Creating a customized intracellular niche: subversion of host cell signaling by Legionella type IV secretion system effectors. Can J Microbiol doi:10.1139/cjm-2015-0166:1-19.
252. Alouf JE, Popoff MR (ed). 2006. The Comprehensive Sourcebook of Bacterial Protein Toxins. Academic Press,

253. Gavin HE, Satchell KJ. 2015. MARTX toxins as effector delivery platforms. Pathog Dis 73:ftv092.
254. Lee BC, Lee JH, Kim MW, Kim BS, Oh MH, Kim KS, Kim TS, Choi SH. 2008. Vibrio vulnificus rtxE is important for virulence, and its expression is induced by exposure to host cells. Infect Immun 76:1509-17.
255. Li L, Rock JL, Nelson DR. 2008. Identification and characterization of a repeat-in-toxin gene cluster in Vibrio anguillarum. Infect Immun 76:2620-32.
256. Liu M, Naka H, Crosa JH. 2009. HlyU acts as an H-NS antirepressor in the regulation of the RTX toxin gene essential for the virulence of the human pathogen Vibrio vulnificus CMCP6. Mol Microbiol 72:491-505.
257. Liu M, Rose M, Crosa JH. 2011. Homodimerization and binding of specific domains to the target DNA are essential requirements for HlyU to regulate expression of the virulence gene rtxA1, encoding the repeat-in-toxin protein in the human pathogen Vibrio vulnificus. J Bacteriol 193:6895-901.
258. Liu M, Crosa JH. 2012. The regulator HlyU, the repeat-in-toxin gene rtxA1, and their roles in the pathogenesis of Vibrio vulnificus infections. Microbiologyopen 1:502-13.
259. Li L, Mou X, Nelson DR. 2011. HlyU is a positive regulator of hemolysin expression in Vibrio anguillarum. J Bacteriol 193:4779-89.
260. Mou X, Spinard EJ, Driscoll MV, Zhao W, Nelson DR. 2013. H-NS is a negative regulator of the two hemolysin/cytotoxin gene clusters in Vibrio anguillarum. Infect Immun 81:3566-76.
261. Guo RH, Lim JY, Tra My DN, Jo SJ, Park JU, Rhee JH, Kim YR. 2018. Vibrio vulnificus RtxA1 Toxin Expression Upon Contact With Host Cells Is RpoS-Dependent. Front Cell Infect Microbiol 8:70.
262. Boardman BK, Satchell KJ. 2004. Vibrio cholerae strains with mutations in an atypical type I secretion system accumulate RTX toxin intracellularly. J Bacteriol 186:8137-43.
263. Stanley P, Koronakis V, Hughes C. 1998. Acylation of *Escherichia coli* hemolysin: a unique protein lipidation mechanism underlying toxin function. Microbiol Mol Biol Rev 62:309-333.
264. Basar T, Havlicek V, Bezouskova S, Hackett M, Sebo P. 2001. Acylation of lysine 983 is sufficient for toxin activity of Bordetella pertussis adenylate cyclase. Substitutions of alanine 140 modulate acylation site selectivity of the toxin acyltransferase CyaC. J Biol Chem 276:348-54.
265. Cheong TG, Chan M, Kurunathan S, Ali SA, ZiNing T, Zainuddin ZF, Lalitha P, Ravichandran M. 2010. Construction and characterization of rtxA and rtxC mutants of auxotrophic O139 Vibrio cholerae. Microb Pathog 48:85-90.
266. Gulig PA, Tucker MS, Thiaville PC, Joseph JL, Brown RN. 2009. USER friendly cloning coupled with chitin-based natural transformation enables rapid mutagenesis of Vibrio vulnificus. Appl Environ Microbiol 75:4936-49.
267. Bina JE, Mekalanos JJ. 2001. *Vibrio cholerae tolC* is required for bile resistance and colonization. Infect Immun 69:4681-5.
268. Andersen C, Hughes C, Koronakis V. 2000. Chunnel vision. Export and efflux through bacterial channel-tunnels. EMBO Rep 1:313-8.

269. Bielaszewska M, Aldick T, Bauwens A, Karch H. 2014. Hemolysin of enterohemorrhagic Escherichia coli: structure, transport, biological activity and putative role in virulence. Int J Med Microbiol 304:521-9.
270. Boardman BK, Meehan BM, Fullner Satchell KJ. 2007. Growth phase regulation of Vibrio cholerae RTX toxin export. J Bacteriol 189:1827-35.
271. Shen A, Lupardus PJ, Albrow VE, Guzzetta A, Powers JC, Garcia KC, Bogyo M. 2009. Mechanistic and structural insights into the proteolytic activation of Vibrio cholerae MARTX toxin. Nat Chem Biol 5:469-78.
272. Gray MC, Donato GM, Jones FR, Kim T, Hewlett EL. 2004. Newly secreted adenylate cyclase toxin is responsible for intoxication of target cells by Bordetella pertussis. Mol Microbiol 53:1709-19.
273. Hozbor D, Rodriguez ME, Fernandez J, Lagares A, Guiso N, Yantorno O. 1999. Release of outer membrane vesicles from Bordetella pertussis. Curr Microbiol 38:273-8.
274. Kim YR, Kim BU, Kim SY, Kim CM, Na HS, Koh JT, Choy HE, Rhee JH, Lee SE. 2010. Outer membrane vesicles of Vibrio vulnificus deliver cytolysin-hemolysin VvhA into epithelial cells to induce cytotoxicity. Biochem Biophys Res Commun 399:607-12.
275. Satchell KJ. 2007. MARTX, multifunctional autoprocessing repeats-in-toxin toxins. Infect Immun 75:5079-84.
276. Linhartova I, Bumba L, Masin J, Basler M, Osicka R, Kamanova J, Prochazkova K, Adkins I, Hejnova-Holubova J, Sadilkova L, Morova J, Sebo P. 2010. RTX proteins: a highly diverse family secreted by a common mechanism. FEMS Microbiol Rev 34:1076-112.
277. Blenner MA, Shur O, Szilvay GR, Cropek DM, Banta S. 2010. Calcium-induced folding of a beta roll motif requires C-terminal entropic stabilization. J Mol Biol 400:244-56.
278. Chenal A, Guijarro JI, Raynal B, Delepierre M, Ladant D. 2009. RTX calcium binding motifs are intrinsically disordered in the absence of calcium: implication for protein secretion. J Biol Chem 284:1781-9.
279. Sotomayor-Perez AC, Ladant D, Chenal A. 2015. Disorder-to-order transition in the CyaA toxin RTX domain: implications for toxin secretion. Toxins (Basel) 7:1-20.
280. Thomas S, Bakkes PJ, Smits SH, Schmitt L. 2014. Equilibrium folding of pro-HlyA from Escherichia coli reveals a stable calcium ion dependent folding intermediate. Biochim Biophys Acta 1844:1500-10.
281. Kudryashova E, Heisler D, Zywiec A, Kudryashov DS. 2014. Thermodynamic properties of the effector domains of MARTX toxins suggest their unfolding for translocation across the host membrane. Mol Microbiol 92:1056-71.
282. Prochazkova K, Shuvalova LA, Minasov G, Voburka Z, Anderson WF, Satchell KJ. 2009. Structural and molecular mechanism for autoprocessing of MARTX toxin of Vibrio cholerae at multiple sites. J Biol Chem 284:26557-68.
283. Sheahan KL, Cordero CL, Satchell KJ. 2007. Autoprocessing of the Vibrio cholerae RTX toxin by the cysteine protease domain. EMBO J 26:2552-61.
284. Egerer M, Satchell KJ. 2010. Inositol hexakisphosphate-induced autoprocessing of large bacterial protein toxins. PLoS Pathog 6:e1000942.

285. Prochazkova K, Satchell KJ. 2008. Structure-function analysis of inositol hexakisphosphate-induced autoprocessing of the Vibrio cholerae multifunctional autoprocessing RTX toxin. J Biol Chem 283:23656-64.
286. Sheahan KL, Cordero CL, Satchell KJ. 2004. Identification of a domain within the multifunctional Vibrio cholerae RTX toxin that covalently cross-links actin. Proc Natl Acad Sci U S A 101:9798-803.
287. Kudryashov DS, Durer ZA, Ytterberg AJ, Sawaya MR, Pashkov I, Prochazkova K, Yeates TO, Loo RR, Loo JA, Satchell KJ, Reisler E. 2008. Connecting actin monomers by iso-peptide bond is a toxicity mechanism of the Vibrio cholerae MARTX toxin. Proc Natl Acad Sci U S A 105:18537-42.
288. Cordero CL, Kudryashov DS, Reisler E, Satchell KJ. 2006. The Actin cross-linking domain of the Vibrio cholerae RTX toxin directly catalyzes the covalent cross-linking of actin. J Biol Chem 281:32366-74.
289. Murciano C, Hor LI, Amaro C. 2015. Host-pathogen interactions in Vibrio vulnificus: responses of monocytes and vascular endothelial cells to live bacteria. Future Microbiol 10:471-87.
290. Toma C, Higa N, Koizumi Y, Nakasone N, Ogura Y, McCoy AJ, Franchi L, Uematsu S, Sagara J, Taniguchi S, Tsutsui H, Akira S, Tschopp J, Nunez G, Suzuki T. 2010. Pathogenic Vibrio activate NLRP3 inflammasome via cytotoxins and TLR/nucleotide-binding oligomerization domain-mediated NF-kappa B signaling. J Immunol 184:5287-97.
291. Kim YR, Lee SE, Kim CM, Kim SY, Shin EK, Shin DH, Chung SS, Choy HE, Progulske-Fox A, Hillman JD, Handfield M, Rhee JH. 2003. Characterization and pathogenic significance of Vibrio vulnificus antigens preferentially expressed in septicemic patients. Infect Immun 71:5461-71.
292. Lee TH, Kim MH, Lee CS, Lee JH, Rhee JH, Chung KM. 2014. Protection against Vibrio vulnificus infection by active and passive immunization with the C-terminal region of the RtxA1/MARTXVv protein. Vaccine 32:271-6.
293. Charpentier X, Oswald E. 2004. Identification of the secretion and translocation domain of the enteropathogenic and enterohemorrhagic Escherichia coli effector Cif, using TEM-1 beta-lactamase as a new fluorescence-based reporter. J Bacteriol 186:5486-95.
294. Zlokarnik G, Negulescu PA, Knapp TE, Mere L, Burres N, Feng L, Whitney M, Roemer K, Tsien RY. 1998. Quantitation of transcription and clonal selection of single living cells with beta-lactamase as reporter. Science 279:84-8.
295. Geddes K, Cruz F, Heffron F. 2007. Analysis of cells targeted by Salmonella type III secretion in vivo. PLoS Pathog 3:e196.
296. Yamamoto K, Ichinose Y, Shinagawa H, Makino K, Nakata A, Iwanaga M, Honda T, Miwatani T. 1990. Two-step processing for activation of the cytolysin/hemolysin of Vibrio cholerae O1 biotype El Tor: nucleotide sequence of the structural gene (hlyA) and characterization of the processed products. Infect Immun 58:4106-16.
297. Yamamoto K, Wright AC, Kaper JB, Morris JG, Jr. 1990. The cytolysin gene of Vibrio vulnificus: sequence and relationship to the Vibrio cholerae E1 Tor hemolysin gene. Infect Immun 58:2706-9.

298. Lee VT, Pukatzki S, Sato H, Kikawada E, Kazimirova AA, Huang J, Li X, Arm JP, Frank DW, Lory S. 2007. Pseudolipasin A is a specific inhibitor for phospholipase A2 activity of Pseudomonas aeruginosa cytotoxin ExoU. Infect Immun 75:1089-98.
299. Aiello D, Williams JD, Majgier-Baranowska H, Patel I, Peet NP, Huang J, Lory S, Bowlin TL, Moir DT. 2010. Discovery and characterization of inhibitors of Pseudomonas aeruginosa type III secretion. Antimicrob Agents Chemother 54:1988-99.
300. Bowlin NO, Williams JD, Knoten CA, Torhan MC, Tashjian TF, Li B, Aiello D, Mecsas J, Hauser AR, Peet NP, Bowlin TL, Moir DT. 2014. Mutations in the Pseudomonas aeruginosa needle protein gene pscF confer resistance to phenoxyacetamide inhibitors of the type III secretion system. Antimicrob Agents Chemother 58:2211-20.
301. Delepelaire P. 2004. Type I secretion in gram-negative bacteria. Biochim Biophys Acta 1694:149-61.
302. Palzkill T, Botstein D. 1992. Identification of amino acid substitutions that alter the substrate specificity of TEM-1 beta-lactamase. J Bacteriol 174:5237-43.
303. Diaz MH, Hauser AR. 2010. Pseudomonas aeruginosa cytotoxin ExoU is injected into phagocytic cells during acute pneumonia. Infect Immun 78:1447-56.
304. Sakamoto H, Bellalou J, Sebo P, Ladant D. 1992. Bordetella pertussis adenylate cyclase toxin. Structural and functional independence of the catalytic and hemolytic activities. J Biol Chem 267:13598-602.
305. Lee CT, Pajuelo D, Llorens A, Chen YH, Leiro JM, Padros F, Hor LI, Amaro C. 2013. MARTX of Vibrio vulnificus biotype 2 is a virulence and survival factor. Environ Microbiol 15:419-32.
306. Biancucci M, Satchell KJ. 2015. A bacterial toxin that cleaves Ras oncoprotein. Oncotarget 6:18742-3.
307. Guimaraes JC, Rocha M, Arkin AP. 2014. Transcript level and sequence determinants of protein abundance and noise in Escherichia coli. Nucleic Acids Res 42:4791-9.
308. Chung KJ, Cho EJ, Kim MK, Kim YR, Kim SH, Yang HY, Chung KC, Lee SE, Rhee JH, Choy HE, Lee TH. 2010. RtxA1-induced expression of the small GTPase Rac2 plays a key role in the pathogenicity of Vibrio vulnificus. J Infect Dis 201:97-105.
309. Feldhusen F. 2000. The role of seafood in bacterial foodborne diseases. Microbes Infect 2:1651-60.
310. Chen CL, Chien SC, Leu TH, Harn HI, Tang MJ, Hor LI. 2017. Vibrio vulnificus MARTX cytotoxin causes inactivation of phagocytosis-related signaling molecules in macrophages. J Biomed Sci 24:58.
311. Dixon LJ, Barnes M, Tang H, Pritchard MT, Nagy LE. 2013. Kupffer cells in the liver. Compr Physiol 3:785-97.
312. Borges da Silva H, Fonseca R, Pereira RM, Cassado Ados A, Alvarez JM, D'Imperio Lima MR. 2015. Splenic Macrophage Subsets and Their Function during Blood-Borne Infections. Front Immunol 6:480.
313. Wesche J, Elliott JL, Falnes PO, Olsnes S, Collier RJ. 1998. Characterization of membrane translocation by anthrax protective antigen. Biochemistry 37:15737-46.

314. Spyres LM, Qa'Dan M, Meader A, Tomasek JJ, Howard EW, Ballard JD. 2001. Cytosolic delivery and characterization of the TcdB glucosylating domain by using a heterologous protein fusion. Infect Immun 69:599-601.
315. Harris J. 2011. Autophagy and cytokines. Cytokine 56:140-4.
316. Lawrence T. 2009. The nuclear factor NF-kappaB pathway in inflammation. Cold Spring Harb Perspect Biol 1:a001651.
317. Jones B, Burkhart J, Sonpavde G. 2015. Danger on a half shell: Vibrio vulnificus septicemia. Am J Med 128:475-6.
318. Chao CH, Duh RW, Liu CY, Lou JP, Chen CK. 1992. Experience of six patients with Vibrio vulnificus septicemia. Zhonghua Yi Xue Za Zhi (Taipei) 49:335-42.
319. Inoue Y, Ono T, Matsui T, Miyasaka J, Kinoshita Y, Ihn H. 2008. Epidemiological survey of Vibrio vulnificus infection in Japan between 1999 and 2003. J Dermatol 35:129-39.
320. Olfert ED, Godson, Dale L. 2000. Humane Endpoints for Infectious Disease Animal Models. Institute for Laboratory Animal Research Journal 41:99-104.
321. Trammell RA, Toth LA. 2011. Markers for predicting death as an outcome for mice used in infectious disease research. Comp Med 61:492-8.
322. Vlach KD, Boles JW, Stiles BG. 2000. Telemetric evaluation of body temperature and physical activity as predictors of mortality in a murine model of staphylococcal enterotoxic shock. Comp Med 50:160-6.
323. Wong JP, Saravolac EG, Clement JG, Nagata LP. 1997. Development of a murine hypothermia model for study of respiratory tract influenza virus infection. Lab Anim Sci 47:143-7.
324. Soothill JS, Morton DB, Ahmad A. 1992. The HID50 (hypothermia-inducing dose 50): an alternative to the LD50 for measurement of bacterial virulence. Int J Exp Pathol 73:95-8.
325. Toth LA. 2000. Defining the moribund condition as an experimental endpoint for animal research. iLAR J 41:72-9.
326. Fullner KJ, Mekalanos JJ. 1999. Genetic characterization of a new type IV-A pilus gene cluster found in both classical and El Tor biotypes of Vibrio cholerae. Infect Immun 67:1393-404.
327. Gargiulo S, Greco A, Gramanzini M, Esposito S, Affuso A, Brunetti A, Vesce G. 2012. Mice Anesthesia, Analgesia, and Care, Part 1: Anexthetic Considerations in Preclinical Research. ILAR J 53:E55-69.
328. Toth LA. 1997. The moribund state as an experimental endpoint. Contemp Top Lab Anim Sci 36:44-8.
329. Toth LA, Rehg JE, Webster RG. 1995. Strain differences in sleep and other pathophysiological sequelae of influenza virus infection in naive and immunized mice. J Neuroimmunol 58:89-99.
330. Stiles BG, Campbell YG, Castle RM, Grove SA. 1999. Correlation of temperature and toxicity in murine studies of staphylococcal enterotoxins and toxic shock syndrome toxin 1. Infect Immun 67:1521-5.

331. Bast DJ, Yue M, Chen X, Bell D, Dresser L, Saskin R, Mandell LA, Low DE, de Azavedo JC. 2004. Novel murine model of pneumococcal pneumonia: use of temperature as a measure of disease severity to compare the efficacies of moxifloxacin and levofloxacin. Antimicrob Agents Chemother 48:3343-8.
332. Hankenson FC, Ruskoski N, van Saun M, Ying GS, Oh J, Fraser NW. 2013. Weight loss and reduced body temperature determine humane endpoints in a mouse model of ocular herpesvirus infection. J Am Assoc Lab Anim Sci 52:277-85.
333. Warn PA, Brampton MW, Sharp A, Morrissey G, Steel N, Denning DW, Priest T. 2003. Infrared body temperature measurement of mice as an early predictor of death in experimental fungal infections. Lab Anim 37:126-31.
334. Clement JG. 1993. Experimentally induced mortality following repeated measurement of rectal temperature in mice. Lab Anim Sci 43:381-2.
335. Kort WJ, Hekking-Weijma JM, TenKate MT, Sorm V, VanStrik R. 1998. A microchip implant system as a method to determine body temperature of terminally ill rats and mice. Lab Anim 32:260-9.
336. Newsom DM, Bolgos GL, Colby L, Nemzek JA. 2004. Comparison of body surface temperature measurement and conventional methods for measuring temperature in the mouse. Contemp Top Lab Anim Sci 43:13-8.
337. Fiser R, Masin J, Bumba L, Pospisilova E, Fayolle C, Basler M, Sadilkova L, Adkins I, Kamanova J, Cerny J, Konopasek I, Osicka R, Leclerc C, Sebo P. 2012. Calcium influx rescues adenylate cyclase-hemolysin from rapid cell membrane removal and enables phagocyte permeabilization by toxin pores. PLoS Pathog 8:e1002580.
338. Osickova A, Masin J, Fayolle C, Krusek J, Basler M, Pospisilova E, Leclerc C, Osicka R, Sebo P. 2010. Adenylate cyclase toxin translocates across target cell membrane without forming a pore. Mol Microbiol 75:1550-62.
339. Thelestam M, Mollby R. 1983. Survival of cultured cells after functional and structural disorganization of plasma membrane by bacterial haemolysins and phospholipases. Toxicon 21:805-15.
340. Walev I, Bhakdi SC, Hofmann F, Djonder N, Valeva A, Aktories K, Bhakdi S. 2001. Delivery of proteins into living cells by reversible membrane permeabilization with streptolysin-O. Proc Natl Acad Sci U S A 98:3185-90.
341. Bischofberger M, Iacovache I, van der Goot FG. 2012. Pathogenic pore-forming proteins: function and host response. Cell Host Microbe 12:266-75.
342. Husmann M, Beckmann E, Boller K, Kloft N, Tenzer S, Bobkiewicz W, Neukirch C, Bayley H, Bhakdi S. 2009. Elimination of a bacterial pore-forming toxin by sequential endocytosis and exocytosis. FEBS Lett 583:337-44.
343. Keyel PA, Loultcheva L, Roth R, Salter RD, Watkins SC, Yokoyama WM, Heuser JE. 2011. Streptolysin O clearance through sequestration into blebs that bud passively from the plasma membrane. J Cell Sci 124:2414-23.
344. Alouf JE. 1980. Streptococcal toxins (streptolysin O, streptolysin S, erythrogenic toxin). Pharmacol Ther 11:661-717.

345. Kennedy CL, Smith DJ, Lyras D, Chakravorty A, Rood JI. 2009. Programmed cellular necrosis mediated by the pore-forming alpha-toxin from Clostridium septicum. PLoS Pathog 5:e1000516.
346. Knapp O, Maier E, Mkaddem SB, Benz R, Bens M, Chenal A, Geny B, Vandewalle A, Popoff MR. 2010. Clostridium septicum alpha-toxin forms pores and induces rapid cell necrosis. Toxicon 55:61-72.
347. Lin CF, Chen CL, Huang WC, Cheng YL, Hsieh CY, Wang CY, Hong MY. 2010. Different types of cell death induced by enterotoxins. Toxins (Basel) 2:2158-76.
348. Pedelacq JD, Cabantous S, Tran T, Terwilliger TC, Waldo GS. 2006. Engineering and characterization of a superfolder green fluorescent protein. Nat Biotechnol 24:79-88.
349. Nenasheva TA, Mashanov GI. 2006. [Visualizing single fluorophores in live cells]. Biofizika 51:454-65.
350. Nguyen AH, Nguyen VT, Kamio Y, Higuchi H. 2006. Single-molecule visualization of environment-sensitive fluorophores inserted into cell membranes by staphylococcal gamma-hemolysin. Biochemistry 45:2570-6.
351. Khelef N, Sakamoto H, Guiso N. 1992. Both adenylate cyclase and hemolytic activities are required by Bordetella pertussis to initiate infection. Microb Pathog 12:227-35.
352. Gross MK, Au DC, Smith AL, Storm DR. 1992. Targeted mutations that ablate either the adenylate cyclase or hemolysin function of the bifunctional cyaA toxin of Bordetella pertussis abolish virulence. Proc Natl Acad Sci U S A 89:4898-902.
353. Kucharzik T, Lugering N, Rautenberg K, Lugering A, Schmidt MA, Stoll R, Domschke W. 2000. Role of M cells in intestinal barrier function. Ann N Y Acad Sci 915:171-83.
354. Owen RL, Pierce NF, Apple RT, Cray WC, Jr. 1986. M cell transport of Vibrio cholerae from the intestinal lumen into Peyer's patches: a mechanism for antigen sampling and for microbial transepithelial migration. J Infect Dis 153:1108-18.
355. Neutra MR, Frey A, Kraehenbuhl JP. 1996. Epithelial M cells: gateways for mucosal infection and immunization. Cell 86:345-8.
356. Neutra MR, Pringault E, Kraehenbuhl JP. 1996. Antigen sampling across epithelial barriers and induction of mucosal immune responses. Annu Rev Immunol 14:275-300.
357. Nikitas G, Deschamps C, Disson O, Niault T, Cossart P, Lecuit M. 2011. Transcytosis of Listeria monocytogenes across the intestinal barrier upon specific targeting of goblet cell accessible E-cadherin. J Exp Med 208:2263-77.
358. Tamplin ML, Specter S, Rodrick GE, Friedman H. 1985. Vibrio-Vulnificus Resists Phagocytosis in the Absence of Serum Opsonins. Infection and Immunity 49:715-718.
359. Lee BC, Kim MS, Cho D, Choi SH, Kim TS. 2010. Co-culture supernatants from Vibrio vulnificus-infected INT-407 cells induce IL-8 production in intestinal epithelial cells: crucial role of V. vulnificus rtxE. Int J Mol Med 26:651-9.
360. Bone RC, Sibbald WJ, Sprung CL. 1992. The ACCP-SCCM consensus conference on sepsis and organ failure. Chest 101:1481-3.
361. Harris J, Hartman M, Roche C, Zeng SG, O'Shea A, Sharp FA, Lambe EM, Creagh EM, Golenbock DT, Tschopp J, Kornfeld H, Fitzgerald KA, Lavelle EC. 2011. Autophagy controls IL-1beta secretion by targeting pro-IL-1beta for degradation. J Biol Chem 286:9587-97.

362. Mattox TA, Thayne, K.A., Anderson, E.J. 2013. Prohibitin coordinates an anti-inflammatory/antioxidant feedback loop from mitochondria to nucleus to protect the heart from severe inflammatory stress. FASEB J 27.
363. Cai Y, Sukhova GK, Wong HK, Xu A, Tergaonkar V, Vanhoutte PM, Tang EH. 2015. Rap1 induces cytokine production in pro-inflammatory macrophages through NFkappaB signaling and is highly expressed in human atherosclerotic lesions. Cell Cycle 14:3580-92.
364. Munoz L, Yeung YT, Grewal T. 2016. Oncogenic Ras modulates p38 MAPK-mediated inflammatory cytokine production in glioblastoma cells. Cancer Biol Ther 17:355-63.
365. Catanzaro JM, Sheshadri N, Pan JA, Sun Y, Shi C, Li J, Powers RS, Crawford HC, Zong WX. 2014. Oncogenic Ras induces inflammatory cytokine production by upregulating the squamous cell carcinoma antigens SerpinB3/B4. Nat Commun 5:3729.
366. Perona R, Montaner S, Saniger L, Sanchez-Perez I, Bravo R, Lacal JC. 1997. Activation of the nuclear factor-kappaB by Rho, CDC42, and Rac-1 proteins. Genes Dev 11:463-75.
367. Tong L, Tergaonkar V. 2014. Rho protein GTPases and their interactions with NFkappaB: crossroads of inflammation and matrix biology. Biosci Rep 34.
368. Woida PJ, Satchell KJF. 2018. Coordinated delivery and function of bacterial MARTX toxin effectors. Mol Microbiol 107:133-141.
369. Adiba S, Nizak C, van Baalen M, Denamur E, Depaulis F. 2010. From grazing resistance to pathogenesis: the coincidental evolution of virulence factors. PLoS One 5:e11882.
370. Miller VL, Mekalanos JJ. 1988. A novel suicide vector and its use in construction of insertion mutations: osmoregulation of outer membrane proteins and virulence determinants in Vibrio cholerae requires toxR. J Bacteriol 170:2575-83.
371. Simon R, Priefer U, Puhler A. 1983. A Broad Host Range Mobilization System for Invivo Genetic-Engineering - Transposon Mutagenesis in Gram-Negative Bacteria. Bio-Technology 1:784-791.
372. Kim HU, Kim SY, Jeong H, Kim TY, Kim JJ, Choy HE, Yi KY, Rhee JH, Lee SY. 2011. Integrative genome-scale metabolic analysis of Vibrio vulnificus for drug targeting and discovery. Mol Syst Biol 7:460.
373. Philippe N, Alcaraz JP, Coursange E, Geiselmann J, Schneider D. 2004. Improvement of pCVD442, a suicide plasmid for gene allele exchange in bacteria. Plasmid 51:246-55.
374. Clement JG, Mills P, Brockway B. 1989. Use of telemetry to record body temperature and activity in mice. J Pharmacol Methods 21:129-40.
375. Krarup A, Chattopadhyay P, Bhattacharjee AK, Burge JR, Ruble GR. 1999. Evaluation of surrogate markers of impending death in the galactosamine-sensitized murine model of bacterial endotoxemia. Lab Anim Sci 49:545-50.
376. Donato RP, El-Merhibi, A., Gundsambuu, B., Mak, K.Y., Formosa, E.R., Wang, X, Abbott, C.A., Powell, B.C. 2011. Chapter 8: Studying Permeability in a Commonly Used Epithelial Cell Line: T84 Intestinal Epithelial Cells. *In* Turksen K (ed), Permeability Barrier. Humana Press.

APPENDIX I – Parisa Noorian, PhD (UNSW) and Hannah Gavin

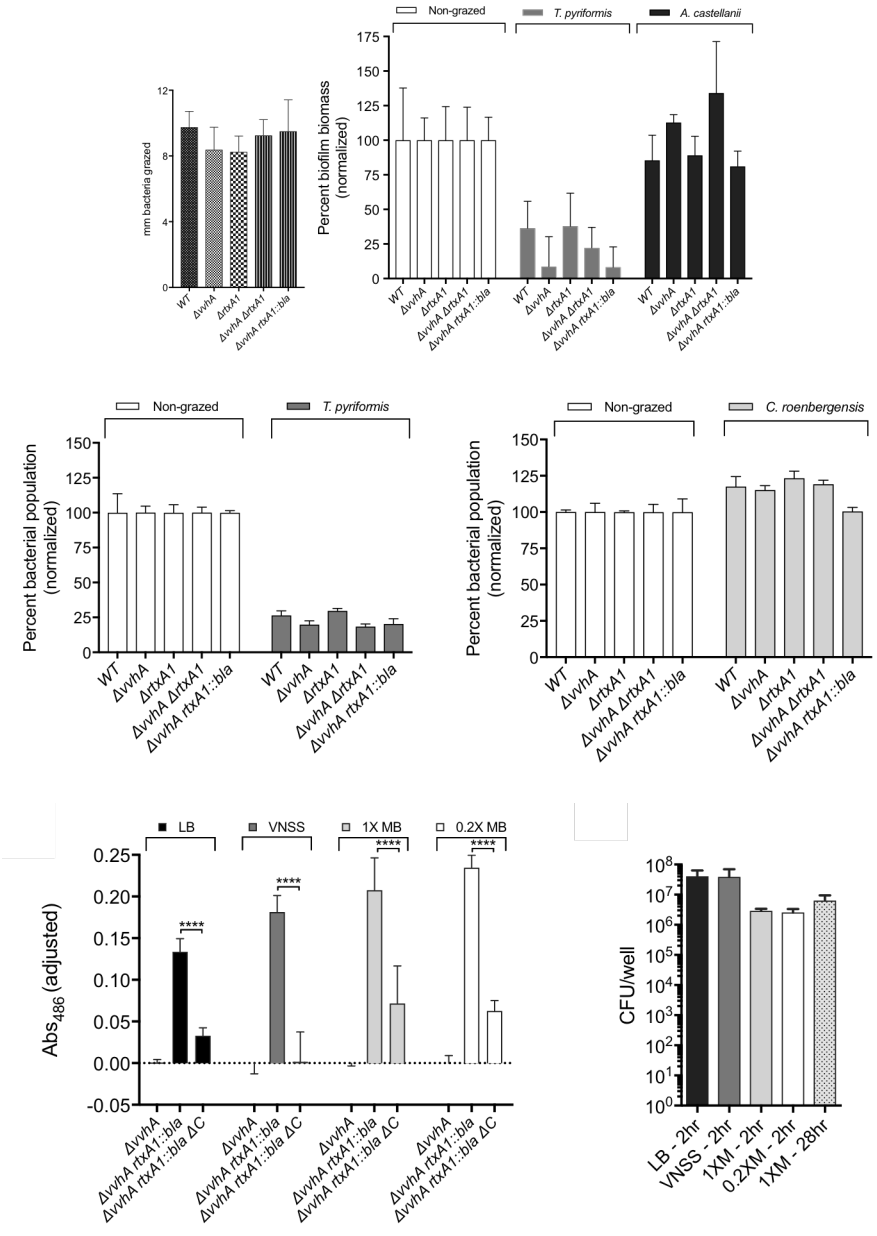

Neither of the secreted toxins VvhA or MARTX protect *V. vulnificus* from predation by protists. *V. vulnificus* was exposed to grazing by various protists (as indicated) in both biofilm and planktonic states (experimetns by Parisa Noorian, PhD, University of New South Wales). All strains of *V. vulnificus* were equivalently susceptible to predation by protists, despite confirmation of *rtxA1* expression and MARTX secretion into the culture media.

APPENDIX II –Hannah Gavin in the laboratory of Nuno Santos, PhD

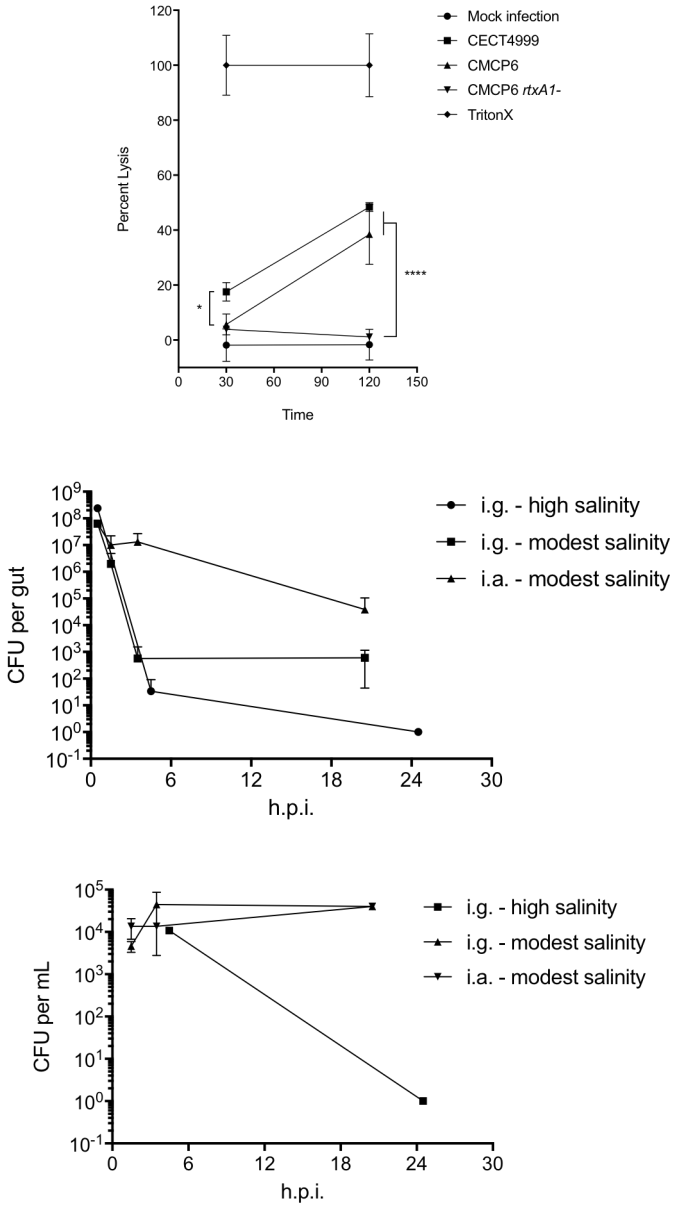

Preliminary data on development of a seabass gut colonization model for *V. vulnificus.* Seabass peritoneal exudate cells are susceptible to MARTX-mediated killing ex-vivo, despite fish resistance to bacterial infection at $>10^{10}$ CFU (top). When water is kept at modest salinity (e.g. <28), *V. vulnificus* can survive in the seabass gut and mucus to 20 hpi.